

## University of Southampton Research Repository ePrints Soton

Copyright © and Moral Rights for this thesis are retained by the author and/or other copyright owners. A copy can be downloaded for personal non-commercial research or study, without prior permission or charge. This thesis cannot be reproduced or quoted extensively from without first obtaining permission in writing from the copyright holder/s. The content must not be changed in any way or sold commercially in any format or medium without the formal permission of the copyright holders.

When referring to this work, full bibliographic details including the author, title, awarding institution and date of the thesis must be given e.g.

AUTHOR (year of submission) "Full thesis title", University of Southampton, name of the University School or Department, PhD Thesis, pagination

**UNIVERSITY OF SOUTHAMPTON**

FACULTY OF ENGINEERING, SCIENCE AND MATHEMATICS

School of Civil Engineering and the Environment

**Three Dimensional Numerical Modelling of Rows of Discrete  
Piles used to Stabilise Large Landslides**

By

**Sasokanthan Kanagasabai**

Thesis for the degree of Doctor of Philosophy

July 2010

UNIVERSITY OF SOUTHAMPTON

ABSTRACT

FACULTY OF ENGINEERING, SCIENCE AND MATHEMATICS

SCHOOL OF CIVIL ENGINEERING AND THE ENVIRONMENT

Doctor of Philosophy

THREE DIMENSIONAL NUMERICAL MODELLING OF ROWS OF DISCRETE PILES  
USED TO STABILISE LARGE LANDSLIDES

by Sasokanthan Kanagasabai

A number of three dimensional finite difference analyses using *FLAC<sup>3D</sup>* have been carried out to investigate the complex pile-soil interaction effects of single isolated pile and groups of piles. The three-dimensional numerical models developed to carry out these analyses are able to model the full pile-soil interaction problem including three dimensional and surface effects which cannot be understood fully using two dimensional analyses.

*FLAC<sup>3D</sup>* analyses are initially carried out to investigate the response of a single pile subjected to lateral soil movements. These analyses explore and verify the failure mechanisms for landslide stabilising piles categorised by Viggiani (1981). The effect of the strength of the slip plane interface and a sloping ground surface on the behaviour of the pile is then investigated. The initial numerical results from models with a rigid pile, a distinct plane of sliding and a horizontal ground surface, as assumed by Viggiani, agree well with his limit equilibrium solutions. The further analyses show that the strength of the slip plane interface has a considerable influence on the pile behaviour, and that the slope of the ground surface is only significant above certain angles.

The behaviour of single and two pile rows with increasing pile spacing is analysed numerically. The *FLAC<sup>3D</sup>* analyses show that pile-soil interaction within a group of piles has a significant influence on performance. If the performance of a single pile row is compared with that of two pile rows, the single pile row installed at a spacing of  $2d$  (where  $d$  is the diameter of the pile) and the two piles rows installed at a spacing between piles in a row of  $3d$  provide a stabilising force equivalent to the force obtained from a solid retaining wall. For both cases, soil movement through the piles remains very small, as a passive wedge type failure mechanism forms in front of the piles.

The behaviour of rows of piles used to stabilise a landslide near Ironbridge, Telford is back analysed. The numerical analyses show that the *FLAC<sup>3D</sup>* models can be used to back analyse complex pile stabilised landslides, in a way not possible by simple limit equilibrium analysis. However, detailed material properties, and the location of slip planes and their strength parameters, are very important input parameters if accurate outputs are to be obtained.

**List of Contents**

<b>Abstract .....</b>	<b>i</b>
<b>List of contents .....</b>	<b>ii</b>
<b>List of figures .....</b>	<b>vi</b>
<b>List of tables .....</b>	<b>xvi</b>
<b>Declaration of Authorship .....</b>	<b>xvii</b>
<b>Acknowledgements .....</b>	<b>xviii</b>
<b>Notation .....</b>	<b>ixx</b>
<b>Chapter - 1:      Introduction .....</b>	<b>1</b>
1.1    Introduction .....	1
1.2    Objectives .....	2
1.3    Layout of the thesis .....	3
<b>Chapter - 2:      Literature Review .....</b>	<b>4</b>
2.1    Introduction .....	4
2.2    Potential failure mechanisms of laterally loaded piles .....	4
2.2.1    Actively loaded pile .....	7
2.2.2    Passively loaded pile .....	9
2.3    Group effects due to the pile-soil interaction .....	17
2.3.1    Field test .....	17
2.3.2    Centrifuge modelling .....	20
2.3.3    2D numerical analysis .....	22
2.3.4    3D numerical analysis .....	29
2.4    Summary .....	32
<b>Chapter - 3:      Potential Failure Mechanisms of Single Laterally Loaded Pile .....</b>	<b>34</b>
3.1    Introduction .....	34
3.2 <i>FLAC</i> <sup>3D</sup> computer code .....	35
3.3    Numerical approach for failure mechanisms .....	36
3.4    Routines used to calculate parameters .....	37
3.4.1    Deflection .....	37
3.4.2    Shear force .....	38
3.4.3    Bending moment .....	39
3.4.4    Lateral pile-soil pressure (expressed in unit of N/m) .....	40



3.5	Investigation of the numerical accuracy of the piles .....	42
3.5.1	<i>FLAC<sup>3D</sup></i> analysis.....	42
3.5.2	Results and discussion .....	45
3.6	Investigation of the numerical accuracy of the interface elements.....	49
3.6.1	Behaviour of the interface representing a defined slip plane.....	51
3.6.1.1	Grid generation.....	51
3.6.1.2	Boundary conditions .....	52
3.6.1.3	Constitutive models and material properties .....	52
3.6.1.4	<i>FLAC<sup>3D</sup></i> analysis.....	53
3.6.1.5	Results and discussion.....	55
3.6.2	Behaviour of pile-soil interface with interface cohesion .....	58
3.6.2.1	Grid generation.....	58
3.6.2.2	Boundary conditions .....	59
3.6.2.3	Constitutive models and material properties .....	59
3.6.2.4	<i>FLAC<sup>3D</sup></i> analysis.....	60
3.6.2.5	Ultimate lateral pile-soil pressure ( $p_u$ ) .....	60
3.6.2.6	Results and discussion.....	63
3.7	Investigate the boundary effects on the pile behaviour .....	67
3.8	Failure mechanisms of isolated piles based on Viggiani (1981) .....	70
3.8.1	Geometry of the problem.....	70
3.8.2	Grid generation .....	71
3.8.3	Initial and boundary conditions .....	71
3.8.4	Constitutive models and material properties.....	71
3.8.5	<i>FLAC<sup>3D</sup></i> analysis.....	72
3.8.6	Results and discussion .....	74
3.8.6.1	Mode – A .....	74
3.8.6.2	Mode – C.....	78
3.8.6.3	Mode – B.....	82
3.9	Summary.....	90

#### **Chapter - 4: Extended Analyses on the Failure Mechanisms of Single Laterally**

##### **Loaded Pile ..... 92**

4.1	Introduction .....	92
4.2	Pile behaviour with increasing strength of the slip plane .....	92
4.2.1	<i>FLAC<sup>3D</sup></i> analyses.....	93
4.2.2	Results and discussion .....	93

4.3	Behaviour of the pile in an infinite slope .....	104
4.3.1	<i>FLAC<sup>3D</sup></i> analyses .....	104
4.3.2	Results and discussion .....	105
4.3.2.1	Behaviour of the pile with slope angle (slip plane strength = 0).....	105
4.3.2.2	Behaviour of the pile with slip plane strength (slope angle = 22°) .....	112
4.4	Behaviour of the pile in a finite slope.....	115
4.4.1	<i>FLAC<sup>3D</sup></i> analyses .....	115
4.4.2	Results and discussion .....	118
4.4.2.1	Behaviour of the pile with varying slip plane strength ( $S_h = 10 d$ ) .....	118
4.4.2.2	Behaviour of the pile with varying pile spacing ( $c_{int}/c_u = 0.5$ ) .....	122
4.5	Summary.....	126
<b>Chapter - 5:</b>	<b>Pile-Soil Interaction Effects of Pile Groups .....</b>	<b>127</b>
5.1	Introduction .....	127
5.2	Interaction effects between single row of piles .....	128
5.2.1	<i>FLAC<sup>3D</sup></i> analyses .....	128
5.2.2	Results and discussion .....	130
5.3	Interaction effects between two rows of piles .....	150
5.3.1	<i>FLAC<sup>3D</sup></i> analyses .....	151
5.3.2	Results and discussion .....	151
5.3.2.1	Case – 1 ( $S_h/d = 3$ ).....	152
5.3.2.2	Case – 2 ( $S_h/d = 5$ ).....	157
5.4	Summary.....	163
<b>Chapter - 6:</b>	<b>Back Analysis the Observed Performance of the Pile Stabilised Landslide at Telford.....</b>	<b>165</b>
6.1	Introduction .....	165
6.2	Background to the site .....	165
6.3	Instrumentation and field monitoring .....	167
6.4	Back analyses the pile group behaviour using <i>FLAC<sup>3D</sup></i> .....	168
6.4.1	Grid generation .....	169
6.4.2	Constitutive models and material properties.....	171
6.4.3	Initial and boundary Conditions.....	172
6.4.4	<i>FLAC<sup>3D</sup></i> analyses .....	173
6.4.5	Results and discussion .....	174
6.5	Summary.....	180

<b>Chapter - 7:</b>	<b>Conclusions and Future Work .....</b>	<b>182</b>
7.1	Conclusions .....	182
7.1.1	Chapter 2: Literature review .....	182
7.1.2	Chapter 3: Failure mechanisms of a single pile .....	183
7.1.3	Chapter 4: Extended analyses on the failure mechanisms of single pile .....	184
7.1.4	Chapter 5: Pile-soil interaction effects of pile groups.....	185
7.1.5	Chapter 6: Back analysis of pile stabilised landslide at Telford .....	186
7.2	Future Work.....	187
7.2.1	Pile-soil interaction of asymmetrically spaced pile group .....	187
7.2.2	Long term behaviour of pile group .....	187
7.2.3	Formation of plastic hinges (failure of the pile) .....	188
7.2.4	Extended analyses on the pile stabilised landslide at Ironbridge, Telford .....	188
<b>References.....</b>	<b>.....</b>	<b>189</b>

## **List of Figures**

Figure 2.1: Diagram showing potential failure mechanisms in the laterally loaded piles

Figure 2.2: Schematic illustrations of lateral loading of piles (a) active loading; (b) passive loading (based on Cubrinovski *et al.*, 2006); and (c) an assumed triangular pressure distribution acts onto the pile above the failure surface due to the failing mass (passive loading)

Figure 2.3: Failure modes for free-headed piles (a) short pile; and (b) long pile (based on Broms, 1964)

Figure 2.4: Failure modes for restrained piles (a) long pile; (b) intermediate length pile; and (c) short pile (based on Broms, 1964)

Figure 2.5: Schematic diagram showing Viggiani's approach

Figure 2.6: Pile failure modes, reproduced from Viggiani (1981)

Figure 2.7: Basic problem of a pile in an unstable slope (based on Poulos, 1995)

Figure 2.8: Pile behaviour characteristics for various failure modes at ultimate loading state (taken from Poulos, 1995)

Figure 2.9: Imposed soil displacements used in *ALP* (taken from Smethurst and Powrie, 2007)

Figure 2.10: The results of the *ALP* analyses and the calculated pressures plotted with the pressure distributions determined by differentiating the fitted bending moment distributions for imposed soil displacement profile (a) *D1*; and (b) *D2* (taken from Smethurst and Powrie, 2007)

Figure 2.11: Average pile load versus deflection curves for each row of piles in comparison with single pile (taken from Rollins *et al.*, 1998)

Figure 2.12: Ratio of average load carried by pile in each row and load carried by single pile as function of lateral pile head deflection (taken from Rollins *et al.*, 1998)

Figure 2.13: Schematic drawing illustrating reduction in load capacity in pile groups due to the overlapping of failure zones (shadow stress zones) and gap formation behind piles (taken from Rollins *et al.*, 1998)

Figure 2.14: Interim design curves for *p*-multipliers ( $P_M = P_{GP}/P_{SP}$ ) as function of pile spacing: (a) leading row piles; and (b) trailing row piles (taken from Rollins *et al.*, 1998)

Figure 2.15: Photograph taken at end of test where piles were spaced at 3 *d* centre-to-centre spacing (taken from Hayward *et al.*, 2001)

Figure 2.16: Plan view of displacement vectors measured in centrifuge tests for piles spaced at (a) 3 *d*; and (b) 6 *d* (taken from Hayward *et al.*, 2001)

Figure 2.17: Measured bending moment profiles of piles spaced at (a) 3 *d*; (b) 4 *d*; and (c) 6 *d* (taken from Hayward *et al.*, 2001)

- Figure 2.18: Infinite and finite element mesh for a single isolated pile loaded laterally in extended soil medium (taken from Chen and Poulos, 1993)
- Figure 2.19: Four analyses of pile groups (based on Chen and Poulos, 1993)
- Figure 2.20:  $p$ - $y$  relationship for piles in an infinitely long row (taken from Chen and Poulos, 1993)
- Figure 2.21:  $p$ - $y$  relationship for piles in two infinitely long rows (taken from Chen and Poulos, 1993)
- Figure 2.22:  $p$ - $y$  relationship for 3-pile group of piles of  $S_h/w = 4$  (taken from Chen and Poulos, 1993)
- Figure 2.23:  $p$ - $y$  relationship 6-pile group (taken from Chen and Poulos, 1993)
- Figure 2.24: Group effects for (a) granular soil (friction angle =  $30^\circ$ ); and (b) undrained state (undrained shear strength = 25 kPa), where bulk modulus =  $7.5 \times 10^4$  kPa, shear modulus =  $1.26 \times 10^4$  kPa, and unit weight = 21 kN/m<sup>3</sup> (taken from Chen and Martin, 2002)
- Figure 2.25: State of soil and  $y$ -direction displacement contours on two rows of piles in granular/drained conditions at the ultimate loading state (taken from Chen and Martin, 2002)
- Figure 2.26: View of the three dimensional mesh with piles displaced laterally (taken from Brown and Shie, 1990b)
- Figure 2.27:  $p$ - $y$  curves of single row of piles spaced at  $2D$ ,  $3D$ ,  $5D$  and  $10D$  centre to centre (c-c) spacing, where  $D$  is diameter of the pile: (a) undrained clay; (b) drained sand (taken from Brown and Shie, 1990b)
- Figure 2.28:  $p$ - $y$  curves for group piles in undrained clay spaced at  $3D$  and  $5D$  centre to centre (c-c) spacing, between the pile rows, where  $D$  is diameter of the pile: (a) front row; (b) back row (taken from Brown and Shie, 1990b)
- Figure 2.29:  $P_m$  values from numerical experiments (taken from Brown and Shie, 1990b)
- Figure 3.1: View of the  $FLAC^{3D}$  history plot of the maximum unbalanced force
- Figure 3.2: Geometry of the  $FLAC^{3D}$  model to represent Viggiani's approach
- Figure 3.3:  $FLAC^{3D}$  pile model: a) pile, before lateral loading; b) pile, after lateral loading
- Figure 3.4: A section showing stress in  $x$ -direction in an element
- Figure 3.5: A section showing stress in  $z$ -direction in an element
- Figure 3.6: Plan view of  $FLAC^{3D}$  mesh showing location of interface elements in between the pile and the soil
- Figure 3.7: Representative area of an interface node (Itasca, 2006)
- Figure 3.8: Typical pile-soil system with interface elements between them
- Figure 3.9: Grid model of piles: a) full pile model; b) half pile model used in the analyses

- Figure 3.10: Schematic diagram of a laterally loaded pile, denoting variables
- Figure 3.11: Variation of deflection with number of vertical elements
- Figure 3.12: Variation of shear force with number of vertical elements
- Figure 3.13: Variation of bending moment with number of vertical elements
- Figure 3.14: Location of interface elements in the model
- Figure 3.15: Element dimension used in stiffness calculation (taken from Itasca, 2006)
- Figure 3.16: *FLAC*<sup>3D</sup> model used to analyse the behaviour of a defined slip plane
- Figure 3.17: *FLAC*<sup>3D</sup> mesh showing equilibrium of vertical stress after gravitational loading
- Figure 3.18: Deformed mesh of Case 1:  $c_{int}/c_u = 0$
- Figure 3.19: Deformed mesh of Case 3:  $c_{int}/c_u = 1$
- Figure 3.20: *FLAC*<sup>3D</sup> history plot showing the  $x$ -direction movement of Point  $G$  (0,0,-5) with boundary soil displacement
- Figure 3.21: Movement of  $z$ -axis nodes with boundary soil movement
- Figure 3.22: Before the pile moves into contact with interface elements
- Figure 3.23: Distribution of lateral earth pressures (taken from Broms, 1964)
- Figure 3.24: Ultimate lateral resistance of different shape of piles (taken from Broms, 1964)
- Figure 3.25: Characteristic meshes for circular piles (taken from Randolph and Houlsby, 1984)
- Figure 3.26: Normalised lateral pressure versus pile displacement curves (taken from Chen and Martin, 2002)
- Figure 3.27: Variation in deflection with pile-soil interface strength
- Figure 3.28: Variation in shear force with pile-soil interface strength
- Figure 3.29: Variation in bending moment with pile-soil interface strength
- Figure 3.30: Variation in normalised lateral pile-soil pressure with pile-soil interface strength
- Figure 3.31: Development of normalised lateral pile-soil pressure with boundary soil movement; rough pile-soil interface model
- Figure 3.32: Comparison of normalised lateral pile-soil pressure with different methods
- Figure 3.33: Plan view of *FLAC*<sup>3D</sup> mesh (a) boundaries at 8  $d$ ; (b) boundaries at 16  $d$
- Figure 3.34: Variation in deflection with distance between pile and boundary locations
- Figure 3.35: Variation in shear force with distance between pile and boundary locations
- Figure 3.36: Variation in bending moment with distance between pile and boundary locations
- Figure 3.37: Variation in normalised lateral pile-soil pressure with distance between pile and boundary locations
- Figure 3.38: Geometry of the *FLAC*<sup>3D</sup> model
- Figure 3.39: Development of normalised lateral pile-soil pressure with soil movement in failure mode A with applied boundary soil displacement of 400 mm and 800 mm
- Figure 3.40: History plot of the normalised lateral pile-soil pressure development at pile top and pile bottom with boundary soil displacement for mode A

- Figure 3.41: Typical diagram explaining failure mode A (based on Viggiani, 1981)
- Figure 3.42: Displacement of pile with soil movement in failure mode A with applied boundary soil displacement
- Figure 3.43: Development of normalised lateral pile-soil pressure with soil movement in failure mode A with applied boundary soil displacement
- Figure 3.44: Development of shear force in the pile with soil movement in failure mode A with applied boundary soil displacement
- Figure 3.45: Development of bending moment in the pile with soil movement in failure mode A with applied boundary soil displacement
- Figure 3.46: Typical diagram explaining failure mode C (based on Viggiani, 1981)
- Figure 3.47: Displacement of pile with soil movement in failure mode C with applied boundary soil displacement
- Figure 3.48: Development of normalised lateral pile-soil pressure with soil movement in failure mode C with applied boundary soil displacement
- Figure 3.49: Development of shear force in the pile with soil movement in failure mode C with applied boundary soil displacement
- Figure 3.50: Development of bending moment in the pile with soil movement in failure mode C with applied boundary soil displacement
- Figure 3.51: History plot of the normalised shear force development at slip plane, with normalised pile top displacement and normalised boundary soil displacement for mode C
- Figure 3.52: Typical diagram explaining failure mode B (based on Viggiani, 1981)
- Figure 3.53: Displacement of pile with soil movement in failure mode B with applied boundary soil displacement
- Figure 3.54: Development of normalised lateral pile-soil pressure with soil movement in failure mode B with applied boundary soil displacement
- Figure 3.55: Development of shear force in the pile with soil movement in failure mode B with applied boundary soil displacement
- Figure 3.56: Development of bending moment in the pile with soil movement in failure mode B with applied boundary soil displacement
- Figure 3.57: Section of the mesh showing vectors of soil and pile movement: (a) mode C; (b) mode A; and (c) mode B.
- Figure 3.58: Development of shear force (absolute value) at the slip plane with boundary soil movement, where  $A=\pi d^2/4$ ,  $c_u=60$  kPa and  $d=1$  m
- Figure 3.59: Development of shear force (absolute value) at the slip plane with pile top movement, where  $A=\pi d^2/4$ ,  $c_u=60$  kPa and  $d=1$  m

- Figure 3.60: Deformed  $FLAC^{3D}$  mesh of mode B analysis, after 200 mm boundary soil displacement
- Figure 4.1: Movement of pile versus depth for three different slip plane strengths, for mode A at 400 mm of boundary soil movement
- Figure 4.2: Normalised lateral pile-soil pressures versus depth for three different slip plane strengths, for mode A at 400 mm of boundary soil movement
- Figure 4.3: Pile shear forces versus depth for three different slip plane strengths, for mode A at 400 mm of boundary soil movement
- Figure 4.4: Bending moments developed in pile versus depth for three different slip plane strengths, for mode A at 400 mm of boundary soil movement
- Figure 4.5: Soil movement calculated at 5 m distance from pile centre in  $y$ -direction for mode A at 400 mm of boundary soil displacement
- Figure 4.6: Movement of pile versus depth for three different slip plane strengths, for mode B at 400 mm of boundary soil movement
- Figure 4.7: Normalised lateral pile-soil pressures versus depth for three different slip plane strengths, for mode B at 400 mm of boundary soil movement
- Figure 4.8: Pile shear forces versus depth for three different slip plane strengths, for mode B at 400 mm of boundary soil movement
- Figure 4.9: Bending moments developed in pile versus depth for three different slip plane strengths, for mode B at 400 mm of boundary soil movement
- Figure 4.10: Soil movement calculated at 5 m distance from pile centre in  $y$ -direction for mode B at 400 mm of boundary soil displacement
- Figure 4.11: Soil movement calculated at 5 m distance from pile centre in  $y$ -direction for mode C at 400 mm of boundary soil displacement
- Figure 4.12: Movement of pile versus depth for three different slip plane strengths, for mode C at 400 mm of boundary soil movement
- Figure 4.13: Normalised lateral pile-soil pressures versus depth for three different slip plane strengths, for mode C at 400 mm of boundary soil movement
- Figure 4.14: Pile shear forces versus depth for three different slip plane strengths, for mode C at 400 mm of boundary soil movement
- Figure 4.15: Bending moments developed in pile versus depth for three different slip plane strengths, for mode C at 400 mm of boundary soil movement
- Figure 4.16: Development of shear force (absolute value) at the slip plane with strength of the slip plane; where  $A=\pi d^2/4$ ,  $c_u=60$  kPa and  $d=1$  m
- Figure 4.17:  $FLAC^{3D}$  slope model with  $14^\circ$  slope angle. The model has been rotated for a better three dimensional view.



Figure 4.18: *FLAC*<sup>3D</sup> slope model with 14 degrees slope angle

Figure 4.19: *FLAC*<sup>3D</sup> slope model with 22 degrees slope angle

Figure 4.20: Movement of pile versus depth for different slope angles at 400 mm of boundary soil movement along the slope

Figure 4.21: Normalised lateral pile-soil pressure versus depth for different slope angles at 400 mm of boundary soil displacement along the slope

Figure 4.22: Pile shear forces versus depth for different slope angles at 400 mm of boundary soil displacement along the slope

Figure 4.23: Bending moment developed in pile versus depth for different slope angles at 400 mm of boundary soil displacement along the slope

Figure 4.24: Diagram showing the stresses acting on the plane at a depth  $d$  below the ground level in an infinite slope (reproduced from Powrie, 2004)

Figure 4.25: The effect of the unit weight of the soil on the stability of the slope, where  $c_{int}/c_u = 1$  and  $d = 5$  m

Figure 4.26: The effect of the depth of the slip plane from the slope surface on the stability of the slope, where  $c_{int}/c_u = 1$  and  $\gamma = 18$  kN/m<sup>3</sup>

Figure 4.27: The effect of the strength of the slip plane on the stability of the slope, where  $\gamma = 18$  kN/m<sup>3</sup> and  $d = 5$  m

Figure 4.28: Deflection of pile and soil movement on a vertical line through a point located 1 m from pile centre in  $y$ -direction, for three different slip plane strengths at 400 mm of boundary soil displacement along the slope

Figure 4.29: Normalised lateral pile-soil pressure versus depth for three different slip plane strengths at 400 mm of boundary soil displacement along the slope

Figure 4.30: Pile shear forces versus depth for three different slip plane strengths at 400 mm of boundary soil displacement along the slope

Figure 4.31: Bending moment developed in pile versus depth for three different slip plane strengths at 400 mm of boundary soil displacement along the slope

Figure 4.32: *FLAC*<sup>3D</sup> mesh of finite slope with 22 degrees slope angle, where  $S_H/d = 10$

Figure 4.33: Displacement vectors showing failure of the unstable soil for  $c_{int}/c_u = 0$  after  $5 \times 10^5$  *FLAC*<sup>3D</sup> steps, where  $S_H/d = 10$

Figure 4.34: Movement of pile versus depth for three different slip plane strengths, after  $5 \times 10^5$  *FLAC*<sup>3D</sup> steps

Figure 4.35: Normalised lateral pile-soil pressure versus depth for three different slip plane strengths, after  $5 \times 10^5$  *FLAC*<sup>3D</sup> steps

Figure 4.36: Soil movement calculated at 1 m distance from pile centre in  $y$ -direction for three different slip plane strengths, after  $1 \times 10^5$  *FLAC*<sup>3D</sup> steps

- Figure 4.37: Pile shear forces versus depth for three different slip plane strengths, after  $5 \times 10^5$   $FLAC^{3D}$  steps
- Figure 4.38: Bending moments developed in pile versus depth for three different slip plane strengths, after  $5 \times 10^5$   $FLAC^{3D}$  steps
- Figure 4.39:  $FLAC^{3D}$  mesh showing the piles in a row at  $S_h$  spacing
- Figure 4.40: Deflection of pile and soil movement on a vertical line through a point located 1 m from pile centre in  $y$ -direction, for three different pile spacings after  $2 \times 10^5$   $FLAC^{3D}$  steps
- Figure 4.41: Normalised lateral pile-soil pressure versus depth for different pile spacings after  $2 \times 10^5$   $FLAC^{3D}$  steps
- Figure 4.42: Pile shear forces versus depth for different pile spacings after  $2 \times 10^5$   $FLAC^{3D}$  steps
- Figure 4.43: Bending moment developed in pile versus depth for different pile spacings after  $2 \times 10^5$   $FLAC^{3D}$  steps
- Figure 5.1: Plan view of  $FLAC^{3D}$  model (a) mesh used in Chapter 3 analyses; (b) modified mesh developed for pile group analyses
- Figure 5.2:  $FLAC^{3D}$  mesh showing the piles in a row at  $S_h/d = 5$  spacing
- Figure 5.3: Plan view of  $FLAC^{3D}$  mesh used for single pile row analyses
- Figure 5.4: Pile behaviour at different pile spacings for a soil boundary displacement of 300 mm: (a) normalised pile displacement; (b) normalised shear force; (c) normalised bending moment; and (d) normalised ultimate lateral pile-soil pressure
- Figure 5.5: (a) Soil flow around the pile and piles act individually; (b) Soil flow around the pile but deforming soil regions start to interact; and (c) Formation of passive wedge in front of closely spaced piles
- Figure 5.6: Relative pile-soil displacement vectors (= displacement vectors, after 300 mm boundary soil displacement – 300 mm displacement, in  $x$ -direction) plotted on the plane through pile axis and parallel to the soil movement ( $y = 0$ ) for the discrete piles spaced at: (a)  $S_h/d = 2$ ; and (b)  $S_h/d = 5$
- Figure 5.7: (a) Plan view of the mesh showing the location  $G$  at which soil movement has been recorded; (b) Movement of soil through Point  $G$  in  $y = 1$  m plane for 300 mm of boundary soil displacement; and (c) Relative soil movement at different pile spacings for soil boundary displacement of 300 mm
- Figure 5.8: Development of normalised ultimate lateral pile-soil pressure for piles spaced at: (a)  $S_h/d = 5$ , (c)  $S_h/d = 2$ ; Movement of soil measured vertically below Point  $G$  in the direction of the applied boundary soil displacement for piles spaced at: (b)  $S_h/d = 5$ , (d)  $S_h/d = 2$

- Figure 5.9:  $x$ -displacement contours at 300 mm boundary soil displacement (a) piles at 2  $d$  spacing; (b) piles at 5  $d$  spacing. Label values are in metre.
- Figure 5.10:  $z$ -displacement contours at 300 mm boundary soil displacement (a) piles at 2  $d$  spacing; (b) piles at 5  $d$  spacing. Label values are in metre.
- Figure 5.11: Ultimate lateral piles-soil pressure developed on the piles with different pile spacing, after 300 mm of boundary soil displacement
- Figure 5.12 Scaled ultimate lateral pile-soil pressure for different pile spacing after 300 mm of boundary soil displacement
- Figure 5.13: Active and passive pressure distribution on a solid retaining wall
- Figure 5.14: Comparison of normalised stabilising force with increasing pile spacing, where  $c_u = 30$  kPa,  $L = 10$  m,  $d = 1$  m and  $\gamma = 18$  kN/m<sup>3</sup>
- Figure 5.15: Comparison of normalised stabilising force with increasing pile spacing for soils with  $c_u = 30$  kPa and 60 kPa (Stabilising forces normalised by appropriate  $c_u$  values)
- Figure 5.16: Block state of  $FLAC^{3D}$  model at 300 mm boundary soil displacement for piles at 2  $d$  spacing: (a) model with  $c_u = 30$  kPa; and (b) model with  $c_u = 60$  kPa
- Figure 5.17: Diagrams shows how pile increases factor of safety ( $FoS$ ) of unstable slope
- Figure 5.18: Comparison of normalised stabilising force calculated using ultimate lateral pile-soil pressure and maximum shear force, where  $c_u = 30$  kPa and  $d = 1$  m
- Figure 5.19: (a) & (b) The normalised lateral pile-soil pressure developed on pile at 20% of ultimate displacement for  $S_h/d = 2$  and 5; (c) & (d) The soil movement measured through Point  $G$  with depth at 20% of ultimate displacement. 300 mm of boundary soil displacement was assumed to be sufficient to develop the ultimate load
- Figure 5.20: Comparison of normalised stabilising force with increasing pile spacing for 20% of ultimate boundary soil movement and ultimate boundary soil movement, where  $c_u = 30$  kPa,  $L = 10$  m,  $d = 1$  m and  $\gamma = 18$  kN/m<sup>3</sup>
- Figure 5.21:  $FLAC^{3D}$  mesh showing two pile rows spaced at  $S_h/d = 3$  and  $S_v/d = 3$
- Figure 5.22: Plan view of two infinitely long rows of piles
- Figure 5.23: Behaviour of two pile rows at different  $S_v/d$  pile spacings for soil boundary displacement of 300 mm. The spacing between piles along the pile row,  $S_h = 3 d$ : (a) normalised pile displacement; (b) normalised shear force; (c) normalised bending moment; and (d) normalised ultimate lateral pile-soil pressure
- Figure 5.24: (a) Mesh showing where soil movement was monitored; (b) Movement of soil at 1 m away from pile centres in the  $y = 1$  plane after 300 mm of boundary soil displacement for  $S_h/d = 3$  arrangement
- Figure 5.25: (a)  $x$ -displacement contours at 300 mm boundary soil displacement for two pile rows spaced at  $S_h/d = 3$  and  $S_v/d = 3$ ; (b)  $x$ -displacement contours at 300 mm

boundary soil displacement for single pile row at  $3d$  spacing. Label values are in metre.

Figure 5.26: Relative displacement vectors (= displacement vectors, after 300 mm boundary soil displacement – 300 mm displacement, in  $x$ -direction) plotted on the plane through pile axis and parallel to the soil movement ( $y = 0$ ) (a) for the discrete piles spaced at  $S_h/d = 3$  and  $S_v/d = 3$ ; (b) for single discrete pile row spaced at  $S_h/d = 3$

Figure 5.27: Behaviour of two pile rows at different  $S_v/d$  pile spacings for soil boundary displacement of 300 mm. The spacing between piles along the pile row,  $S_h = 5d$ : (a) normalised pile displacement; (b) normalised shear force; (c) normalised bending moment; and (d) normalised ultimate lateral pile-soil pressure

Figure 5.28: (a) Mesh showing where soil movement was monitored; (b) Movement of soil at 1 m away from pile centres in the  $y = 1$  plane after 300 mm of boundary soil displacement for  $S_h/d = 5$  arrangement

Figure 5.29:  $x$ -displacement contours at 300 mm boundary soil displacement for two pile rows spaced at (a)  $S_h/d = 5$  and  $S_v/d = 3$ ; (b)  $S_h/d = 5$  and  $S_v/d = 5$ . Label values are in metre.

Figure 5.30: Comparison of normalised stabilising force per metre run of slope along pile row with increasing pile spacing in single and double discrete pile rows, where  $c_u = 30$  kPa,  $L = 10$  m,  $d = 1$  m  $\gamma = 18$  kN/m<sup>3</sup>

Figure 6.1: Site plan of Lloyd's cottage landslide (not to scale)

Figure 6.2: Damage to The Lloyd's Road caused by development of a large landslide in 2004 near Ironbridge, Telford. (Photograph Dr J Smethurst)

Figure 6.3: Cross-section of the site through A-B (not to scale)

Figure 6.4: Simplified slope geometry used to model  $FLAC^{3D}$  mesh

Figure 6.5: Plan view of positions of pile group

Figure 6.6:  $FLAC^{3D}$  model used to back analyse the behaviour of stabilising piles installed at Ironbridge, Telford

Figure 6.7: Plan view of  $FLAC^{3D}$  mesh showing positions of piles and location of pile cap

Figure 6.8:  $FLAC^{3D}$  model showing installation of pile cap

Figure 6.9:  $FLAC^{3D}$  mesh showing equilibrium of pore water pressure after gravitational loading

Figure 6.10 : Comparison of pile behaviour (centre row) plotted from field data and  $FLAC^{3D}$  results (a) pile deflection versus depth; and (b) bending moment developed in the pile versus depth. Field data was analysed by Bicocchi, 2010).

Figure 6.11: Comparison of pile behaviour (centre row) plotted from field data and different  $FLAC^{3D}$  results (a) pile deflection versus depth; and (b) bending moment developed in the pile versus depth. Field data was analysed by Bicocchi, 2010).

Figure 6.12: Comparison between the field data and the *FLAC*<sup>3D</sup> result of pile deflections of all three pile rows

Figure 6.13: Comparison of pile behaviour (centre row) for two different stiffness variations of weak sand stone layer: (a) pile shear forces versus depth; and (b) lateral pile-soil pressures developed in the pile versus depth

Figure 6.14: New slope geometry showing the compound slip plane

**List of Tables**

Table 3.1: Properties of the pile

Table 3.2: Error percentages in variables and the required steps

Table 3.3: Material properties for unstable and stable soils

Table 3.4: Material properties for the pile and the soil

Table 3.5: Material properties for the pile and the soil

Table 3.6: Properties of interface elements used in the analyses

Table 3.7: Shear resistance  $T/Ac_u$  (where  $A=\pi d^2/4$ ,  $c_u=60$  kPa and  $d=1$  m) provided by piles calculated from Viggiani (1981) and  $FLAC^{3D}$  analyses.

Table 5.1: Pile group arrangements

Table 6.1: Properties of the pile

Table 6.2: Assumed plastic-strength properties of the soil layers

Table 6.3: Elastic-strength properties of the soil layers

## **Declaration of Authorship**

I, *Sasokanthan Kanagasabai* declare that the thesis entitled, ‘Three dimensional numerical modelling of rows of discrete piles used to stabilise large landslides’ and the work presented in the thesis are both my own, and have been generated by me as the result of my own original research. I confirm that:

- this work was done wholly or mainly while in candidature for a research degree at this University;
- where any part of this thesis has previously been submitted for a degree or any other qualification at this University or any other institution, this has been clearly stated;
- where I have consulted the published work of others, this is always clearly attributed;
- where I have quoted from the work of others, the source is always given. With the exception of such quotations, this thesis is entirely my own work;
- I have acknowledged all main sources of help;
- where the thesis is based on work done by myself jointly with others, I have made clear exactly what was done by others and what I have contributed myself;
- none of this work has been published before submission.

**Signed:**

---

**Date:**

---

## **Acknowledgements**

I would like to express my sincere gratitude to Professor William Powrie and Dr Joel Smethurst for their invaluable supervision, guidance, and support throughout my PhD. This thesis would not have been possible without their continuous encouragement and patience. I would also like to thank Professor Richard Harkness for his advice in carrying out the numerical analyses in *FLAC<sup>3D</sup>*. My thanks also go to Professor David Richards for his invaluable remarks as the examiner for both my nine-month report and the MPhil-PhD transfer report.

I am also thankful to the School of Civil Engineering and the Environment and the United Kingdom Engineering and Physical Sciences Research Council (EPSRC) that provided the studentship for pursuing this research. I would also like to express my gratitude to other members of Geomechanics Research Group, past and present, who have helped me on several occasions on a variety of issues ranging from report writing to administrative procedures: especially Dr Lucy Ivanova, Dr Qaiser Iqbal and Dr Emily Rees.

I am in great debt to numerous friends who have made my life in the UK enjoyable. Without them, I would never have got this PhD finished. I would like to acknowledge all of them.

Finally, I cannot sufficiently thank my parents, brother and sister for their endless support, love, and care that they have showered upon me throughout my life. In appreciation of all that support, this thesis is dedicated to them.



## **Notation**

### ***Abbreviations***

2D	two-dimensional
3D	three-dimensional
BGL	below ground level
BSD	boundary soil displacement
FLAC <sup>3D</sup>	Fast Lagrangian Analysis of Continua in 3 dimensions

### ***Symbols***

$a$	adhesion at the pile-soil interface
$A$	cross-sectional area of the pile
$c_{\text{int}}$	pile-soil adhesion or undrained shear strength on the sliding plane
$c_u$	undrained shear strength of soil
$d$	pile diameter
$D$	applied boundary displacement
$E$	Young's modulus
$g$	acceleration due to gravity
$G$	elastic shear modulus
$H$	depth from the ground surface to the sliding surface
$I$	second moment of area of the pile
$k$	bearing capacity factor
$k_n$	normal stiffness of interface elements
$k_s$	shear stiffness of interface elements
$K$	elastic bulk modulus
$K_0$	earth pressure coefficient at rest
$K_R$	pile flexibility factor
$L$	pile length
$M$	pile bending moment
$M_p$	yield bending moment
$N$	number of <i>FLAC</i> <sup>3D</sup> calculation steps
$p$	lateral pile-soil pressure (or, force acting on pile per unit length along the pile axis)
$p_{\text{pw}}$	force provided by discrete piles per metre run of slope along the direction of pile row
$p_{\text{rw}}$	force provided by retaining wall per metre run of slope along the wall
$p_u$	ultimate lateral pile-soil pressure
$p_{u,s}$	scaled ultimate lateral pile-soil pressure

$P$	point load
$r$	radius of pile
$S_h$	spacing between two pile in a row
$S_v$	spacing between two pile rows
$T$	pile shear force
$V$	applied boundary velocity in <i>FLAC</i> <sup>3D</sup>
$w$	constant distributed load per unit length
$x$	co-ordinate direction
$y$	lateral pile deflection or co-ordinate direction
$z$	co-ordinate direction
$z_0$	depth of soil in tension between ground surface and depth $z_0$ in the active side
$\alpha$	adhesion ratio
$\beta$	slope angle
$\phi$	frictional soil resistance
$\gamma$	unit weight of soil
$\nu$	Poisson's ratio
$\rho$	density
$\sigma$	normal stress
$\tau$	shear stress
$\psi$	dilation angle

## Chapter - 1: Introduction

### 1.1 Introduction

“A landslide devil seems to laugh at human incompetence”. This is a saying from Bjerrum, 1967. Landslides are frequently responsible for considerable loss of both money and lives, and the severity of the consequences of a landslide usually increases with the size and extent of the slipping mass.

Landslides form in two different ways: a) reactivation of movements on a pre-existing failure surface (e.g. Weeks, 1969; Skempton and Weeks, 1976) and b) where no previous failure surface exists but failure is triggered by a change in the balance of stabilising and resisting forces (e.g. Skempton, 1970; Vaughan and Walbancke, 1973). Many landslides are initiated from pre-existing failure surfaces which may have originally formed as a result of coastal or river erosion, or glacial / postglacial events such as rapid ice melting. The second type of landslide is generated by changes in the pore water pressure of the soil caused by heavy rain fall, or changes to the weight and balance of the unstable mass due to construction activities, excavations or costal / river erosion. However, rain induced failures are most common (Fourie, 1996) and the incidence of these is expected to increase due to climate change (Hulme *et al.*, 2002).

Unstable ground which underlies infrastructure, including buildings, roads, railways and bridges, has to be stabilised to prevent loss or damage to that infrastructure. While the cost of this may be considerable, it is almost always less than the cost of re-routing the infrastructure concerned. However, landslide stabilisation works are expensive and are now the subject of research with the intention of producing more economical designs. There are many slope stabilisation methods available such as shear keys, re-profiling the ground surface, carrying out surface and subsurface drainage, etc. All of these methods have at least one serious limitation. For example, shear keys are only possible where the failure surface is not very deep, and re-profiling is often ruled out for environmental and economic reasons.

Discrete piles have been used to stabilise landslides for many decades (De Beer and Wallays, 1970; Ito and Matsui, 1975; Fokuoka, 1977; Sommer, 1977). When they are placed through deforming ground such as a landslide or slope failure, it is considered that they act to reduce ground movements (Ito and Matsui, 1975). Discrete piles have some significant merits. For example, in heavily built up areas, they can act as foundations for new buildings as well as to stabilise lateral movements.

Current design approaches of discrete piles are aimed at evaluating the restoring force required to stabilise the slope, the required shear and bending moment capacities of the piles, and pile dimensions and layout (Carder, 2005). To determine the shear forces and bending moments developed in the piles, the distribution of the ultimate lateral pile-soil pressures acting along the pile length generated by the movement of the unstable slope is required.

There are a number of analytical and theoretical methods available to estimate the ultimate lateral pile-soil pressures and forces; however, most give the solution for a single or isolated pile and not for a pile group. In general practice, piles are used in groups rather than singly. When piles are installed in a group, there is likely to be a reduction in the ultimate lateral pile-soil pressures acting on each individual pile due to interaction effects with neighbouring piles (Broms, 1964; Randolph, 1981; Chen and Poulos, 1997). Although a number of successful applications of slope stabilisation by means of piles have been reported in the literature, in general there is a lack of clear knowledge of the exact behaviour and potential failure mechanisms of these piles, especially when they are used in rows or groups. Therefore, understanding the behaviour and potential failure mechanisms of piles is very important to the design of effective stabilisation schemes.

Since numerical modelling is quite economical compared to full scale field experiments on a pile group, it can be used to gain an improved understanding of some of the assumptions currently made in discrete pile design procedures. For example, the effect of the spacing between piles in a single row can be investigated using a computational model. This thesis investigates the behaviour of a single isolated pile and pile groups loaded externally by lateral soil movement using a numerical model. Pile-soil interaction is a complex three dimensional problem in nature, and therefore all the analyses presented in this thesis were carried out using three dimensional finite difference computer code *FLAC<sup>3D</sup>* (Itasca, 2006).

## **1.2 Objectives**

The objectives of this thesis are to:

- Gain an improved understanding of the mechanisms of behaviour and potential failure of piles used to stabilise major landslides.
- Gain an improved understanding of the load distribution behaviour when rows of piles are used.
- Back analyse the observed performance of the pile stabilised landslide at Ironbridge, Telford; and
- Test the robustness of simplified analyses for use in the design of pile stabilised slopes.

### 1.3 Layout of the thesis

The layout of the thesis is described below:

#### Chapter 1: Introduction

An introduction to the use of discrete piles to stabilise landslides is given, the significance of the research project are addressed, and the objectives are defined.

#### Chapter 2: Literature review

A review of the behaviour and potential failure mechanisms of actively and passively loaded single isolated piles is presented. Then the pile-soil interaction effects within a single pile row and two pile rows are reviewed by considering field tests, centrifuge modelling, and numerical modelling.

#### Chapter 3: Potential failure mechanisms of single laterally loaded pile

*FLAC<sup>3D</sup>* analyses are carried out to investigate the behaviour of a single pile used to stabilise a slipping mass of soil, by embedment into a stable stratum. Many analyses are carried out, prior to the main analyses, for validation purposes (for example, a numerical investigation into the accuracy of the pile and interface elements) to ensure reliable results. The analyses also explore the failure mechanisms for landslide stabilising piles categorised by Viggiani (1981).

#### Chapter 4: Extended analyses on the failure mechanisms of single laterally loaded pile

The effects of varying the strength of the interface between the sliding and stable strata, and of a sloping ground surface on the behaviour of the pile are investigated in this chapter.

#### Chapter 5: Pile-soil interaction effects of pile groups

The behaviour of single and double rows of passively loaded piles with increasing spacing between piles in a row and distance between two pile rows are analysed numerically. This chapter then provides recommendations for selecting an appropriate pile group arrangement, considering the stabilising force per metre run along the slope by each pile, and soil movement through the piles.

#### Chapter 6: Back analysis the observed performance of the pile stabilised slope at Telford

Back analysis of the behaviour of piles installed to stabilise a landslide in the Severn Gorge at Telford are carried out using *FLAC<sup>3D</sup>*, and compared with field measurements.

#### Chapter 7: Conclusions and future work

The conclusions and new findings drawn from this research are summarised, and suggestions for further research are made.

## Chapter - 2: Literature Review

### 2.1 Introduction

Discrete piles have been used to increase the stability of landslides for many decades (De Beer and Wallays, 1970; Ito and Matsui, 1975; Fokuoka, 1977; Sommer, 1977; Allison *et al.*, 1991; Hong and Han, 1996; Carder and Barker, 2005). The piles are installed to provide resistance against a laterally moving soil mass, transferring the loads into more stable underlying ground. As the soil displaces laterally into the piles, it induces shear forces and bending moments in the piles which they must be able to resist without serviceability or ultimate failure. The piles have to be adequately designed to resist these forces, and to calculate them it is necessary to understand the mechanism by which piles will act to stabilise the slope.

Although there are a number of uncertainties in the design of laterally loaded piles, this thesis concentrates mainly on: (a) trying to understand the behaviour by which the piles stabilise the slope and the ultimate potential failure mechanism, and (b) group effects on laterally loaded piles. A brief literature review of these two areas is presented in the following sections.

### 2.2 Potential failure mechanisms of laterally loaded piles

The resisting force which each pile can provide against the sliding soil mass depends on many factors including the diameter, length and stiffness of the pile, the length of pile embedded into the firm layer, the size and extent of the slipping mass and the stiffness of the soil layers. However, some of these (e.g. stiffness) will not affect the ultimate load, but will affect the load developed at a 'reasonable' (i.e. a serviceable) movement. Due to the interaction of these many factors, failure mechanisms of laterally loaded pile are complex.

There are two main types of potential failure mechanism for laterally loaded piles. If the piles can be designed with sufficient bending capacity, the first group of failure mechanisms involves a flow of soil around the pile associated with failure of the soil. This may involve a failure of the soil within the slipping mass (Fig. 2.1a), or if the piles do not penetrate far below the failure surface, failure in the underlying soil (Fig. 2.1b).

A second group of failure mechanisms involves the formation of one or more plastic hinges in the pile (Fig. 2.1c). The plastic hinges will form at the points where maximum bending moments occur.

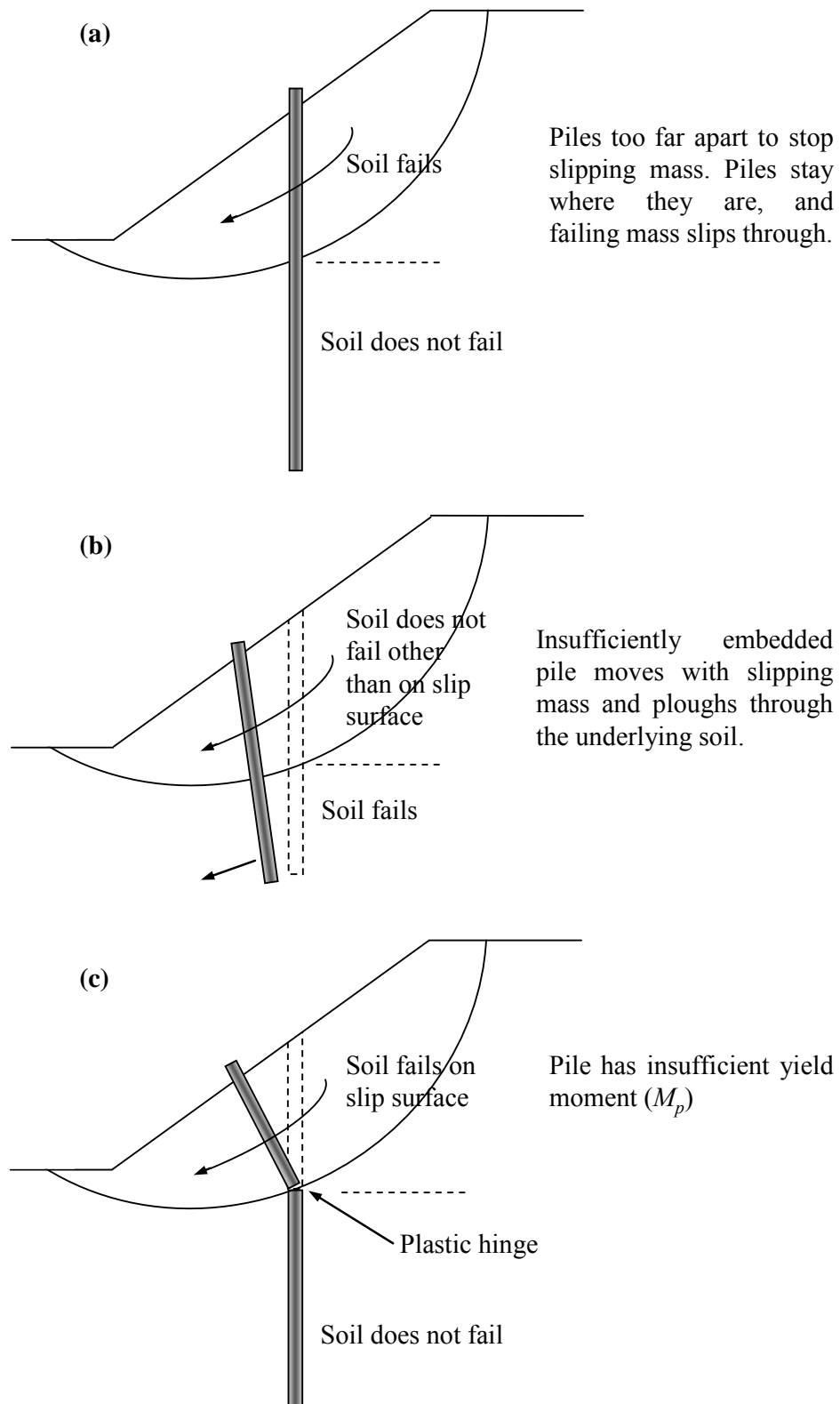


Figure 2.1: Diagram showing potential failure mechanisms in the laterally loaded piles

There is a difference in potential failure mechanisms between a pile loaded ‘actively’ (where external loads are applied to the pile head) in case of Broms (1964), and piles loaded ‘passively’ via global ground movement (Figs. 2.2b and 2.2c). The potential failure mechanisms for a passively loaded pile were first analysed by Viggiani (1981).

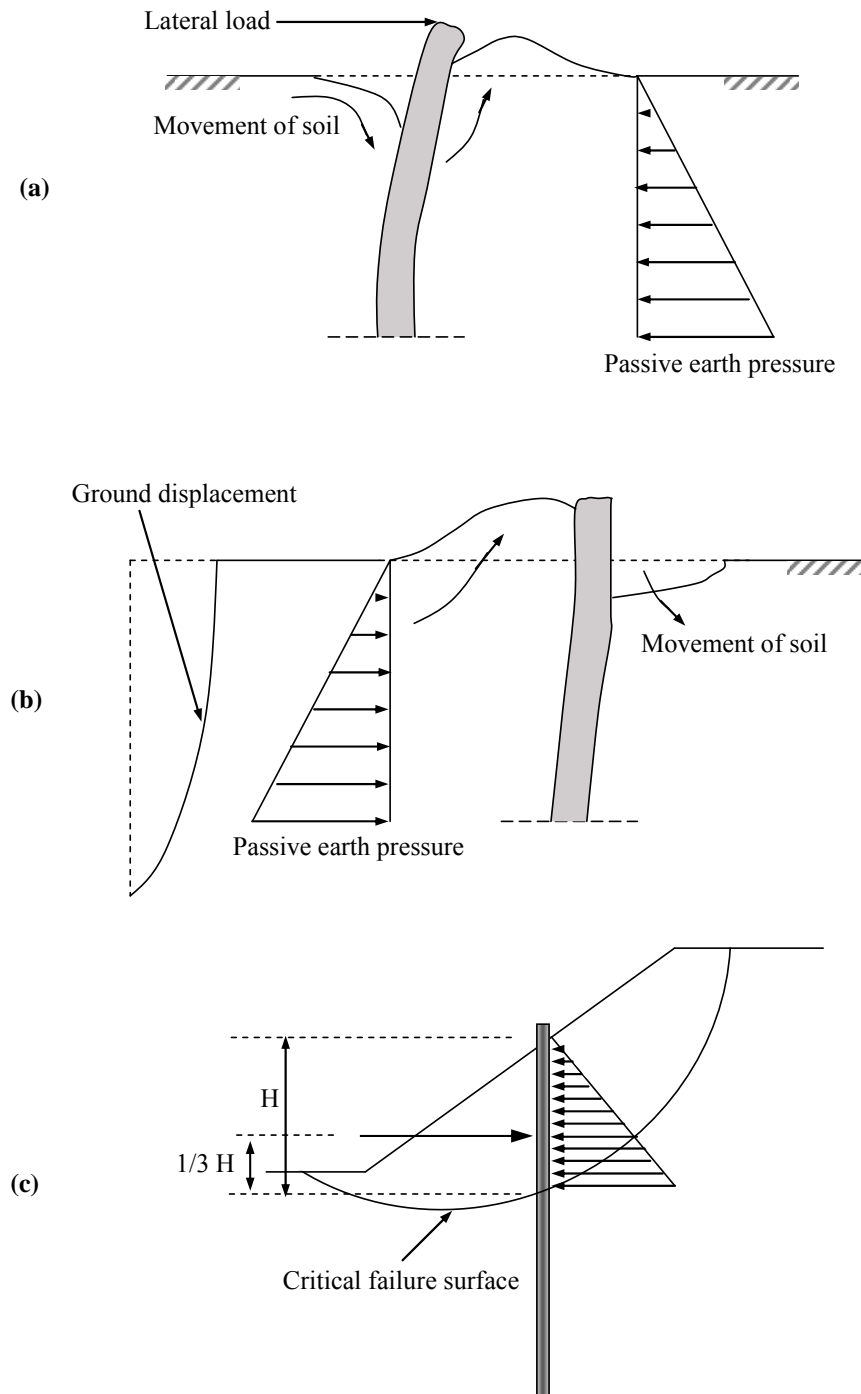


Figure 2.2: Schematic illustrations of lateral loading of piles (a) active loading; (b) passive loading (based on Cubrinovski et al., 2006); and (c) an assumed triangular pressure distribution acts onto the pile above the failure surface due to the failing mass (passive loading)



### 2.2.1 Actively loaded pile

Broms (1964) analysed the possible modes of failure of isolated or single laterally loaded piles driven into saturated cohesive soils. He categorised the failure mechanisms by considering the status of the pile head (free or restrained) and the length of the pile (short, intermediate or long) for a pile loaded laterally at the head by a point force ( $P$ ).

He found that in a short unrestrained pile, failure takes place when the resulting lateral earth pressures reach the lateral resistance of the supporting soil along the full length of the pile and the pile rotates as a rigid body about a point located at some depth below the ground surface (Fig. 2.3a). This kind of failure takes place only when the length of the pile and its penetration depth are small. In a long unrestrained pile, failure occurs when the maximum bending moment in the pile exceeds the moment causing yielding or failure of the pile section (Fig. 2.3b).

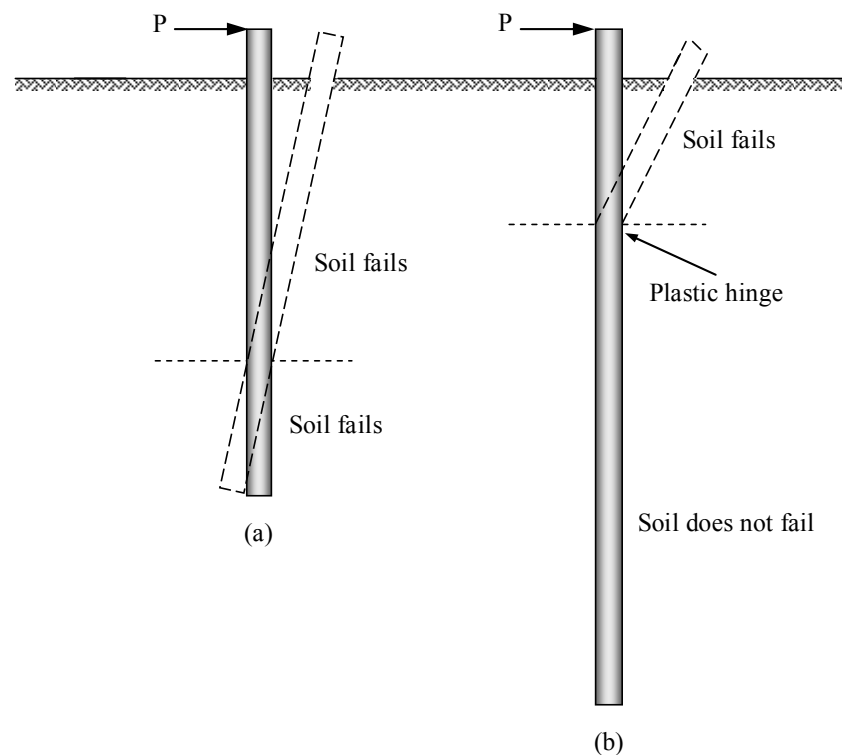


Figure 2.3: Failure modes for free-headed piles (a) short pile; and (b) long pile (based on Broms, 1964)

Broms (1964) also defined possible failure modes for piles restrained at the head by a pile cap. In the case of a long pile, failure takes place when two plastic hinges form along the pile. The first hinge is located at the section of maximum negative bending moment (which is at the level of restraint, usually at the bottom of a pile cap) and the second hinge at the section of maximum

positive bending moment, at some depth below the ground surface. This kind of failure is possible when the length of the piles and the penetration depth are large (Fig. 2.4a). In an intermediate length pile with an intermediate penetration depth, failure takes place after the formation of the first plastic hinge at the top end of the pile and the pile rotates about a point located at some depth below the ground surface (Fig. 2.4b). Short restrained piles fail when the applied lateral load is equal to the ultimate lateral resistance of the soil and the pile moves as a unit through the soil (Fig. 2.4c).

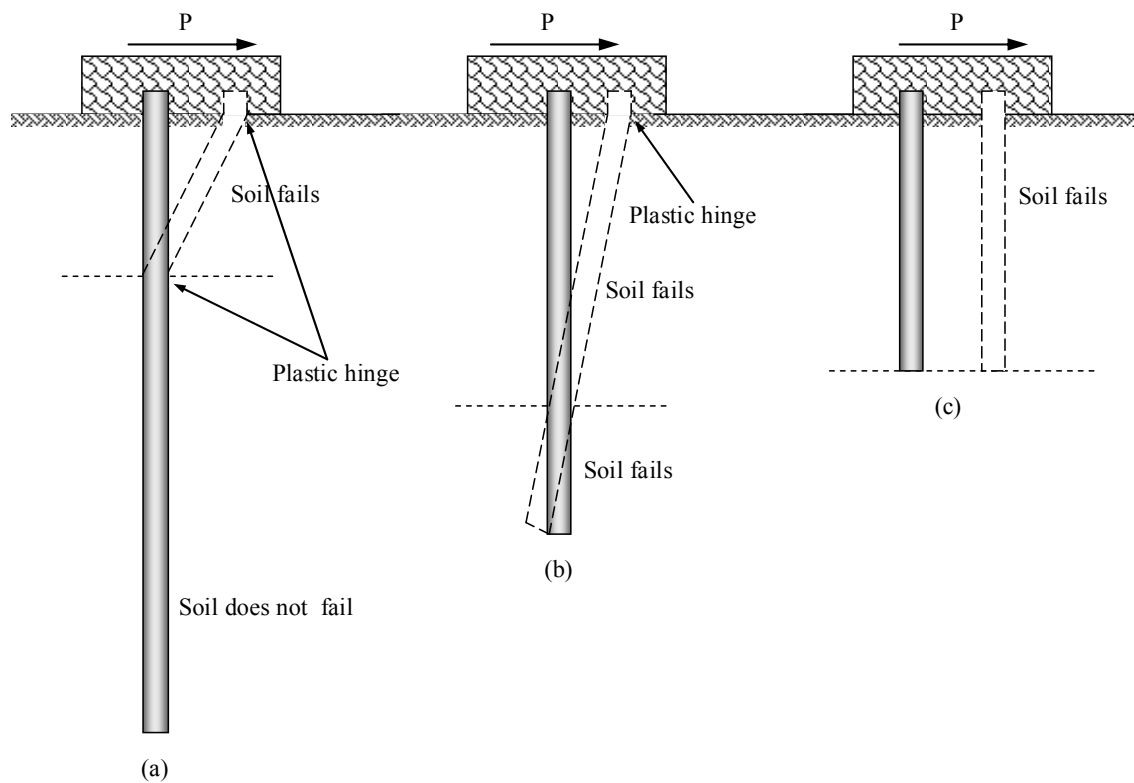


Figure 2.4: Failure modes for restrained piles (a) long pile; (b) intermediate length pile; and (c) short pile (based on Broms, 1964)

Broms (1964) concentrated solely on failure mechanisms of isolated piles in purely cohesive soil. Also, Broms's analysis considered a point force at the pile top, while in terms of stabilising a slope, a pile may be subjected to a distributed lateral soil force along its length (i.e. passive loading).

### 2.2.2 Passively loaded pile

Viggiani (1981) categorised the failure mechanisms of piles loaded by moving ground by considering different factors. He identified six different failure mechanisms for piles driven into a two layered purely cohesive soil, which depend on the yield moment of the pile section, the strength parameters of the stable and sliding soil layers, the thickness of the sliding soil mass and the length and diameter ( $d$ ) of the pile. His proposed approach was based on the concepts developed by Broms (1964) to evaluate the ultimate load of a vertical pile subjected to a horizontal point load.

Viggiani (1981) simplified the real pile-soil interaction problem by making the following assumptions.

- 1) The ground has two layers of soil, with the top layer sliding uniformly over a layer of underlying soil.
- 2) Both the ground surface and the slip surface are horizontal.
- 3) Both soil layers are saturated clays in undrained conditions.
- 4) The undrained shear strength ( $c_u$ ) is constant in each layer.

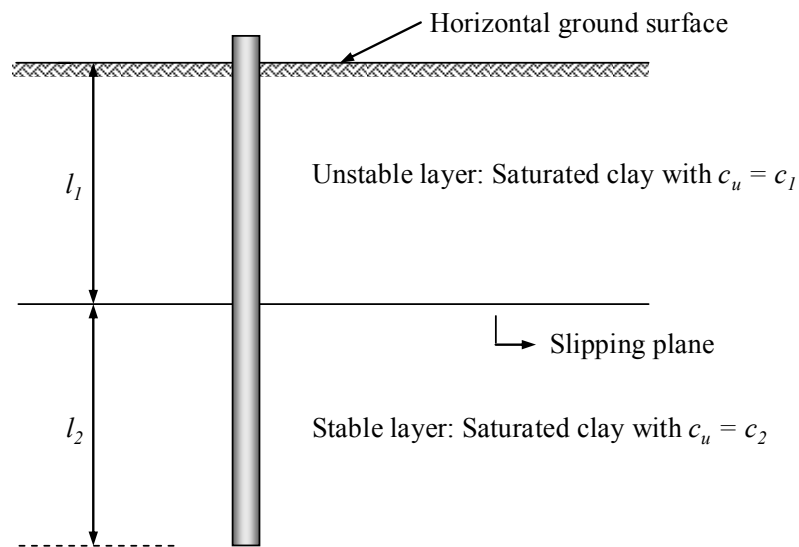


Figure 2.5: Schematic diagram showing Viggiani's approach

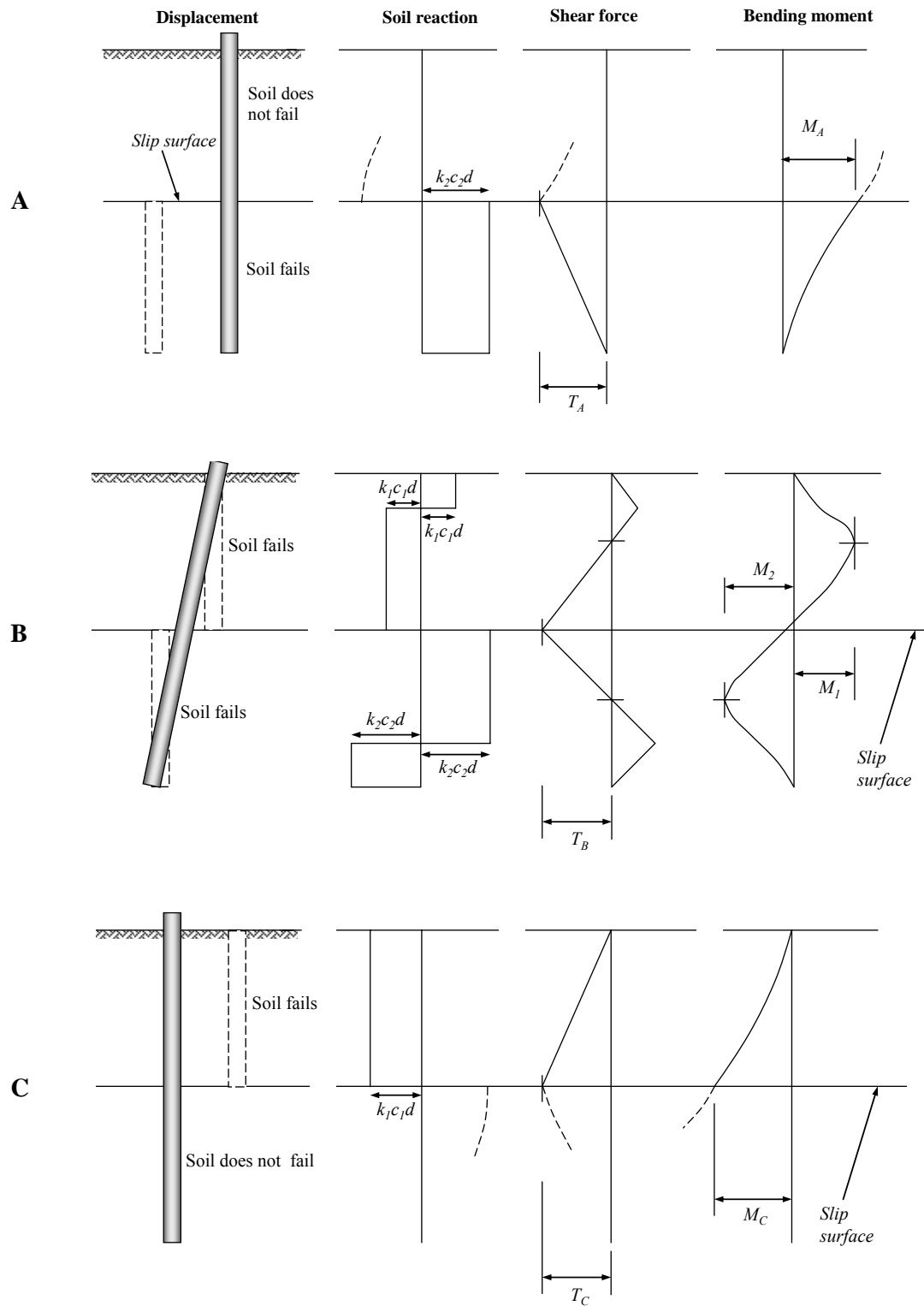


Figure 2.6: Pile failure modes, reproduced from Viggiani (1981)

Viggiani (1981) presents three failure mechanisms assuming that only the soil can fail; these are reproduced in Figure 2.6, labelled A to C. Mechanism A represents a short pile that only penetrates a small distance below the sliding plane. The pile is assumed to be carried along with the sliding soil mass, with the portion of the pile below the sliding plane ploughing through the underlying ground; the soil is then in a state of failure around this lower portion of pile. The earth pressures above the sliding surface do not reach the ultimate value but are otherwise unknown, as are the distributions of shear force and bending moment for this section of the pile. Failure mechanism B is a rigid body rotation of the pile, with two points at which the direction of relative pile-soil movement changes, one above and one below the sliding plane. In this mechanism, the soil is assumed to be at failure over the full depth of the pile, and the full shear force and bending moment distributions can be calculated. Mechanism C relates to a pile which extends some distance below the sliding surface. In this case, the sliding soil fails around the upper section of the pile, but the soil in the underlying stratum is not at failure. The lateral pile-soil pressure, shear force and bending moment are calculable only above the sliding surface.

Viggiani derived dimensionless solutions for shear force and bending moment for each potential failure mechanism, based on an idealised distribution of ultimate lateral pile-soil pressure ( $p_u$ ). The maximum shear force always occurs at the level of the failure surface, and corresponds to the maximum resistance that the system is able to provide to resist ground movements (Eqs. 2.1-2.3).

$$\text{Mode A:} \quad \frac{T_A}{k_1 c_1 d l_1} = \frac{\lambda}{\chi} \quad \text{Equation 2.1}$$

$$\text{Mode B:} \quad \frac{T_B}{k_1 c_1 d l_1} = \sqrt{\left(\frac{1+\lambda}{1+\chi}\right)^2 + \left(\frac{\lambda^2 + \chi}{\chi(1+\chi)}\right)} - \left(\frac{1+\lambda}{1+\chi}\right) \quad \text{Equation 2.2}$$

$$\text{Mode C:} \quad \frac{T_C}{k_1 c_1 d l_1} = 1 \quad \text{Equation 2.3}$$

Where,

$$\lambda = \frac{l_2}{l_1}$$

$$\chi = \frac{k_1 c_1}{k_2 c_2}$$

$c_1 = c_u$  of the unstable soil layer

$c_2 = c_u$  of the stable soil layer

$k_1 = p_u/c_u d$  of the unstable soil layer

$k_2 = p_u/c_u d$  of the stable soil layer

$l_1 =$  pile length embedded in the unstable soil layer

$l_2 =$  pile length embedded in the stable soil layer

$T =$  shear force developed at a particular pile section

Failure mode A occurs if

$$\lambda < \lambda' = \chi \left( \frac{\sqrt{(2+2\chi)} - 1}{1+2\chi} \right) \quad \text{Equation 2.4}$$

Failure mode C occurs if

$$\lambda > \lambda'' = \chi + \sqrt{2\chi^2 + 2\chi} \quad \text{Equation 2.5}$$

And failure mode B occurs when

$$\lambda' \leq \lambda \leq \lambda'' \quad \text{Equation 2.6}$$

Viggiani defined the equivalent coefficient of normalised ultimate lateral pile-soil pressure ( $p_u/c_u d$ ) as a bearing capacity factor ( $k$ ) and assumed values of 4 and 8 for the unstable and stable soils respectively.

Viggiani's solutions are idealised, but enable the potential failure mechanisms of piles subjected to lateral soil movement to be categorised and understood. Many aspects of real landslides, such as a sloping ground surface and slip plane, and long-term drained strength parameters, are not considered. Viggiani's approach is applicable only to the ultimate state and it does not give any indication of the development of pile resistance, or any change in displacement mechanism with soil movement. In design, piles would normally be distanced from ultimate failure using appropriate safety factors; a serviceability limit state in terms of a maximum acceptable displacement may also be specified.

Poulos (1995) carried out a number of simplified boundary element analyses using a computer programme, *ERCAP* (CPI, 1992), to overcome some of Viggiani's (1981) limitations, and presented an approach for the design of slope stabilising piles by assessing their response to lateral ground movement. The pile was modelled as a simple elastic beam, and the soil as an elastic continuum. A limiting lateral pile-soil stress was specified to allow for the local failure of the soil and to obtain a non-linear response. To impose the lateral load on the pile, the unstable soil was moved downslope along the drag zone (or slip surface) as a rigid body (Fig. 2.7).

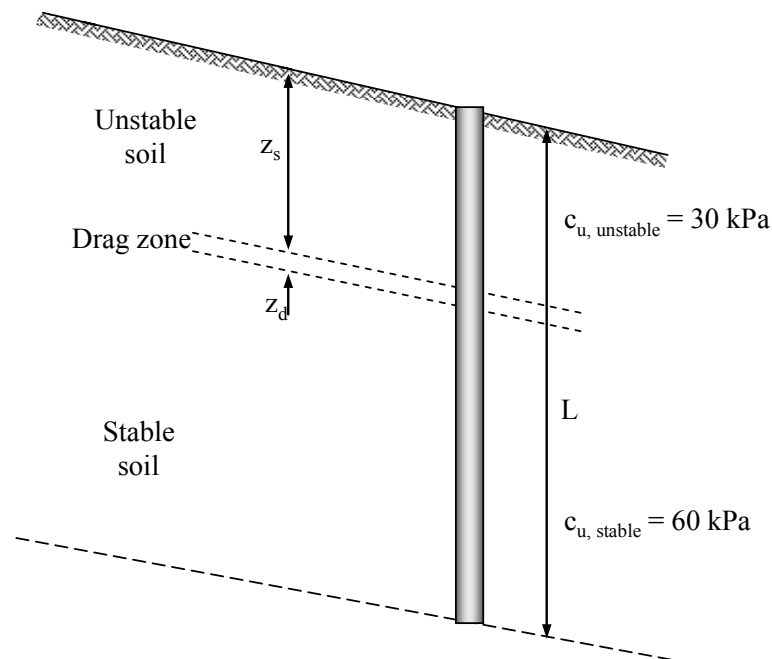


Figure 2.7: Basic problem of a pile in an unstable slope (based on Poulos, 1995)

Poulos also reported three different failure modes similar to Viggiani (1981).

- Flow mode: when the depth of the slip plane is shallow, the unstable soil becomes plastic and flows around the stationary pile (Fig. 2.8a) (equivalent to Viggiani's mode C).
- Short pile mode: when the slip plane is relatively deep and the length of the pile in the stable soil is relatively shallow, the unstable sliding soil carries the pile through the stable soil layer (Fig. 2.8c) (equivalent to Viggiani's mode A).
- Intermediate mode: when the soil strength in both the unstable and stable soil is mobilised along the pile length (Fig. 2.8b) (equivalent to Viggiani's mode B).

Poulos (1995) observed that the highest shear force and bending moment were developed in the piles in the intermediate failure mode. He also observed that the maximum shear force in the pile was developed at the level of the slip plane. Finally, Poulos concluded that the maximum shear force developed in a pile is governed by a number of factors, primarily the shear strength of the soil above and below the potential slide plane, the depth of the slide plane relative to the pile length and the structural strength (yield moment) of the pile.

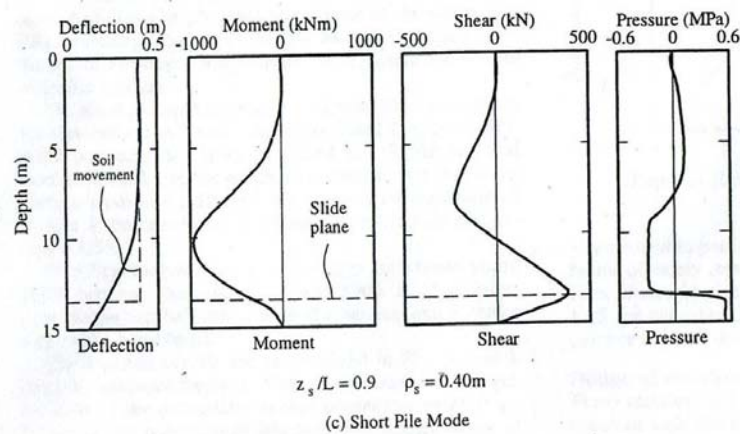
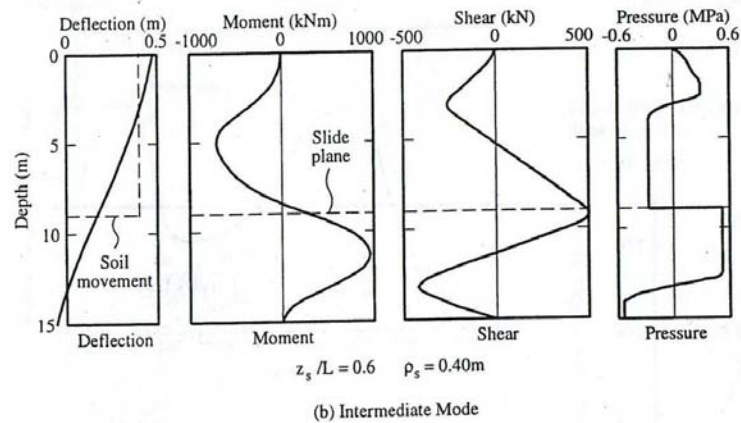
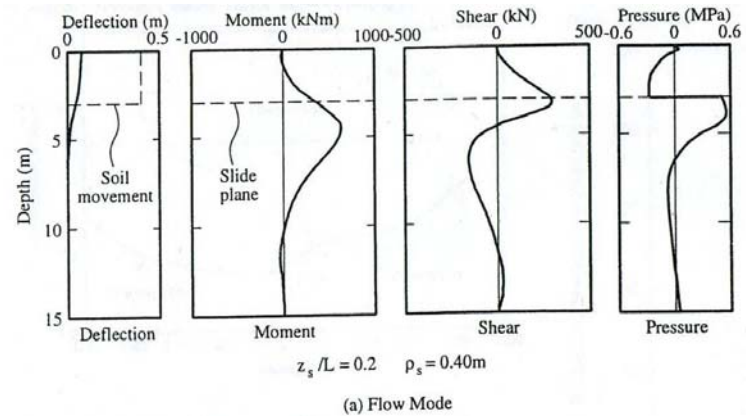


Figure 2.8: Pile behaviour characteristics for various failure modes at ultimate loading state (taken from Poulos, 1995)



The analyses carried out by Viggiani (1981) and Poulos (1995) explain the pile behaviour at the ultimate loading state. However, in general, the slope stabilising piles are designed to carry a serviceability load than the ultimate load, and therefore understanding the behaviour of piles at a serviceability loading state would be useful.

Smethurst and Powrie (2007) back analysed the behaviour of real piles used to stabilise a railway embankment (passively loaded piles) under serviceability loading state. The back analyses were carried out using the programme *ALP* (Oasys, 2004), in which the pile is modelled as a series of finite beam elements and the soil as the elastic-plastic springs. The pile was loaded by displacing the soil into the top section of the model pile, with soil displacement profiles *D1* and *D2*, as shown in Figure 2.9.

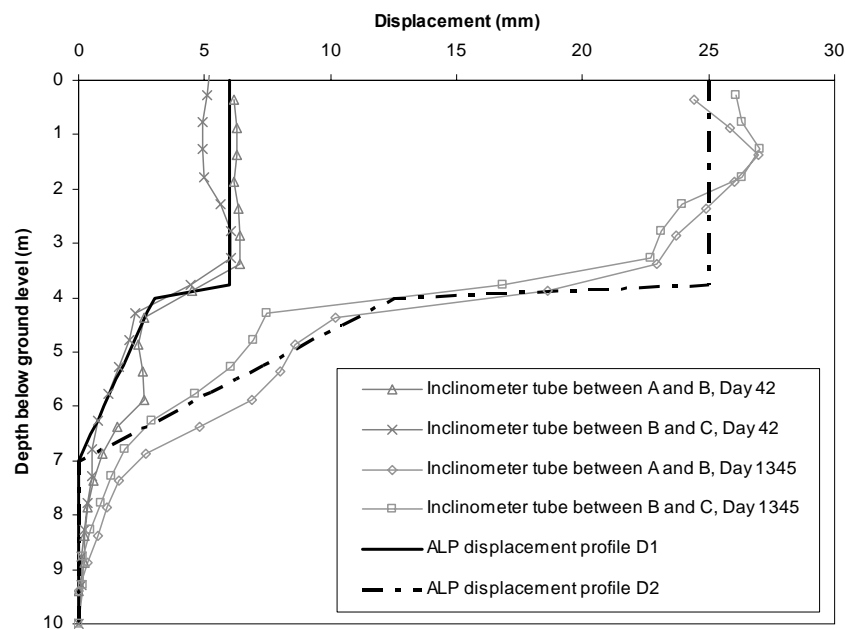


Figure 2.9: Imposed soil displacements used in ALP (taken from Smethurst and Powrie, 2007)

Figure 2.10(a) shows the *ALP* net pressure results for the analysis with imposed soil displacements *D1*, together with the net pressure distributions obtained by differentiating splines fitted to bending moment distributions from the strain gauge data points and the inclinometer data. Figure 2.10 clearly shows that the developed net pressures along the pile shaft for the imposed soil displacement profiles *D1* and *D2*, is distant from the limiting or ultimate pressures, and increases with imposed soil displacements. These back-analysis results therefore confirm that the pile stabilised embankment experiences a serviceability loading conditions and would need more soil displacement to reach its ultimate limit state.

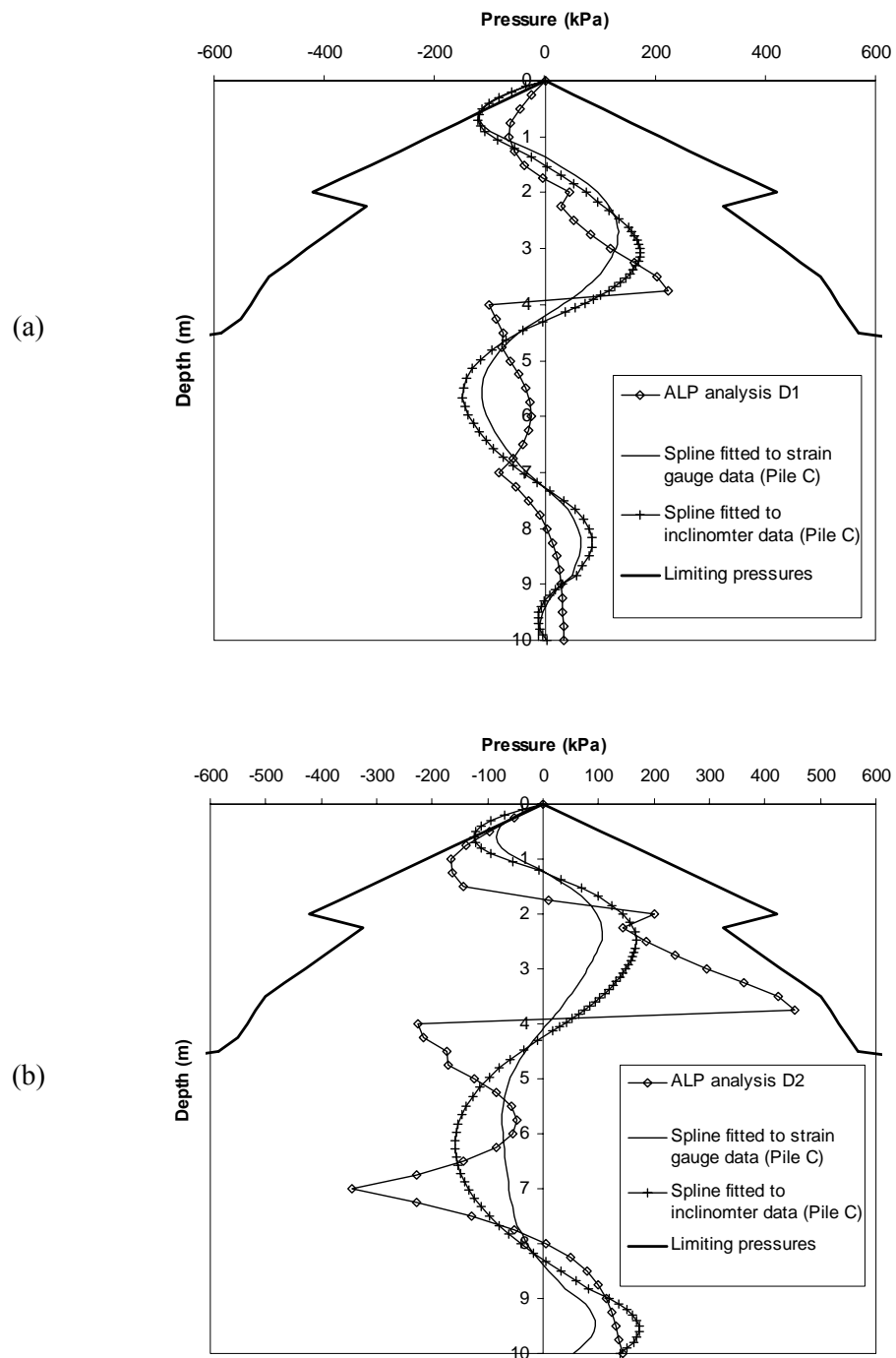


Figure 2.10: The results of the ALP analyses and the calculated pressures plotted with the pressure distributions determined by differentiating the fitted bending moment distributions for imposed soil displacement profile (a) D1; and (b) D2 (taken from Smethurst and Powrie, 2007)

### 2.3 Group effects due to the pile-soil interaction

In practice, piles are frequently used in groups. When piles are closely spaced in a pile group, the presence of loaded piles nearby affects the behaviour of each individual pile (Bransby and Springman, 1999). Many researchers (Broms, 1964; Randolph, 1981; Chen and Poulos, 1997) have recognised that the piles within a group may suffer some reduction in capacity compared with single isolated piles due to interaction effects.

However, the solution obtained for a single pile is often used in design, even for pile groups, due to the lack of a clear quantitative understanding of the pile group interaction effects (Cai and Ugai, 2003). Therefore, it is important to obtain a better understanding of pile-soil-pile interaction within a group of piles.

#### 2.3.1 Field test

Rollins *et al.* (1998) carried out a full scale static lateral load test on a pile group to determine the resulting pile-soil-pile interaction effects. They instrumented, using inclinometers and strain gauges, a 3×3 pile group driven at three-diameter spacings into a layer of soft to medium stiffness clays and silts underlain by a layer of sand. They also instrumented a single isolated pile for comparison.

Rollins *et al.* (1998) applied the lateral load to the single pile and the pile group at the pile head (active loading) in an incremental manner and plotted average pile load versus average pile head deflection curve (Fig. 2.11). From the result, they found that the load distribution in the pile group was not uniform and was a function of the row position. Figure 2.12 shows the ratio between the average horizontal load carried by a pile in each row  $H_{group}$ , and the load carried by a single pile  $H_{single}$ . Rollins *et al.* observed that for a given deflection, piles in trailing rows carried significantly less load than piles in the leading row, and that piles in all rows carried less load than a single isolated pile. When the pile rows are closely spaced, the failure zones for individual piles overlap (Fig. 2.13), and therefore the trailing row carries less load.

The next stage of their work was involved with re-calculating the  $p$ -multiplier  $P_M = P_{GP}/P_{SP}$  (Eq. 2.7) using the computer programme *GROUP* (Reese *et al.*, 1996). Figure 2.14 shows the interim design curves showing  $p$ -multipliers for leading and tailing row piles as a function of pile spacing for low plasticity silts and clays. From this, it can be concluded that pile rows spaced at more than 6 times the pile diameter behave as two different rows.

$$P_M = \frac{P_{GP}}{P_{SP}}$$

Equation 2.7

Where,

$P_{GP}$  = Horizontal soil resistance of a pile from pile group

$P_{SP}$  = Horizontal soil resistance of a single isolated pile

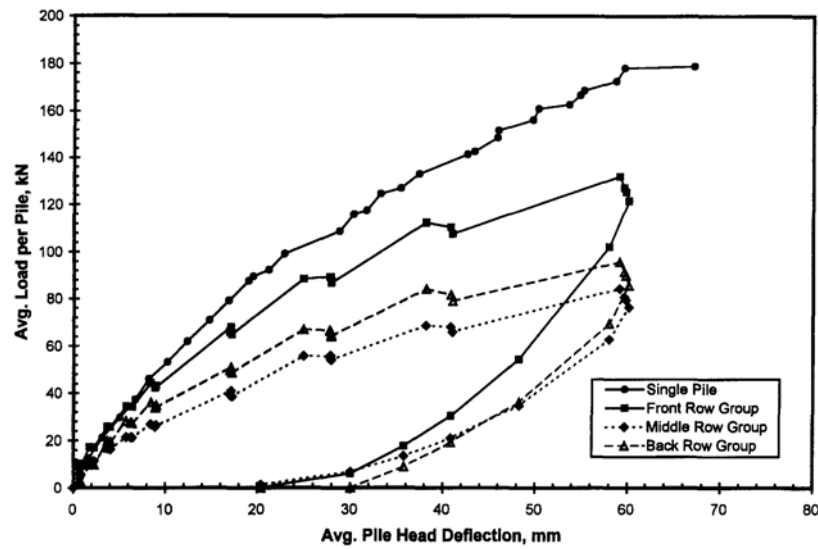


Figure 2.11: Average pile load versus deflection curves for each row of piles in comparison with single pile (taken from Rollins et al., 1998)

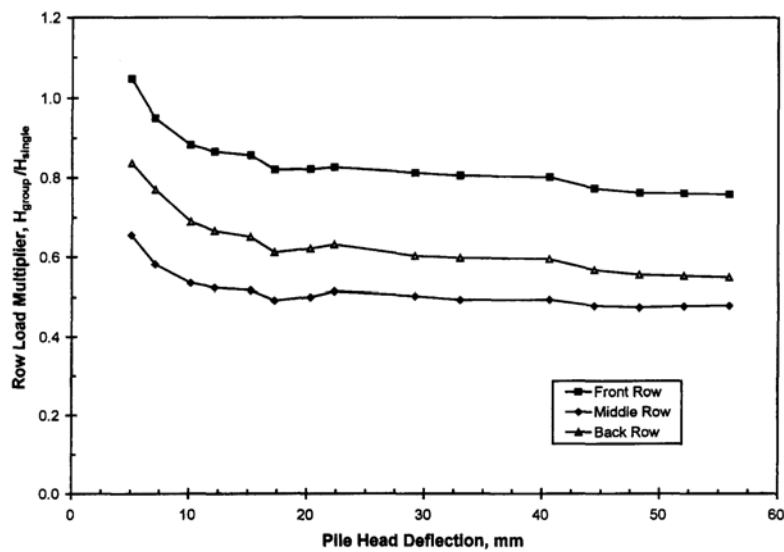


Figure 2.12: Ratio of average load carried by pile in each row and load carried by single pile as function of lateral pile head deflection (taken from Rollins et al., 1998)

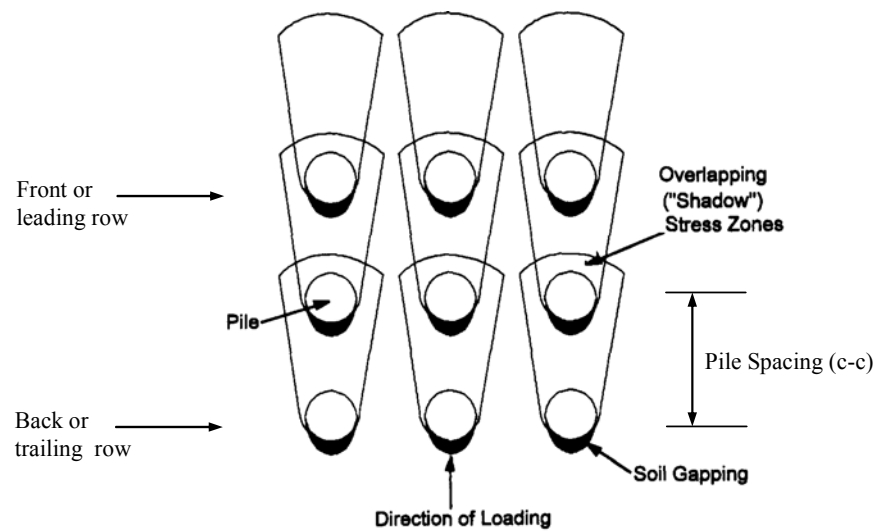


Figure 2.13: Schematic drawing illustrating reduction in load capacity in pile groups due to the overlapping of failure zones (shadow stress zones) and gap formation behind piles (taken from Rollins et al., 1998)

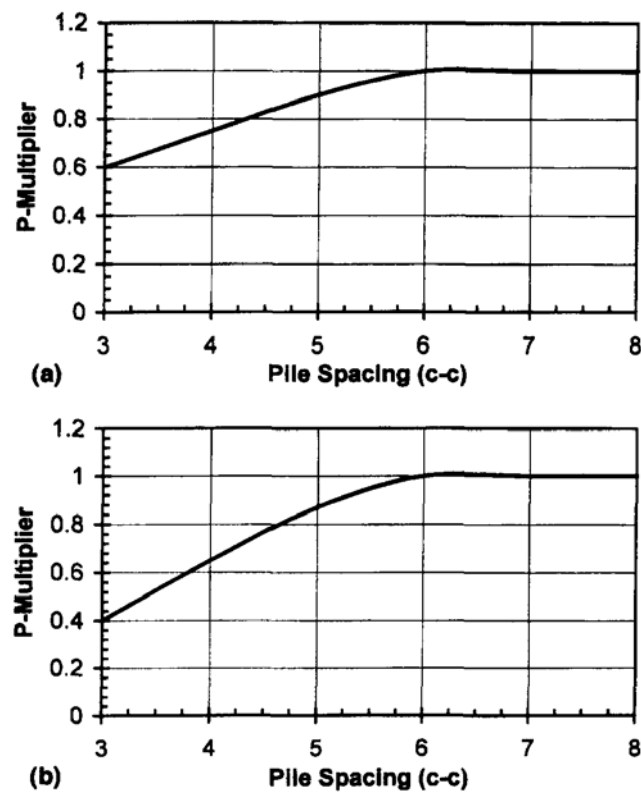
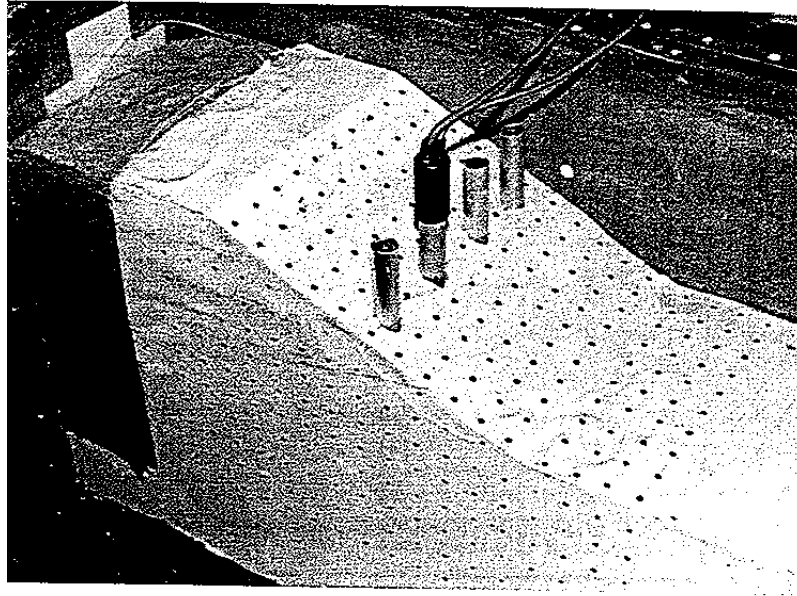


Figure 2.14: Interim design curves for  $p$ -multipliers ( $P_M = P_{GP}/P_{SP}$ ) as function of pile spacing: (a) leading row piles; and (b) trailing row piles (taken from Rollins et al., 1998)

### 2.3.2 Centrifuge modelling

Hayward *et al.* (2001) carried out a series of centrifuge tests to investigate the use of discrete piles for slope stabilisation. A slope without piles, and with piles (Fig. 2.15) spaced at about 3, 4 and 6 pile diameters ( $d$ ) were modelled, and the long term behaviour was then investigated. The tests showed that the slope without piles and with piles spaced at 6  $d$  failed while others did not.



*Figure 2.15: Photograph taken at end of test where piles were spaced at 3  $d$  centre-to-centre spacing (taken from Hayward *et al.*, 2001)*

Figure 2.16 shows the plan view of displacement vectors, plotted at end of the test, for the piles spaced at 3  $d$  and 6  $d$ . When the piles were spaced at 6  $d$ , more soil flow through the piles was observed (Fig. 2.16b), than with the piles at 3  $d$  spacing. This behaviour was explained by Hayward *et al.* as a decrease in the pile-soil interaction when the spacing between piles increases, such that beyond a certain spacing each pile behaves like a single isolated pile. The results from centrifuge tests showed that increasing the spacing between the piles also increased the bending moment developed on the piles (Fig. 2.17). It was argued that when the piles are installed at a high spacing, each pile has to resist a wider strip of the slope, and therefore a higher bending moment is developed on the piles. In other words, the load per pile increases when the spacing between the piles increases.

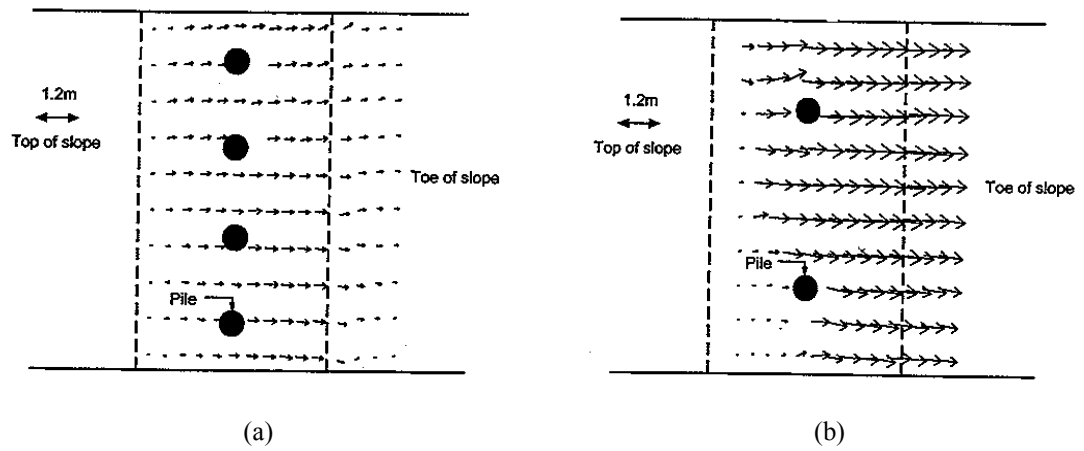


Figure 2.16: Plan view of displacement vectors measured in centrifuge tests for piles spaced at (a) 3 d; and (b) 6 d (taken from Hayward et al., 2001)

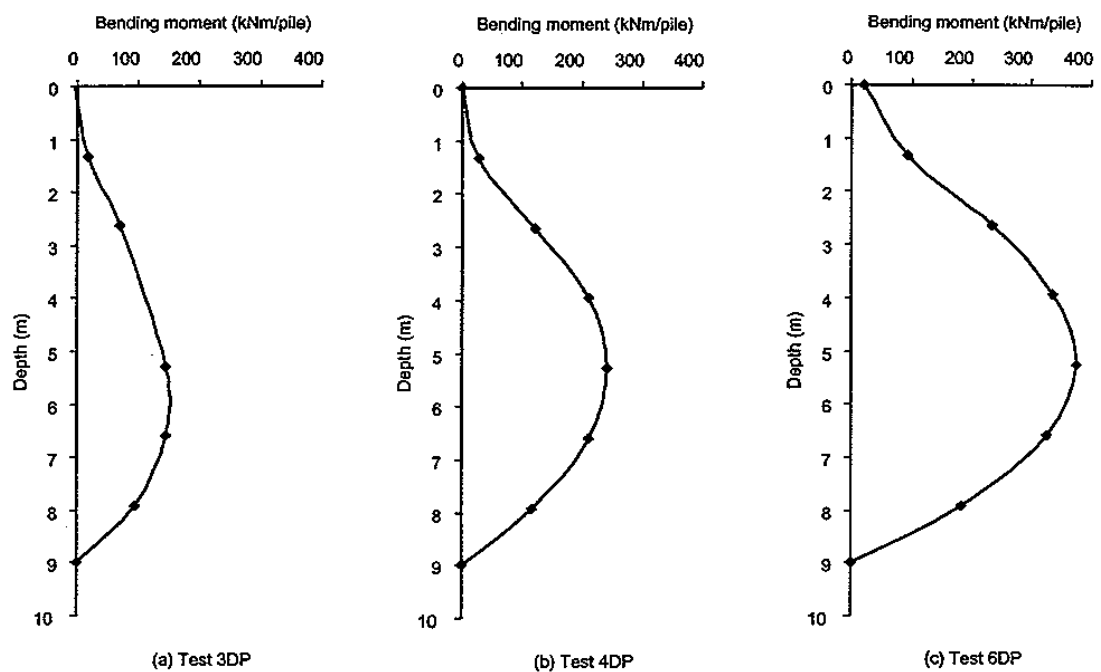


Figure 2.17: Measured bending moment profiles of piles spaced at (a) 3 d; (b) 4 d; and (c) 6 d (taken from Hayward et al., 2001)

### 2.3.3 2D numerical analysis

Chen and Poulos (1993) carried out a numerical analysis combining infinite and finite element methods to investigate how the ultimate soil resistance (or the ultimate lateral pile-soil pressure,  $p_u$ ) changes when the piles are in groups. In this method, the infinite elements were used to simulate the far-field behaviour of the soil medium and standard finite elements to model the pile and the soil immediately surrounding it.

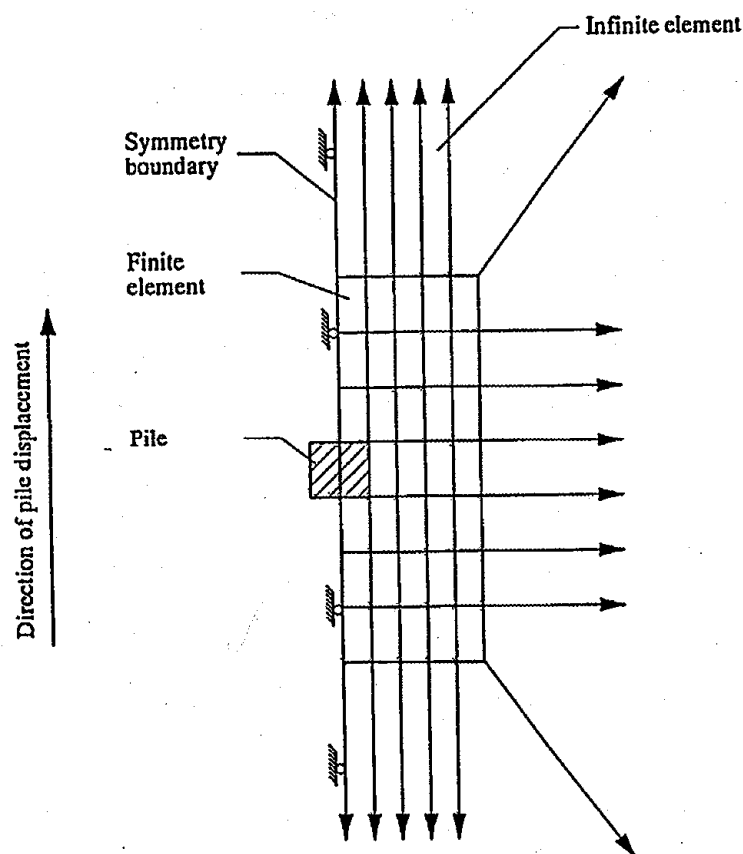


Figure 2.18: Infinite and finite element mesh for a single isolated pile loaded laterally in extended soil medium (taken from Chen and Poulos, 1993)

Chen and Poulos (1993) used a 2D plane stress analysis for two main reasons. It can be applied to a horizontal plane within the soil mass, as the vertical displacement is small compared with the horizontal displacement during lateral loading of piles. Secondly, they felt that 2D plane strain analysis should provide an adequate solution since the ultimate lateral pile-soil pressure was the primary concern in their analysis. It is also much less demanding computationally than a full 3D analysis.



Chen and Poulos analysed four different pile group arrangements (Fig. 2.19). These were:

- Case – A: An infinitely long row of piles
- Case – B: Two infinitely long rows of piles
- Case – C: A three pile group
- Case – D: A six pile group

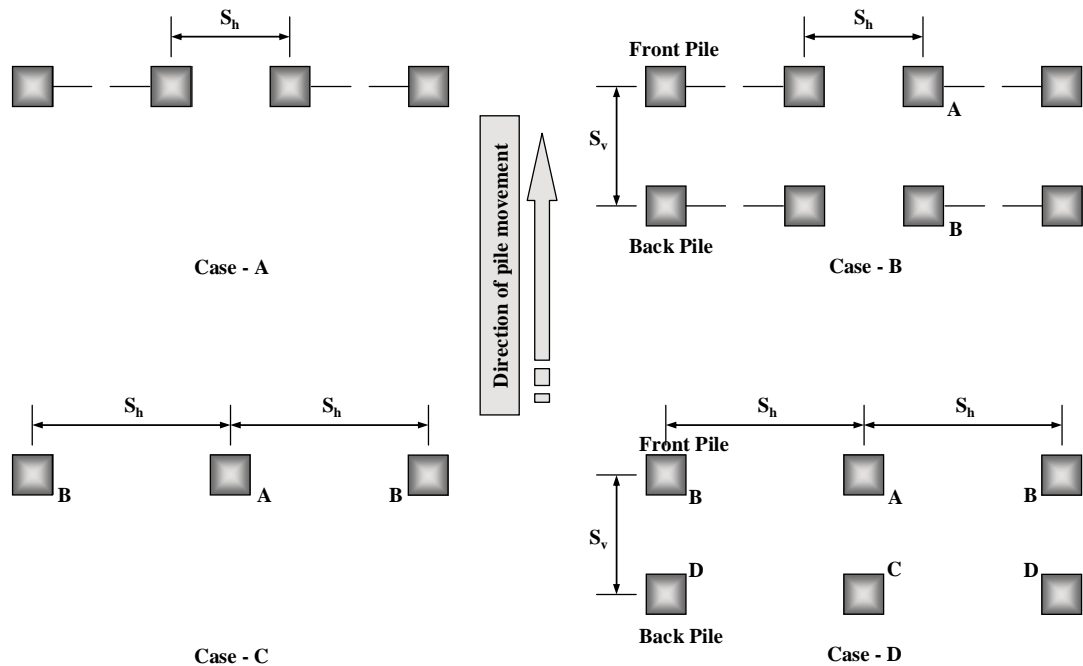


Figure 2.19: Four analyses of pile groups (based on Chen and Poulos, 1993)

Chen and Poulos (1993) assumed that the piles were connected by a rigid pile cap, and were sufficiently rigid to displace equally at all levels. The soil was assumed to be uniform with undrained shear strength ( $c_u$ ). They then incrementally applied a uniform displacement to the pile in the direction of pile movement (active loading).

It is important to note that Chen and Poulos (1993) named the pile row which was pushed into the virgin soil as the ‘front row’ and the one pushed into the shadow soil as the ‘back row’.

From these analyses, they drew many important conclusions on pile group effects. For an infinitely long single row of piles (Case-A), when  $S_h$  is greater than  $2w$  where  $w$  is the width of the pile, there is a trend for  $p_u$  to decrease as the spacing between the piles decreases, but the reduction is fairly small. When the spacing is small (i.e.  $S_h = 2w$ ),  $p_u$  becomes slightly greater than that for a single isolated pile (Fig. 2.20). Although this behaviour is unusual and unexplained, Chen and Poulos (1993) suggested that in practice the spacing between piles is rarely less than  $2.5w$ , and from a practical point of view, it may be concluded that for a single row of piles, group interaction has a relatively small influence on  $p_u$ .

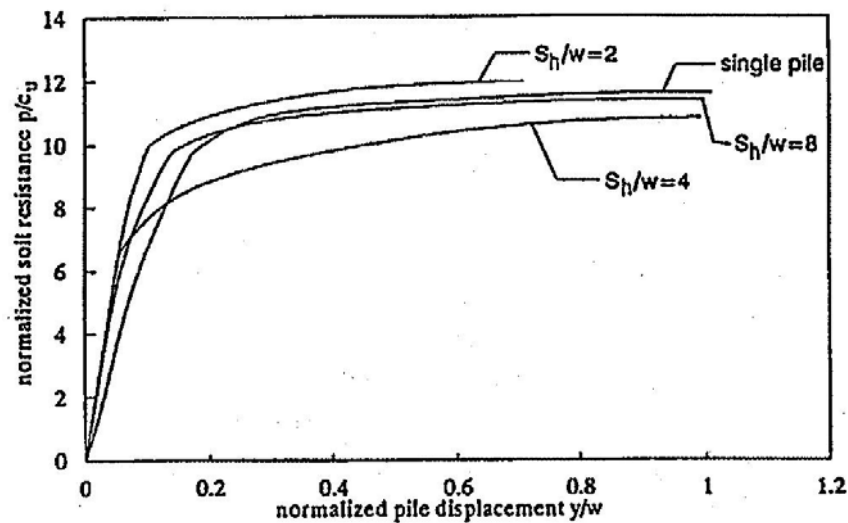


Figure 2.20:  $p$ - $y$  relationship for piles in an infinitely long row (taken from Chen and Poulos, 1993)

For piles in two infinitely long rows (Case-B), the spacing  $S_h$  in the direction perpendicular to that of the loading within the range of  $3w$  to  $6w$  has little effect on  $p_u$  (Figs. 2.21a and 2.21b), while the spacing  $S_v$  in the direction parallel to the direction of loading has a substantial effect for the same spacing range, especially for the piles in the front row (Figs. 2.21a and 2.21c).

For the 3-pile group arrangement (Case-C), a significant group effect was found only when the pile spacing was less than  $2.5w$ . Chen and Poulos (1993) mentioned that the spacing between piles is rarely less than  $2.5w$  in practice; so that, no significant effect needs to be taken into account in this case from a practical point of view.

For the 6 pile group arrangement (Case-D), they found that the capacity of all the piles decreased dramatically from that of a single isolated pile due to the effects of the other piles (Fig. 2.23). They also found that the back piles develop higher  $p_u$  values than the front piles.

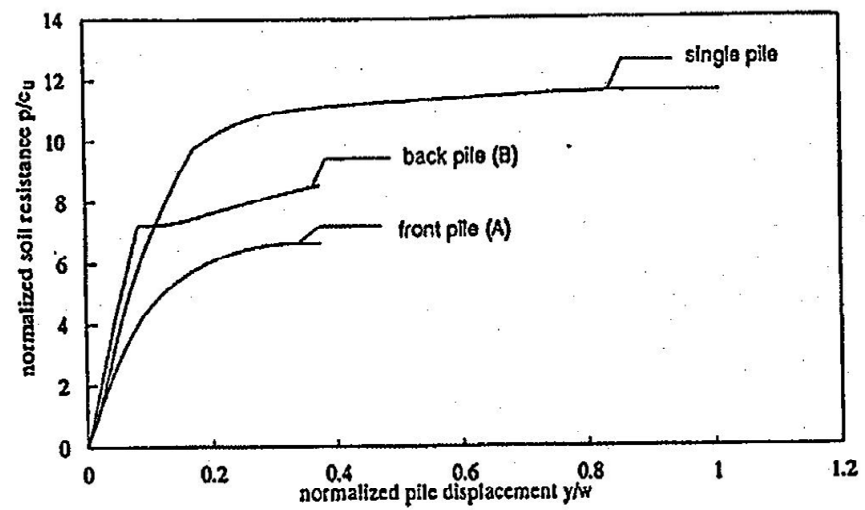
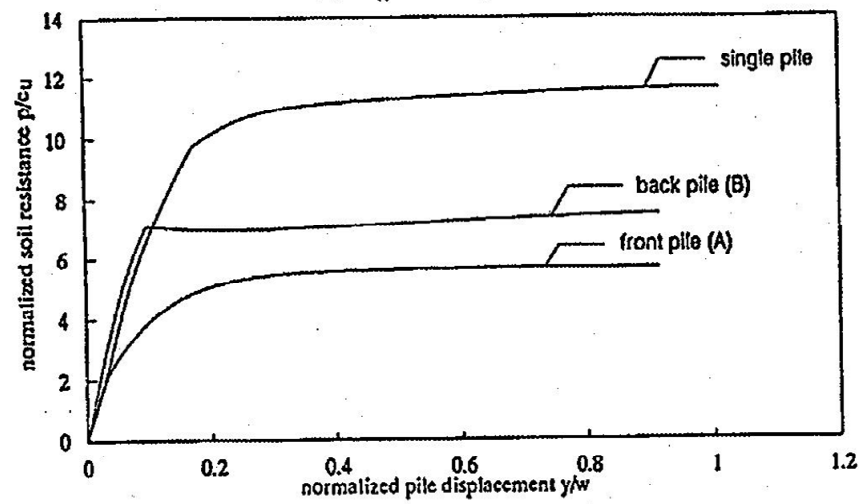
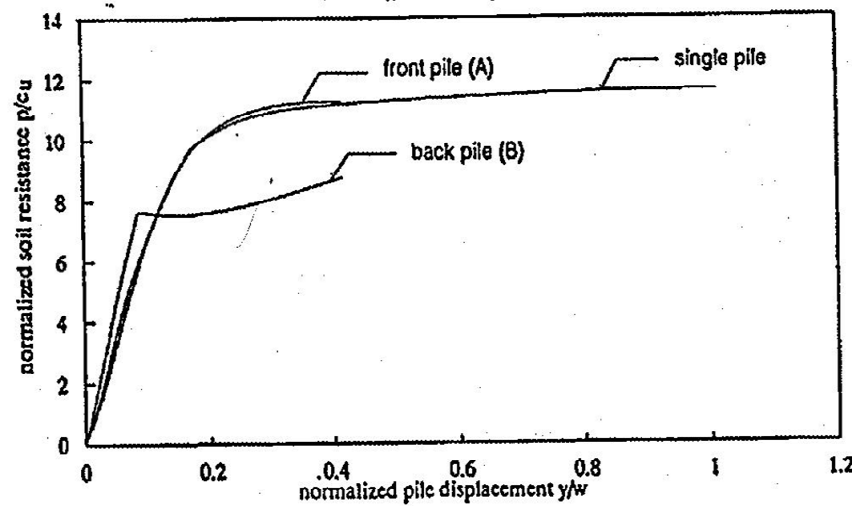
(a)  $S_h = 3w, S_v = 3w$ (b)  $S_h = 6w, S_v = 3w$ (c)  $S_h = 3w, S_v = 6w$ 

Figure 2.21:  $p$ - $y$  relationship for piles in two infinitely long rows (taken from Chen and Poulos, 1993)

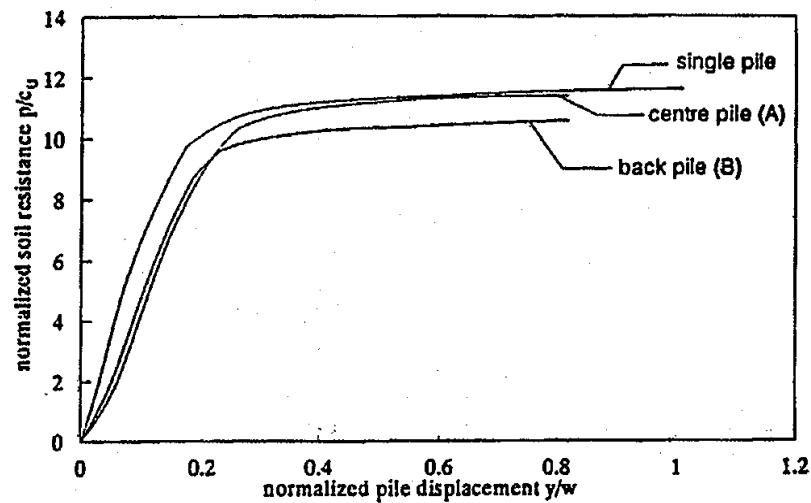


Figure 2.22:  $p$ - $y$  relationship for 3-pile group of piles of  $S_h/w = 4$  (taken from Chen and Poulos, 1993)

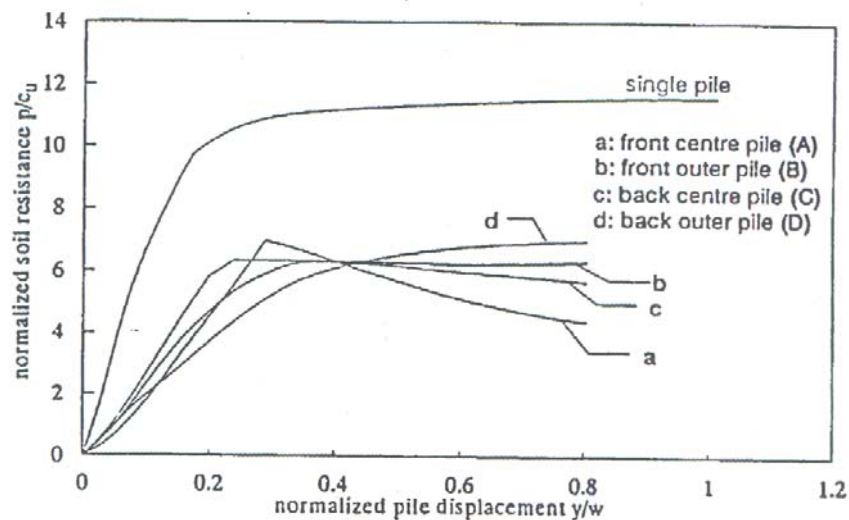


Figure 2.23:  $p$ - $y$  relationship 6-pile group (taken from Chen and Poulos, 1993)

Chen and Poulos (1993) concluded the following points. The ultimate soil resistance is generally lower for a pile in a group than that for a single isolated pile. The extent of the reduction depends on the arrangement of piles. For piles in one row (i.e. in a line perpendicular to the direction of the pile movement) the reduction is not significant, whereas a substantial reduction is found for piles in two rows if the pile rows are close enough (Figs. 2. 20 and 2.21).

Chen and Martin (2002) investigated the effect on the load transfer mechanism of using one or two rows of passively loaded piles in drained conditions. They developed a plane-strain model using the finite difference programme *FLAC<sup>2D</sup>* (Itasca, 1998) to investigate the load transfer mechanism and then to understand the soil plastic flow around the pile.

They compared the group effects of piles subjected to active and passive loading, for one row of stabilising piles in drained soil conditions. Figure 2.24(a) shows the pressure acting on the piles for a pile spacing varying from  $2d$  to  $6d$  where  $d$  is the pile diameter. They found that the ultimate lateral pressure decreased as the pile spacing decreased.

Chen and Martin (2002) examined how ultimate pressures vary with pile spacing in clay in undrained plane strain conditions. They found that the ultimate pressures acting on one row of passively loaded piles reduced with increasing pile spacing (Fig. 2.24b). This behaviour seems counter-intuitive since a higher ultimate pressure might be expected when the spacing between the piles is bigger. *FLAC<sup>3D</sup>* analyses are carried out as part of this thesis to understand clearly this behaviour, and are presented in Chapter 5.

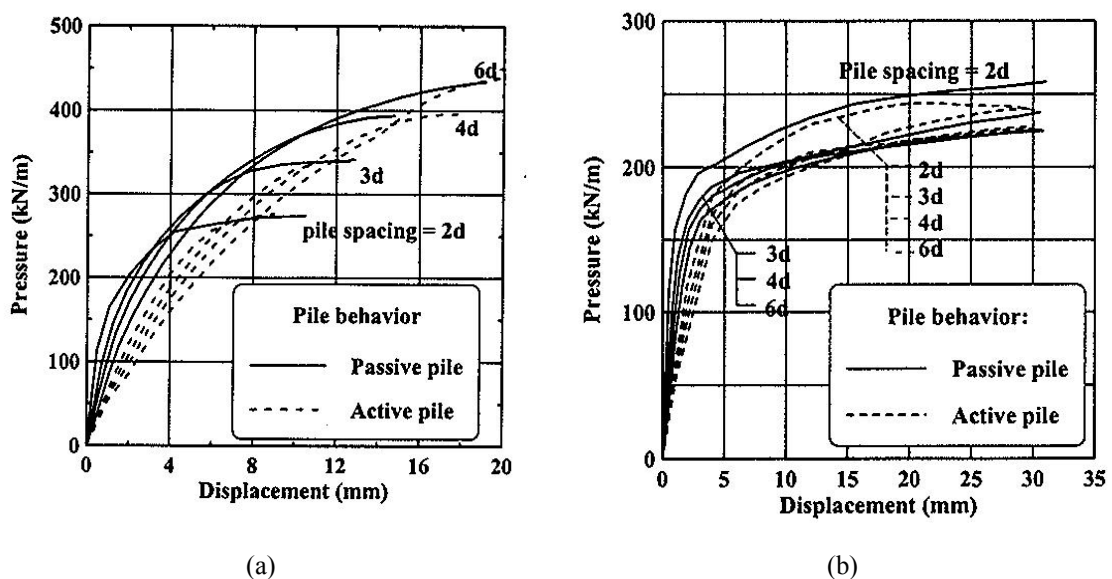


Figure 2.24: Group effects for (a) granular soil (friction angle =  $30^\circ$ ); and (b) undrained state (undrained shear strength = 25 kPa), where bulk modulus =  $7.5 \times 10^4$  kPa, shear modulus =  $1.26 \times 10^4$  kPa, and unit weight =  $21 \text{ kN/m}^3$  (taken from Chen and Martin, 2002)

They carried out further analyses on a passively loaded pile group comprising two pile rows in drained conditions. Parallel and zigzag arrangements of piles were considered in the analysis. The  $y$ -direction displacement contours (Fig. 2.25) clearly show that the parallel arrangement extends the zone of soil movement to the rear row of the piles much more effectively than piles arranged in the zigzag pattern.

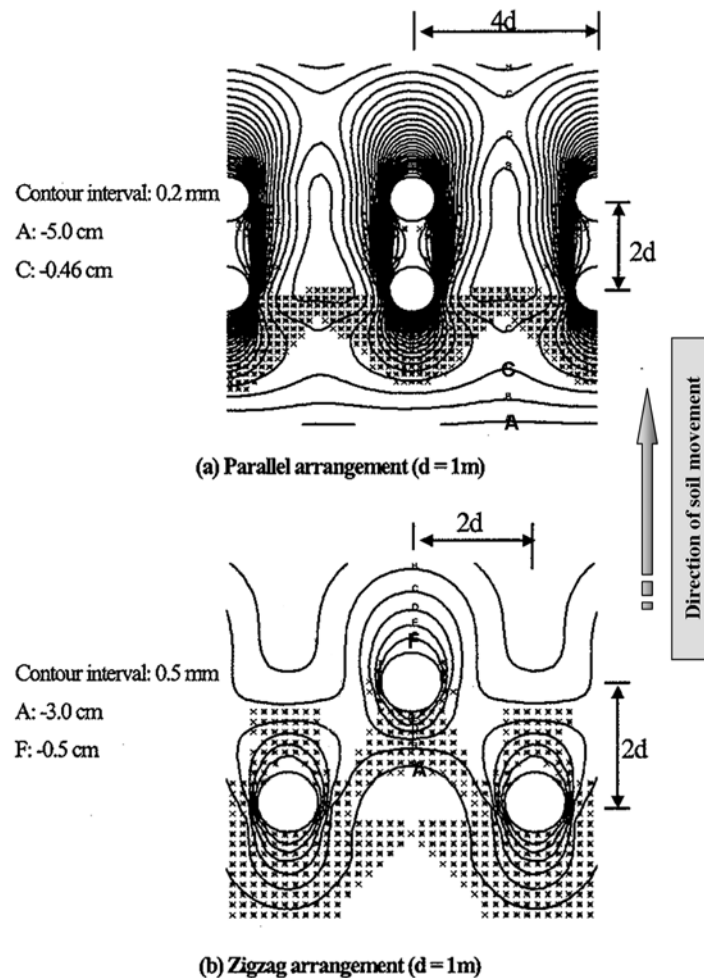


Figure 2.25: State of soil and  $y$ -direction displacement contours on two rows of piles in granular/draind conditions at the ultimate loading state (taken from Chen and Martin, 2002)

In summary, Chen and Martin (2002) concluded that the ultimate lateral pressure increases as the pile spacing becomes larger in drained conditions, and decreases when the pile spacing increases in undrained conditions, in a single passively loaded pile row. However, no significant interaction or group effects occur if pile spacing is over  $4d$ . Chen and Martin (2002) also show that group effects are more significant for drained than undrained conditions.

### 2.3.4 3D numerical analysis

Brown and Shie (1990b) analysed the response of one or two rows of closely spaced piles subjected to lateral load at the pile head (active loading) using a three dimensional finite element model. The primary aim of their finite element analyses was to evaluate the effect of pile spacing within a row and between rows of piles to produce design guidelines for pile groups. Figure 2.26 shows the three dimensional finite element model, which consists of two infinite rows of piles in a uniform soil stratum with the piles fixed at the base.

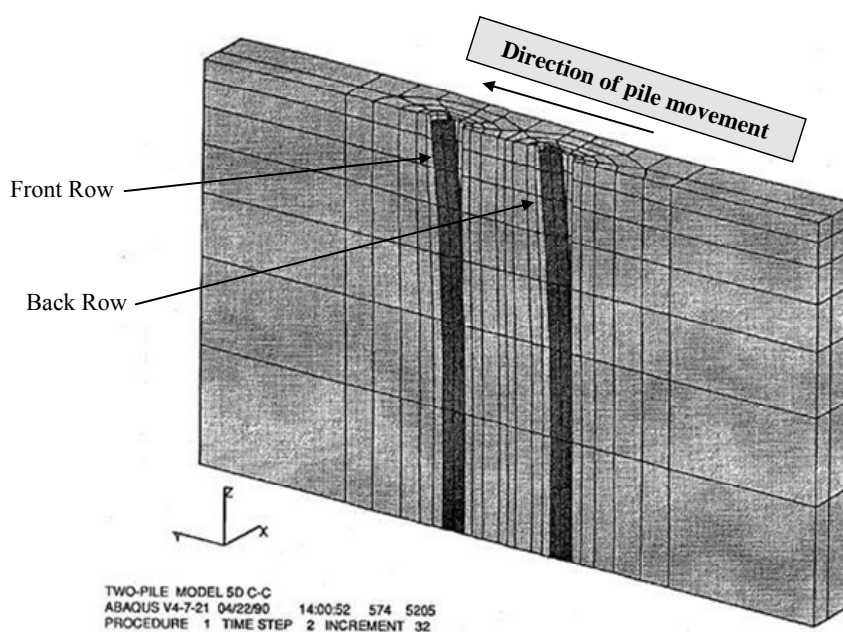


Figure 2.26: View of the three dimensional mesh with piles displaced laterally (taken from Brown and Shie, 1990b)

Brown and Shie (1990b) carried out a series of numerical experiments for an undrained clay and a drained sand, changing the centre-to-centre pile spacing within and between the rows of piles, from which they drew a number of conclusions. They found that the effect of pile spacing within a single row of piles (or the front row of a group) was relatively small for piles spaced at a centre-to-centre distance of three times the diameter of the pile or more in undrained clay soil (Fig. 2.27a). The influence of pile spacing within a single row in sand was somewhat larger, but still relatively small at the same spacing (Fig. 2.27b).

Figure 2.28 shows the  $p$ - $y$  curves for a two row pile group in undrained clay soil. From the figures, it is possible to say that the maximum soil resistance was affected slightly by the pile spacing in the front row piles, while for the piles in the back row a significant reduction was found.

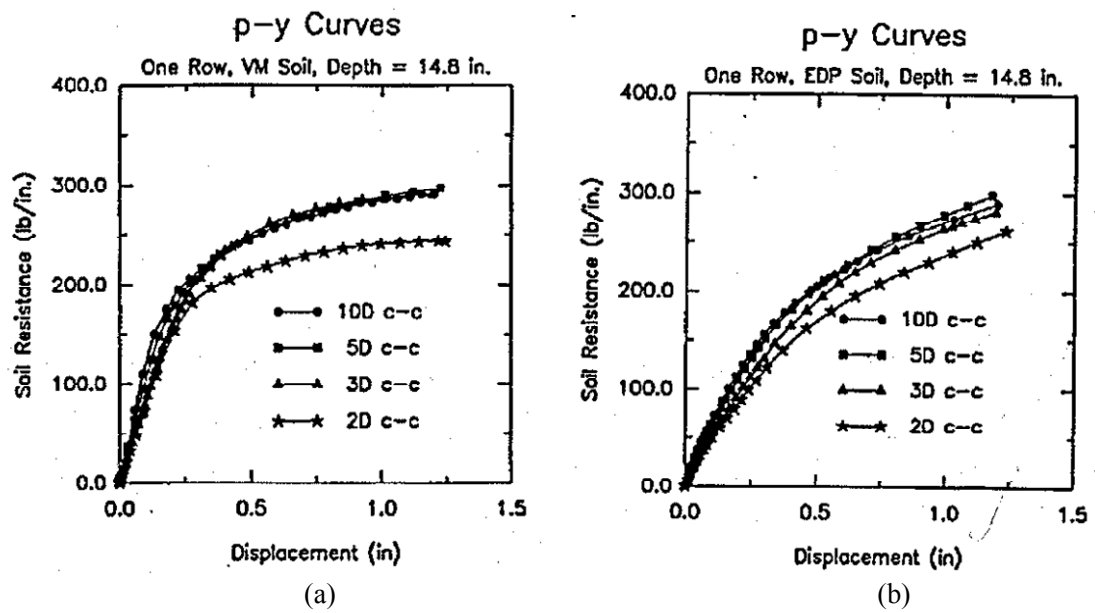


Figure 2.27:  $p$ - $y$  curves of single row of piles spaced at 2D, 3D, 5D and 10D centre to centre (c-c) spacing, where  $D$  is diameter of the pile: (a) undrained clay; (b) drained sand (taken from Brown and Shie, 1990b)

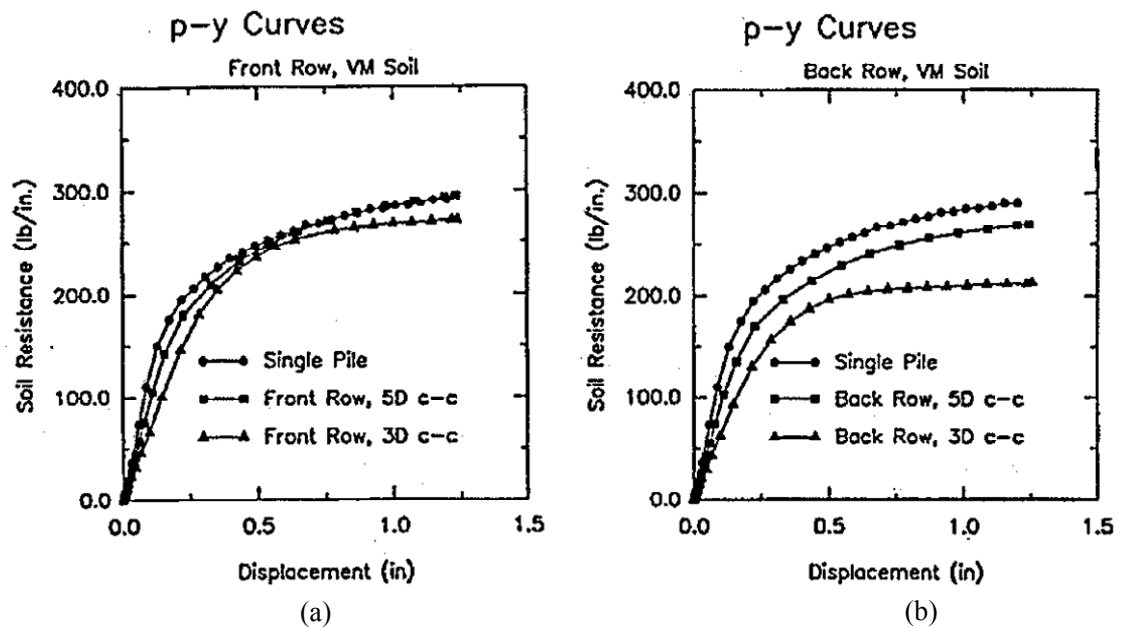


Figure 2.28:  $p$ - $y$  curves for group piles in undrained clay spaced at 3D and 5D centre to centre (c-c) spacing, between the pile rows, where  $D$  is diameter of the pile: (a) front row; (b) back row (taken from Brown and Shie, 1990b)



Based on these results, Brown and Shie concluded the following points:

- 1) The group effects were most influenced by row position, with piles in a trailing row subjected to a significant loss of soil resistance compared to an isolated pile or a single row of piles
- 2) Group effects were significant at a centre-to-centre spacing of three times the pile diameter, and much less at a spacing of five times the diameter of the pile.

Finally, using all these numerical results Brown and Shie (1990b) produced a design guideline. The value of  $P_m$  (Eq. 2.8) gives an indication of the group interaction effect at a certain depth along the pile. From Figure 2.29, it is possible to say that the limiting lateral pile-soil pressure increases in both piles rows (front and back) as the spacing between the piles increases.

$$p_{\text{group pile}} = P_m \times p_{\text{single pile}}$$

Equation 2.8

Where,

$p_{\text{group pile}}$  = soil resistance on a pile in pile group

$p_{\text{single pile}}$  = soil resistance on a single isolated pile

$P_m$  = multiplying factor of soil resistance

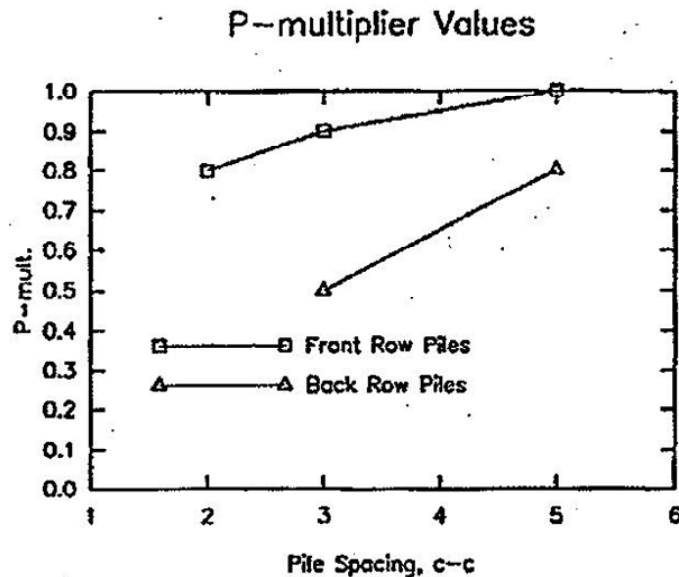


Figure 2.29:  $P_m$  values from numerical experiments (taken from Brown and Shie, 1990b)

## 2.4 Summary

This chapter has reviewed the literature on two areas of laterally loaded piles: potential failure mechanisms of a single isolated pile and group effects due to the pile interaction.

The potential failure modes of a laterally loaded pile depend on many factors such as the shear strength of the soil layers, the depth of the slide plane relative to the pile length and the yield moment of the pile. To be effective, stabilisation piles need to be of sufficiently large diameter and to have a sufficient yield moment (Poulos, 1995).

Assuming the pile has adequate moment capacity, Viggiani (1981) identified three failure modes for a passively loaded pile, based on the embedded length of the pile in the layer beneath the sliding surface. He derived expressions for the maximum shear force and bending moment at the slip surface based on the shearing resistance attained by the pile in each mechanism. Viggiani's solutions are idealised, but enable the potential failure mechanisms of piles subjected to lateral soil movement to be categorised and understood.

A number of studies undertaken subsequently to investigate interaction effects in pile group arrangements, especially for clay soil in undrained conditions were reviewed. Researchers have found both experimentally and numerically that when the piles are grouped, they experience a different ultimate lateral pile-soil pressure ( $p_u$ ) than when isolated.

In a single pile row in undrained conditions, Chen and Poulos (1993) and Brown and Shie (1990b) showed that  $p_u$  increases with the increasing pile spacing. However, Chen and Martin (2002) reported that  $p_u$  decreased while the spacing between the piles increased, which is counter-intuitive and contradictory to the other studies. Further investigations are needed to understand this behaviour. When two pile rows (actively loaded) were investigated, the results obtained from the field tests (Rollins *et al.*, 1998) and the 3D numerical analysis (Brown and Shie, 1990b) showed that the front row of piles developed higher  $p_u$  than the rear rows for any  $S_v$  values. However, the 2D numerical analysis carried out by Chen and Poulos (1993) showed that for  $S_v/w = 3$ , the back row of piles developed higher  $p_u$  than the front rows, and for  $S_v/w = 6$ , the front row of piles developed higher  $p_u$  than the back rows. Further investigations are also needed to clearly understand the behaviour of two pile rows.

Comprehensive  $FLAC^{3D}$  analyses will be carried out in Chapters 3-5,

- to gain an improved understanding of the potential failure mechanisms and behaviour of single isolated pile based on Viggiani (1981)

- to gain an improved understanding of the pile-soil interaction mechanism when piles are grouped, and
- to reconcile some of the discrepancies revealed by the review of earlier literature, and fill some of the gaps in the knowledge.

## Chapter - 3: Potential Failure Mechanisms of Single Laterally Loaded Pile

### 3.1 Introduction

This chapter includes a comprehensive numerical study of the potential failure mechanisms of laterally loaded isolated piles, based on the work of Viggiani (1981), as presented in Section 2.2.2. The main aim of the analyses presented in this chapter is to show how numerical modelling can be used to explore and verify the failure mechanisms categorised by Viggiani. Many analyses were carried out, prior to the main analyses, for validation purposes (for example, a numerical investigation into the accuracy of the pile and interface elements) to ensure reliable results. These analyses are described in Sections 3.5 to 3.7.

Fan and Long (2005) classified methods for the analysis of laterally loaded single piles into five categories: (1) limit equilibrium (Broms, 1964); (2) subgrade reaction (Matlock and Reese, 1960); (3)  $p$ - $y$  (Reese *et al.*, 1974); (4) elasticity (Banerjee and Davis, 1978); and (5) finite element or difference (Chen and Poulos, 1993; Ellis *et al.*, 2010). Although the increased complexity of finite element and finite difference methods means they are less widely used than the others for routine analyses, they can model the pile-soil interaction more rigorously and include effects such as vertical movement at the pile-soil interface, non-linear soil stiffness, sloping ground surfaces, and interaction between adjacent piles.

Two dimensional (2D) plane-strain finite element or difference analyses have been used to investigate the behaviour of passively loaded piles (Bransby and Springman, 1999; Chen and Martin, 2002), and can be carried out in either the horizontal or vertical plane. However, relative vertical soil and pile displacements including surface ground heave, pile flexibility and pile head conditions are not taken into account in the former, while soil flow around the pile and pile spacing effects cannot be modelled in the latter. To model the full pile-soil interaction mechanism, a three dimensional (3D) analysis is necessary.

In this study, three dimensional finite difference analyses were carried out to investigate the response of piles subjected to lateral soil movements, using the finite difference computer code *FLAC<sup>3D</sup>* (Fast Lagrangian Analysis of Continua in 3 Dimensions, Version 3.1, Manual [2006]).

### 3.2 *FLAC*<sup>3D</sup> computer code

*FLAC*<sup>3D</sup> is a commercial geotechnical finite difference programme. It uses an explicit Lagrangian calculation scheme and the mixed-discretization zoning technique (Itasca, 2006) to ensure that plastic failure and flow, as well as elastic behaviour, are modelled accurately.

The calculation scheme used by *FLAC*<sup>3D</sup> takes a large number of calculation steps, each progressively redistributing an unbalanced force caused by changes to stress or displacement boundaries through the mesh (Itasca, 2006). The unbalanced force is the algebraic sum of the net nodal-force vectors for all of the nodes within the mesh. The model is considered to be in equilibrium when the maximum unbalanced force is small compared with the total applied forces within the problem. If the unbalanced force approaches a constant non-zero value, this normally indicates that failure and plastic flow are occurring within the model. By default the model is assumed to be in equilibrium when the maximum unbalanced force ratio (i.e. the ratio between the magnitude of the maximum unbalanced force and the magnitude of the average applied mechanical force within the mesh) falls below  $1 \times 10^{-5}$  (Itasca, 2006).

There are several reasons why *FLAC*<sup>3D</sup> was selected for the analyses. One of the main aims of the numerical study was to model situations in which physical instability or plastic flow may occur. As mentioned earlier, *FLAC*<sup>3D</sup> is suitable for simulating this type of problem.

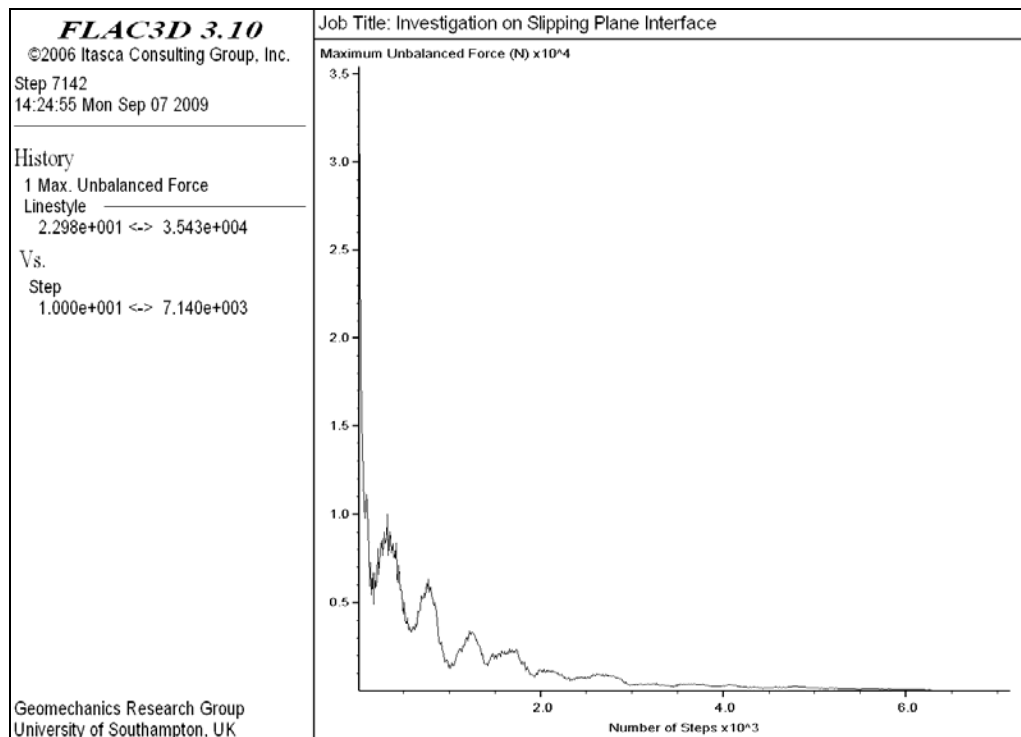


Figure 3.1: View of the *FLAC*<sup>3D</sup> history plot of the maximum unbalanced force

By default,  $FLAC^{3D}$  operates in small-strain mode; that is, nodal coordinates are not changed even if the computed displacements are large compared with the typical element size. In large-strain mode, nodal coordinates are updated at each step according to computed displacements. In large-strain mode, geometric nonlinearity is possible.

The intrinsic *FISH* language is one of the most useful features in  $FLAC^{3D}$ . *FISH* can be used to include conditional ‘*if*’ statements and loops for repetitive tasks within a programme and to carry out mathematical operations, define new variables or functions, and extract stresses and displacements from the analysis.

### 3.3 Numerical approach for failure mechanisms

As explained earlier, the failure modes defined by Viggiani (1981) for a single pile depend on the depth of the failure surface ( $H$ ) relative to the pile length ( $L$ ). Three different geometries of  $FLAC^{3D}$  meshes were created each with a different depth of failure surface, but with the same pile geometry. In each case a wide soil block underlay a narrower upper soil block, representing stable and unstable soil layers, respectively. The  $FLAC^{3D}$  analysis procedures including mesh creation, pile installation, boundary and fixity conditions, constitutive models and properties, gravity loading and lateral load application concept are explained in Section 3.8.

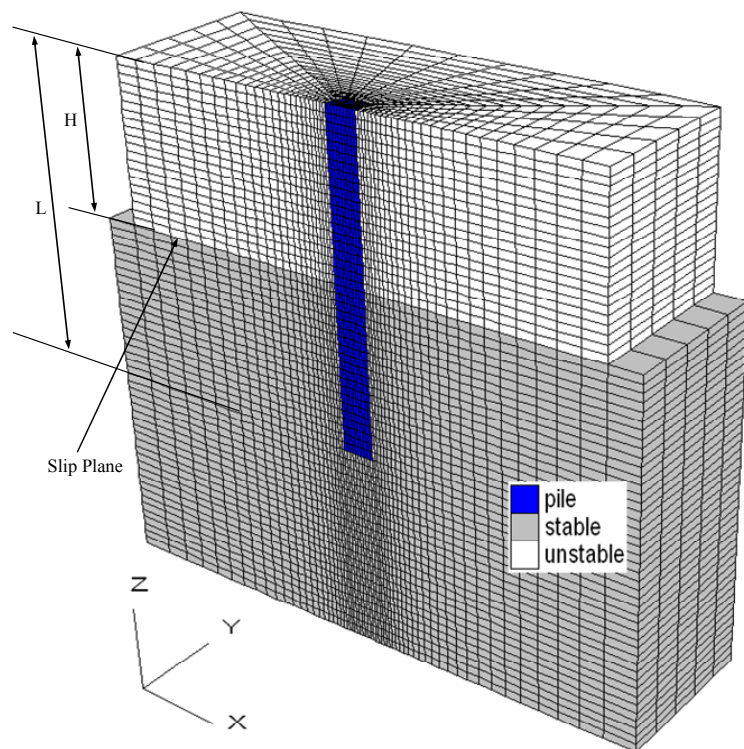


Figure 3.2: Geometry of the  $FLAC^{3D}$  model to represent Viggiani's approach

### 3.4 Routines used to calculate parameters

The intrinsic *FISH* language was used to develop routines to calculate the required parameters directly. The deflection, shear force, bending moment and the lateral pile-soil pressure were the parameters to be calculated in the analyses. The routines used to calculate these parameters are described below.

#### 3.4.1 Deflection

When a pile is laterally loaded, the nodes move along the direction of applied load in large-strain mode (Fig. 3.3b). Therefore, it is not possible to identify a particular node after loading using its original coordinate. To calculate the displacement of the pile, first the coordinates of all the nodes of the vertical pile axis were stored in the memory of the computer. Once the model reached equilibrium, the same nodes were identified and their displacements calculated by subtracting their initial and final  $x$ -coordinate position, where  $x$  is the direction of loading (Fig. 3.3).

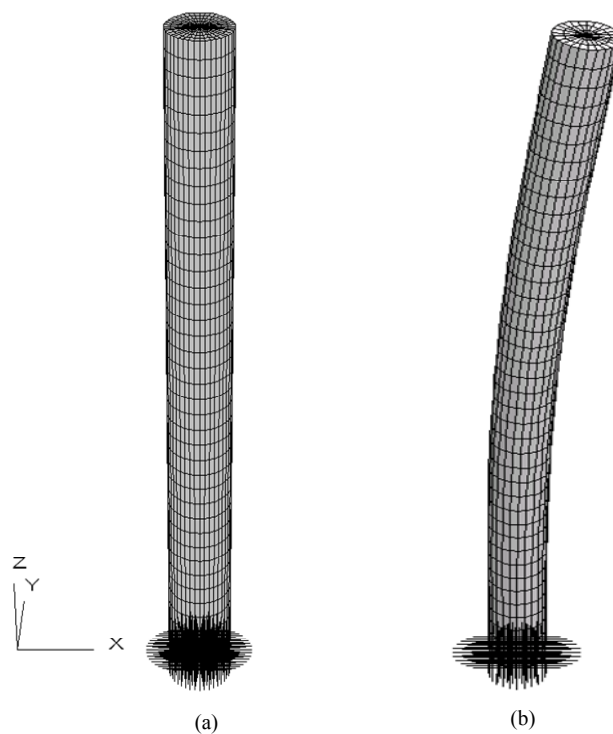


Figure 3.3: *FLAC<sup>3D</sup> pile model: a) pile, before lateral loading; b) pile, after lateral loading*

### 3.4.2 Shear force

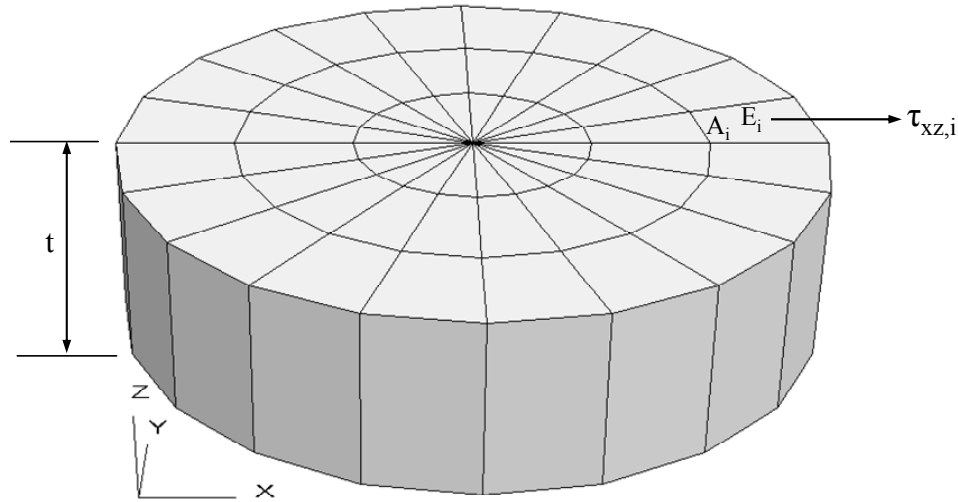


Figure 3.4: A section showing stress in x-direction in an element

The shear force ( $T$ ) in each horizontal pile section was calculated by multiplying the  $x$ -direction horizontal shear stress of each element by its plan surface area. The plan area of each element was calculated by dividing its volume by its thickness in the  $z$ -direction, as it is not possible in  $FLAC^{3D}$  to calculate surface area directly.

Mathematically,

$$T = \sum_{i=1}^n \tau_{xz,i} \times A_i \quad \text{Equation 3.1}$$

Where,

- $T$  = shear force in each horizontal pile section
- $\tau_{xz,i}$  = horizontal shear stress ( $sxz$ ) in element  $E_i$
- $A_i$  = plan area of element  $E_i$
- $n$  = total number of elements in a horizontal pile section



### 3.4.3 Bending moment

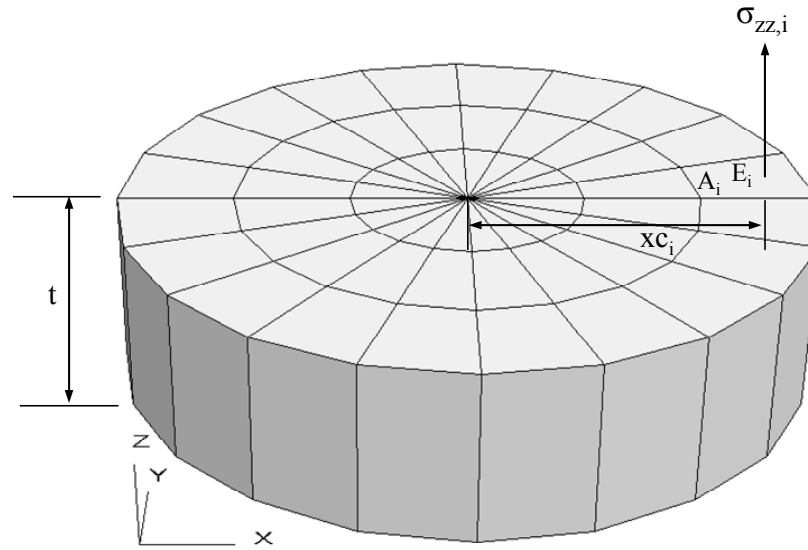


Figure 3.5: A section showing stress in z-direction in an element

The bending moment ( $M$ ) developed in each pile section was obtained by summation of the product of the vertical stress at each element, the plan area of that element and the  $x$ -distance from the centre of the pile to the centroid of the element.

$$M = \sum_{i=1}^n \sigma_{zz,i} \times A_i \times xc_i \quad \text{Equation 3.2}$$

Where,

- $M$  = bending moment in each horizontal pile section
- $\sigma_{zz,i}$  = vertical normal stress ( $s_{zz}$ ) in element  $E_i$
- $A_i$  = plan area of element  $E_i$
- $xc_i$  = centroid distance of element  $E_i$  from the centre of the pile, in  $x$ -direction
- $n$  = total number of elements in a horizontal pile section

### 3.4.4 Lateral pile-soil pressure (expressed in unit of N/m)

The lateral pile-soil pressure (i.e. the force acting on the pile per unit length along the axis,  $p$ ) on each pile section was computed by summing the forces in the  $x$ -direction acting on the interface nodes at the same level. Each interface node is associated with a normal force and a shear force.  $FLAC^{3D}$  does not allow users to determine either of these directly; they were therefore calculated by multiplying the interface node stresses by the representative area of the interface, which is indicated in Figure 3.7. A plan view of the pile-soil system, showing the interface elements, is given in Figure 3.8.

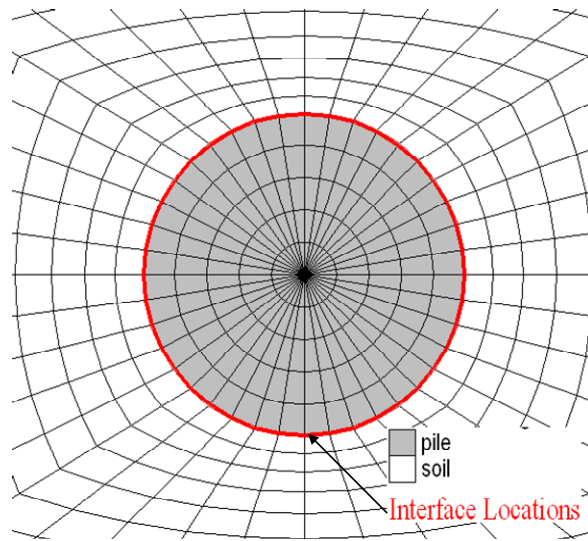


Figure 3.6: Plan view of  $FLAC^{3D}$  mesh showing location of interface elements in between the pile and the soil

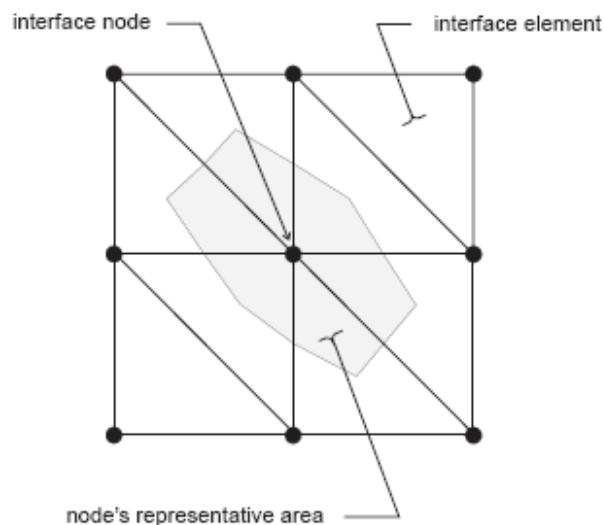


Figure 3.7: Representative area of an interface node (Itasca, 2006)

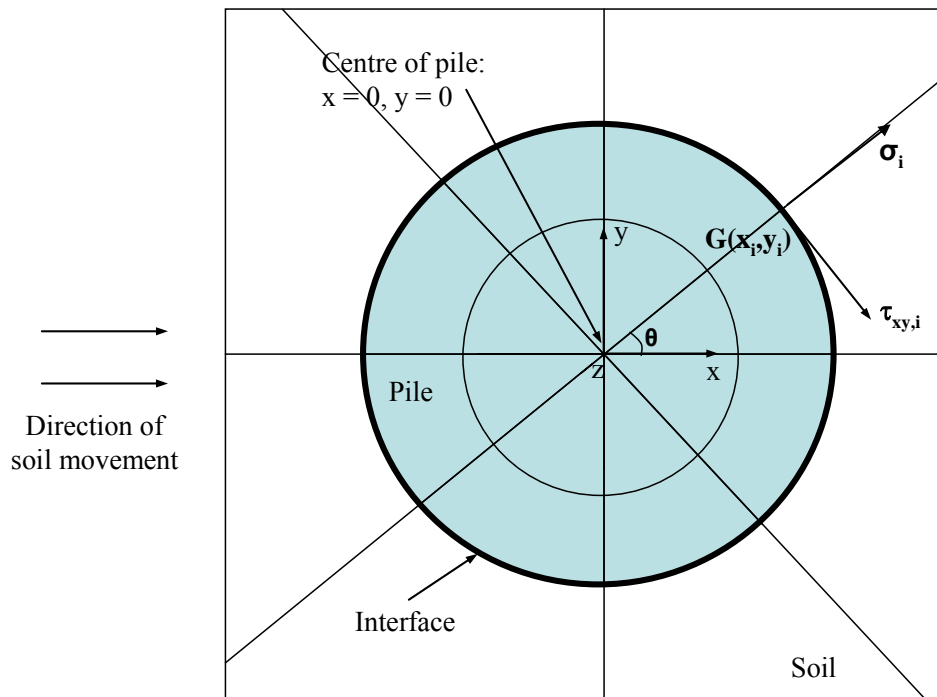


Figure 3.8: Typical pile-soil system with interface elements between them

The  $x$ -component ( $p_{x,i}$ ) of the lateral pile-soil pressure at point  $G$  can be represented as follows:

$$p_{x,i} = (\sigma_i n_{x,i} + \tau_{xy,i} n_{y,i}) \times A_i \quad \text{Equation 3.3}$$

Where,

$$n_{x,i} = \cos \theta = \frac{x_i}{\sqrt{x_i^2 + y_i^2}}$$

$$n_{y,i} = \sin \theta = \frac{y_i}{\sqrt{x_i^2 + y_i^2}}$$

$\sigma_i$  = normal stress at the interface node at point  $G$

$\tau_{xy,i}$  = shear stress at the interface node at point  $G$

$x_i$  =  $x$ -coordinate of the interface node at point  $G$

$y_i$  =  $y$ -coordinate of the interface node at point  $G$

$A_i$  = representative area of interface node (see Fig. 3.7)

The  $x$ -component of the lateral pile-soil pressure is summed over all the interface nodes to calculate the lateral pile-soil pressure ( $p$ ) per unit length along the pile at a particular pile section and is expressed as:

$$p = \sum_{i=1}^n ((\sigma_i n_{x,i} + \tau_{xy,i} n_{y,i}) \times A_i) \quad \text{Equation 3.4}$$

Where,

$n$  = total number of interface nodes in a pile section at a certain depth

### 3.5 Investigation of the numerical accuracy of the piles

The number of elements used to model the pile in the vertical direction can make a substantial difference to its apparent bending behaviour (Ellis *et al.*, 2010). The stresses within each element are uniform in  $FLAC^{3D}$ ; therefore finer meshes tend to give more accurate results as they provide a better representation of high stress gradients (Itasca, 2006). A series of numerical analyses was carried out to understand how the numerical accuracy of the results (deflection, shear force and bending moment) varies with the number of pile elements. In all of the analyses, the pile was modelled using a semi-circular arrangement of brick elements (Fig. 3.9b) with 100 elements in the plan section. More attention was paid to the variation of the number of elements in the vertical direction than in the plan section.

#### 3.5.1 $FLAC^{3D}$ analysis

A cylindrical pile of diameter  $d = 1$  m was modelled using brick elements arranged into a cylindrical shaped mesh. The pile was assumed to be linear elastic. Poulos (1995) proposed a pile flexibility factor  $K_R$  (Eq. 3.5), and the Young's modulus of the pile ( $E_p$ ) was calculated using Equation 3.6, by assuming  $K_R = 0.1$  corresponding to a rigid pile. The Poisson's ratio and density of the pile were assumed to be 0.3 and 2500 kg/m<sup>3</sup>, respectively. Only one half of a pile was modelled, assuming and exploiting symmetry about the  $x$ - $z$  plane (Fig. 3.9b). The pile was fixed at the base and subjected to a constant distributed load ( $w$ ) in the  $x$ -direction perpendicular to the vertical pile axis.

$$K_R = \frac{E_p I_p}{E_s L^4} \quad \text{Equation 3.5}$$

$$E_p = \frac{0.1 \times E_s L^4}{I_p} \quad \text{Equation 3.6}$$

Where,

$E_p$  = Young's modulus of the pile

$I_p$  = second moment of area of the pile

$E_s$  = Young's modulus of soil

$K_R$  = pile flexibility factor

$L$  = pile length

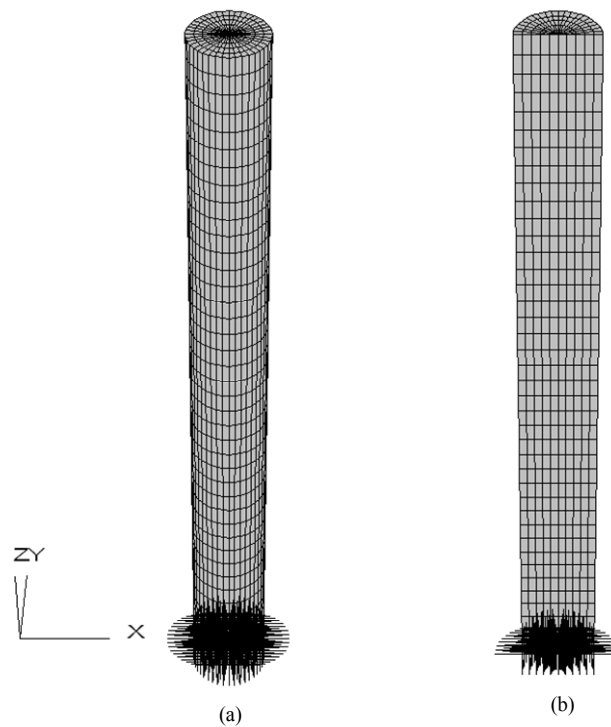


Figure 3.9: Grid model of piles: a) full pile model; b) half pile model used in the analyses

The bulk modulus ( $K$ ) and shear modulus ( $G$ ), rather than Young's modulus ( $E$ ) and Poisson's ratio ( $\nu$ ), are recommended as input parameters in *FLAC<sup>3D</sup>* (Itasca, 2006); the equivalent bulk modulus and shear modulus were calculated using Equations 3.7 and 3.8 respectively. The following analyses were carried out in large strain mode until the maximum unbalanced force ratio fell below  $1 \times 10^{-6}$ .

$$K = \frac{E}{3(1 - 2\nu)} \quad \text{Equation 3.7}$$

$$G = \frac{E}{2(1 + \nu)} \quad \text{Equation 3.8}$$

Table 3.1 summarises the pile properties.

Length (m)	10
Diameter (m)	1.0
Young's Modulus (GPa)	122.2
Poisson's Ratio	0.30
Bulk Modulus (GPa)	101.8
Shear Modulus (GPa)	47.0
Density (kg/m <sup>3</sup> )	2500

*Table 3.1: Properties of the pile*

### 3.5.2 Results and discussion

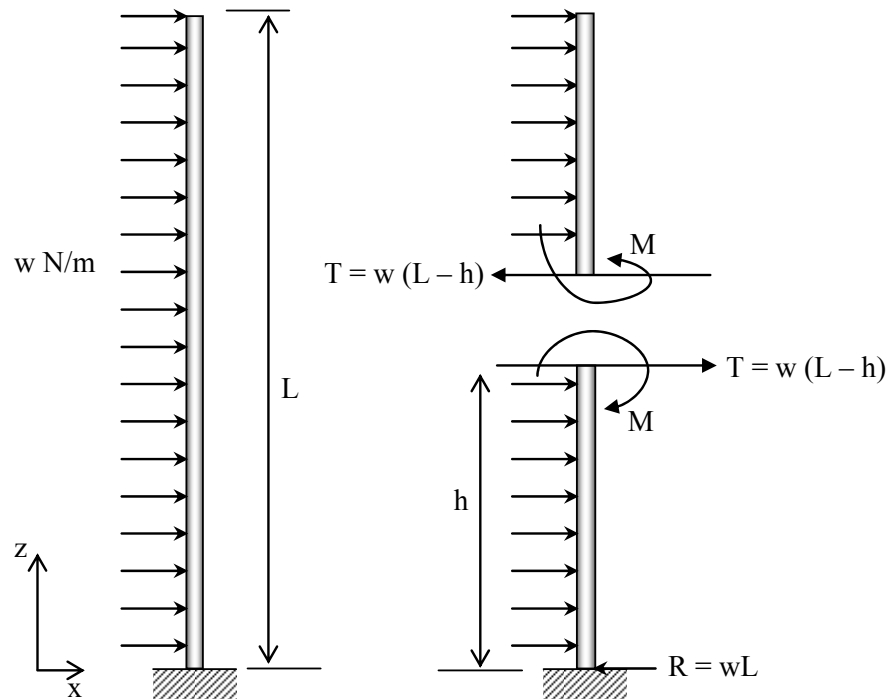


Figure 3.10: Schematic diagram of a laterally loaded pile, denoting variables

Equation 3.9 is the general formula used to calculate the deflection of a pile due to a constant distributed load (Nash, 1972).

$$E_p I x = \frac{w}{24} (L - z)^4 + \frac{w z L^3}{6} - \frac{w L^4}{24} \quad \text{Equation 3.9}$$

Where,

$E_p$  = Young's modulus of the pile

$I$  = second moment of inertia =  $\frac{1}{4} \pi r^4$  for a circular section

$r$  = radius of pile

$x$  = lateral deflection

$z$  = distance of the pile section from the cantilever end

$w$  = constant distributed load per unit length

$L$  = length of pile

The magnitude of the constant distributed load required to give a 20 mm lateral displacement of the pile top was calculated using elastic theory as 48 kN/m (Eq. 3.10).

The maximum deflection ( $x_{\max}$ ) will occur when  $z = L$ .

$$E_p I x_{\max} = 0 + \frac{wL^4}{6} - \frac{wL^4}{24}$$

$$E_p I x_{\max} = \frac{wL^4}{8}$$

$$w = \frac{8E_p I x_{\max}}{L^4}$$

Equation 3.10

The effect on computed pile behaviour of increasing the number of tiers of elements in the vertical direction from 10 to 20, 40, 80 and 100 was examined (Figs. 3.11-3.13). The calculated behaviour is significantly influenced by the number of elements used to model the pile in the vertical direction.

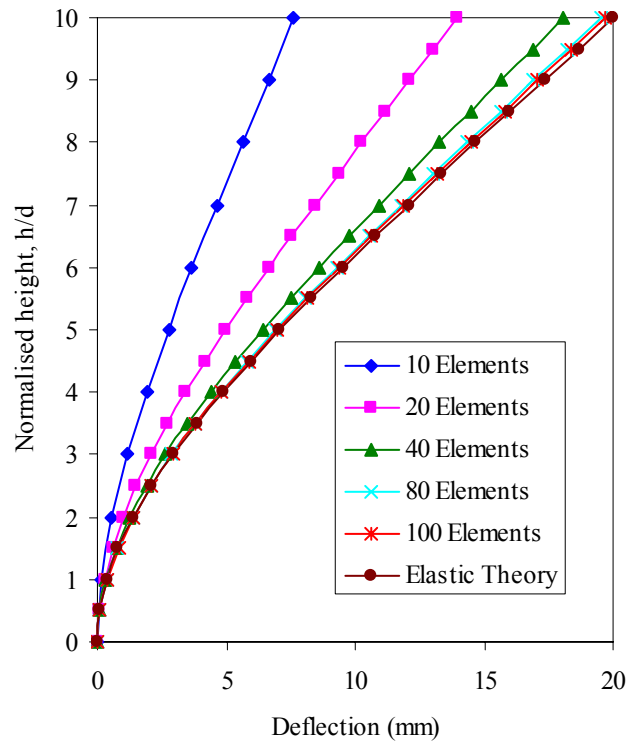


Figure 3.11: Variation of deflection with number of vertical elements



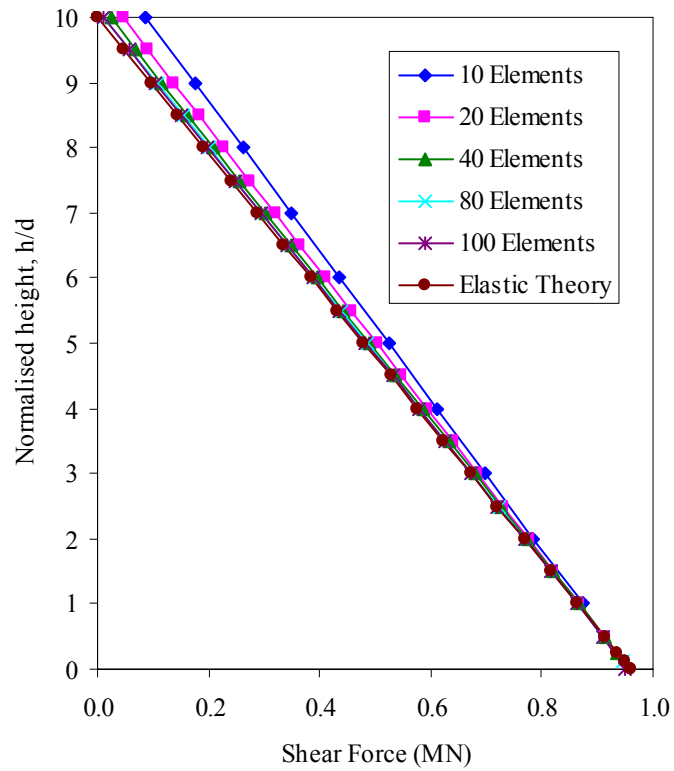


Figure 3.12: Variation of shear force with number of vertical elements

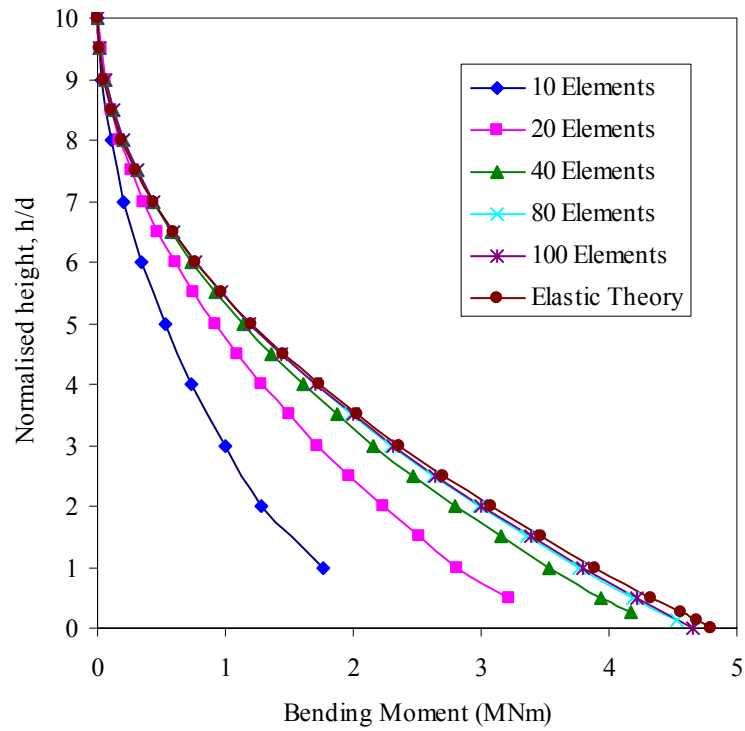


Figure 3.13: Variation of bending moment with number of vertical elements

Table 3.2 shows the percentage errors in deflection, shear force and bending moment for each number of vertical elements. Based on the results, the following key points are observed:

- 1) The model with 100 tiers of elements gave a close match to elastic theory, with errors of 1.44%, 1.15% and 2.93% in the maximum deflection, shear force and bending moment respectively. These values include errors inherent within the *FLAC<sup>3D</sup>* code, such as round-off errors (Itasca, 2006).
- 2) The model with 40 tiers of elements model reached the target maximum unbalanced force ratio limit of  $1.0 \times 10^{-6}$  in 263,092 *FLAC<sup>3D</sup>* calculation steps, taking 1 hour 20 minutes while the model with 100 tiers of elements needed a further 18,645 steps to reach the same ratio, taking 3 hours 31 minutes.

Error % Elements	Deflection	Shear Force	Bending Moment	Total Number of Elements used to Model the Pile	Required Number of Steps to Reach Equilibrium
10	61.82	9.10	54.67	1,000	223,146
20	30.10	4.85	25.54	2,000	258,084
40	9.61	2.53	8.58	4,000	264,053
80	2.36	1.37	3.11	8,000	277,688
100	1.44	1.15	2.93	10,000	280,667

*Table 3.2: Error percentages in variables and the required steps*

As would be expected, the discrepancy between the numerical analysis and the closed form elastic solution reduced as the number of element layers was increased. However, this was at the expense of a substantially increased computational time (e.g. 263,092 steps / 80 minutes for the 40 layer model, compared with 281,737 steps / 211 minutes for the 100 layer model). The 40 layer model was considered to represent a reasonable compromise between accuracy and speed of analysis, and was used for the remainder of the analyses reported in this thesis.

### 3.6 Investigation of the numerical accuracy of the interface elements

It is necessary to use interface elements to allow relative movements between the soil and the pile, and between moving and stable soil layers. Interface elements are used in three places in this numerical problem; between the unstable and stable soil layers to represent a sliding surface, between the pile wall and the soil, and between the pile tip and the soil.

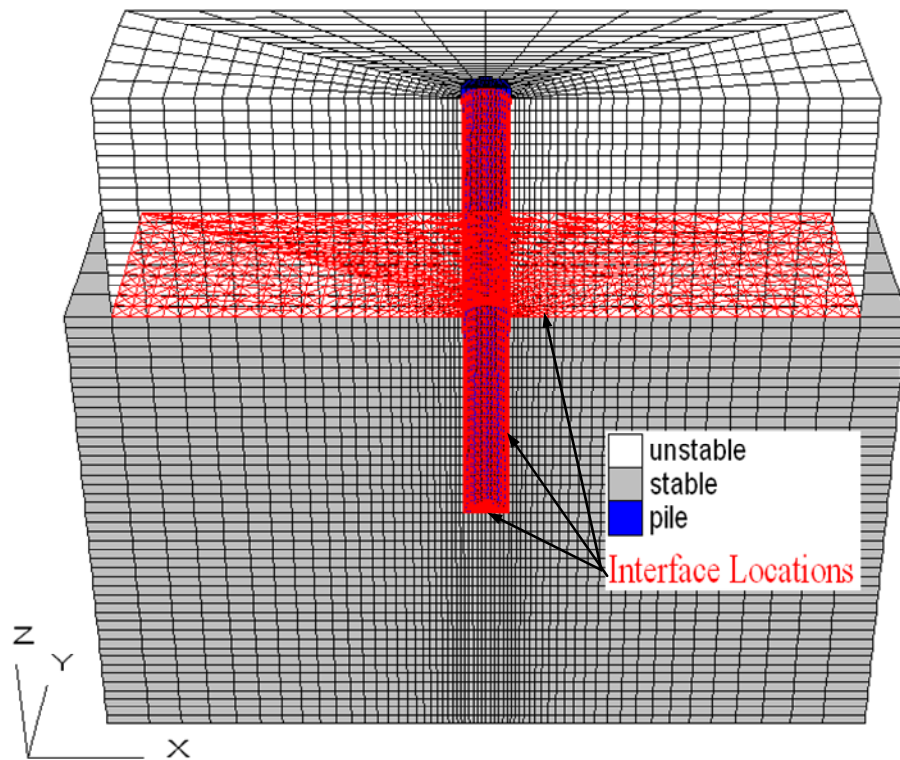


Figure 3.14: Location of interface elements in the model

The interface properties play an important role in a pile-soil model, governing whether slip or the opening of a gap between the pile and the soil may occur, both of which are possibilities in an undrained analysis. *FLAC<sup>3D</sup>* interface elements have properties of friction, cohesion, dilation, normal and shear stiffness, and tensile strength. Itasca (2006) recommends the use of normal and shear stiffnesses ten times those of the stiffest neighbouring element.

The apparent stiffness (expressed in units of stress-per-unit length) of an element (or zone) in the normal direction ( $k_n$ ) is

$$k_n = 10 \times \max \left[ \frac{\left( K + \frac{4}{3} G \right)}{\Delta Z_{\min}} \right] \quad \text{Equation 3.11}$$

Where,

$K$  = bulk modulus of the stiffest neighbouring element

$G$  = shear modulus of the stiffest neighbouring element

$\Delta Z_{\min}$  = smallest dimension of an adjoining element in the normal direction (see Fig. 3.15)

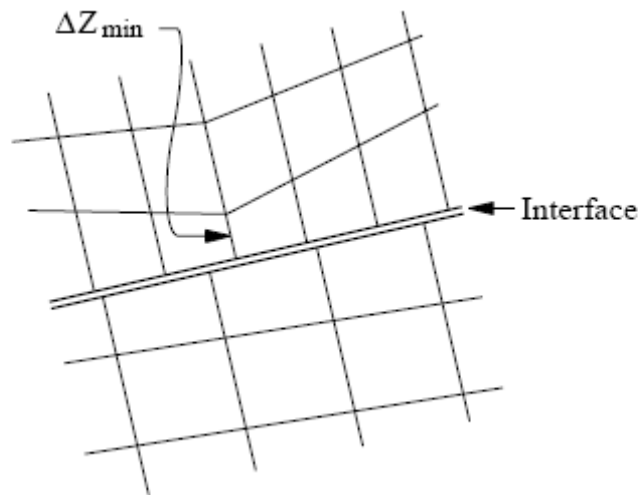


Figure 3.15: Element dimension used in stiffness calculation (taken from Itasca, 2006)

However, Itasca (2006) does not explain how to choose other properties (e.g. cohesion) for an interface. The friction angle ( $\phi'$ ) of the interface elements was assumed to be zero, as the analyses presented in this chapter model only undrained conditions. The analyses presented in Sections 3.6.1 and 3.6.2 were carried out to choose a suitable cohesive strength for the interface elements (slip plane interface and pile-soil interface) to reproduce Viggiani's analyses.

### 3.6.1 Behaviour of the interface representing a defined slip plane (First stage: No pile)

Viggiani (1981) categorised different failure mechanisms for an isolated pile in a two layer soil system in which the overlying unstable soil layer has the capability to slide over an underlying stable soil layer along a well-defined slip plane. The following analyses were carried out to determine an interface cohesive strength ( $c_{int}$ ) representative of a well defined slip plane.

#### 3.6.1.1 Grid generation

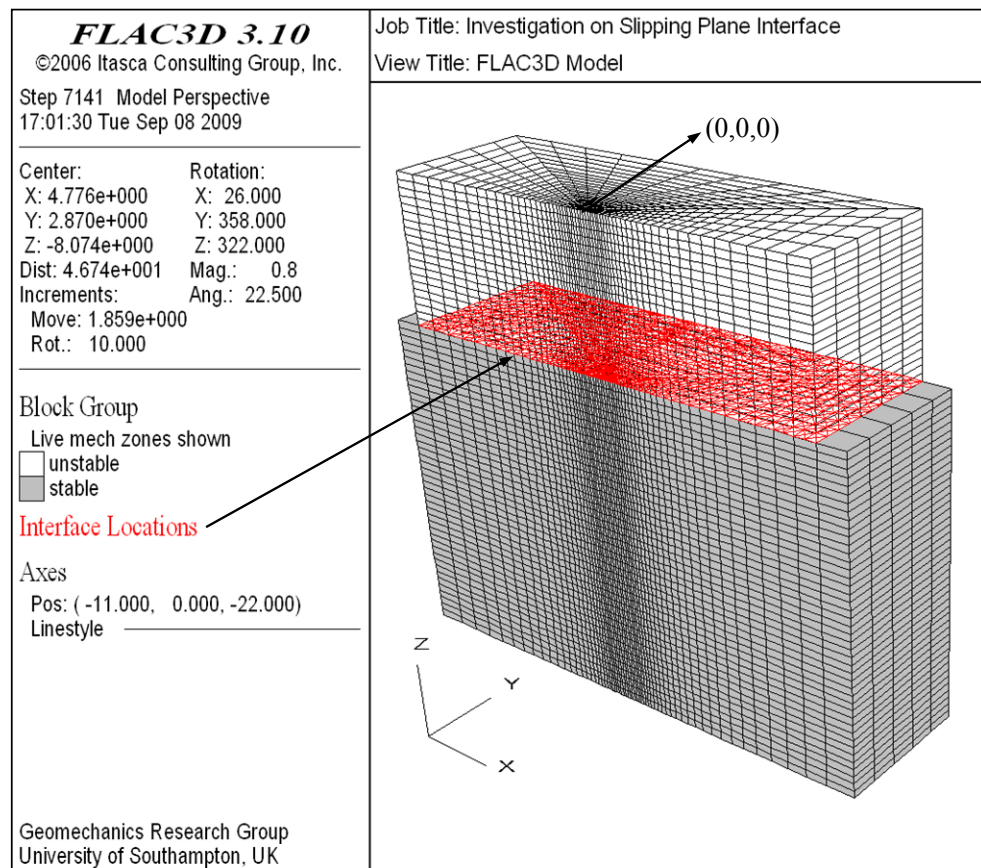


Figure 3.16:  $FLAC^{3D}$  model used to analyse the behaviour of a defined slip plane

A 16 m long  $\times$  5 m wide  $\times$  5 m high mesh representing the unstable soil layer was first created. Then, an 18 m long  $\times$  5 m wide  $\times$  11 m high soil block was modelled below the upper block with a 1 m gap between them. This 1 m gap was specified, because Itasca (2006) recommends that there should be a gap between the planes so that the interface elements can be installed before the planes are brought into contact. The interface elements were created and attached to the bottom face of the upper soil block. This is because here also, Itasca (2006) recommends that interface elements are attached to the block having the smaller surface area.

After the creation of the interface elements, the lower block was lifted up by 1 m to complete the initial geometry. Using the symmetry of the geometry and the loading, the mesh was simplified by modelling just half the pile (reflected about the  $y = 0$  plane). Figure 3.16 shows the  $FLAC^{3D}$  mesh used for the analyses.

### 3.6.1.2 Boundary conditions

The nodes on the bottom face of the soil were restrained in all three directions while the nodes on the top face were free to move. The nodes on the symmetrical faces were prevented from moving in the  $y$ -direction, but were free to move in the  $x$  and  $z$ -directions. The nodes at the right and left faces were restrained from moving in the direction of the applied soil movements (i.e. the  $x$ -direction) during gravity loading, and the nodes at the upper soil layer only were then freed to move during lateral loading.

### 3.6.1.3 Constitutive models and material properties

An elastic-Mohr-Coulomb plastic model was assumed for both soils. The unstable and stable soil layers were assumed to be uniform with undrained shear strengths ( $c_u$ ) of 30 kPa and 60 kPa respectively, and Poisson's ratio = 0.495. A gravitational acceleration vector ( $g$ ) of  $10 \text{ ms}^{-2}$  was applied in the negative  $z$ -direction. To develop a gravitational body force, a mass density of  $1800 \text{ kgm}^{-3}$  was used for all soil elements in the model. Stresses within the model were initialised assuming the earth pressure coefficient at rest ( $K_0$ ) equal to one.

For clay soils, Young's modulus  $E_s$  may be related to the undrained shear strength ( $c_u$ ) as follows (Banerjee and Davies, 1978; Poulos and Davis, 1980; Chow, 1996; Miao *et al.*, 2006):

$$E_s = A c_u \quad \text{Equation 3.12}$$

where the value of  $A$  typically lies between 150 and 400. It was set at 200 in all the analyses. Equations 3.7 and 3.8 were then used to calculate the corresponding bulk modulus and shear modulus respectively for both the soil layers. The normal and shear stiffnesses of the interface elements were determined using Equation 3.11. Table 3.3 shows the material properties used in the analyses.

<i>Material Properties</i>	<i>Unstable Soil</i>	<i>Stable Soil</i>
Density (kg/m <sup>3</sup> )	1800	1800
Strength Properties:		
Cohesion (kPa)	30	60
Friction	0	0
Elastic Properties:		
Young's modulus (MPa)	6	12
Poisson's ratio	0.495	0.495
Bulk modulus (MPa)	200	400
Shear modulus (MPa)	2.007	4.013

Table 3.3: Material properties for unstable and stable soils

#### 3.6.1.4 *FLAC*<sup>3D</sup> analysis

The model was first brought to an equilibrium stress state under gravitational loading. The vertical stress distribution at the equilibrium state is shown in Figure 3.17. Then, the coordinates of all nodes located at  $(x,y) = (0,0)$  and parallel to the  $z$ -direction were stored in array format in the computer's memory. These coordinates were later used to monitor the displacement of the upper soil layer.

After the model had reached initial equilibrium, the nodes at the left and the right faces of upper soil block only were freed to move in the  $x$ -direction (i.e. from left to right) and a uniform horizontal soil movement from the left to the right was imposed incrementally on all the nodes. In *FLAC*<sup>3D</sup>, a given displacement at a boundary ( $D$ ) is created by applying a certain velocity ( $V$ ) to boundary grid points over a given number of steps ( $N$ ).

$$N = \frac{D}{V} \quad \text{Equation 3.13}$$

In the analyses, a velocity of  $4 \times 10^{-6}$  m/step in the  $x$ -direction was applied over 62,500 steps to displace the boundaries by 250 mm. This velocity was selected to ensure that the maximum unbalanced force in the mesh generated by the boundary movement remained small compared with the general magnitude of forces in the problem.

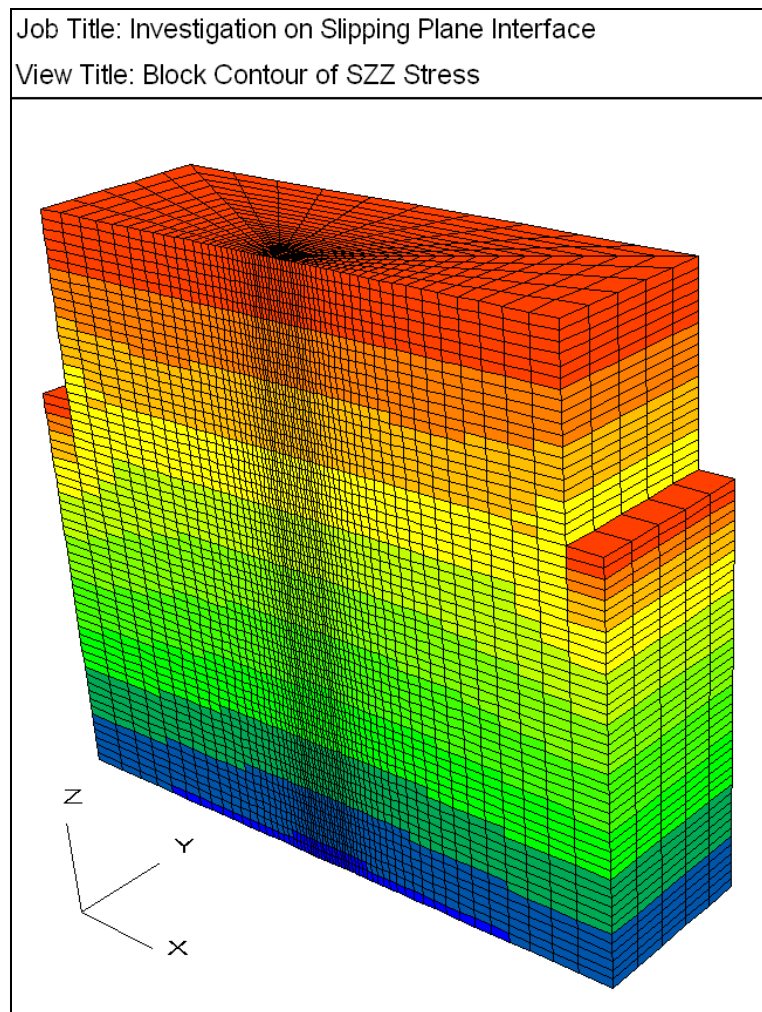


Figure 3.17:  $FLAC^{3D}$  mesh showing equilibrium of vertical stress after gravitational loading

Three different cases were selected by changing the cohesion of the interface elements as follows:

Case 1:  $c_{int}/c_u = 0$  (zero strength, where  $c_u = 30$  kPa)

Case 2:  $c_{int}/c_u = 0.5$  (half strength)

Case 3:  $c_{int}/c_u = 1$  (full strength)



### 3.6.1.5 Results and discussion

Figures 3.18 and 3.19 show the deformed mesh after 250 mm of lateral displacement for Case 1 and Case 3 respectively.

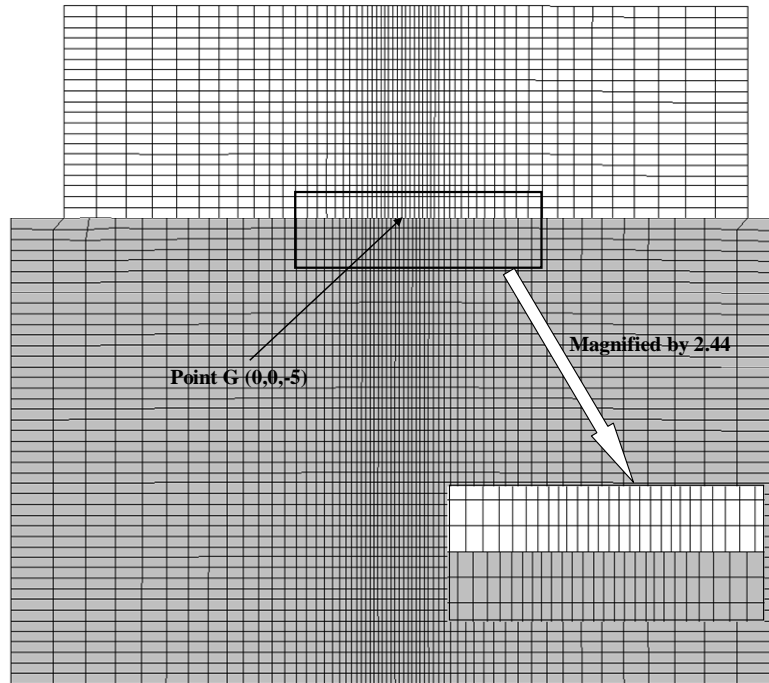


Figure 3.18: Deformed mesh of Case 1:  $c_{int}/c_u = 0$

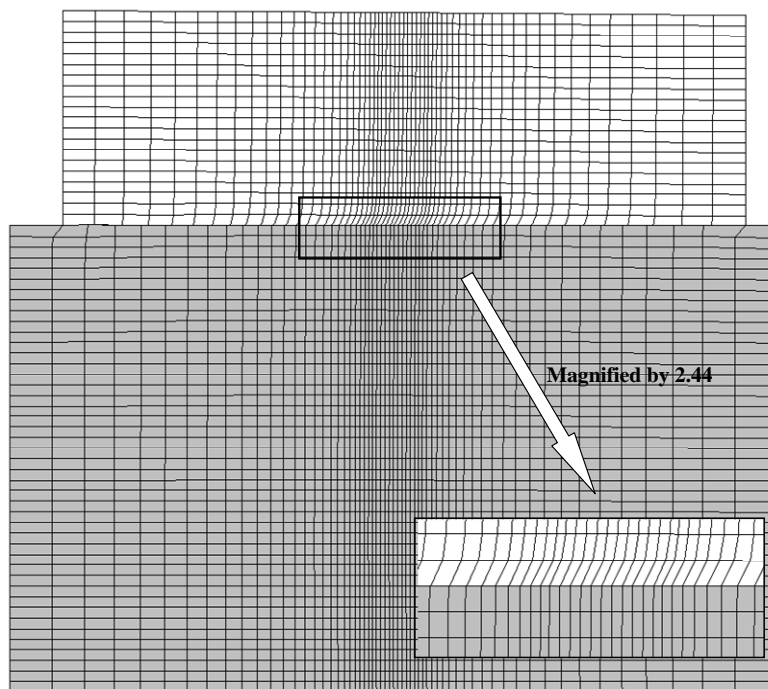


Figure 3.19: Deformed mesh of Case 3:  $c_{int}/c_u = 1$

Figure 3.18 (for the case of zero cohesion) shows that the unstable upper soil layer has slipped perfectly over the stable layer. The lateral movement of grid point *G* was monitored using a *FLAC*<sup>3D</sup> history plot, and is shown in Figure 3.20. The point *G* did not initially move uniformly with applied boundary soil displacement. However, a uniform displacement was observed with further boundary soil displacement, approximately after 60 mm.

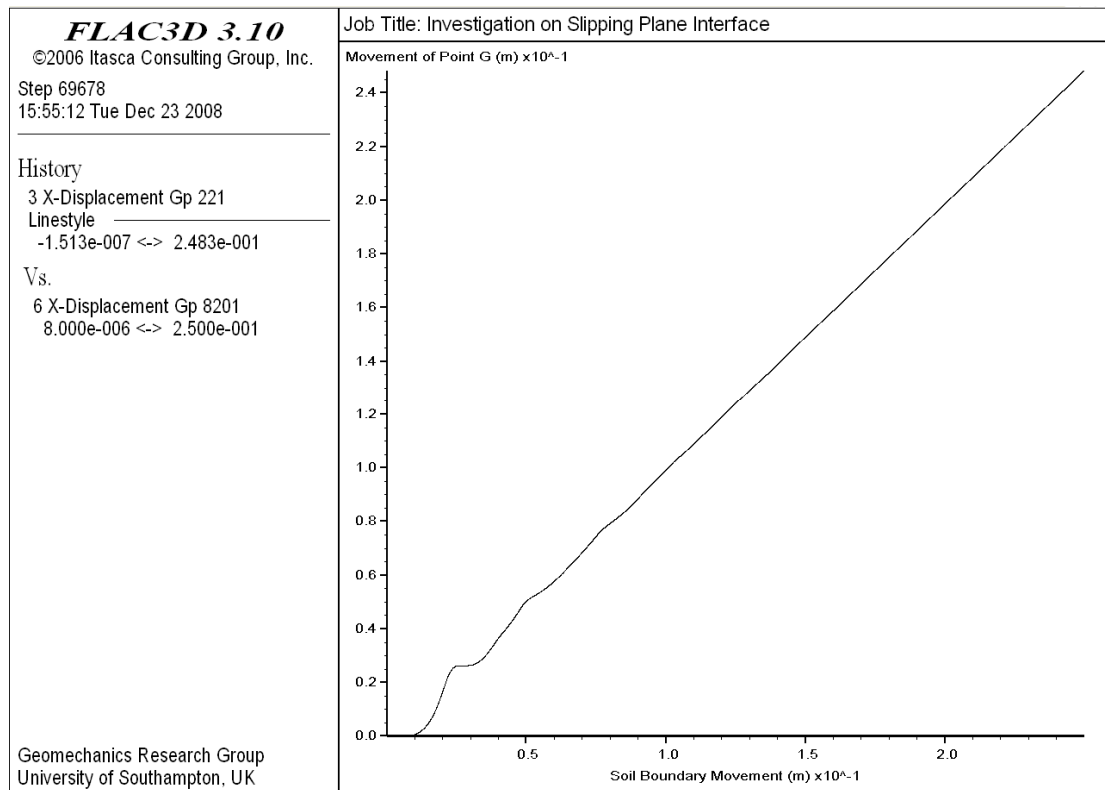


Figure 3.20: *FLAC*<sup>3D</sup> history plot showing the *x*-direction movement of Point *G* (0,0,-5) with boundary soil displacement

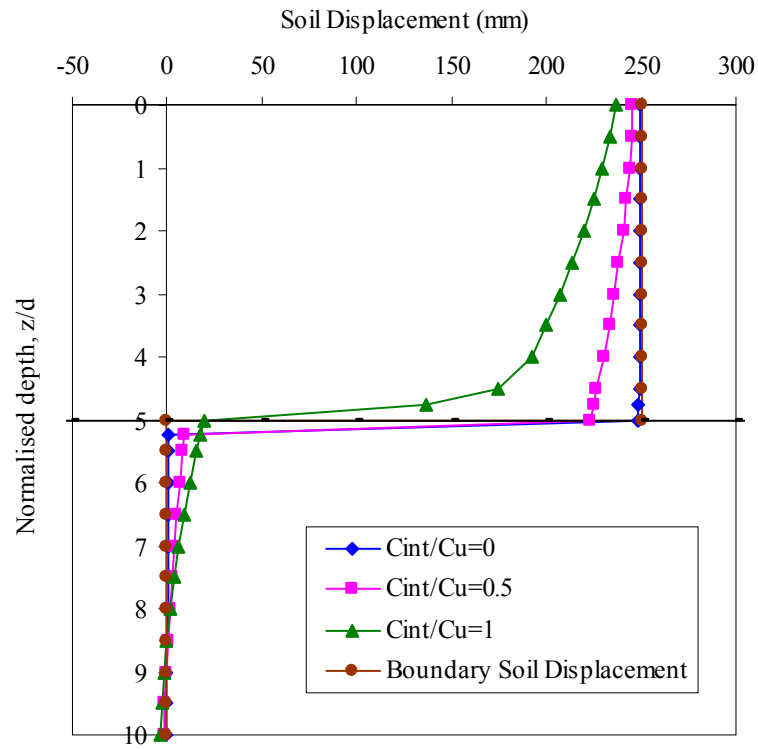


Figure 3.21: Movement of z-axis nodes with boundary soil movement

Figure 3.21 shows the variation in nodal displacement with depth. When the interface strength is equal to the strength of unstable soil, the nodes on the interface slip plane move only by 19.28 mm for 250 mm of boundary soil displacement. The movement of the nodes at the slip plane increases with reducing interface strength, and is similar to the soil boundary movement when the interface strength is zero. While the shear movement becomes more smeared with increasing interface strength, it is still quite well defined up to at least  $c_{int}/c_u = 0.5$ .

In summary, analyses have been carried out to investigate the more realistic cases of a weakened slip plane (but with non-zero strength) and a zero strength slip plane. From the results of these analyses, it was concluded that to represent a well defined slip plane, the interface elements should have zero strength, or perhaps  $c_{int}/c_u$  up to 0.5 can be adopted.

### 3.6.2 Behaviour of pile-soil interface with interface cohesion (Second stage: No slip plane)

To analyse numerically the failure mechanism of a laterally loaded pile based on Viggiani (1981), two more sets of interface elements have to be placed in between the pile perimeter and the soil, and between the pile tip and the soil. The normal and shear stiffnesses of the interface elements can be specified using Equation 3.11. The following analyses were carried out as a check on the calculation of the lateral pile-soil pressures using forces obtained from the interface elements, and to investigate how the pile behaviour varies with the cohesive strength (adhesion) of the interface elements between the pile and the soil.

#### 3.6.2.1 Grid generation

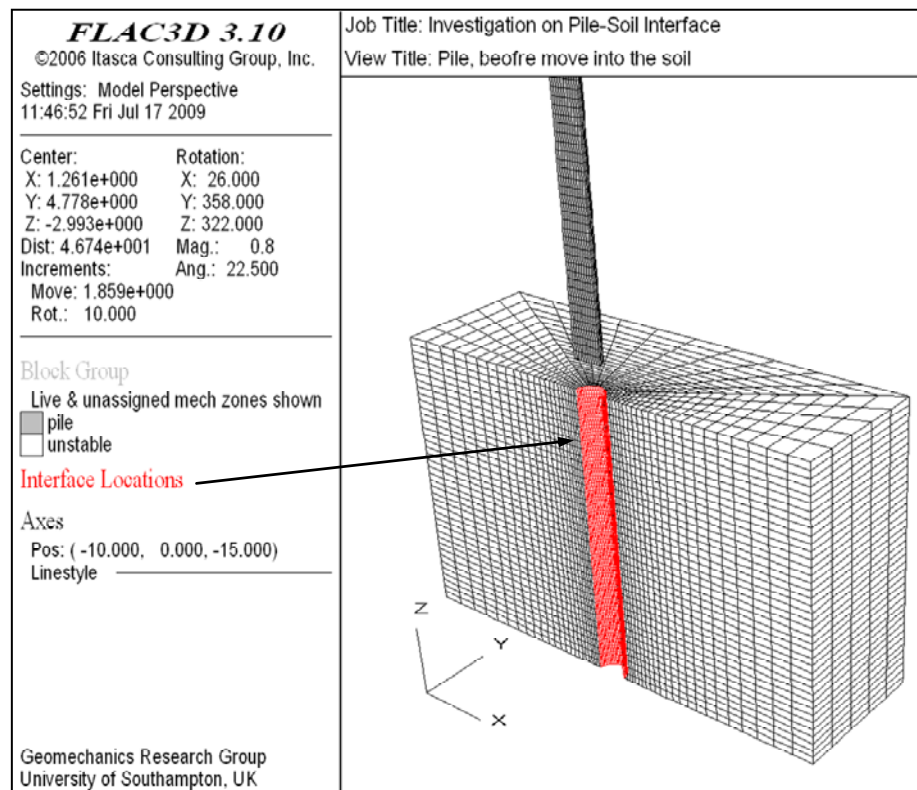


Figure 3.22: Before the pile moves into contact with interface elements

A  $16 \text{ m} \times 5 \text{ m} \times 10 \text{ m}$  graded mesh, representing a soil layer, was created using brick elements extending radially from a semi-circular hole into which the pile was inserted later (Fig. 3.22). Before inserting the pile, interface elements were attached to the soil elements where the pile comes into contact with the soil. A semi-circular pile of diameter 1 m and height 10 m, and 40 elements tall, was created separately and moved into contact with the interface elements. Only half a pile was modelled owing to the symmetry of the geometry. The boundary opposite the

pile centre plane represents a second line of symmetry, so that a row of piles is modelled. The initial pile centre-to-centre spacing was selected as  $10d$  (where  $d$  is the pile diameter), which is large enough for the behaviour to represent a single isolated pile (Brown and Shie, 1990b).

### 3.6.2.2 Boundary conditions

The boundary conditions were similar to those explained in Section 3.6.1.2, except for the bottom face of the soil mesh where the nodes were restrained to move in the vertical direction only. The bottom end of the pile was fixed.

### 3.6.2.3 Constitutive models and material properties

The pile was modelled as a linear elastic material having the properties given in Table 3.4. The soil properties were determined in the same way as described in Section 3.6.1.3. An elastic-Mohr-Coulomb plastic model was assumed for the soil, which was given a uniform undrained shear strength ( $c_u$ ) of 30 kPa and Poisson's ratio of 0.495. Table 3.4 shows the complete material properties used in the analyses.

<i>Material Properties</i>	<i>Pile</i>	<i>Soil</i>
Density ( $\text{kg/m}^3$ )	2500	1800
Strength Properties:		
Cohesion (kPa)	N/A	30
Friction	N/A	0
Elastic Properties:		
Young's modulus (MPa)	$122.2 \times 10^3$	6
Poisson's ratio	0.3	0.495
Bulk modulus (MPa)	$101.8 \times 10^3$	200
Shear modulus (MPa)	$47 \times 10^3$	2.007

*Table 3.4: Material properties for the pile and the soil*

Two different interface cohesion values were selected to investigate the behaviour of the pile-soil interface:

Rough interface:  $c_{int}/c_u = 1$  (full strength), and

Smooth interface:  $c_{int}/c_u = 0$  (zero strength).

### 3.6.2.4 *FLAC*<sup>3D</sup> analysis

Before pile insertion, the model was brought into equilibrium under gravity loading, after which the addresses of mesh nodes, elements and interface nodes were stored in the computer memory. A uniform lateral ( $x$ -direction) soil movement of 600 mm was applied incrementally to the left and right boundaries, at a rate of  $2 \times 10^{-6}$  m/step over 300,000 steps. The analyses were conducted in small strain mode, because in large strain mode (which allows a deformed mesh to be viewed) the analysis stopped with an illegal geometry error when the deformation of an element exceeded its maximum permissible value. Large soil boundary displacements of 600 mm (or  $0.6 d$ ) were applied to enable the ultimate lateral pile-soil pressure ( $p_u$ ) to be developed.

### 3.6.2.5 Ultimate lateral pile-soil pressure ( $p_u$ )

The distribution of ultimate lateral pile-soil pressure (or ultimate lateral resistance) along a laterally loaded pile driven in cohesive soil was first examined in detail by Broms (1964). Figure 3.23(b) shows the probable distribution of  $p_u$  for an actively loaded free-headed pile. To simplify the calculations Broms (1964) assumed that  $p_u = 0$  to a depth of  $1\frac{1}{2}$  pile diameters ( $d$ ) and is then equal to  $9 c_u d$  where  $c_u$  is the undrained shear strength of the soil. Broms also showed that  $p_u$  is a function of the shape of the cross-section and the roughness of the pile surface (Fig. 3.24).

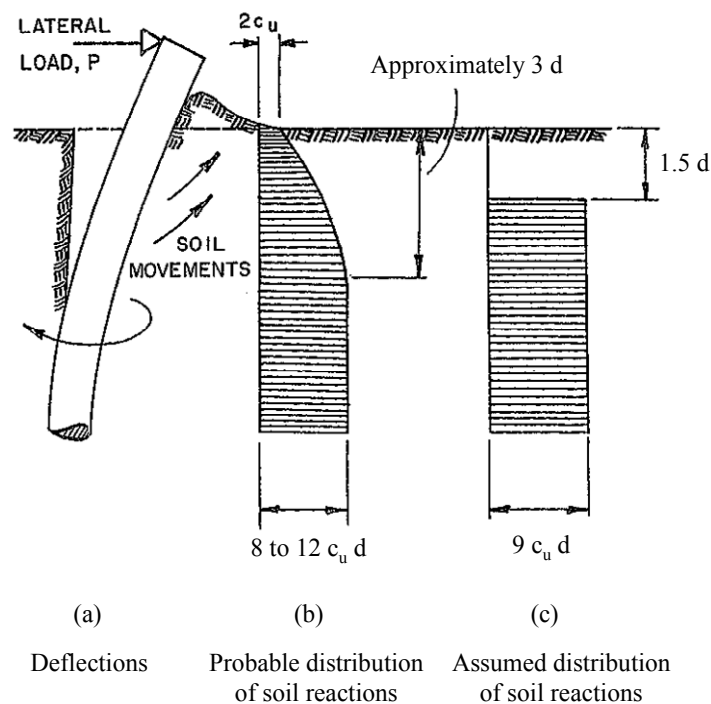


Figure 3.23: Distribution of lateral earth pressures (taken from Broms, 1964)

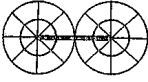
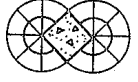


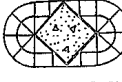
SLIP FIELD PATTERN	SURFACE	ULTIMATE LATERAL RESISTANCE, $q_{ult}/c_u$
	ROUGH	12.56
	ROUGH	11.42
	SMOOTH	11.42
	SMOOTH	9.14
	SMOOTH	8.28

Figure 3.24: Ultimate lateral resistance of different shape of piles (taken from Broms, 1964)

Randolph and Houlsby (1984) derived exact solutions for the ultimate lateral pile-soil pressure (or force per unit length of the pile) of a circular pile in cohesive soil using classical plasticity theory. The solutions developed were based on a rigid, perfectly plastic response of the soil, with an undrained shear strength independent of the total stress level. Randolph and Houlsby reported that the extent of the deforming zone around the pile (Fig. 3.25) varies with the adhesion ( $a$ ) at the pile-soil interface, where the adhesion was related to soil cohesion as shown in Equation 3.14.

$$a = \alpha \times c$$

Equation 3.14

Where,

$a$  = adhesion at the pile-soil interface

$c$  = soil cohesion or undrained shear strength of the soil

$\alpha$  = adhesion ratio ranges between zero (smooth pile) and one (rough pile)

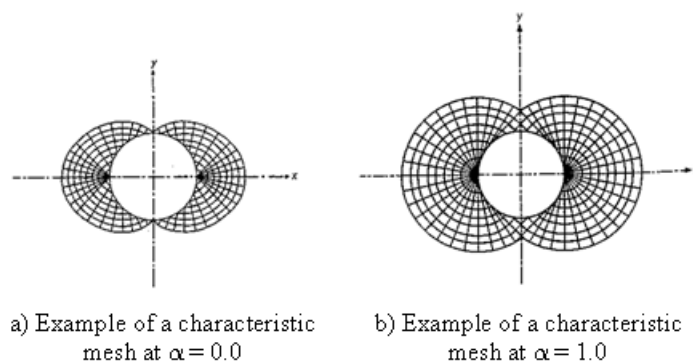


Figure 3.25: Characteristic meshes for circular piles (taken from Randolph and Houlsby, 1984)

Randolph and Houlsby concluded the following points:

- 1) A higher  $p_u$  was found when  $\alpha = 1.0$  (rough pile), owing to the larger deforming region (see Fig. 3.25b).
- 2)  $p_u$  ranges from  $9.14\,cd$  (where  $d$  is diameter of the pile) for a smooth pile up to  $11.94\,cd$  for a perfectly rough pile ( $\alpha = 1.0$ ).

Chen and Martin (2002) carried out plane strain analyses using  $FLAC^{2D}$  to investigate the influence of interface properties on the ultimate lateral pile-soil pressure (or limiting lateral pressure). They modelled the interface without either cohesion or frictional strength to simulate the condition of a perfectly smooth interface between the soil and the pile, and chose an interface strength ( $c_{int}$ ) equal to  $5\,c_u$  to represent a perfectly rough pile-soil interface. Figure 3.26 shows the normalised lateral pressure ( $p/c_u d$ ), plotted against the displacement of the pile. It also shows that the normalised limiting lateral pressure was 9.11 and 11.94 for the smooth and rough interfaces respectively which agrees with Randolph and Houlsby (1984).

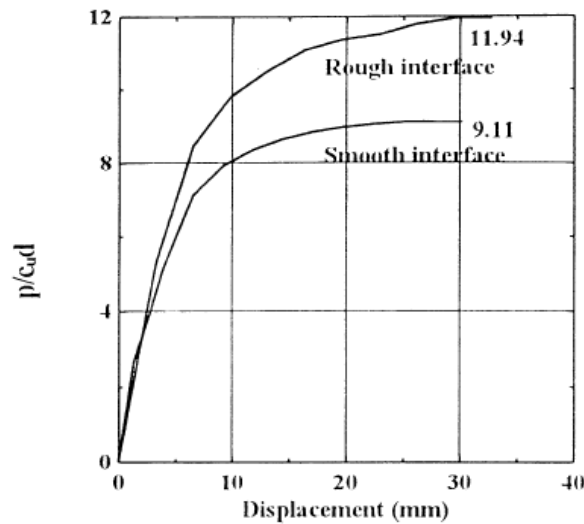


Figure 3.26: Normalised lateral pressure versus pile displacement curves (taken from Chen and Martin, 2002)

Fleming *et al.* (1994) suggest that the ultimate lateral pile-soil pressure (or net lateral force at failure per metre length), acting on a pile of  $d$  diameter moving through a clay of undrained shear strength  $c_u$ , is given by

$$p_u = 2c_u d \quad \text{at the soil surface, } z = 0 \quad \text{Equation 3.15}$$

$$p_u = [2 + (7z/3d)]c_u d \quad \text{for depths } z \leq 3d \quad \text{Equation 3.16}$$

$$p_u = 9c_u d \quad \text{for depths } z \geq 3d \quad \text{Equation 3.17}$$



### 3.6.2.6 Results and discussion

Figures 3.27-3.30 shows the variations in deflection, shear force, bending moment and normalised ultimate lateral pile-soil pressure, for the two different normalised interface cohesions following 600 mm of boundary soil displacement. The analyses show that the behaviour of the pile is influenced by the strength of the pile-soil interface, in accordance with classical theory.

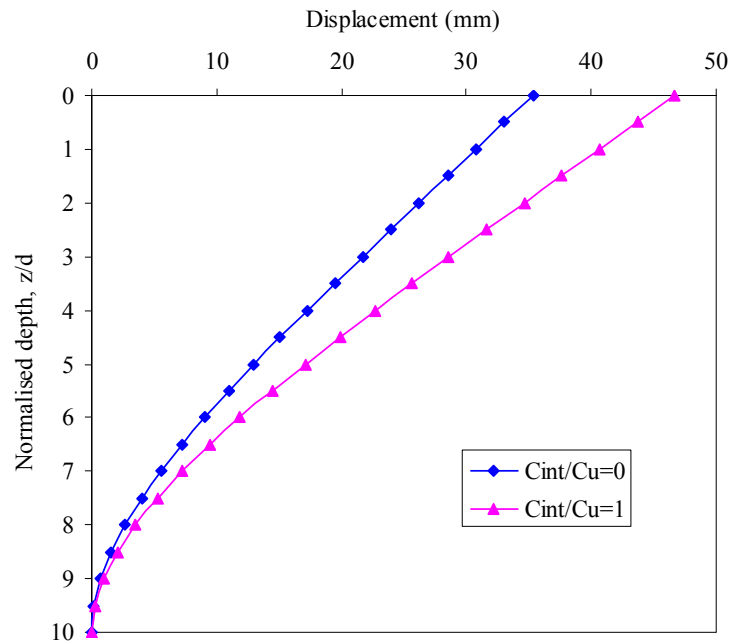


Figure 3.27: Variation in deflection with pile-soil interface strength

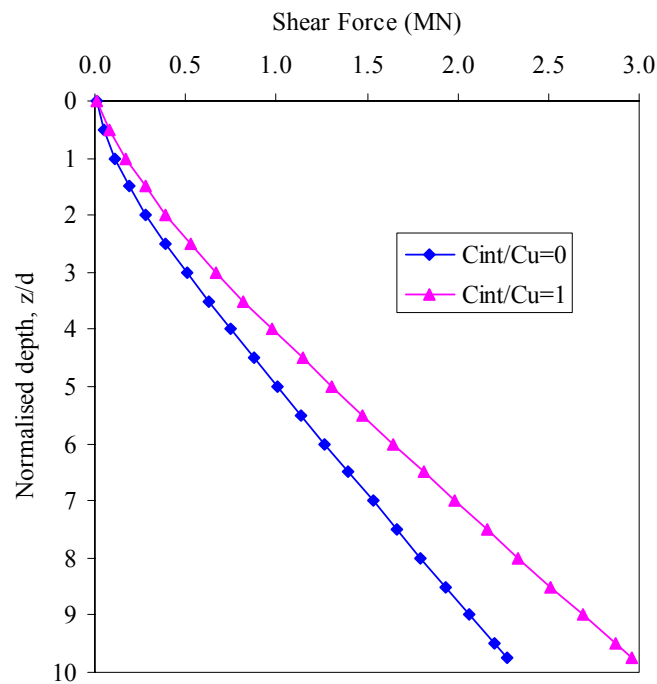


Figure 3.28: Variation in shear force with pile-soil interface strength

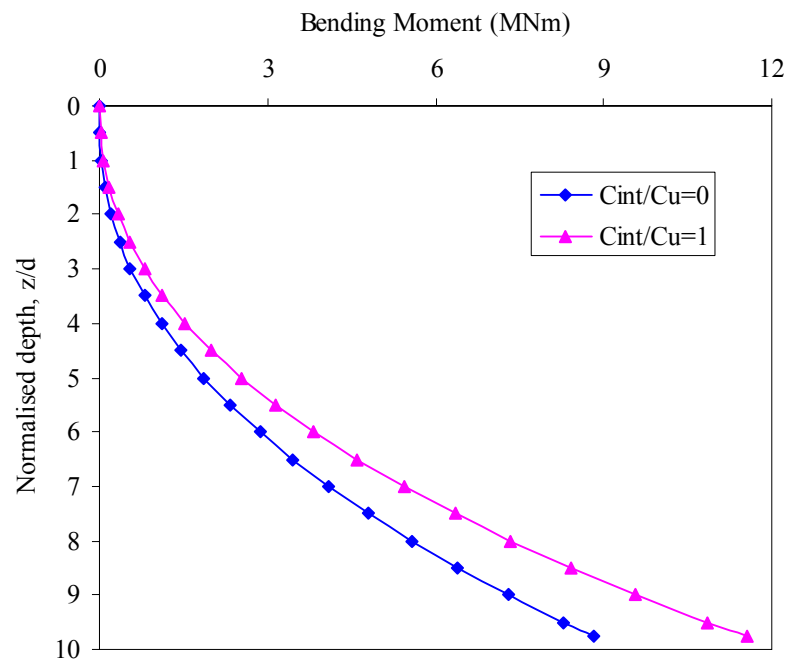


Figure 3.29: Variation in bending moment with pile-soil interface strength

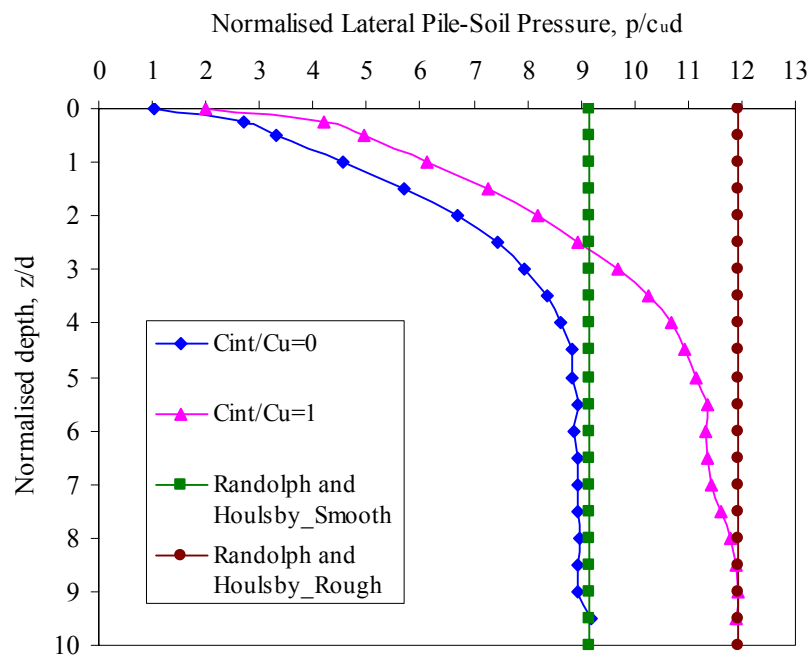


Figure 3.30: Variation in normalised lateral pile-soil pressure with pile-soil interface strength

The values of  $p_u$  found agree well with analytical solutions and numerical 2D plane-strain analyses presented by Broms (1964), Randolph and Houlsby (1984) and Chen and Martin (2002) respectively, of  $9.14 c_u d$  for the adhesionless pile-soil interface and  $11.94 c_u d$  for the rough pile-soil interface (Fig. 3.30). The  $FLAC^{3D}$  analyses attained the ultimate value only in the deeper soil, as surface effects reduced the ultimate lateral pile-soil pressure above about  $z/d = 5$ . The analysis with the rough (full strength) pile-soil interface attained  $p_u = 2.01 c_u d$  at the ground surface while the zero strength pile-soil interface analysis attained  $p_u = 1.04 c_u d$ . The lateral pile-soil pressure reached its ultimate value below a depth of  $5 d$  for the zero strength pile-soil interface, and slightly deeper (6-8  $d$ ) for the full strength interface.

Figure 3.31 shows the development of lateral pile-soil pressure with boundary soil movement for the full strength pile-soil interface. The pile-soil model attains the local value of  $p_u$  initially at shallow and deep levels, and only attains the local value of  $p_u$  at intermediate depths with further lateral soil movement.

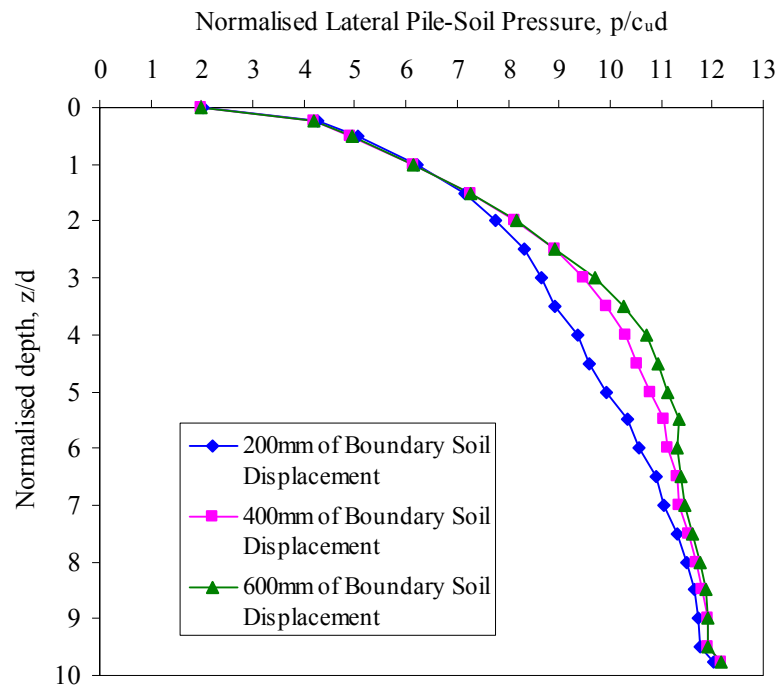


Figure 3.31: Development of normalised lateral pile-soil pressure with boundary soil movement; rough pile-soil interface model

Figure 3.32 compares the reductions in  $p_u$  (below 9.14 or 11.94  $c_u d$ ) suggested by Broms (1964) and Fleming *et al.* (1994) to account for surface effects in active pile loading with the results calculated from the current analyses. The  $p_u$  plot obtained for the zero strength pile-soil interface falls a little below the surface reduction proposed by Fleming *et al.*

The curves coincide with the theoretical maximum values below about 5  $d$  depth, confirming that the interface between the pile and soil is operating correctly in the numerical model and that the interface shear and normal node forces can be used to calculate accurately the lateral pile-soil pressure acting on the pile shaft.

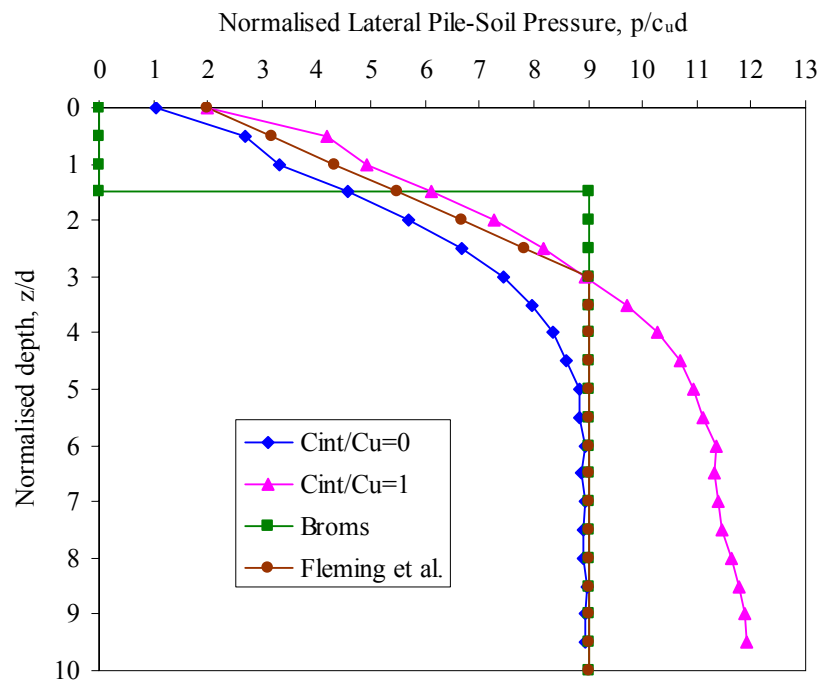


Figure 3.32: Comparison of normalised lateral pile-soil pressure with different methods

### 3.7 Investigate the boundary effects on the pile behaviour

Placement of the model boundaries close to the pile may affect the pile behaviour. Therefore, boundaries have to be placed far enough away to ensure reliable results from the numerical analyses. However, placing the boundaries too far from the pile significantly increases the total number of elements used in the  $FLAC^{3D}$  model, and the calculation time. The left and right boundaries where the lateral load was applied, were placed at a distance of  $8d$  (where  $d$  is the pile diameter) from the pile centre for the analyses presented in Section 3.6.2. The analyses presented in this section were carried out prior to the analyses presented in Section 3.6.2, to check whether the boundaries placed at a distance of  $8d$  are sufficient to get reliable results.

A model similar to that explained in Section 3.6.2 was adopted, but the left and right side boundaries were placed at  $16d$  distance from the pile centre. A rough (full strength) pile-soil interface analyses was placed in between pile and soil, to allow relative movement between them.

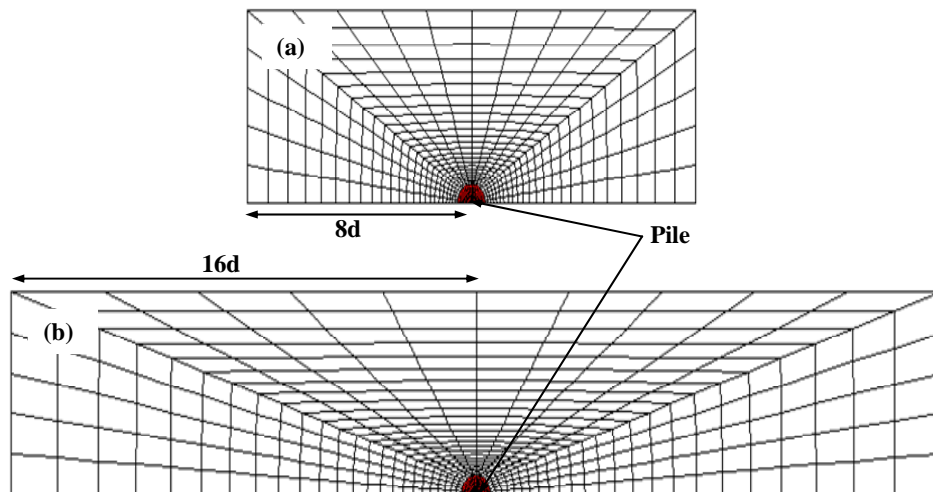


Figure 3.33: Plan view of  $FLAC^{3D}$  mesh (a) boundaries at  $8d$ ; (b) boundaries at  $16d$

Figures 3.34-3.37 show the variation of pile deflection, shear force, bending moment and normalised lateral pile-soil pressure, with the distance of the left and right side soil boundaries from the pile centre, after 300 mm of boundary soil displacement. The reduction that occurred in all four parameters for a boundary distance =  $16d$ , compared with  $8d$ , is small, and may be ignored. When the distance between the boundary and centre of the pile increases, the lateral load exerted on the pile by the boundary soil movement decreases slightly, and therefore the pile deflects slightly less (Fig. 3.34). As a result, slightly less shear force and bending moment is developed on the pile. In conclusion, the chosen distance (i.e.  $8d$ ) at which to place the boundaries is sufficient to minimise the errors generated by the boundary locations, while enabling computational efficiency.

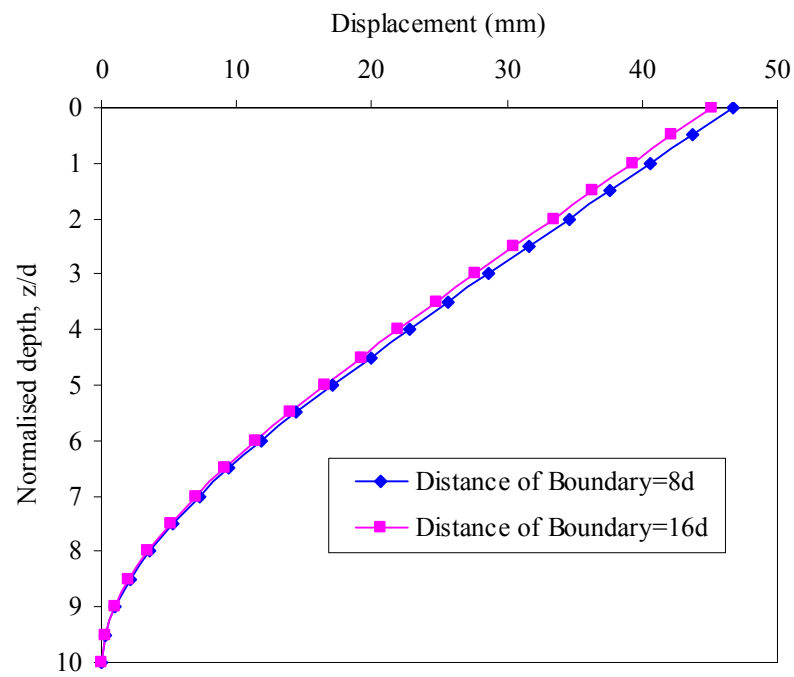


Figure 3.34: Variation in deflection with distance between pile and boundary locations

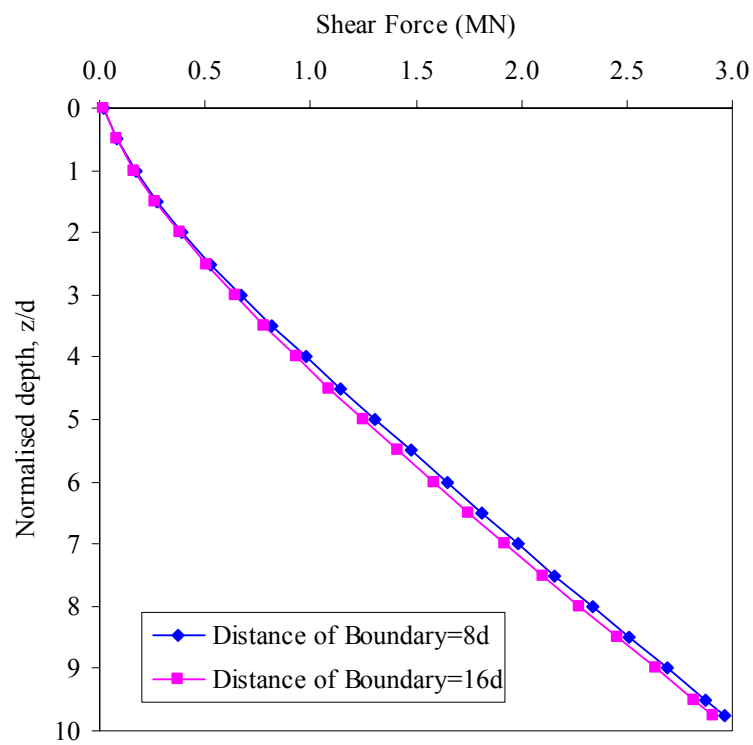


Figure 3.35: Variation in shear force with distance between pile and boundary locations

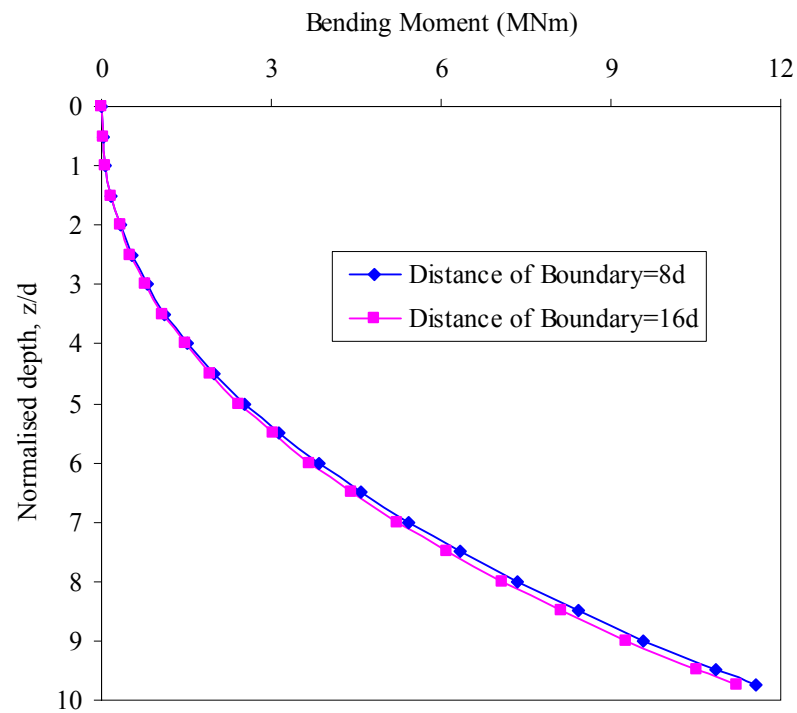


Figure 3.36: Variation in bending moment with distance between pile and boundary locations

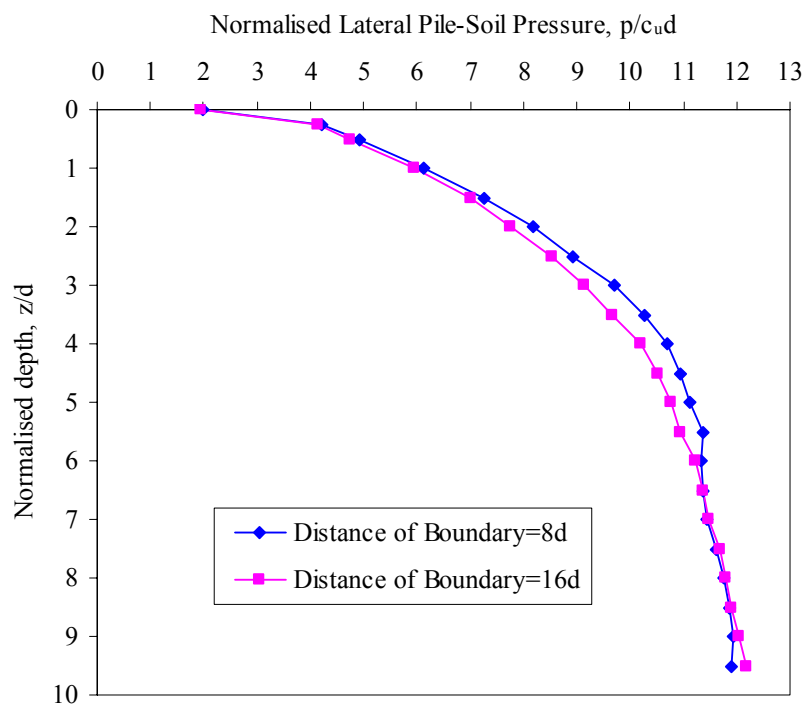


Figure 3.37: Variation in normalised lateral pile-soil pressure with distance between pile and boundary locations

### 3.8 Failure mechanisms of isolated piles based on Viggiani (1981) (Third stage: Slip plane and pile in place)

Numerical studies have been conducted, based on Viggiani's concept, to investigate failure mechanisms for a single circular pile resisting lateral soil movements.

#### 3.8.1 Geometry of the problem

As explained in Section 3.3, the failure modes for a single pile defined by Viggiani (1981) depend on the depth of sliding surface ( $H$ ) relative to the pile length ( $L$ ). Three different geometries of  $FLAC^{3D}$  meshes were created, each with a different depth to the failure surface but with the same pile geometry. The  $FLAC^{3D}$  analysis procedures including  $FLAC^{3D}$  mesh creation, pile installation, boundary and fixity conditions, constitutive models and properties, gravity loading and lateral load application are explained below.

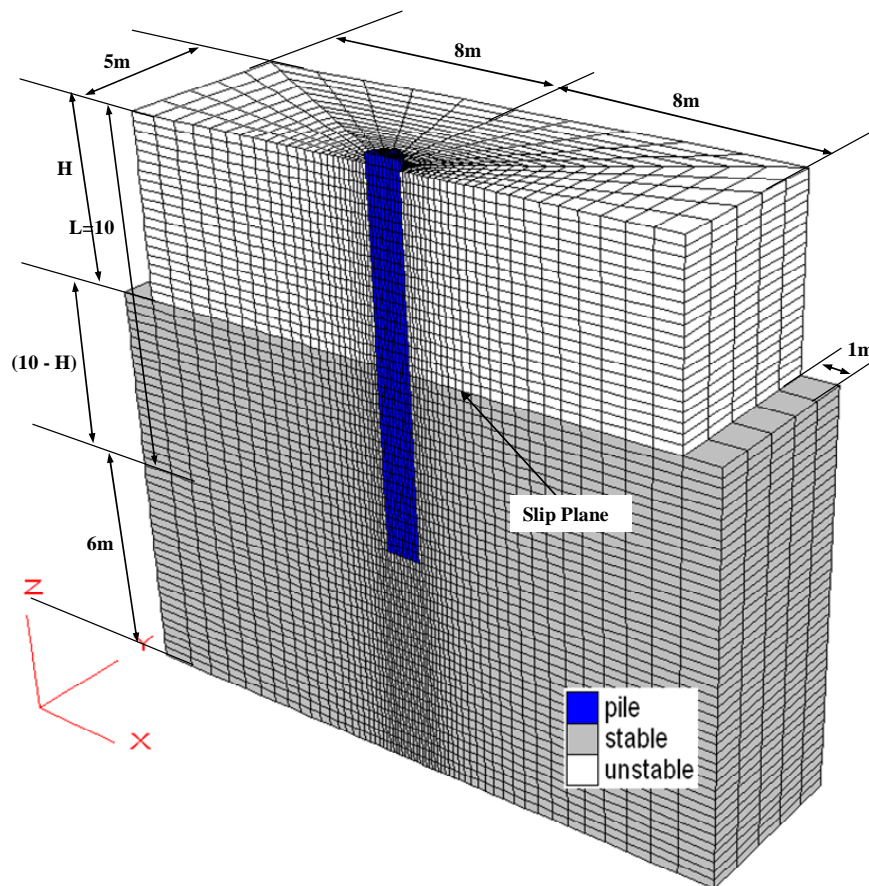


Figure 3.38: Geometry of the  $FLAC^{3D}$  model



### 3.8.2 Grid generation

Figure 3.38 shows the mesh used for the analyses. Using the symmetry of the geometry and loading, the mesh was simplified by modelling just half a pile (reflected about the  $y = 0$  plane). A 16 m long  $\times$  5 m wide  $\times$   $H$  m high (where  $H$  was equal to 9 m, 5 m and 3 m for Viggiani's modes A, B and C respectively) mesh representing the unstable soil layer was created first. The values of  $H$  were chosen based on Viggiani's solutions, but with the normalised ultimate lateral pile-soil pressure ( $p_u/c_u d$ ) taken as 11.94 for the unstable and stable soil layers, rather than 4 and 8 as suggested by Viggiani. An 18 m long  $\times$  5 m wide  $\times$   $(16-H)$  m high soil block was then modelled below the upper block, initially with a 1 m gap between them. A 1 m diameter semi-circular hole was formed at the centre in the front face of both soil blocks, into which the pile was later inserted. The interface elements representing the slip plane were attached to the bottom face of the upper soil block. After the creation of the interface elements, the lower block was lifted up by 1 m to bring it into contact with the upper block, and pile installation was carried out as explained Section 3.6.2 to complete the geometry.

### 3.8.3 Initial and boundary conditions

The nodes on the base of the completed mesh were restrained in all three directions while the nodes on the top face were free to move. The nodes on the faces representing planes of symmetry were prevented from moving in the  $y$ -direction. The nodes on the right and left faces were prevented from moving in the direction of the applied soil movements (i.e.  $x$ -direction) during gravity loading, and the nodes on these faces on the upper soil layer (Fig. 3.38) were freed to move during lateral loading. Stresses were initialised assuming an in situ earth pressure coefficient ( $K_0$ ) equal to 1.

### 3.8.4 Constitutive models and material properties

The pile and soils were modelled as linear elastic and elastic-Mohr-Coulomb plastic materials respectively. The undrained shear strength ( $c_u$ ) of the stable soil layer was set at double that of the unstable soil layer, and the soil stiffness was again calculated as  $E_s = 200 c_u$ . As before, the interface stiffness was set to be ten times that of the stiffest neighbouring element. The interface representing the slip plane was assigned a strength of zero corresponding to Viggiani's (1981) assumption of a perfect sliding plane. The pile-soil adhesion was set to the undrained shear strength of the surrounding soil, corresponding to a perfectly rough (adhesive) interface. Tables 3.5 and 3.6 show the material and interface properties used in the analyses.

<i>Material Properties</i>	<i>Pile</i>	<i>Unstable Soil</i>	<i>Stable Soil</i>
Density (kg/m <sup>3</sup> )	2500	1800	1800
<b>Strength Properties:</b>			
Undrained shear strength (kPa)	N/A	30	60
<b>Elastic Properties:</b>			
Young's modulus (MPa)	122.2×10 <sup>3</sup>	6	12
Poisson's ratio	0.3	0.495	0.495

Table 3.5: Material properties for the pile and the soil

<i>Interface Properties</i>	<i>Interface between the unstable and stable soil</i>	<i>Interface between the pile wall and the unstable soil</i>	<i>Interface between the pile wall and the stable soil</i>	<i>Interface between the pile tip and the soil</i>
Normal stiffness (GPa)	16.21	1.89×10 <sup>4</sup>	1.89×10 <sup>4</sup>	6.579×10 <sup>3</sup>
Shear stiffness (GPa)	16.21	1.89×10 <sup>4</sup>	1.89×10 <sup>4</sup>	6.579×10 <sup>3</sup>
Adhesion (kPa)	0	30	60	60

Table 3.6: Properties of interface elements used in the analyses

### 3.8.5 *FLAC<sup>3D</sup>* analysis

The model was brought into equilibrium under gravity loading and the addresses of required nodes and elements were stored so that stress and displacement outputs could be calculated. The nodes on the left and right faces of the unstable soil block were released to move in the  $x$ -direction (Fig. 3.38), and a velocity of  $2 \times 10^{-7}$  m/step from left to right was applied over  $2 \times 10^6$  steps to move the soil boundaries by 400 mm. The pile deflection, shear force and bending moment developed in the pile, and the lateral pile-soil pressure were calculated at every 100 mm of soil movement up to 400 mm. One analysis was carried out with 800 mm of boundary soil movement for mode A to determine whether 400 mm of boundary soil movement was enough to mobilise fully the lateral pile-soil pressure along the pile shaft. The results showed only a small increase in the lateral pile-soil pressure, compared with the analysis of 400 mm boundary soil movement (Figs. 3.39 and 3.40). From this, it was decided that 400 mm of boundary soil movement would be sufficient to develop the ultimate lateral pile-soil pressure along the pile shaft and therefore all of the remaining analyses were carried out with 400 mm of boundary soil movement.

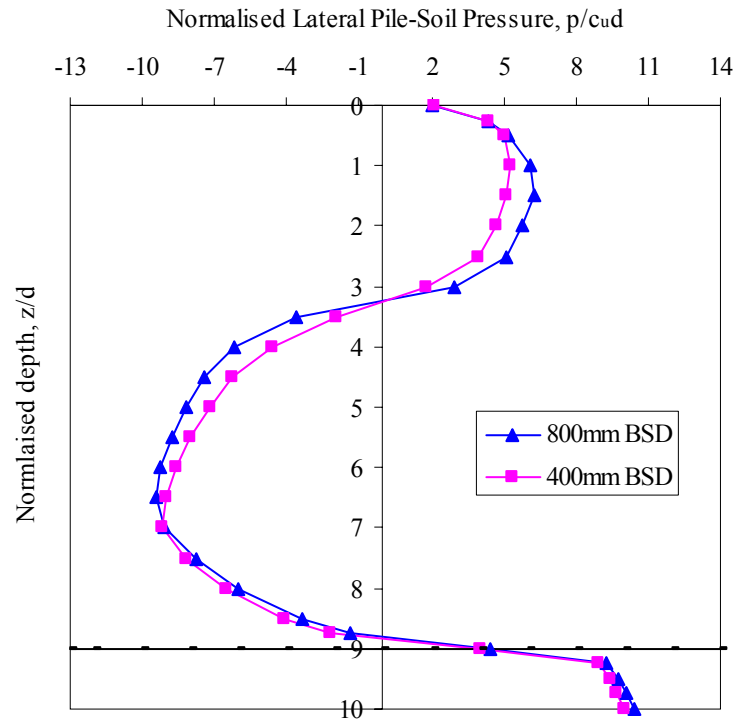


Figure 3.39: Development of normalised lateral pile-soil pressure with soil movement in failure mode A with applied boundary soil displacement of 400 mm and 800 mm

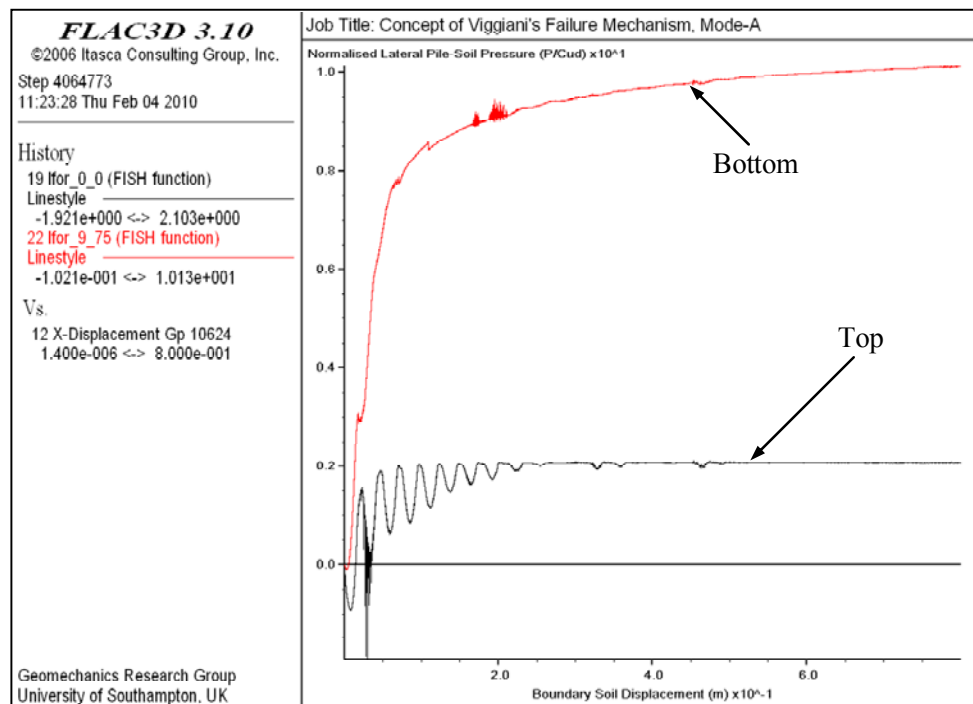


Figure 3.40: History plot of the normalised lateral pile-soil pressure development at pile top and pile bottom with boundary soil displacement for mode A

### 3.8.6 Results and discussion

#### 3.8.6.1 Mode – A

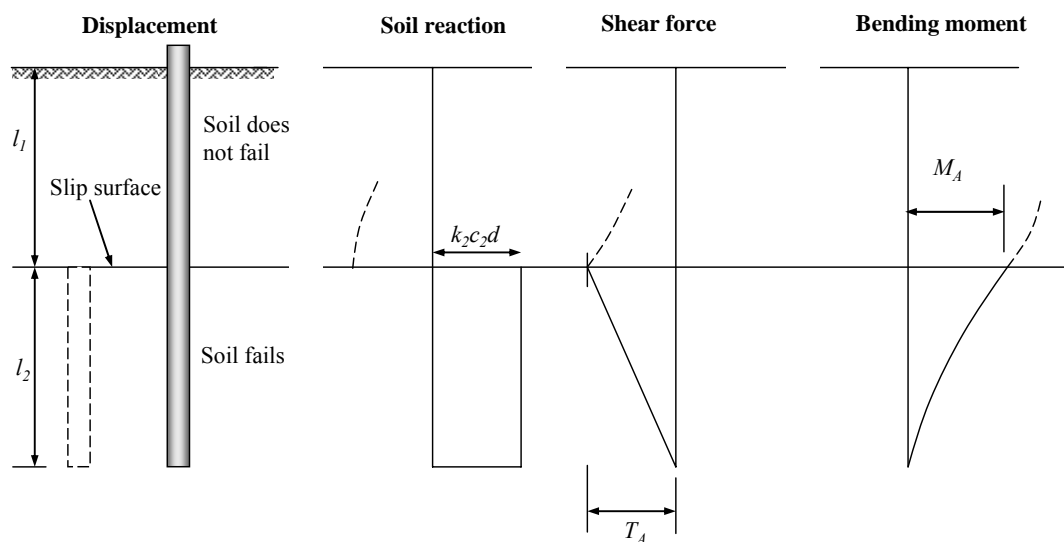


Figure 3.41: Typical diagram explaining failure mode A (based on Viggiani, 1981)

From Equation 2.4, failure mode A occurs if,

$$\lambda < \lambda' = \chi \left( \frac{\sqrt{(2+2\chi)} - 1}{1+2\chi} \right)$$

Where,

$$\lambda = \frac{l_2}{l_1}$$

$$\chi = \frac{k_1 c_1}{k_2 c_2} = \left( \frac{11.94 \times 30000}{11.94 \times 60000} \right) = 0.5 \text{ (refer Section 2.2.2 for details).}$$

By substituting  $\chi = 0.5$  in Equation 2.1,

$$\lambda < \lambda' = 0.5 \left( \frac{\sqrt{2+1} - 1}{1+1} \right) = 0.183$$

$$\Rightarrow \lambda = \frac{l_2}{l_1} < 0.183$$

Equation 3.18

Since

$$l_1 + l_2 = 10 \quad \text{Equation 3.19}$$

By solving Equations 3.18 and 3.19, it was calculated that

$$\left( \frac{10 - l_1}{l_1} \right) < 0.183$$

$$\Rightarrow l_1 > 8.45$$

From this,  $l_1$  and  $l_2$  were approximated to be 9 m and 1 m respectively for failure mode A to occur.

Figures 3.42-3.45 show the deflection, normalised lateral pile-soil pressure, shear force and bending moment developed in the pile with applied boundary displacement respectively, for failure mode A. In the Viggiani (1981) definition of the mode A mechanism, the lower part of the pile is dragged through the soil as the upper part is carried along with the sliding soil layer. Net pile pressures from relative pile-soil movement must be developed above the sliding surface to maintain the pile in equilibrium, although it is assumed that these pressures remain distant from  $p_u$  and it is not possible to calculate their exact distribution with depth from considerations of limiting equilibrium.

In Figure 3.42, the pile has been dragged along with the unstable soil layer and there is a substantial rotation of the pile, which causes the displacement of the top portion of the pile to exceed the applied boundary soil movements. This behaviour is consistent with the normalised lateral pile-soil pressure plot (Fig. 3.43), in which a reversal of the lateral pile-soil pressure is apparent at the top of the pile. The ultimate lateral pile-soil pressure on the part of the pile embedded in the stable layer develops quite rapidly; increasing rotation of the pile with greater boundary soil movement then occurs, increasing the lateral pile-soil pressures on the pile in the sliding layer. Increasing pressures above and below the point of inflexion at about 3.5 m depth (Fig. 3.43) balance each other out, maintaining the pile in equilibrium. As expected, the pressures above the sliding surface remain below  $p_u$  (plotted in Fig. 3.43 from Fig. 3.32, including surface effects).

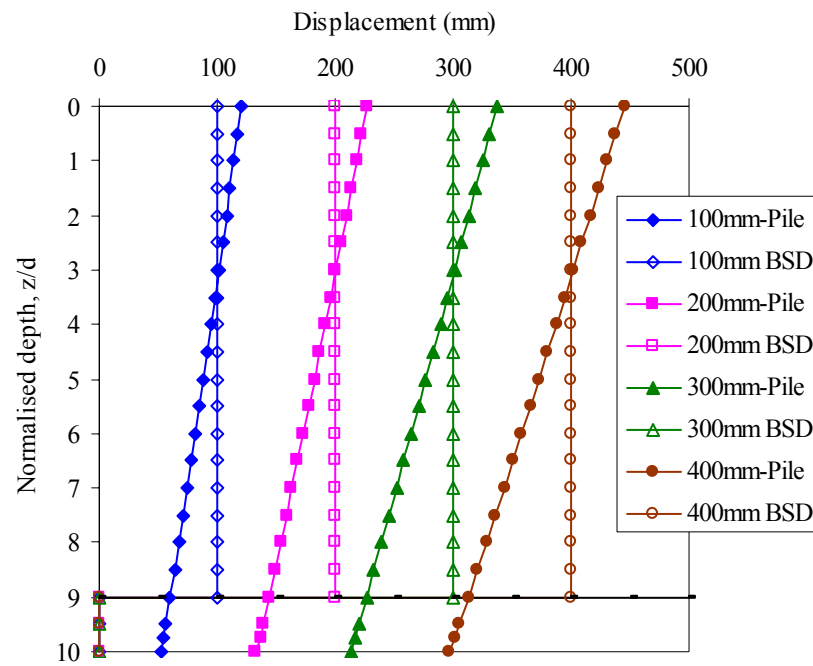


Figure 3.42: Displacement of pile with soil movement in failure mode A with applied boundary soil displacement

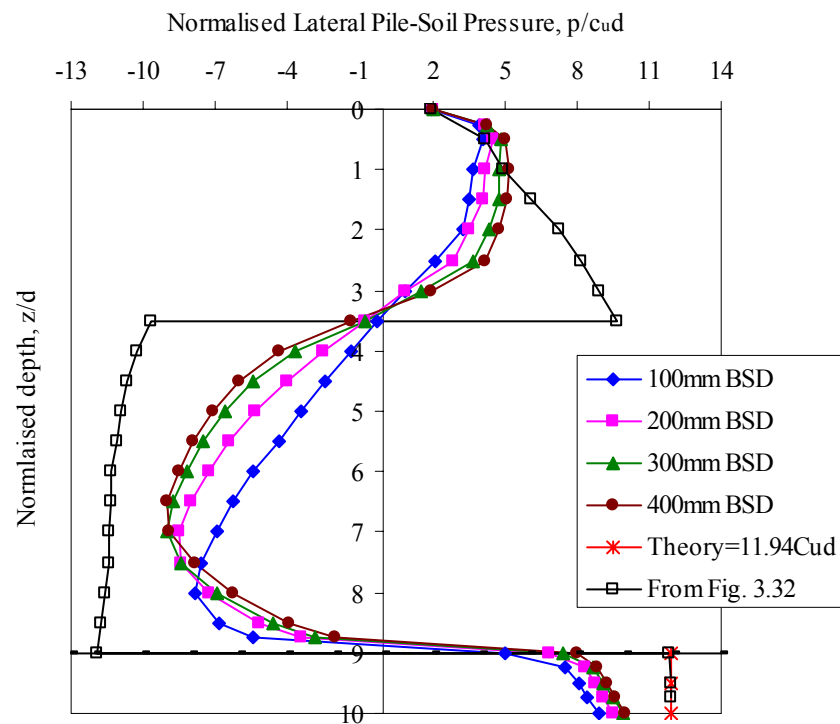


Figure 3.43: Development of normalised lateral pile-soil pressure with soil movement in failure mode A with applied boundary soil displacement

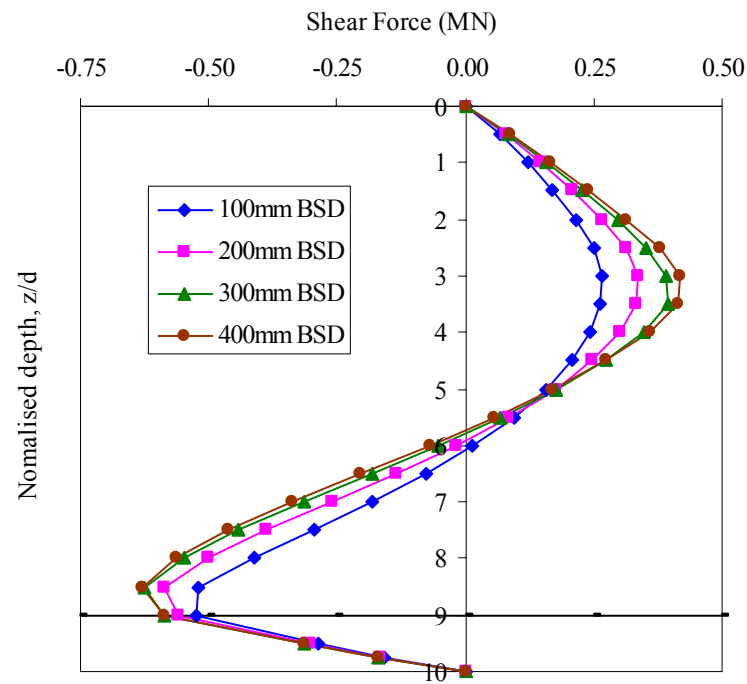


Figure 3.44: Development of shear force in the pile with soil movement in failure mode A with applied boundary soil displacement

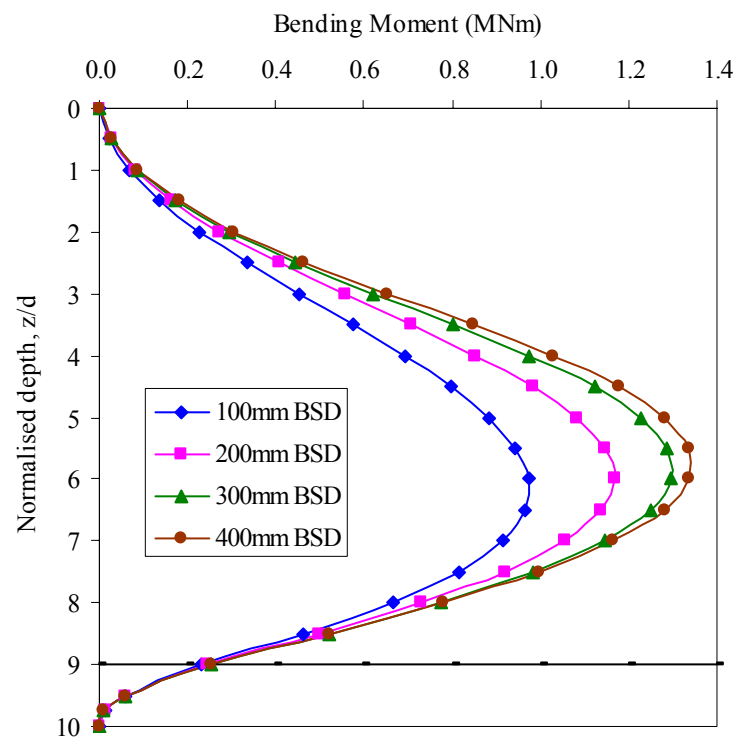


Figure 3.45: Development of bending moment in the pile with soil movement in failure mode A with applied boundary soil displacement

### 3.8.6.2 Mode – C

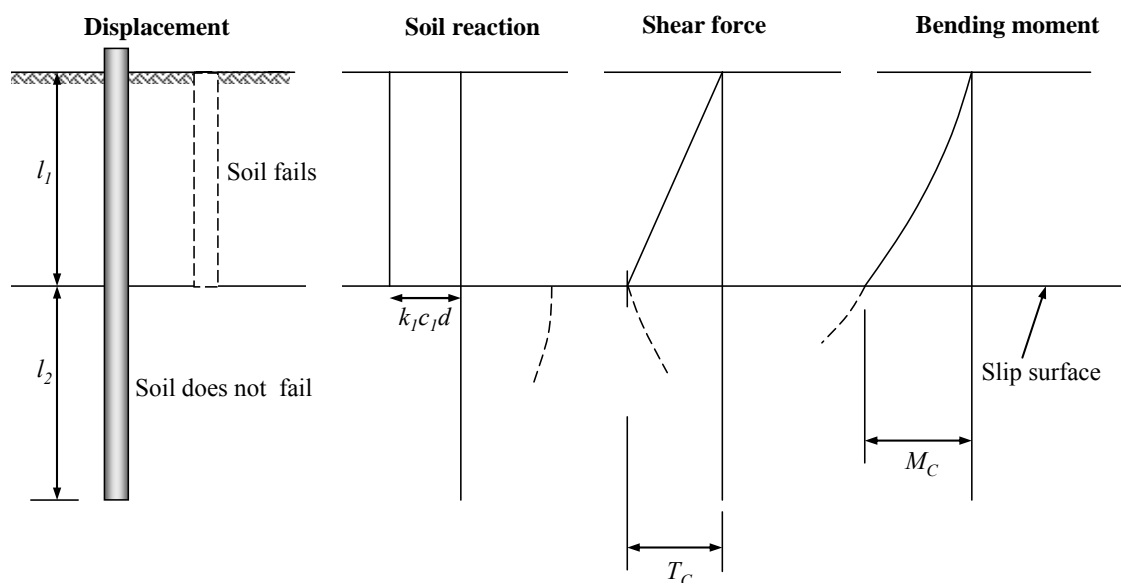


Figure 3.46: Typical diagram explaining failure mode C (based on Viggiani, 1981)

From Equation 2.5, failure mode C occurs if,

$$\lambda > \lambda'' = \chi + \sqrt{2\chi^2 + 2\chi}$$

By substituting  $\chi = 0.5$  in above equation,

$$\lambda > \lambda'' = 0.5 + \sqrt{(2 \times 0.5^2) + (2 \times 0.5)} = 1.725$$

$$\Rightarrow \lambda = \frac{l_2}{l_1} > 1.725$$

Equation 3.20

Since

$$l_1 + l_2 = 10$$

Equation 3.21

By solving Equations 3.20 and 3.21,

$$\left( \frac{10 - l_1}{l_1} \right) > 1.725$$

$$\Rightarrow l_1 < 3.670$$



From this calculation,  $l_1$  and  $l_2$  were approximated to be 3 m and 7 m respectively for failure mode C to occur.

In Figure 3.47, for failure mode C, the soil flows around the top of the pile without significant pile movement, although a small amount of pile rotation does occur. This is because 7 m of the 10 m pile is embedded into the stable soil in this configuration, which provides a much greater resistance to the lateral pile-soil pressure developed by the sliding layer. The ultimate lateral pile-soil pressure  $p_u$  develops over the length of pile in the unstable soil layer, but pressures remain distant from  $p_u$  below this (Fig. 3.48).

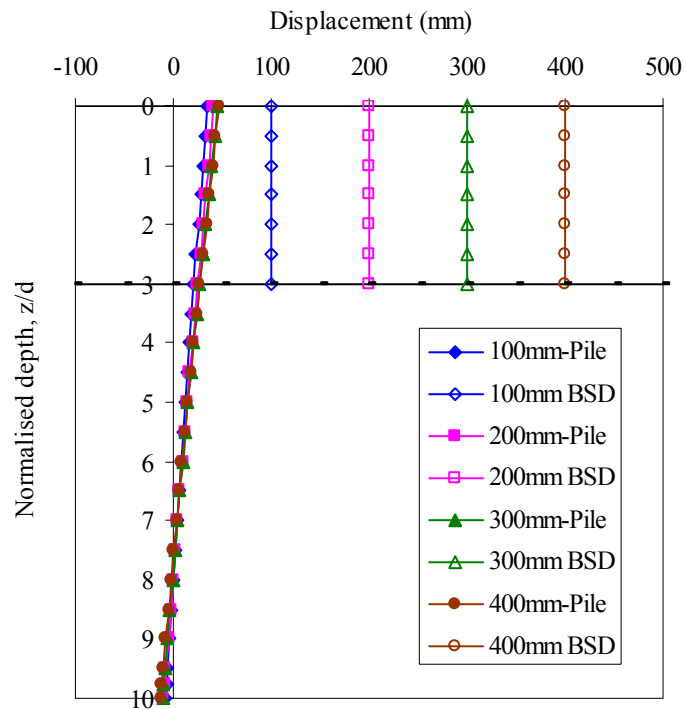


Figure 3.47: Displacement of pile with soil movement in failure mode C with applied boundary soil displacement

Figures 3.49 and 3.50 show the shear force and bending moment developed in the pile with applied boundary displacement respectively. Figure 3.51 shows the history plot of the normalised shear force development at slip plane, with normalised pile top displacement and normalised boundary soil displacement.

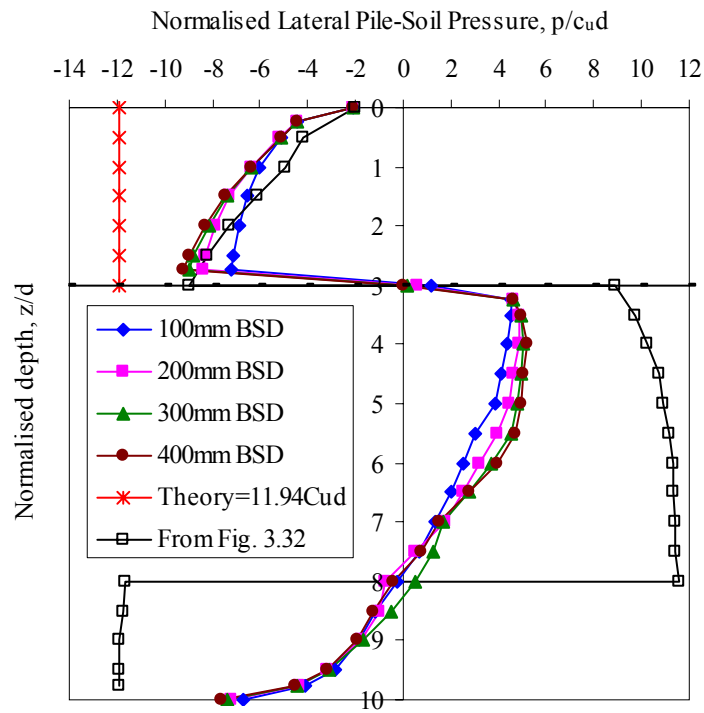


Figure 3.48: Development of normalised lateral pile-soil pressure with soil movement in failure mode C with applied boundary soil displacement

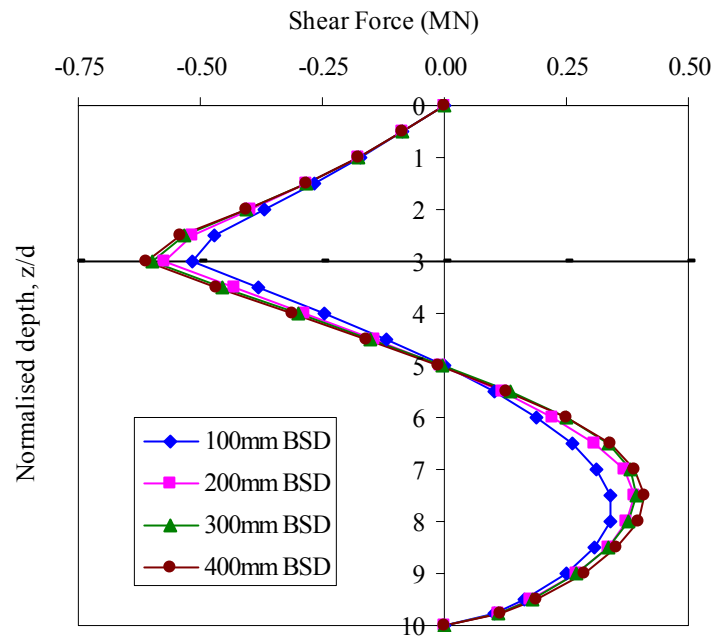


Figure 3.49: Development of shear force in the pile with soil movement in failure mode C with applied boundary soil displacement

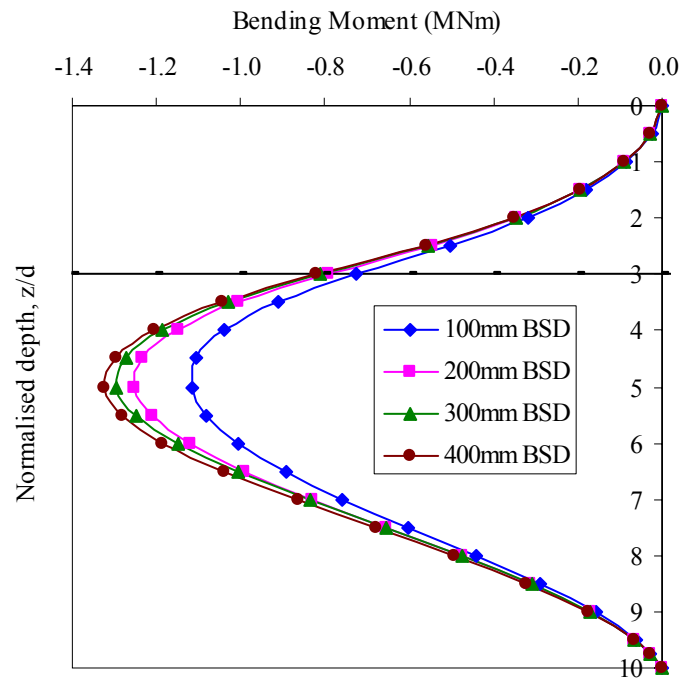


Figure 3.50: Development of bending moment in the pile with soil movement in failure mode C with applied boundary soil displacement

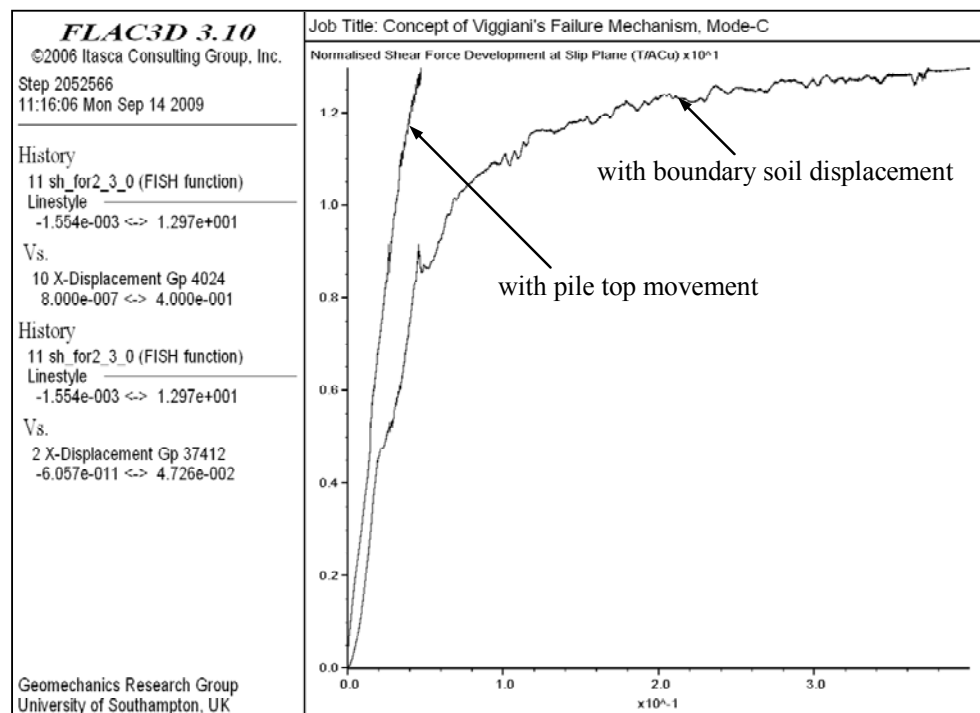


Figure 3.51: History plot of the normalised shear force development at slip plane, with normalised pile top displacement and normalised boundary soil displacement for mode C

### 3.8.6.3 Mode – B

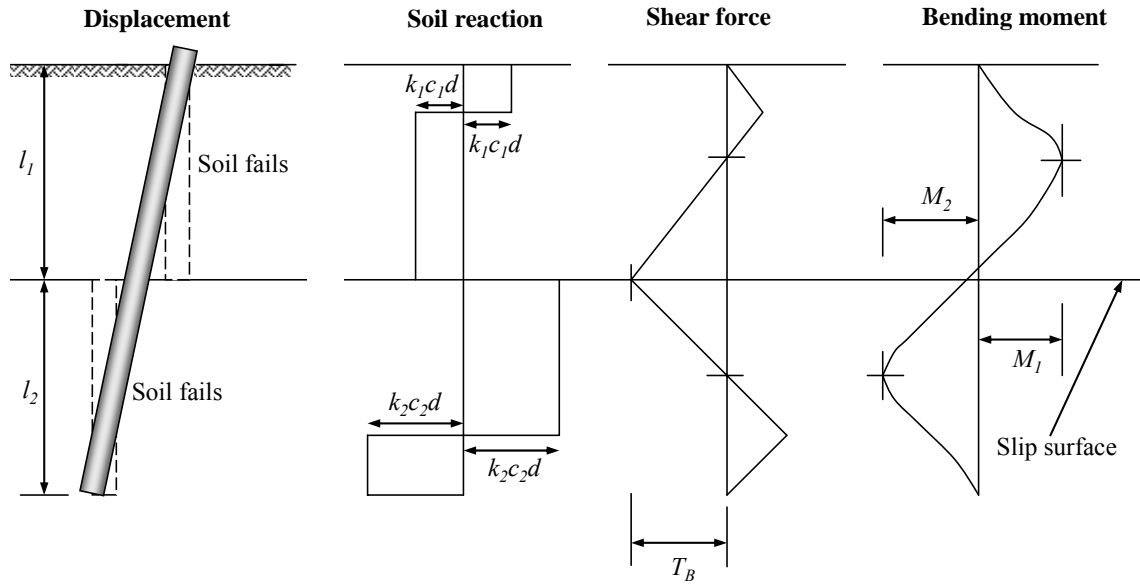


Figure 3.52: Typical diagram explaining failure mode B (based on Viggiani, 1981)

From Equation 2.6, the failure mode B occurs, if

$$\lambda' \leq \lambda \leq \lambda''$$

$$\Rightarrow 0.183 \leq \lambda \leq 1.725$$

$$\Rightarrow 0.183 \leq \frac{l_2}{l_1} \leq 1.725$$

$$0.183l_1 \leq (10 - l_1) \leq 1.725l_1$$

$$1.183l_1 \leq 10 \leq 2.725l_1$$

$$\Rightarrow 3.670 \leq l_1 \leq 8.453$$

In this analysis, both  $l_1$  and  $l_2$  were approximated to be 5 m.

In failure mechanism B, the pile rotates as expected, with two points of inflexion where the relative direction of the pile and soil movements swaps (at about 1.0 and 8.5 m depth in Fig. 3.53). Lateral pile-soil pressures are close to the ultimate values along the full length of the pile (Fig. 3.54, in which the ultimate pressure  $11.94 c_u d$  from Randolph and Houlsby and the ultimate pressures from Fig. 3.32 including surface effects are also plotted). Figures 3.55 and 3.56 show the shear force and bending moment developed in the pile with applied boundary displacement respectively.

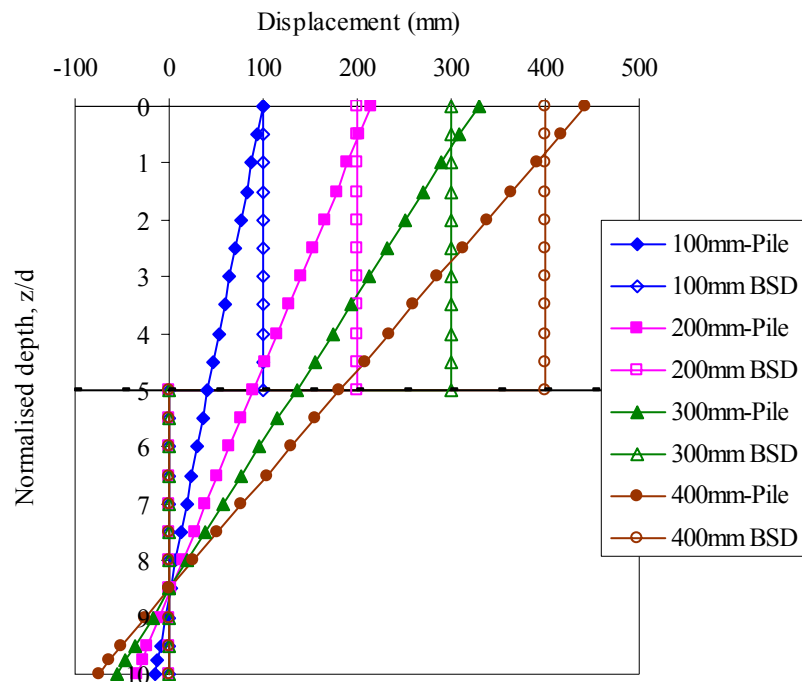


Figure 3.53: Displacement of pile with soil movement in failure mode B with applied boundary soil displacement

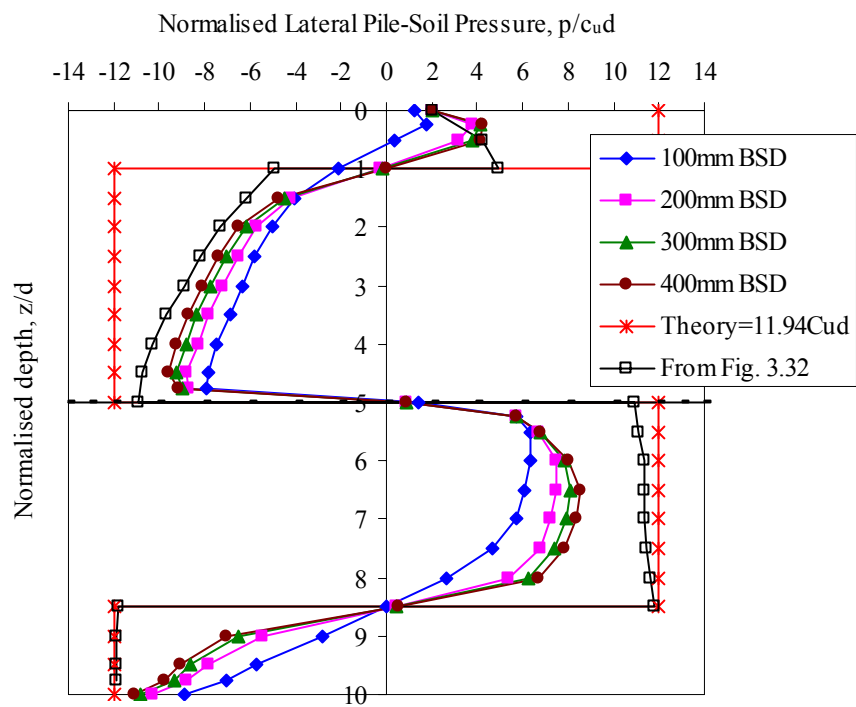


Figure 3.54: Development of normalised lateral pile-soil pressure with soil movement in failure mode B with applied boundary soil displacement

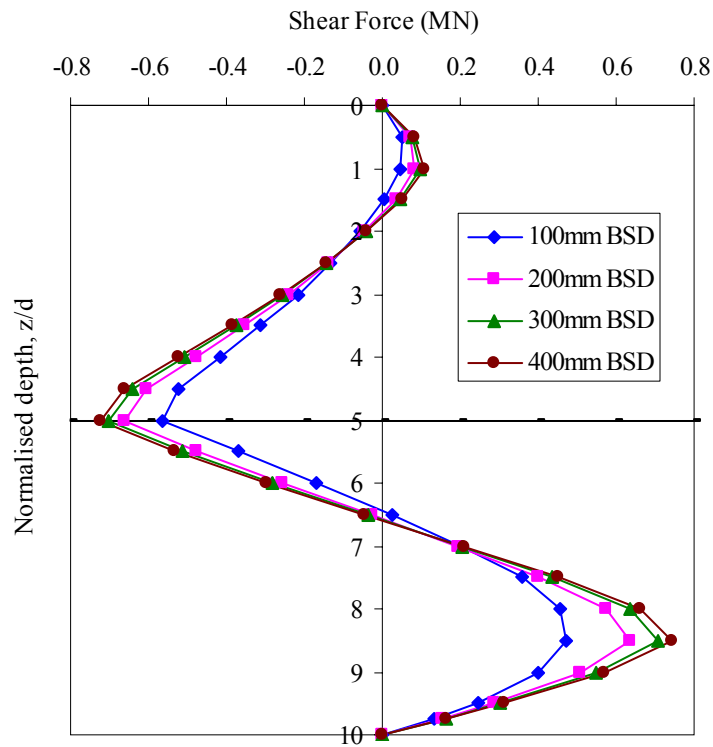


Figure 3.55: Development of shear force in the pile with soil movement in failure mode B with applied boundary soil displacement

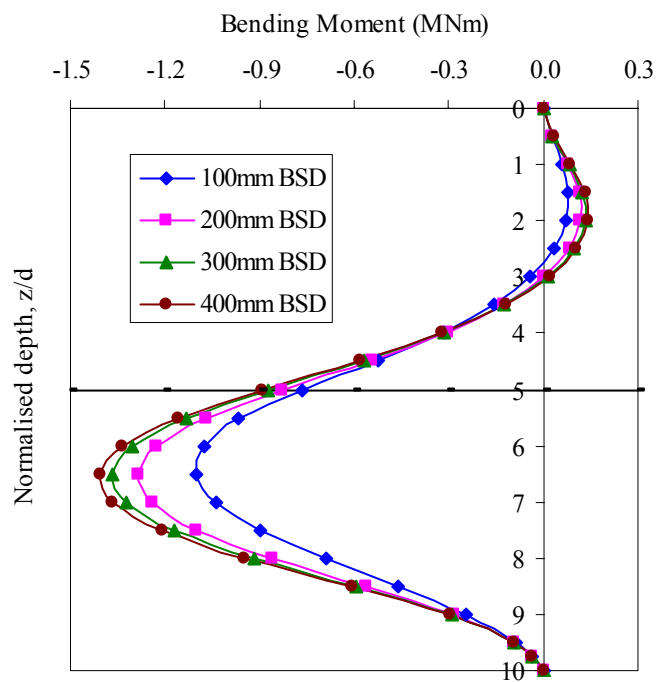


Figure 3.56: Development of bending moment in the pile with soil movement in failure mode B with applied boundary soil displacement

It is worth pointing out that the normalised lateral pile-soil pressure has not attained its theoretical ultimate value ( $11.94 c_u d$ ) for any of the failure modes (Figs. 3.43, 3.48 and 3.54). Figure 3.57(a) shows that at shallow depths the soil in front of the pile tends to move upward, because the ground surface is unconfined. As a result of this surface effect,  $p_u$  is reduced over the top 5 pile diameters or so. At ground level in all failure modes,  $p_u$  is equal to  $2 c_u d$  as in the previous analysis (Fig. 3.32). In a 3D analyses, the soil can also move beneath the pile tip (Fig. 3.57b), so the lateral pile-soil pressure may not attain the theoretical ultimate value of  $11.94 c_u d$  at the base of the pile either (Fig. 3.43). Vertical components of soil displacement are observed in Figures 3.57(b) and (c), just above and below the sliding plane. These result from the large differences in horizontal soil pressure above and below the sliding surface, and may also contribute to the lateral pile-soil pressure not attaining locally the theoretical maximum value of  $11.94 c_u d$ .

Figure 3.58 shows how the shear force in the pile at the slip plane develops with boundary soil displacement. The largest shear force is attained in mode B. The same result was reported by Poulos (1995), who concluded that stabilising piles should be designed to establish mode B behaviour. In all modes, the majority of the ultimate normalised shear force ( $T/Ac_u$ ) at the slip plane has developed by  $0.1 d$  of boundary soil displacement, indicating that in this case, with a rigid pile, the soil boundary displacement required to mobilise the full benefit of the pile is not large. In modes A and C, the increase in  $T/Ac_u$  with further displacement is small. In mode B, the increase in  $T/Ac_u$  with further boundary soil displacement is slightly more significant. This may be explained by the large pile rotation required to develop maximum pressures along the full pile shaft in this mode.

Figure 3.59 shows the normalised shear force on the slip plane as a function of the displacement of the pile top. The mode C mechanism mobilises the full shear force on the slip plane with the smallest pile displacement. This makes it an attractive arrangement for shallower slips, or where small pile displacement and serviceability are important. However, it requires an embedment of 2.3 times the depth of the slipping soil, and for a given slip would be more expensive to construct than the mode B pile which has embedment depth equal to the depth of sliding soil.

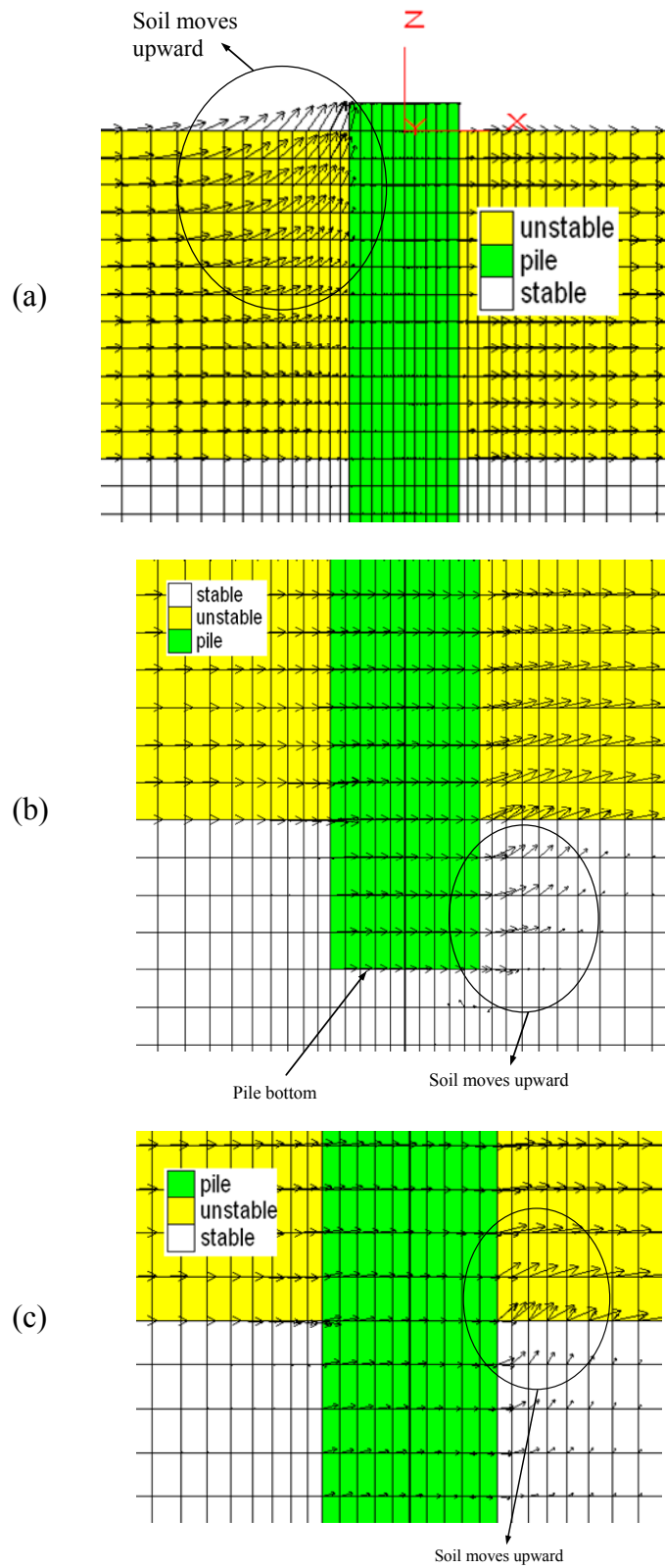


Figure 3.57: Section of the mesh showing vectors of soil and pile movement: (a) mode C; (b) mode A; and (c) mode B.



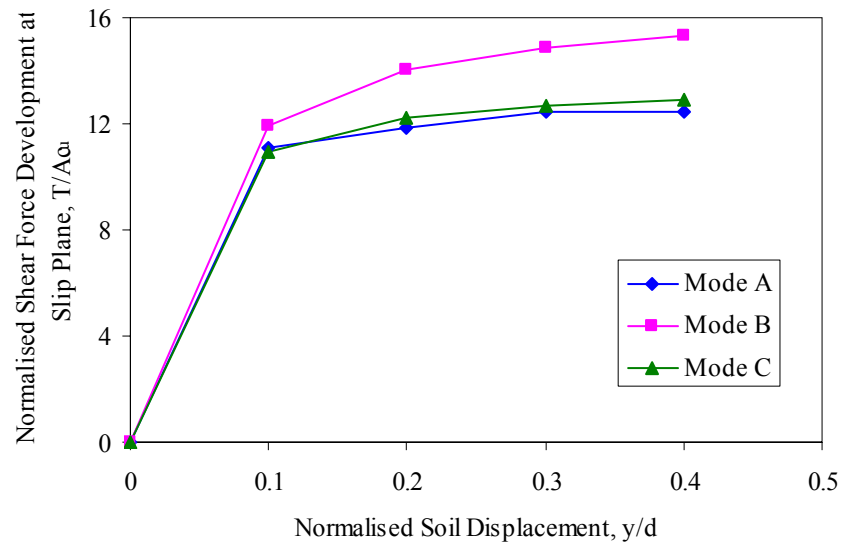


Figure 3.58: Development of shear force (absolute value) at the slip plane with boundary soil movement, where  $A=\pi d^2/4$ ,  $c_u=60$  kPa and  $d=1$  m

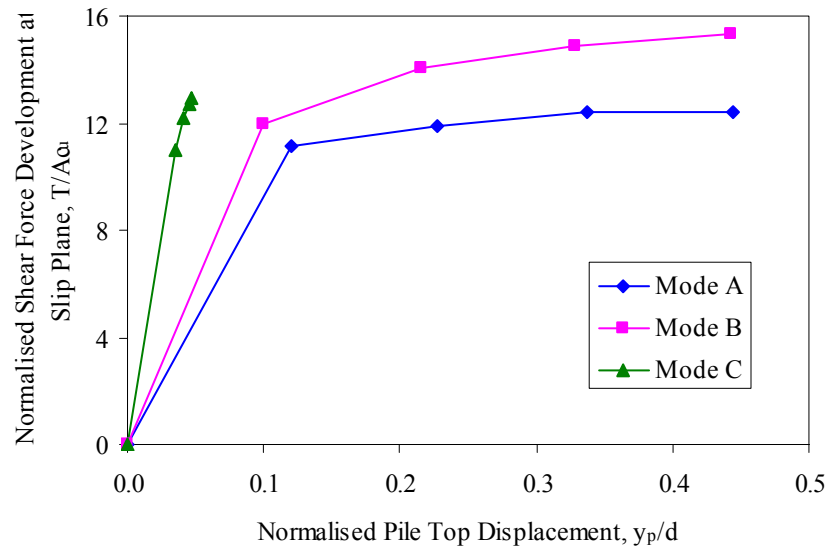


Figure 3.59: Development of shear force (absolute value) at the slip plane with pile top movement, where  $A=\pi d^2/4$ ,  $c_u=60$  kPa and  $d=1$  m

As mentioned earlier, an observation from the analyses is that the value of  $p_u$  achieved is not uniform with depth. This is most noticeable within about  $5d$  of the ground surface, where  $p_u$  is reduced owing to vertical soil movement. Viggiani (1981) suggests taking  $p_u = 0$  over the top

1.5  $d$  of the pile, following Broms (1964). The normalised maximum shear resistances calculated from the Viggiani (1981) equations (Eqs. 2.1-2.3), assuming that  $p_u = 0$  over the top 1.5  $d$  and 11.94  $c_u d$  below this, are given in Table 3.7. For mode C, this value is similar to the maximum shearing resistance calculated in the finite difference analysis. There is a larger difference for modes A and B, with the limit equilibrium equations giving a significantly greater shear force than the finite difference model. The mode A pile in  $FLAC^{3D}$  was apparently unable to develop the full 11.94  $c_u d$  below the sliding surface, which as discussed earlier may be a result of the vertical soil movements observed adjacent to the slip plane and soil movement beneath the pile toe (Fig. 3.57b). The mode B and C piles did not develop 11.94  $c_u d$  over the upper 5  $d$  owing to surface effects. For mode B, which might have been expected to develop ultimate pressures along its full length, the calculated pressures are also some distance from 11.94  $c_u d$  over the lowest 5  $d$  of the pile (Fig. 3.54). This is a consequence of the requirement for equilibrium – if the surface effects prevent development of the full 11.94  $c_u d$  over the top part of the pile, then the full 11.94  $c_u d$  is not needed and cannot be developed over the base part either. This reduces the shear force the pile is able to provide.

Mode (depth to slip surface)	A ( $H = 9\text{ m}$ )	B ( $H = 5\text{ m}$ )	C ( $H = 3\text{ m}$ )
$FLAC^{3D}$ analysis	12.42	15.32	12.93
Viggiani (1981) with no $p_u = 0$ surface adjustment	15.20	23.18	22.80
Viggiani (1981) with $p_u = 0$ surface adjustment	15.20	22.14	11.40
Viggiani (1981) with $p_u = 0$ surface adjustment / $FLAC^{3D}$ analysis	122%	145%	88%

Table 3.7: Shear resistance  $T/Ac_u$  (where  $A = \pi d^2/4$ ,  $c_u = 60\text{ kPa}$  and  $d = 1\text{ m}$ ) provided by piles calculated from Viggiani (1981) and  $FLAC^{3D}$  analyses.

One analysis was carried out in large-strain mode for mode B pile configuration, to demonstrate the actual deformation of the pile-soil system. The left and right hand soil boundaries were displaced by 200 mm, since further displacement caused an illegal geometry error. Figure 3.60 shows the deformed  $FLAC^{3D}$  mesh in which ground heave, gap formation and relative soil movement above and below the slip plane are clearly shown.

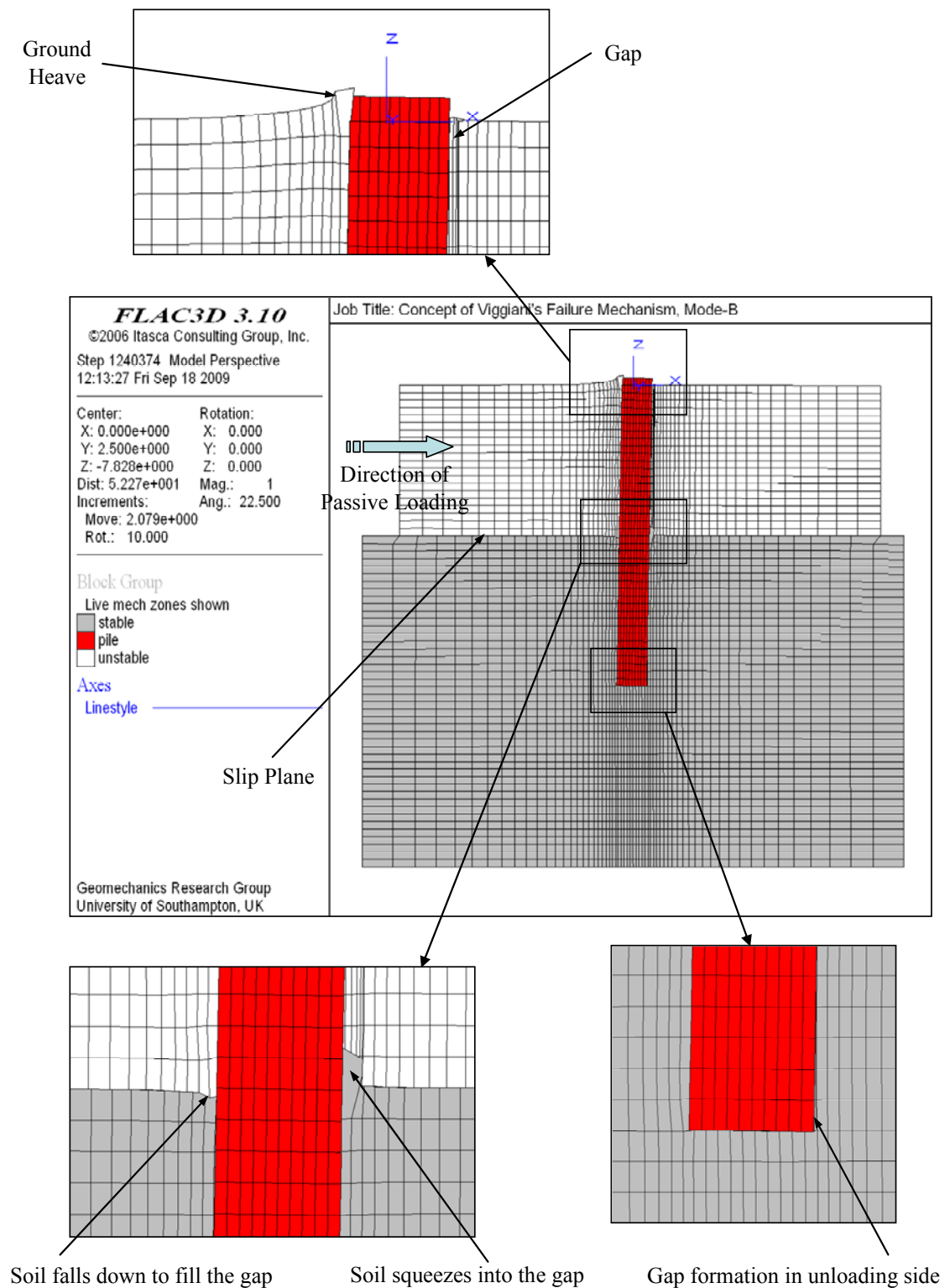


Figure 3.60: Deformed  $FLAC^{3D}$  mesh of mode B analysis, after 200 mm boundary soil displacement

### 3.9 Summary

A number of three dimensional finite difference analyses using *FLAC<sup>3D</sup>* have been carried out to investigate the response of a single pile subjected to lateral soil movements. The analyses aimed mainly to explore and verify the failure mechanisms for landslide stabilising piles categorised by Viggiani (1981).

Before Viggiani's analyses were reproduced, initial investigations were carried out to understand the variation in calculated bending behaviour of a pile with the number of tiers used to model the pile, and the influence of the strengths of the slip plane and pile-soil interfaces. It was found that the model with 40 tiers of elements can be used to represent a 10 m long pile, providing a reasonable compromise between accuracy and computing time. The analyses carried out to investigate the influence of the strength of the slip plane interface show that a well defined slip plane is obtained with zero or 0.5  $c_u$ . The behaviour of a laterally loaded pile is significantly influenced by the strength of the pile-soil interface. As Randolph and Houlsby (1984) reported, increasing the roughness of the pile-soil interface creates a bigger deforming region around the pile, leading the pile to deflect more and developing greater shear forces, bending moments and ultimate lateral pile-soil pressures. These analyses also show that the normalised ultimate lateral pile-soil pressure ( $p_u/c_u d$ ) is not reached within 5  $d$  to 8  $d$  of surface for the zero and full strength pile-soil interfaces. This is different from conventional assumptions based on proposals by Broms (1964) and Fleming *et al.* (1994).

The numerical results from models with a rigid pile, a distinct plane of sliding and a horizontal ground surface, as assumed by Viggiani, agree well with the theoretical solutions. However, three-dimensional surface effects are significant, and that both the unmodified and modified limit equilibrium approach may overestimate the lateral shearing resistance that the piles can provide. Further empirical modifications may be needed to take surface effects fully into account. Care should also be taken with mechanism A, where it may be difficult fully to mobilise  $p_u$  over the short length of pile below the sliding surface. Mode A is however an unusual pile configuration: in practice design would tend to leave a reasonable length below the failure surface, more likely resulting in B and C as failure modes. The highest shear force on the slip plane is attained in mode B and therefore stabilising piles are generally designed to establish mode B behaviour. However, mode C, with a long length embedded below the slip surface may be the preferred pile configuration to stabilise many shallower failures, as the rate of mobilisation of shear force with pile movement (as opposed to sliding soil movement) is greatest.

The *FLAC*<sup>3D</sup> analyses presented in this chapter show that the ultimate limit equilibrium mechanisms proposed by Viggiani (1981) can be replicated reasonably well in a finite difference analysis, if similar idealised horizontal ground and slip surfaces, uniform soil movement, and undrained shear strength properties, and a rigid pile are adopted.

## **Chapter - 4: Extended Analyses on the Failure Mechanisms of Single Laterally Loaded Pile**

### **4.1 Introduction**

The numerical analyses presented in Section 3.8 have some limitations. The first notable limitation is that the interface elements representing the slip plane were assigned zero strength to represent a situation where the unstable layer can slip perfectly over the stable layer, as considered by Viggiani (1981). However, in a real slope, any pre-existing slip planes generally have non-zero strength. The behaviour of a single pile with increasing strength on the slip plane is analysed first in this chapter. These analyses give a better understanding of how relative movement between unstable and stable soil layers influences the behaviour of the laterally loaded pile.

The second major limitation of the analyses presented in Section 3.8 is that the ground surface was assumed to be horizontal. However, in reality the ground is more likely to be sloping and this could influence the development of lateral pile-soil pressures. To overcome this limitation, the behaviour of single pile in an infinitely long slope is analysed and then a pile in a finite slope. All the analyses were carried out with a defined slip plane within the slope.

### **4.2 Pile behaviour with increasing strength of the slip plane**

In the analyses presented in Section 3.8, zero strength ( $c_{int} = 0$ ) was used on the slip plane, replicating the perfect sliding plane assumed by Viggiani (1981). In reality, even if a slip is identifiable it is likely to have a reduced but non-zero shear strength. The strength of the slip plane is likely to influence the pattern of relative movement between the unstable and stable soil layers. In many slope failures movements above and just below the failure surface are observed to be non-uniform (Leroueil *et al.*, 1996; Smethurst and Powrie, 2007).

The effect on the behaviour of the pile during lateral loading and at the ultimate state was investigated by carrying out the analyses with an increased slip plane strength, and the results are compared with those obtained for slip plane interface elements of zero strength (Section 3.8.6).

### 4.2.1 *FLAC*<sup>3D</sup> analyses

The *FLAC*<sup>3D</sup> model used in Section 3.8 was modified to carry out two further analyses for each of Viggiani's (1981) failure modes A, B and C. Two different slip plane shear strengths were used:

Case 1:  $c_{int}/c_u = 0.5$  (half strength, where  $c_u = 30$  kPa), and

Case 2:  $c_{int}/c_u = 1$  (full strength).

### 4.2.2 Results and discussion

The computed deflection, normalised lateral pile-soil pressure, shear force and bending moment are plotted for the different values of normalised interface shear strength for modes A, B and C. Figure 4.1 shows the deflection of the pile with interface shear strength for mode A. The relative movement between the unstable and stable soil layers on the interface, and hence the movement of the pile toe at a given soil boundary displacement decrease as the strength of the slip plane interface increases. This behaviour is demonstrated in Figure 4.5, in which the soil movement on the symmetrical mesh boundary 5 m from the pile centre is plotted against depth for mode A. When the interface strength is equal to the strength of the unstable soil, the nodes on the interface slip plane move by only 13.6 mm for 400 mm of boundary soil displacement. The movement of the nodes at the slip plane increases with reducing interface strength and is similar to the soil boundary movement (about 400 mm) when the interface strength is zero.

Figure 4.1 shows that the pile rotates more as the strength of the slip plane increases, and the amount of rigid body translation is reduced. This is an inevitable consequence of the restriction on pile translation associated with smaller relative movements between the soil layers. The normalised lateral pile-soil pressures for the analyses having different interface strengths are shown in Figure 4.2 for mode A. These match the observed pile deflections in that the lateral pile-soil pressures developed for  $c_{int}/c_u = 0$  and 0.5 are similar, while there is some slight difference in distribution for  $c_{int}/c_u = 1$ .

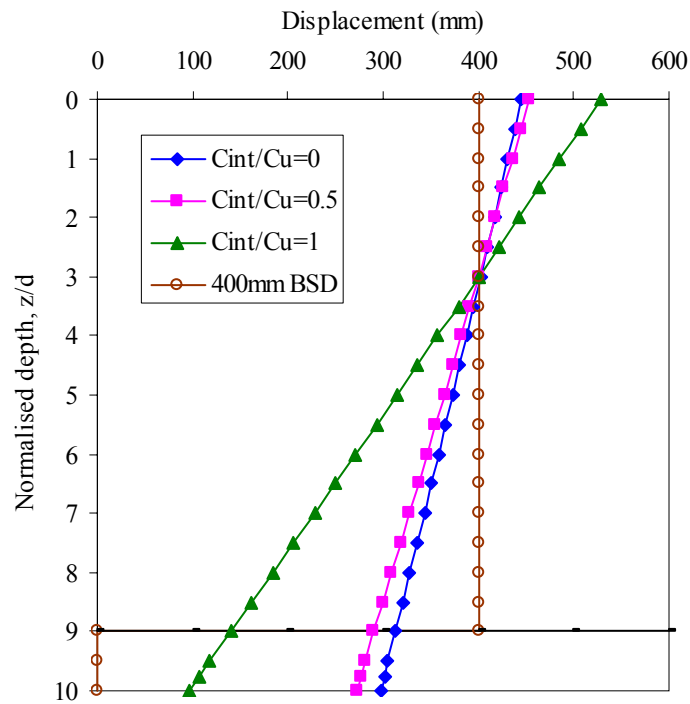


Figure 4.1: Movement of pile versus depth for three different slip plane strengths, for mode A at 400 mm of boundary soil movement

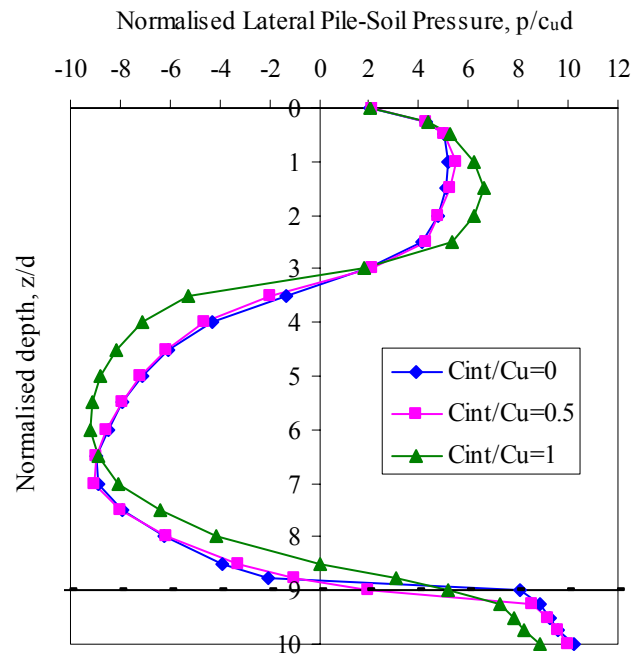


Figure 4.2: Normalised lateral pile-soil pressures versus depth for three different slip plane strengths, for mode A at 400 mm of boundary soil movement



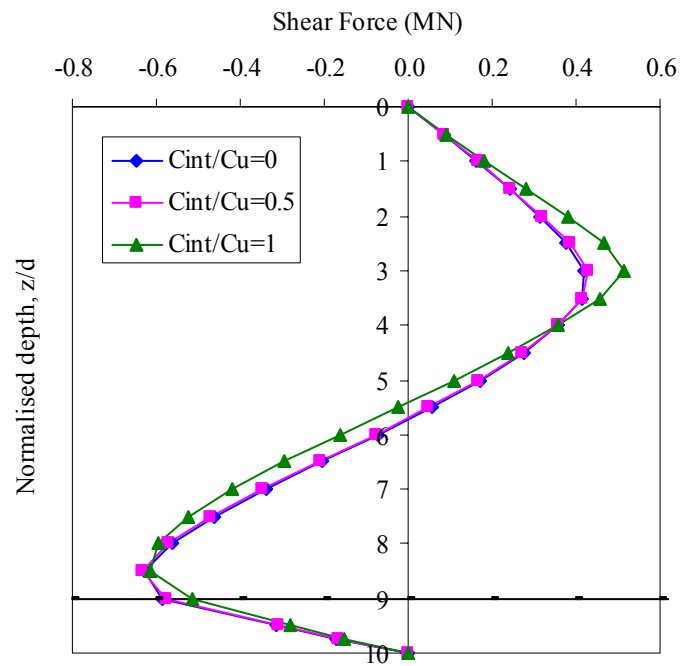


Figure 4.3: Pile shear forces versus depth for three different slip plane strengths, for mode A at 400 mm of boundary soil movement

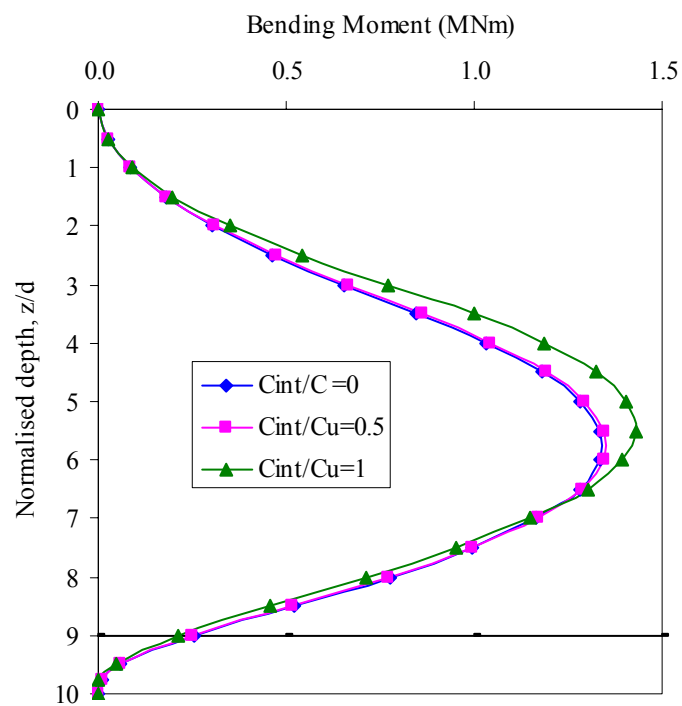


Figure 4.4: Bending moments developed in pile versus depth for three different slip plane strengths, for mode A at 400 mm of boundary soil movement

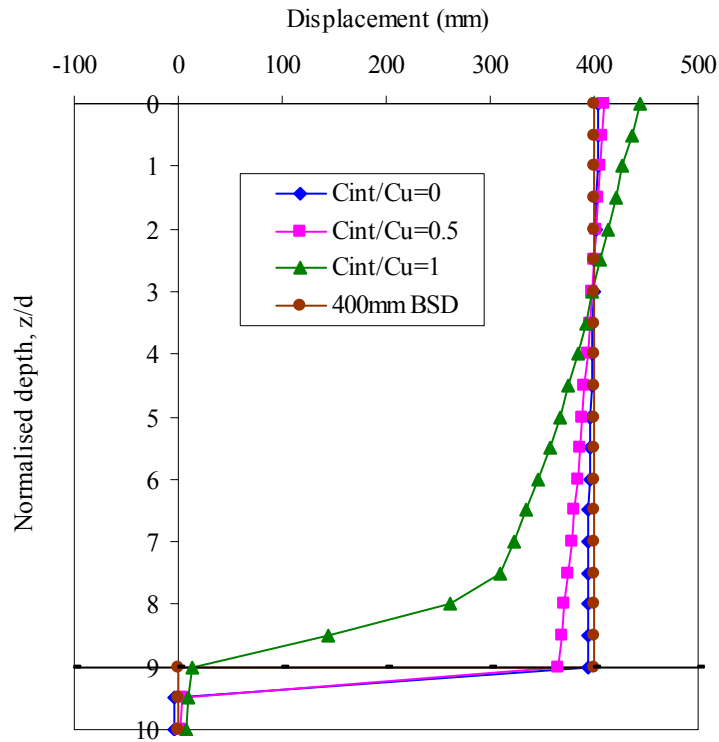


Figure 4.5: Soil movement calculated at 5 m distance from pile centre in y-direction for mode A at 400 mm of boundary soil displacement

Pile deflections after 400 mm of boundary soil movement for different slip plane strengths in mode B are shown in Figure 4.6. The pile top movement exceeds the boundary soil movement when the slip plane interface has zero strength. This behaviour is reflected in the normalised lateral pile-soil pressure graph (Fig. 4.7), in which a reverse lateral pile-soil pressure is developed over the top 1 m of the pile. This reverse pressure is lost as the slip plane strength is increased. Again, as the interface strength increases the relative movement between the soil layers becomes less distinct (Fig. 4.10) leading to a reduction in the lateral pile-soil pressure attained immediately above the slip surface. Correspondingly, the rotation of the pile reduces with increasing slip plane strength and the mechanism changes from mode B into something approaching mode C (Figs. 4.12-4.15).

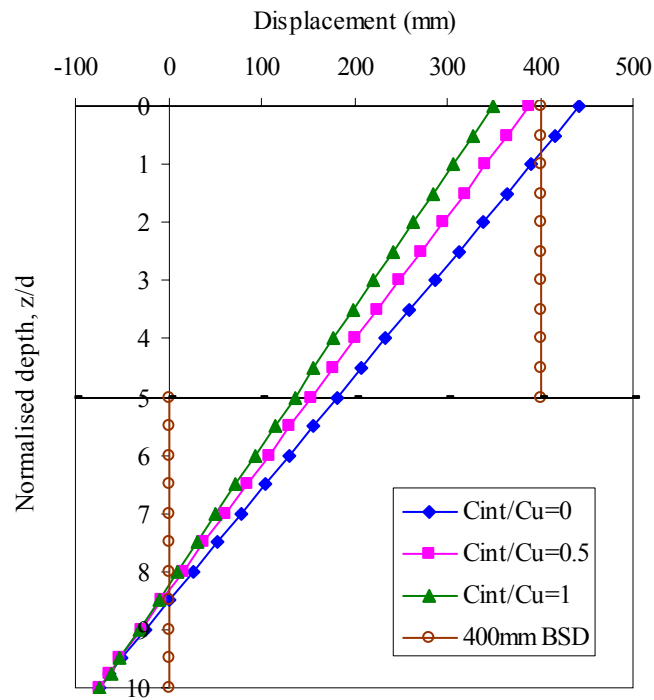


Figure 4.6: Movement of pile versus depth for three different slip plane strengths, for mode B at 400 mm of boundary soil movement

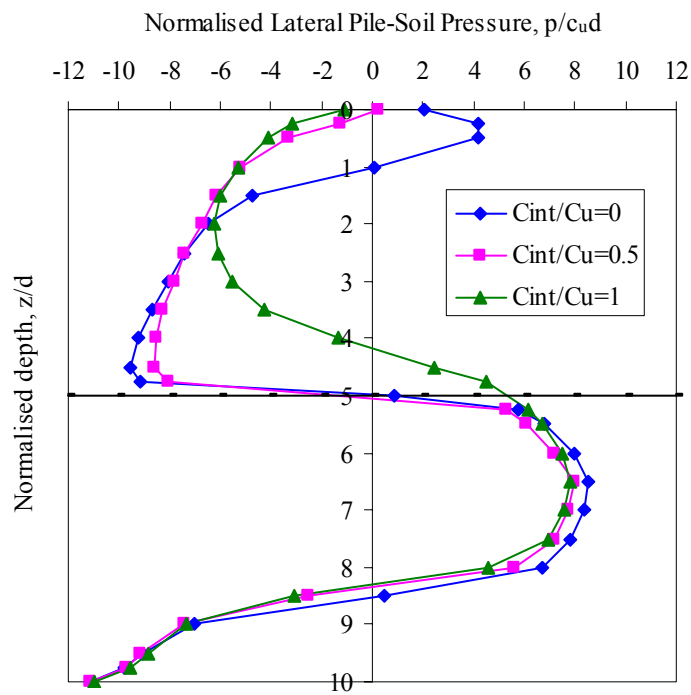


Figure 4.7: Normalised lateral pile-soil pressures versus depth for three different slip plane strengths, for mode B at 400 mm of boundary soil movement

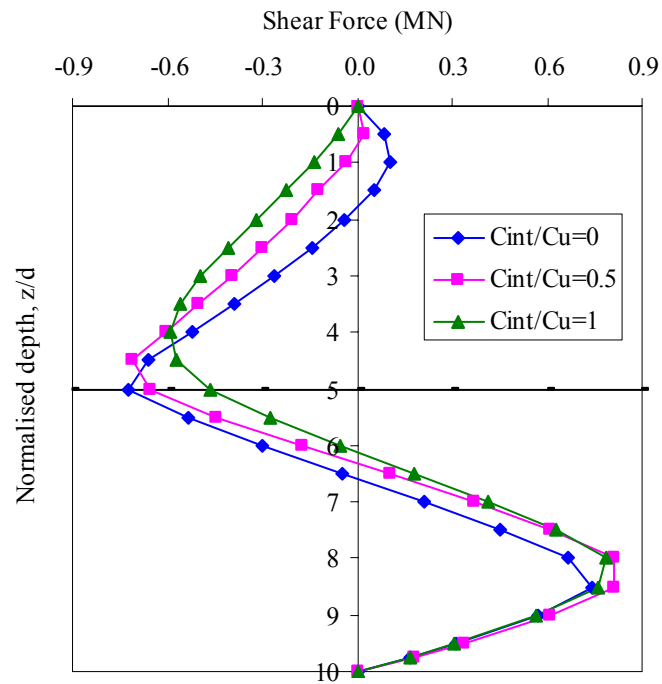


Figure 4.8: Pile shear forces versus depth for three different slip plane strengths, for mode B at 400 mm of boundary soil movement

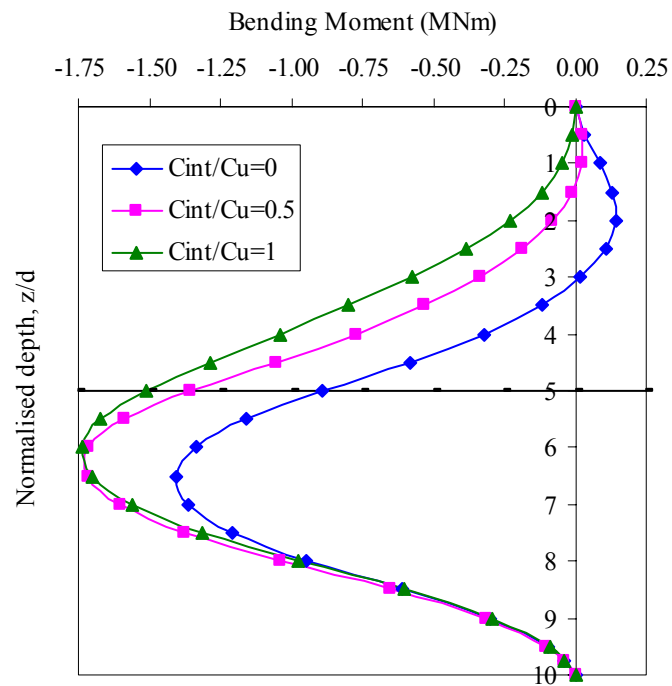


Figure 4.9: Bending moments developed in pile versus depth for three different slip plane strengths, for mode B at 400 mm of boundary soil movement

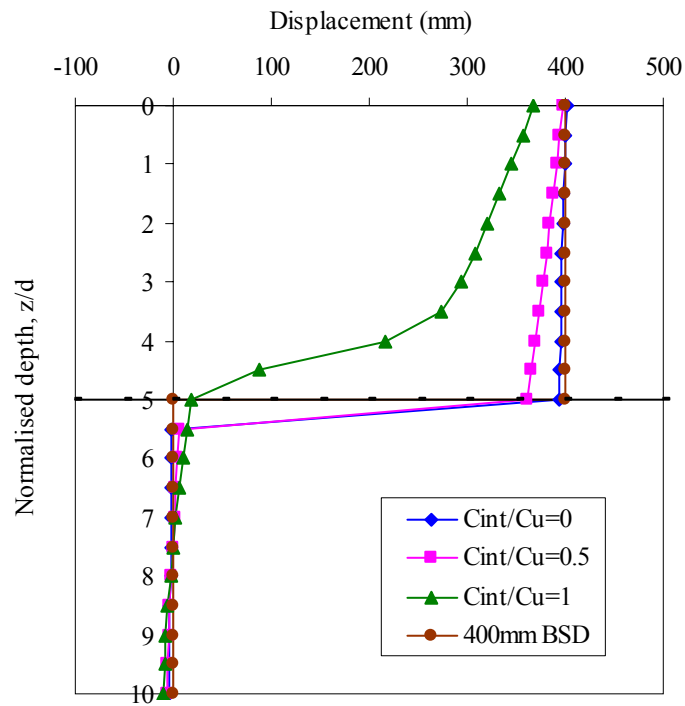


Figure 4.10: Soil movement calculated at 5 m distance from pile centre in y-direction for mode B at 400 mm of boundary soil displacement

In mode C, increasing the slip surface shear strength reduces pile movements, lateral pile-soil pressures, shear forces and bending moments (Figs. 4.12-4.15). The changes from  $c_{int}/c_u = 0$  to  $c_{int}/c_u = 0.5$  are relatively small (e.g. the pile top displacement is reduced very slightly from 46.7 mm to 45.1 mm), but the changes as  $c_{int}/c_u$  is increased for 0.5 to 1 are large (e.g. pile top displacement reduced from 45.1 mm to 23.2 mm).

In all three modes, finite difference models with increased slip plane strength show less movement on the sliding surface, giving a profile of soil movement that decreases with depth. The biggest differences in the soil movement profiles occur as  $c_{int}/c_u$  changes from 0.5 to 1.0. The largest changes in pile rotation, normalised pressure, bending moment and shear force also occurs for the change in  $c_{int}/c_u$  from 0.5 to 1.0, except for mode B, where the larger difference occurs for  $c_{int}/c_u$  from 0 to 0.5. The resistance that the pile is able to provide to soil movement is reduced as  $c_{int}/c_u$  increases, for the same boundary displacement of 400 mm.

The mode C mechanism is most influenced by the change in strength on the failure surface. For the full strength slip plane, mode C is more likely to fail by passive and active wedge failures at the displacement boundaries, rather than a ‘block’ failure with the section of unstable soil sliding over the underlying stable soil. This is probably because of the nature and position of boundary locations in this analysis, combined with a shallow depth of unstable soil layer. If in the mode C analysis the soil layer were deeper and the boundary locations were wider, it is possible that there would be less influence on the shear force and bending moment developed in the pile.

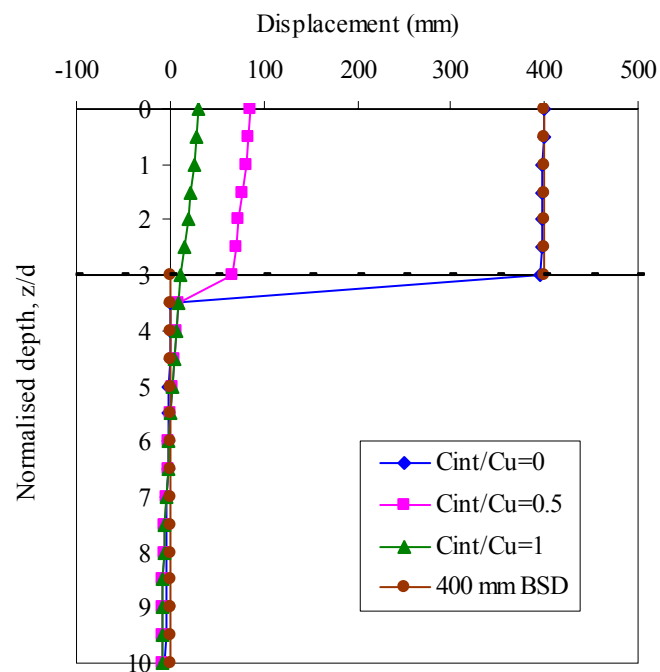


Figure 4.11: Soil movement calculated at 5 m distance from pile centre in y-direction for mode C at 400 mm of boundary soil displacement

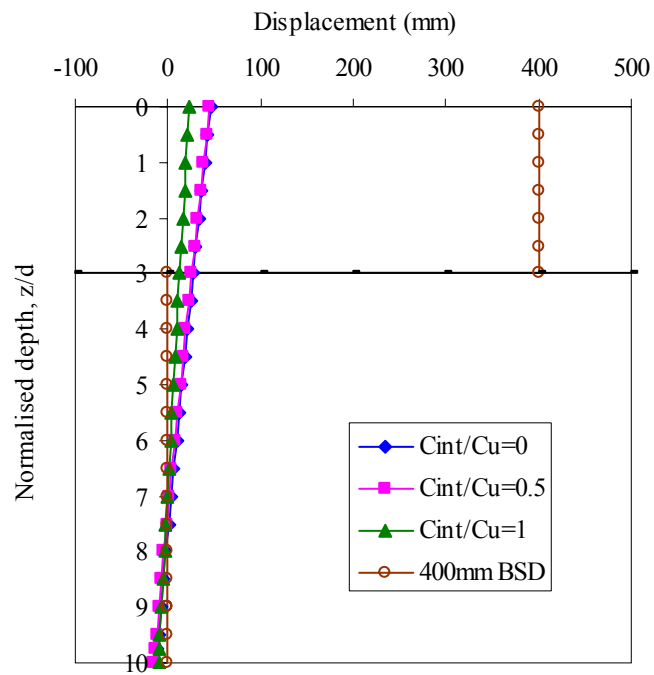


Figure 4.12: Movement of pile versus depth for three different slip plane strengths, for mode C at 400 mm of boundary soil movement

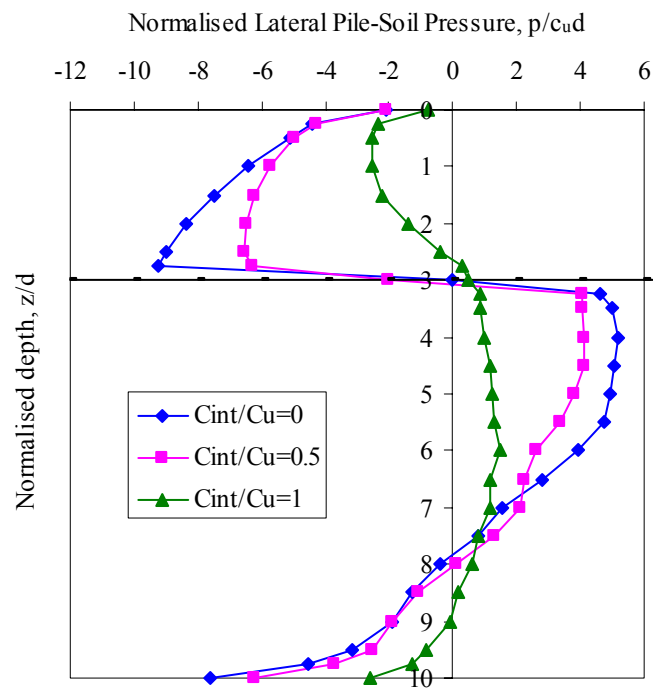


Figure 4.13: Normalised lateral pile-soil pressures versus depth for three different slip plane strengths, for mode C at 400 mm of boundary soil movement

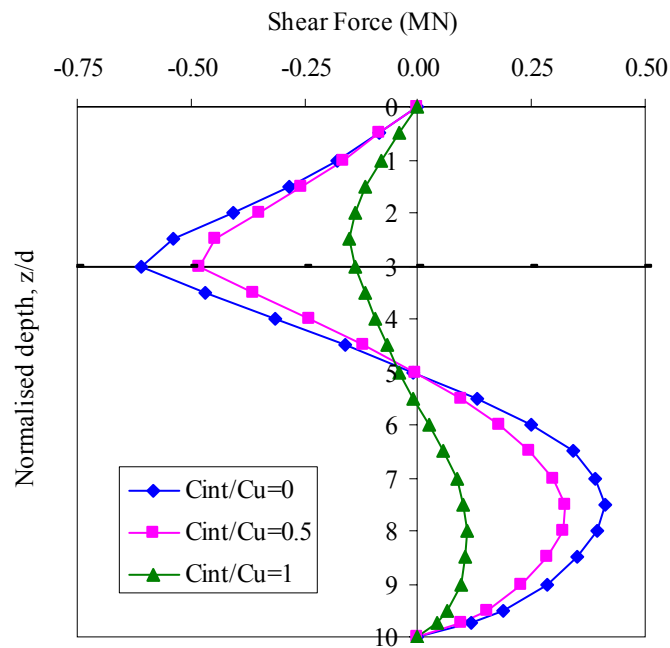


Figure 4.14: Pile shear forces versus depth for three different slip plane strengths, for mode C at 400 mm of boundary soil movement

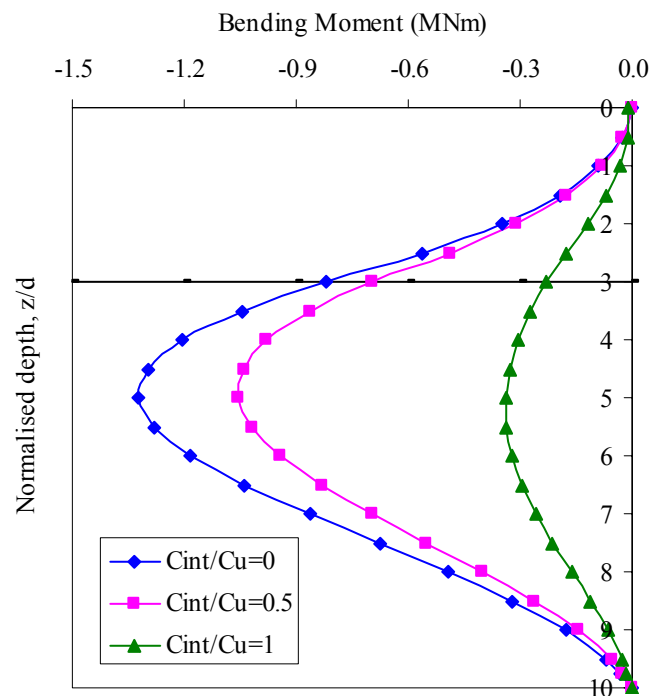


Figure 4.15: Bending moments developed in pile versus depth for three different slip plane strengths, for mode C at 400 mm of boundary soil movement



Figure 4.16 shows the variation in shear force developed within the pile section at the depth of the slip plane with strength of the slip plane. The normalised shear force developed at the slip plane decreases as the normalised slip plane strength  $c_{int}/c_u$  increases from 0 to 1 in all three failure modes. In general, the mode B pile configuration is used for stabilisation pile designs as it usually provides a greater resistance against the laterally moving soil for a given slip plane strength.

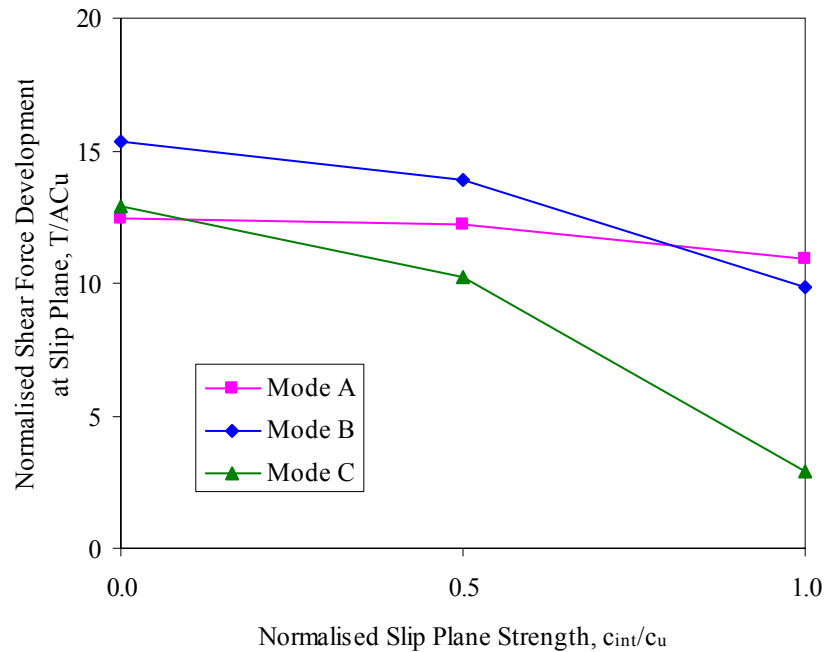


Figure 4.16: Development of shear force (absolute value) at the slip plane with strength of the slip plane; where  $A=\pi d^2/4$ ,  $c_u=60$  kPa and  $d=1$  m

In summary, the analyses show that the behaviour of the laterally loaded pile is significantly influenced by the strength of the slip plane. Generally, a higher slip plane strength leads to a smaller relative soil movement between the unstable and stable soil layers, and this changes the behaviour of the pile.

### 4.3 Behaviour of the pile in an infinite slope

The behaviour of a laterally loaded pile installed in an infinite slope is analysed. The aim of these analyses is to investigate the influence of a sloping ground surface and the strength of the slip surface on the pile behaviour in the ultimate state. This more closely represents the application of laterally loaded piles to slope stabilisation.

#### 4.3.1 *FLAC<sup>3D</sup>* analyses

The *FLAC<sup>3D</sup>* mesh used to carry out the analyses of the 14° inclined slope is shown in Figure 4.17. A 5 m upper sliding soil layer was created above a lower stable soil layer to provide a geometrical arrangement equivalent to Viggiani's mode B, except for the orientation of the ground and slip planes. The interface attachment and pile installation procedures, initial and boundary conditions, and constitutive models and material properties were the same as in Section 3.8. The pile-soil interfaces were given full strengths.

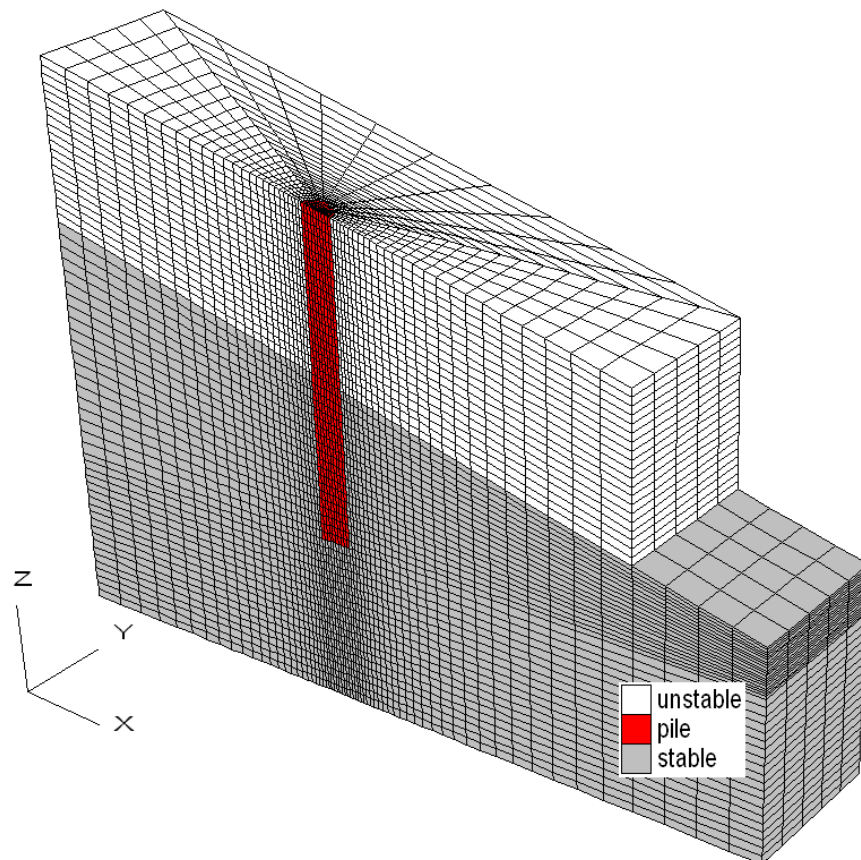


Figure 4.17: *FLAC<sup>3D</sup>* slope model with 14° slope angle. The model has been rotated for a better three dimensional view.

A slightly different approach was necessary in these analyses during the application of gravity loading, because if the model is gravity loaded with the actual soil properties applied it does not come into equilibrium and the soil starts to move along the slip plane. To prevent instability during gravity loading, high shear and tensile strengths were temporarily assigned to both soil layers, which were then reduced to their actual values once the self weight stresses had been initialised in the mesh.

Two different cases are considered in this section.

Case 1: Pile behaviour with slope angle, with the slip plane strength ( $c_{int}$ ) assumed to be zero.

Case 2: Pile behaviour with slip plane strength, where only the slope with a  $22^\circ$  slope angle is considered.

### 4.3.2 Results and discussion

#### 4.3.2.1 Behaviour of the pile with slope angle (slip plane strength = 0)

Two different slope geometries with a ground and sliding surface at  $14^\circ$  (Fig. 4.18) and  $22^\circ$  (Fig. 4.19) to the horizontal were considered. The behaviour of the piles in the sloping ground is compared with that of the piles in level ground in Figures 4.20-4.23. The deflection of the pile is not much affected by the  $14^\circ$  slope, but is increased significantly by the  $22^\circ$  slope. The boundary soil displacements plotted in Figure 4.20 are horizontal  $x$ -direction displacements, and not the displacements along the slip plane.

This increased pile deflection is associated with a larger movement of the soil downslope of the pile. Since the slip plane has zero strength, the soil downslope of the pile has a higher tendency for slippage despite the displacement control on the right hand boundary; thus it offers less resistance to the pile, particularly over the top 1 m, and the pile deflects more (Fig. 4.20). The ultimate lateral pile-soil pressure at ground level, which acts in the reverse direction (upslope) on the top of the pile, is reduced below  $2 c_u d$  as the slope angle increases. In flat ground, where there is better ‘downslope’ support, the pile develops slightly greater shear forces and bending moments (Figs. 4.22 and 4.23). However, there is little difference in the shear forces and bending moments developed in the pile portion below the slip plane.

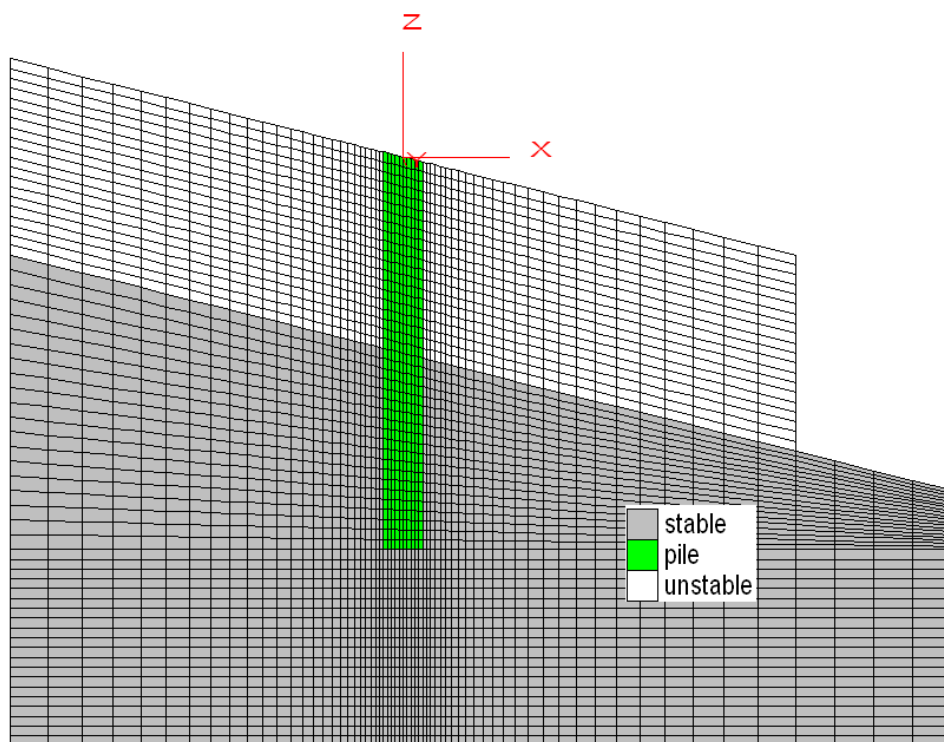


Figure 4.18:  $FLAC^{3D}$  slope model with 14 degrees slope angle

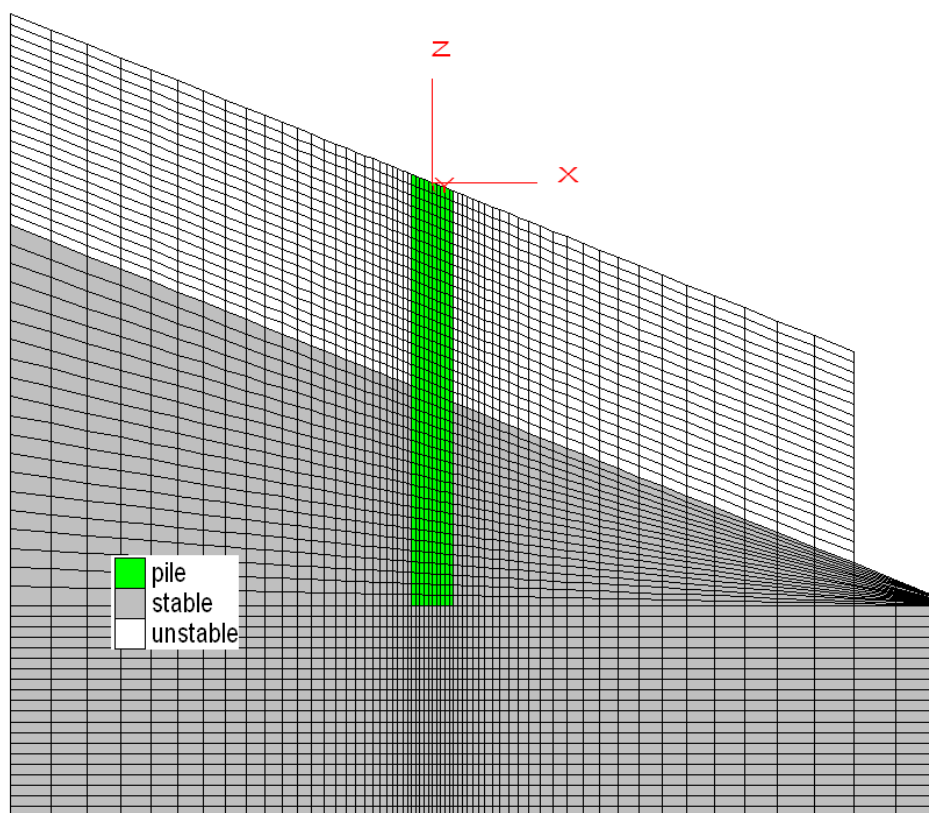


Figure 4.19:  $FLAC^{3D}$  slope model with 22 degrees slope angle

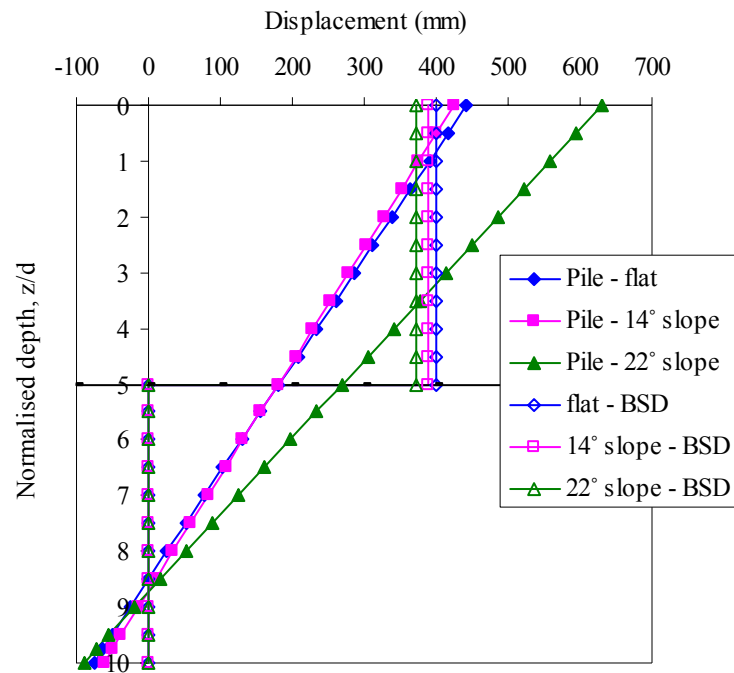


Figure 4.20: Movement of pile versus depth for different slope angles at 400 mm of boundary soil movement along the slope

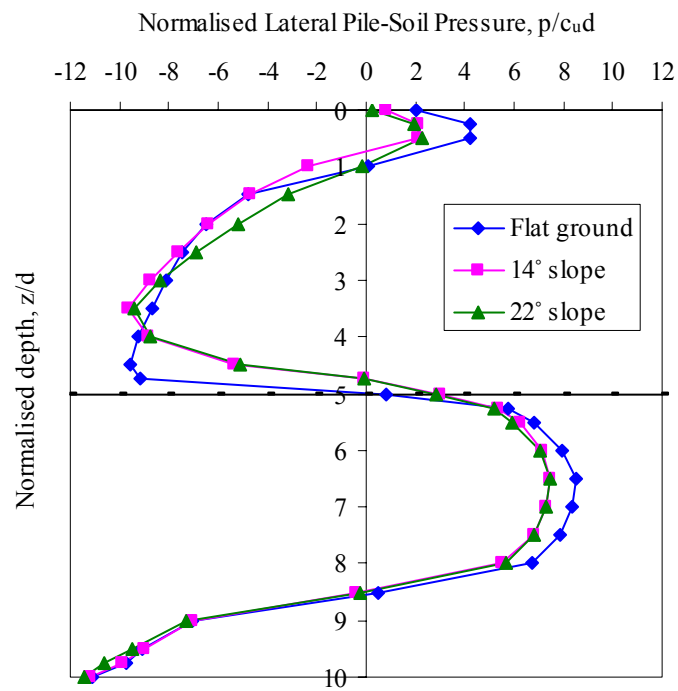


Figure 4.21: Normalised lateral pile-soil pressure versus depth for different slope angles at 400 mm of boundary soil displacement along the slope

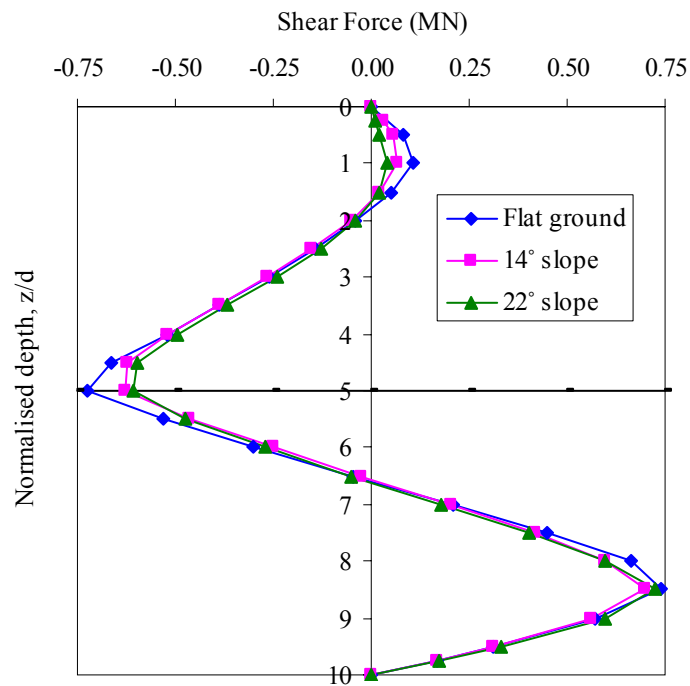


Figure 4.22: Pile shear forces versus depth for different slope angles at 400 mm of boundary soil displacement along the slope

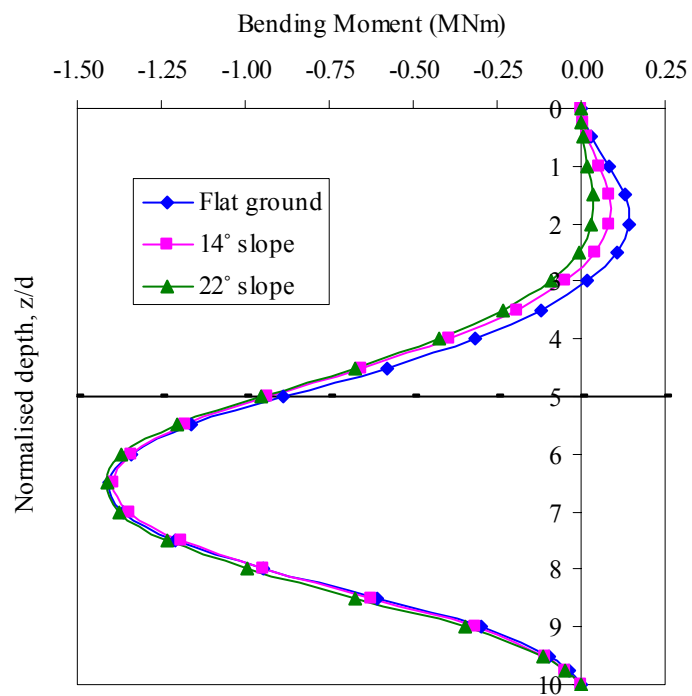


Figure 4.23: Bending moment developed in pile versus depth for different slope angles at 400 mm of boundary soil displacement along the slope

These analyses indicate that a sloping surface is only significant above a certain angle; for shallow slopes, the pile behaves in the same way as for horizontal ground. However, the magnitude of the ‘significant’ slope angle may be influenced by the stability of the slope, and this in turn is influenced by the unit weight of the soil ( $\gamma$ ), the depth of the slip plane from the slope surface ( $d$ ), and the strength of the slip plane ( $c_{int}$ ) for an undrained analysis (Eq. 4.1).

For a unit length down a slope at an angle  $\beta$  to the horizontal (Fig. 4.24),

$$\text{Weight of the block of soil ABCD, } W = \gamma d \cos \beta$$

$$\text{Shear stress acting on the plane CD, } \tau = W \sin \beta = \gamma d \cos \beta \sin \beta$$

$$\text{Factor of safety on slope stability, } FoS = \frac{\tau_{int}}{\tau} = \frac{\tau_{int}}{\gamma d \cos \beta \sin \beta} \quad \text{Equation 4.1}$$

where,

$\tau_{int}$  = available shear strength (for  $\phi = 0$  analysis,  $\tau_{int} = c_{int}$ )

$\tau$  = mobilised shear strength

$$\text{Slope to be stable, } FoS > 1 \Rightarrow \frac{\tau_{int}}{\tau} > 1 \quad \text{Equation 4.2}$$

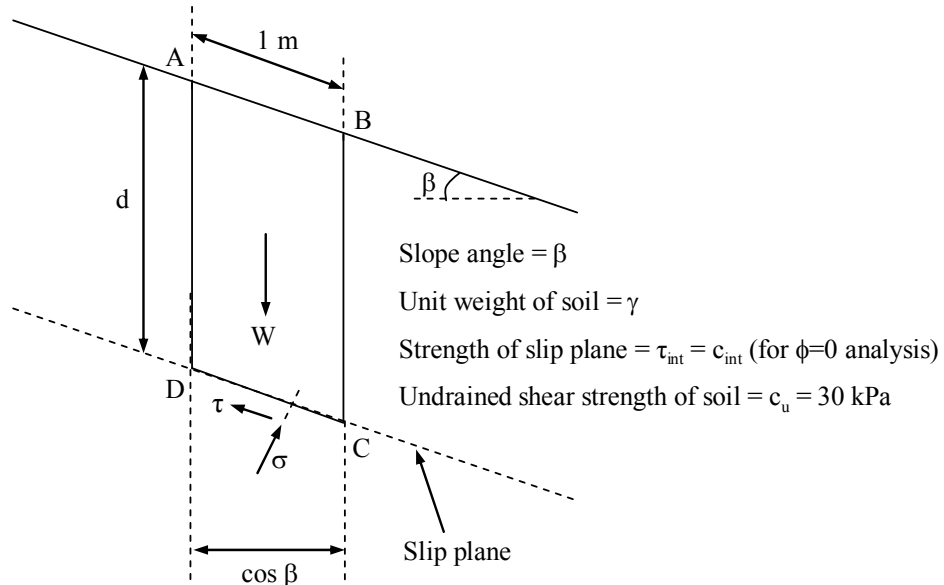


Figure 4.24: Diagram showing the stresses acting on the plane at a depth  $d$  below the ground level in an infinite slope (reproduced from Powrie, 2004)

Simple calculations were carried out using an EXCEL spreadsheet to demonstrate the effect of the unit weight of the soil, the depth of the slip plane from the slope surface, and the slip plane strength on the stability of the slope. According to Equation 4.1, for an infinite slope in undrained conditions (with no pile), the slope is always unstable when the strength of the slip plane is zero. Therefore, a generic case was chosen in which the strength of the slip plane was assumed to be 30 kPa (i.e.  $c_{int}/c_u = 1$ ), and the effect of the unit weight of the soil and the depth of the slip plane on the stability of the slope was investigated.

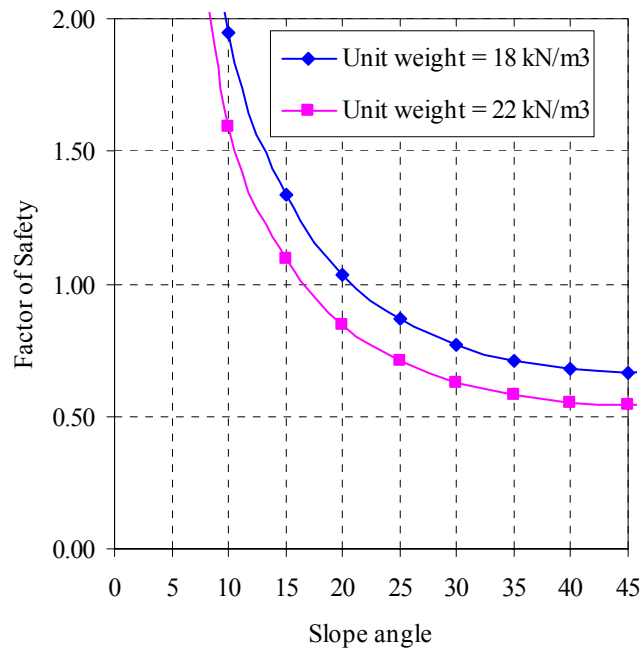


Figure 4.25: The effect of the unit weight of the soil on the stability of the slope, where  $c_{int}/c_u = 1$  and  $d = 5 \text{ m}$

Figure 4.25 shows how the factor of safety (FoS) of slope varies with the unit weight of the soil ( $\gamma$ ). When  $\gamma = 18 \text{ kN/m}^3$ , the slope is stable up to a slope angle around  $21^\circ$ . However, the maximum stable slope angle reduces to about  $17^\circ$  when  $\gamma$  increases to  $22 \text{ kN/m}^3$ . Therefore, it can be said that the stability of the slope (or the magnitude of the slope angle where the slope can be stable) is dependent on the unit weight of the soil.

The influence of the depth of the slip plane on the stability of an infinite slope is shown in Figure 4.26. Increasing the depth  $d$  leads to a reduction of the stability of the slope. For the slope to be stable, the slope angle  $\beta$  should be less than  $21^\circ$  and  $12^\circ$  for the cases  $d = 5 \text{ m}$  and  $d = 8 \text{ m}$ , respectively.



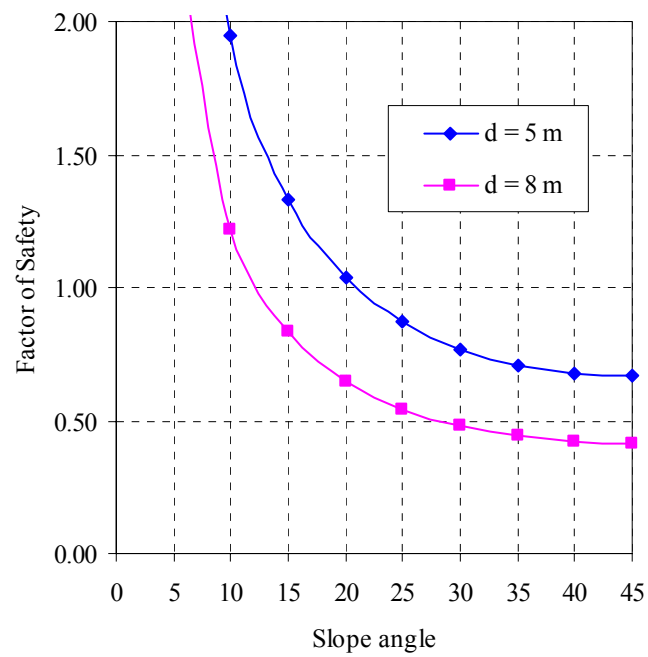


Figure 4.26: The effect of the depth of the slip plane from the slope surface on the stability of the slope, where  $c_{int}/c_u = 1$  and  $\gamma = 18 \text{ kN/m}^3$

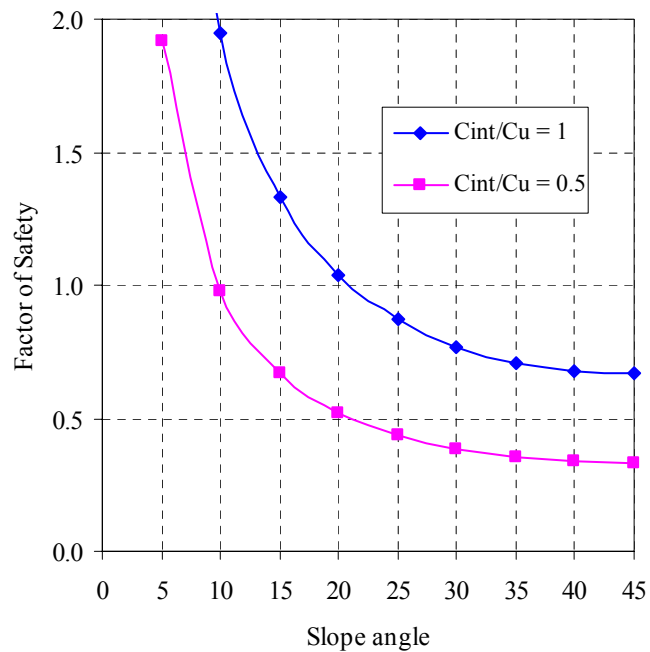


Figure 4.27: The effect of the strength of the slip plane on the stability of the slope, where  $\gamma = 18 \text{ kN/m}^3$  and  $d = 5 \text{ m}$

The third and last factor influencing the stability of the slope is the strength of the slip plane. A simple EXCEL spreadsheet calculation was again carried out and the result is shown in Figure 4.27. When the strength of the slip plane is equal to 30 kPa (i.e.  $c_{int}/c_u = 1$ ), the slope appears to be stable for a slope angle less than around  $21^\circ$ . However, when the strength of the slip plane reduces to 15 kPa, the slope appears to be stable for a slope angle less than around  $10^\circ$ .

From these simple spreadsheet analyses, it can be concluded that the magnitude of the 'significant' slope angle where an infinite slope can be stable in undrained condition is dependent on three parameters: the unit weight of the soil, the depth of the slip plane, and the strength of the slip plane. However, these analyses demonstrate only the stability of a general slope, not of a piled slope. The behaviour of an infinite piled slope with the strength of the slip plane is investigated numerically in Section 4.3.2.2.

#### 4.3.2.2 Behaviour of the pile with slip plane strength (slope angle = $22^\circ$ )

The analyses presented in this section show the effect of slip plane strength on the behaviour of a pile placed in an infinite slope with a  $22^\circ$  slope angle. Figure 4.28 shows the deflection of the pile and the soil movement on a vertical line through a point located 1 m from the pile centre in  $y$ -direction after a boundary soil displacement of 400 mm along the slip plane. The deflection of the pile is quite large when  $c_{int}/c_u = 0$ , compared with  $c_{int}/c_u = 0.5$  and 1, where  $c_u = 30$  kPa. As discussed in Section 4.2, a low slip plane strength leads to a greater downslope soil slippage and thus the pile rotates more due to the lack of downslope support. In this case, the soil movement adjacent to the pile row is larger than the applied boundary displacement.

Figure 4.29 shows the normalised lateral pile-soil pressure developed in the pile for different slip plane strengths. This is consistent with Figure 4.28, in which the reversed pressure is developed over the top 1 m of the pile as the pile movement exceeds the soil movement. The bending moment developed over the pile portion in the unstable soil layer is largest for  $c_{int}/c_u = 0.5$ , and not for  $c_{int}/c_u = 0$ . Although the pile head deflection exceeds the soil movement for  $c_{int}/c_u = 0$ , the overall resistance provided by the soil downslope of the pile is likely to be less for  $c_{int}/c_u = 0$ , than for  $c_{int}/c_u = 0.5$ .

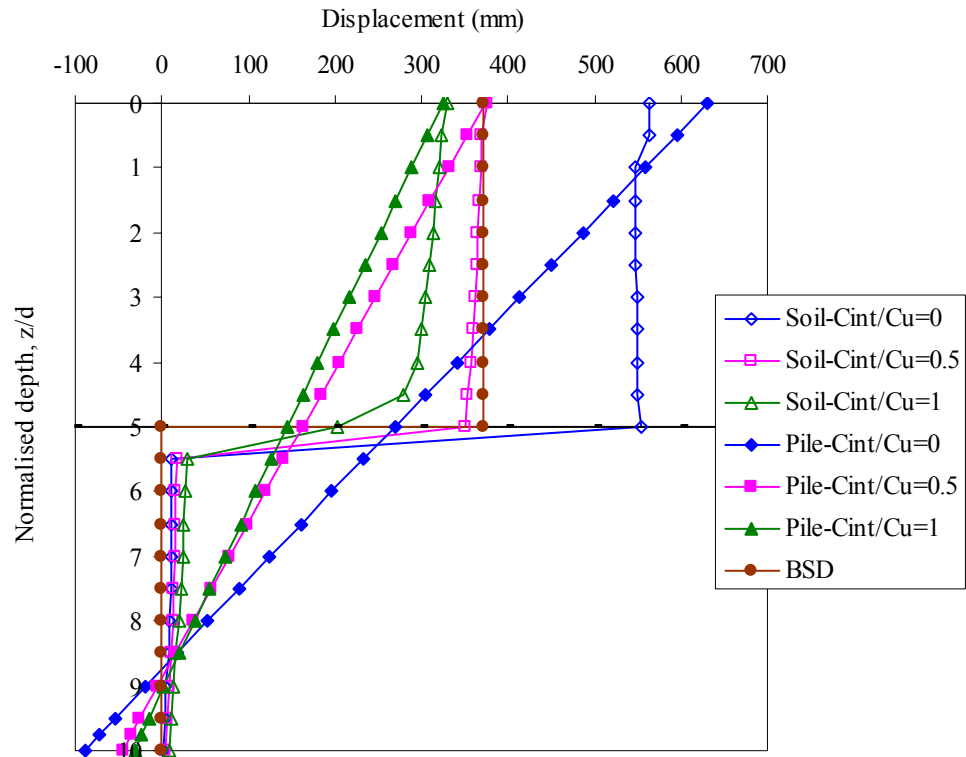


Figure 4.28: Deflection of pile and soil movement on a vertical line through a point located 1 m from pile centre in y-direction, for three different slip plane strengths at 400 mm of boundary soil displacement along the slope

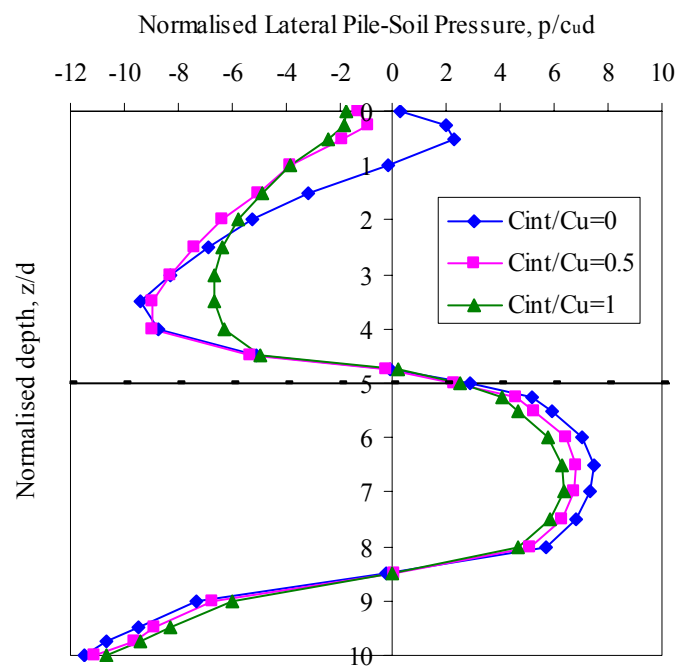


Figure 4.29: Normalised lateral pile-soil pressure versus depth for three different slip plane strengths at 400 mm of boundary soil displacement along the slope

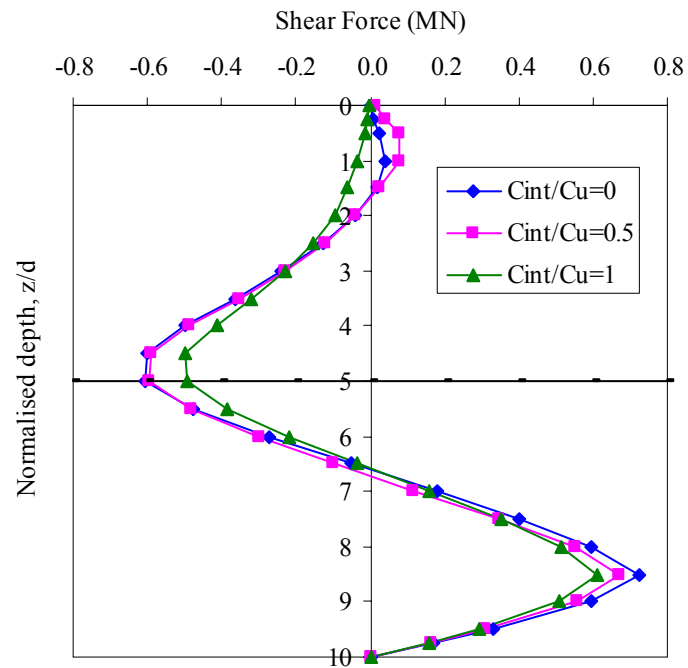


Figure 4.30: Pile shear forces versus depth for three different slip plane strengths at 400 mm of boundary soil displacement along the slope

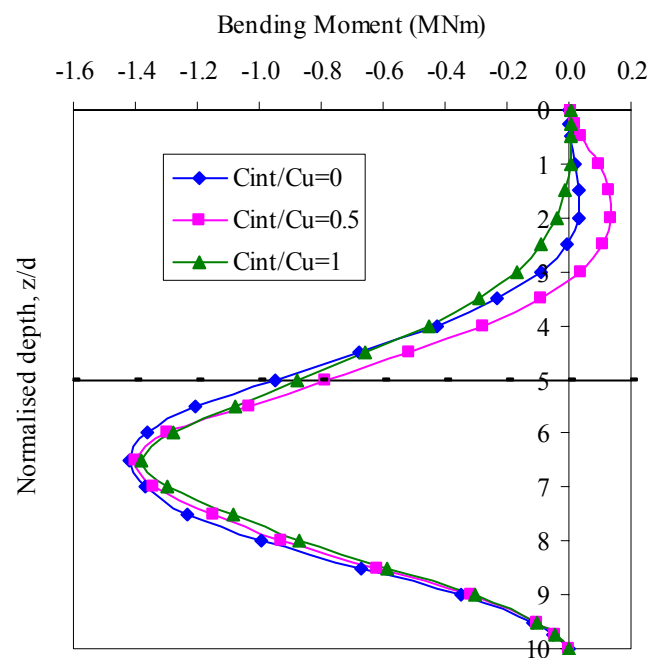


Figure 4.31: Bending moment developed in pile versus depth for three different slip plane strengths at 400 mm of boundary soil displacement along the slope

When  $c_{int}/c_u = 0$ , despite the fact a displacement controlled boundary condition is applied at either side of the unstable soil block, the soil adjacent to the pile tries to run away. Therefore, it could be argued that this velocity controlled boundary condition may influence on the actual pile behaviour. The  $FLAC^{3D}$  analyses were carried out without using this velocity controlled boundary condition to understand this effect and are presented in the following section.

#### 4.4 Behaviour of the pile in a finite slope

The behaviour of the laterally loaded pile placed in a two layered finite slope is investigated in this section. This more realistically represents a pile stabilised slope with a pre-existing slip plane.

##### 4.4.1 $FLAC^{3D}$ analyses

The  $FLAC^{3D}$  mesh used in Section 4.3.2.2 (slope angle =  $22^\circ$ ) was modified to carry out these analyses by adding further soil elements, as shown in Figure 4.32. The left and right side boundaries were placed far from the pile centre to reduce the interaction of the boundaries with the slipping soil. The nodes on the left, right and bottom faces were restrained against movement in all three directions, while the nodes on the ground surface were allowed to move freely.

In all previous analyses, a velocity was applied at the left and right boundaries to impose an external lateral displacement to the model. This velocity acted as a disturbing force to cause soil movement within the model, and development of the ultimate lateral pile-soil pressures along the pile shaft. In this section, no external load was applied to the model, which was allowed to fail due to the effects of gravity and a defined pre-existing failure plane.

The same approach as explained in Section 4.3.1 was used to prevent slope instability during gravity loading. After the model had reached equilibrium, the soil properties were changed to their actual values and the behaviour of the pile was then monitored.

Two different cases are considered in this section.

Case 1: Pile behaviour with slip plane strength, where centre-to-centre spacing between the piles ( $S_h$ ) is 10 times the diameter of the pile ( $d$ )

Case 2: Pile behaviour with spacing between the piles in a row, where only the slope with the slip plane strength  $c_{int}/c_u = 0.5$  is considered.

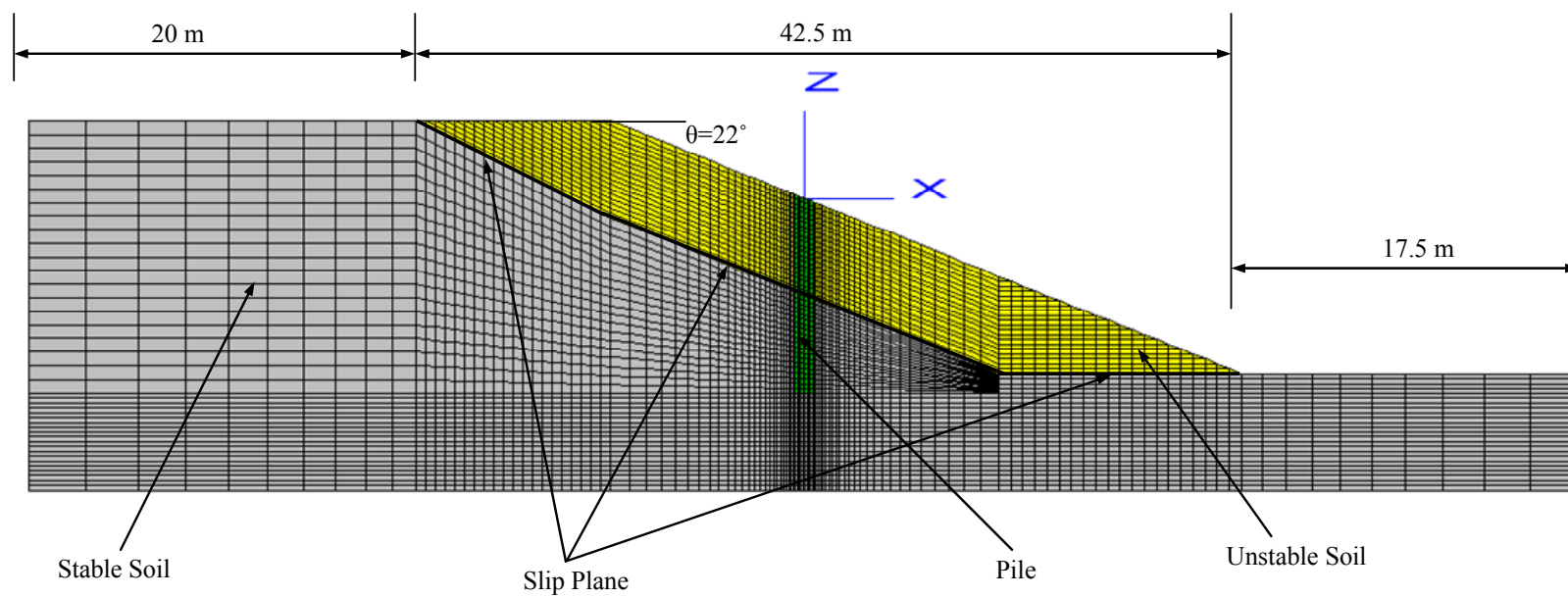


Figure 4.32:  $FLAC^{3D}$  mesh of finite slope with 22 degrees slope angle, where  $S_h/d = 10$

Job Title: Behaviour of a Finite Piled Slope

View Title: Displacement Vectors

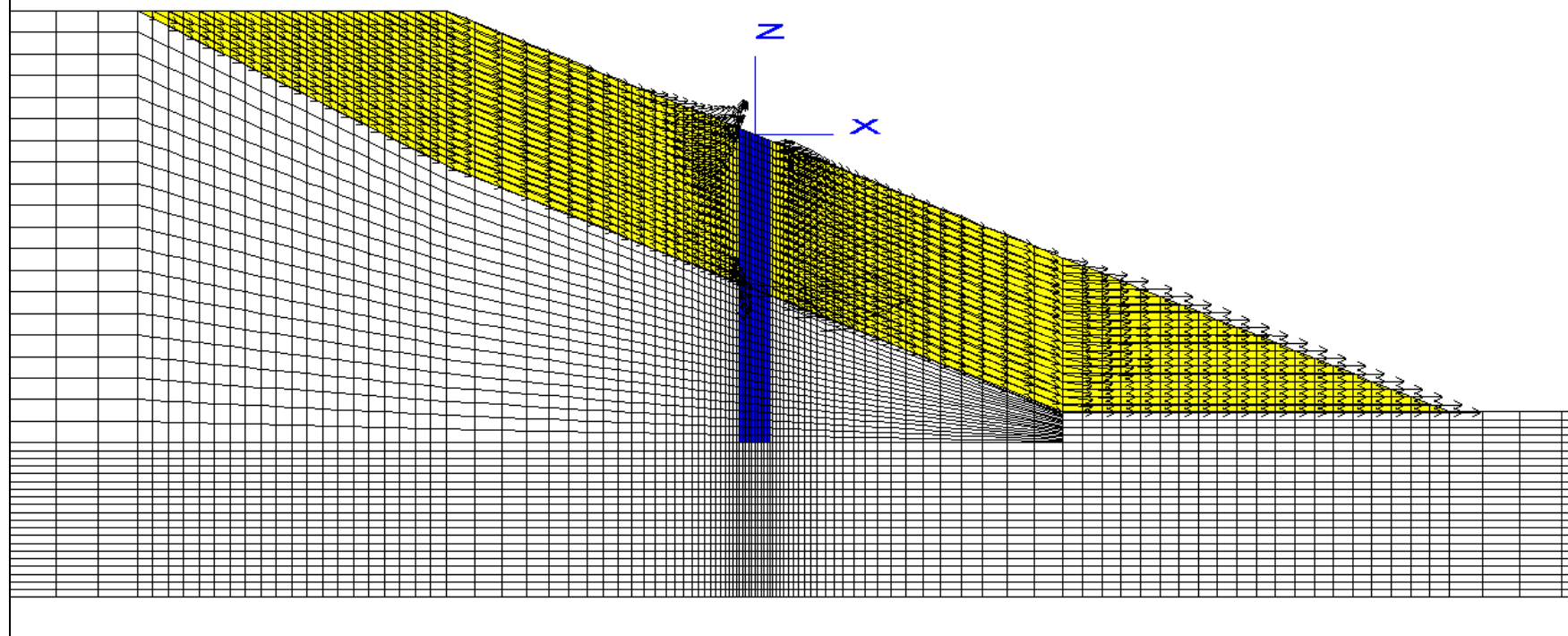


Figure 4.33: Displacement vectors showing failure of the unstable soil for  $c_{int}/c_u=0$  after  $5 \times 10^5$  FLAC<sup>3D</sup> steps, where  $S_H/d = 10$

## 4.4.2 Results and discussion

### 4.4.2.1 Behaviour of the pile with varying slip plane strength ( $S_h = 10 d$ )

The analyses presented in this section show the effect of slip plane strength on the behaviour of the single isolated pile placed in a finite slope with a  $22^\circ$  slope angle. The analyses with the normalised slip plane interface strengths  $c_{int}/c_u = 0$  and  $0.5$  did not reach the maximum unbalanced force ratio of  $1 \times 10^{-5}$  assumed to represent an equilibrium state, even after hundreds of thousands steps. Therefore, it was decided to carry out the analyses for  $5 \times 10^5$  *FLAC*<sup>3D</sup> steps, as in the previous analyses, and assess the equilibrium state at that point.

Deflection profiles of the piles are shown in Figure 4.34. When the slip plane has zero strength, the piles do not stop the soil flow, and the maximum lateral pile-soil pressures reaches on the upslope side of the pile (Fig. 4.35). However, as found in the previous analyses, when the slip plane strength increases, the tendency of the soil to flow through the piles decreases and leading to increased pile-soil interaction (i.e. the pile tries to work hard to stabilise the slope). Due to this increased interaction effect, the soil applies slightly more pressure on the piles walls and therefore the pile rotation increases when  $c_{int}/c_u = 0.5$  (Fig. 4.34). Negligible deflection in pile occurs for  $c_{int}/c_u = 1$ , as the slope is stable for this case.

As in the earlier analyses (Section 4.3.2.2), the unstable soil slips very easily when the slip plane has no strength, and movement decreases as the slip plane strength increases. For  $c_{int}/c_u = 0$ , soil flow around the pile increases with depth (Fig. 4.36) unlike in the previous analyses (Figs. 4.10 and 4.28). This result is plausible: velocity controlled boundaries were employed in the previous analyses and that controlled downslope soil movement. However, no velocity controlled boundaries are used in these analyses; therefore the unstable soil is free to fail in a more rotational mode.

The shear forces and bending moments developed within the pile sections are shown in Figures 4.37 and 4.38, respectively. A higher maximum shear force and bending moment is developed within the pile for  $c_{int}/c_u = 0.5$  than for  $c_{int}/c_u = 0$ . As explained earlier, when the slip plane interface has zero strength, the soil flows past the piles without applying much pressure to the piles. However, when the slip plane strength is  $0.5 c_u$ , the piles works quite hard to stabilise the slope, and as a result a higher shear force and bending moment is developed on the piles. Very small or negligible shear forces and bending moments are obtained for  $c_{int}/c_u = 1$ ; this is because, as explained earlier, the slope was stable in this case, and therefore piles are not needed.



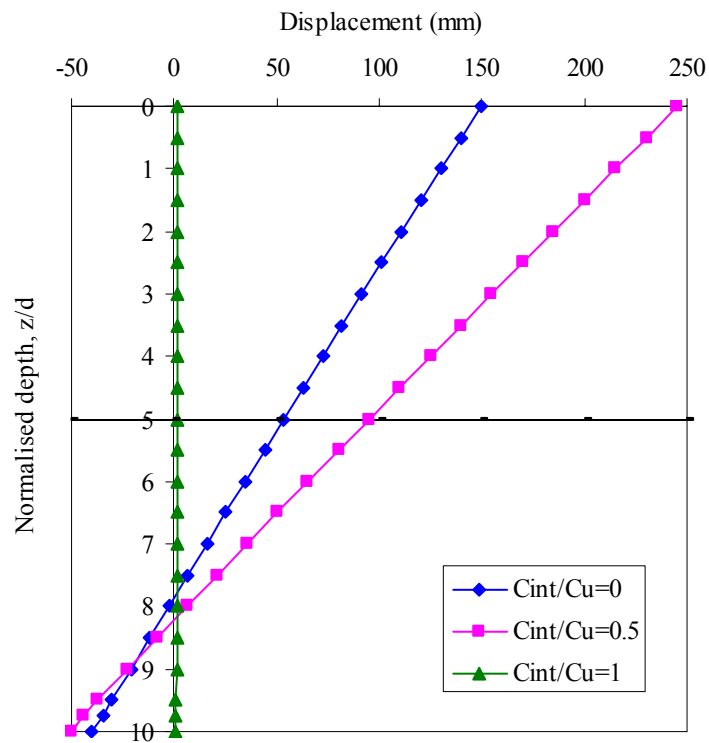


Figure 4.34: Movement of pile versus depth for three different slip plane strengths, after  $5 \times 10^5$   $FLAC^{3D}$  steps

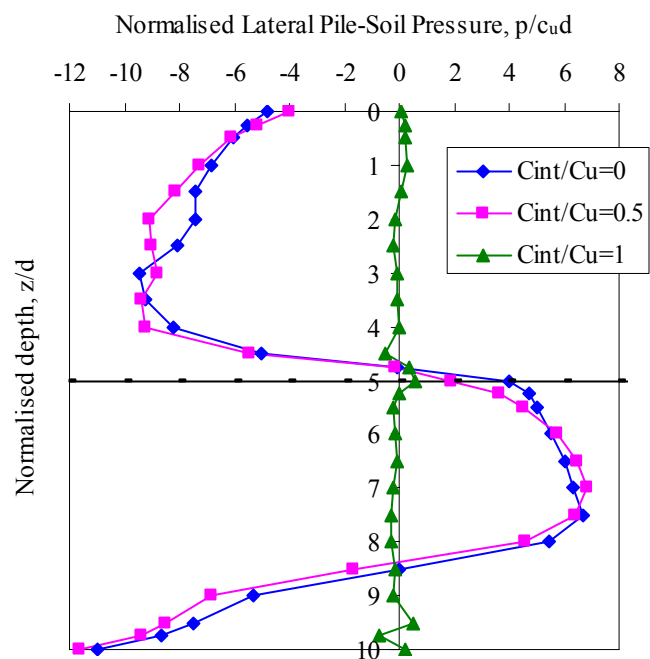


Figure 4.35: Normalised lateral pile-soil pressure versus depth for three different slip plane strengths, after  $5 \times 10^5$   $FLAC^{3D}$  steps

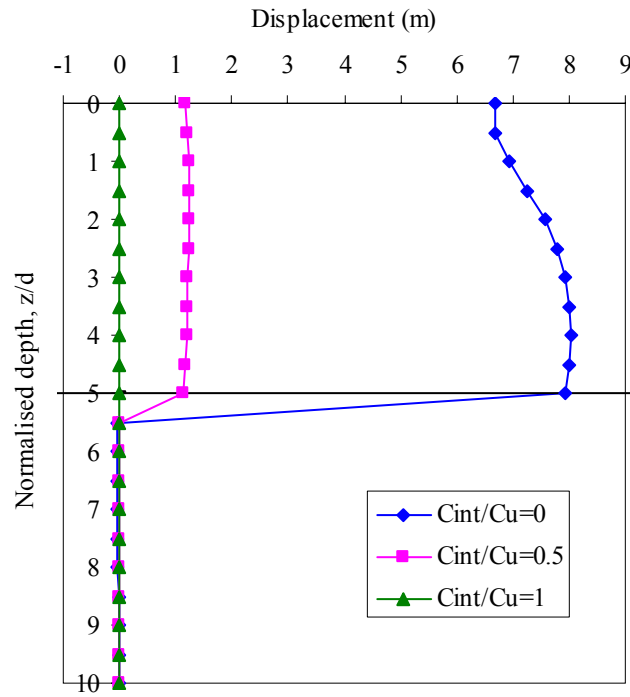


Figure 4.36: Soil movement calculated at 1 m distance from pile centre in y-direction for three different slip plane strengths, after  $1 \times 10^5$   $FLAC^{3D}$  steps

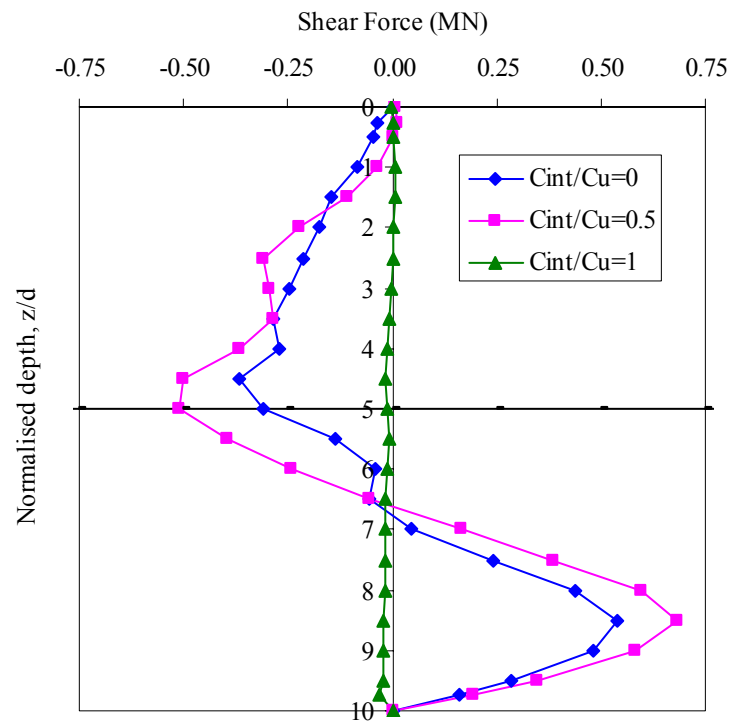


Figure 4.37: Pile shear forces versus depth for three different slip plane strengths, after  $5 \times 10^5$   $FLAC^{3D}$  steps

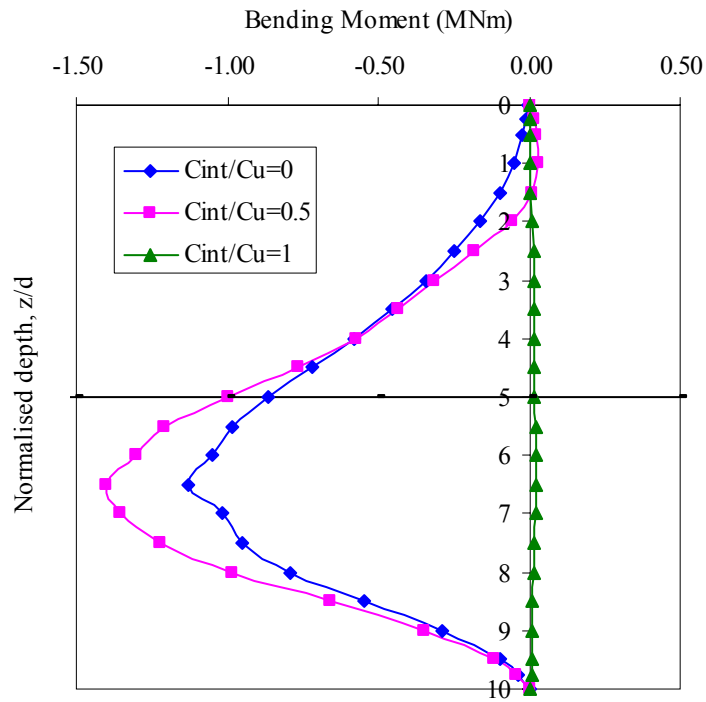


Figure 4.38: Bending moments developed in pile versus depth for three different slip plane strengths, after  $5 \times 10^5$   $FLAC^{3D}$  steps

Although the geometry of this piled finite slope is equivalent to Viggiani's mode B pile configuration (i.e. the slip plane location is at 5 m below ground level and length of the pile is 10 m), the behaviour of the pile is similar to Viggiani's mode C mechanism (i.e. soil flows around the piles) as shown in Figure 3.46. This is mainly because the piles were spaced with a centre-to-centre spacing of 10 times the diameter of the piles in this  $FLAC^{3D}$  analyses, and they did not prevent soil flow for slip plane strengths  $c_{int}/c_u = 0$  and 0.5. The effect of the pile spacing is investigated in the following section.

#### 4.4.2.2 Behaviour of the pile with varying pile spacing ( $c_{int}/c_u = 0.5$ )

The analyses presented in this section investigate the behaviour of piles with different pile spacings. Only the slope with a slip plane strength of  $0.5 c_u$  was considered, and the effect of the pile spacing on the behaviour of the pile was investigated by changing the distance between the planes of symmetry in the  $FLAC^{3D}$  model (Fig. 4.39).

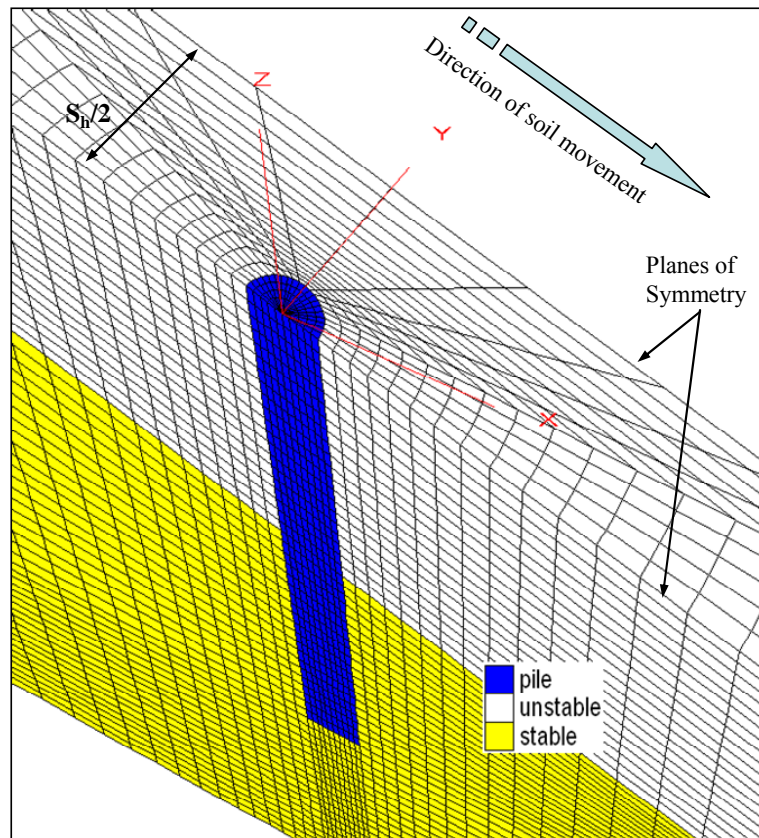


Figure 4.39:  $FLAC^{3D}$  mesh showing the piles in a row at  $S_h$  spacing

Figure 4.40 shows the pile deflection and soil movement on a vertical line through a point located 1 m from the pile centre in the  $y$ -direction for three different pile spacings. When the pile spacing  $S_h/d = 10$ , the pile top moves about 51 mm, while the soil movement monitored on the vertical line was found to be more than a metre. This means that when the piles are placed too far from each other, they do not provide sufficient resistance to prevent slope failure, and the soil just flows around the piles. However, in practice, as the piles are placed further from each other, they should undergo a higher deflection, irrespective of whether the soil just flows around or interacts with the piles. As the  $FLAC^{3D}$  analyses for case  $S_h/d = 10$  did not seem to reach numerical equilibrium, observed pile deflection may not be correct for this case. When the piles are closely spaced (i.e.  $S_h/d = 3$ ), they effectively stabilise the slope with a pile head deflection of 64 mm.

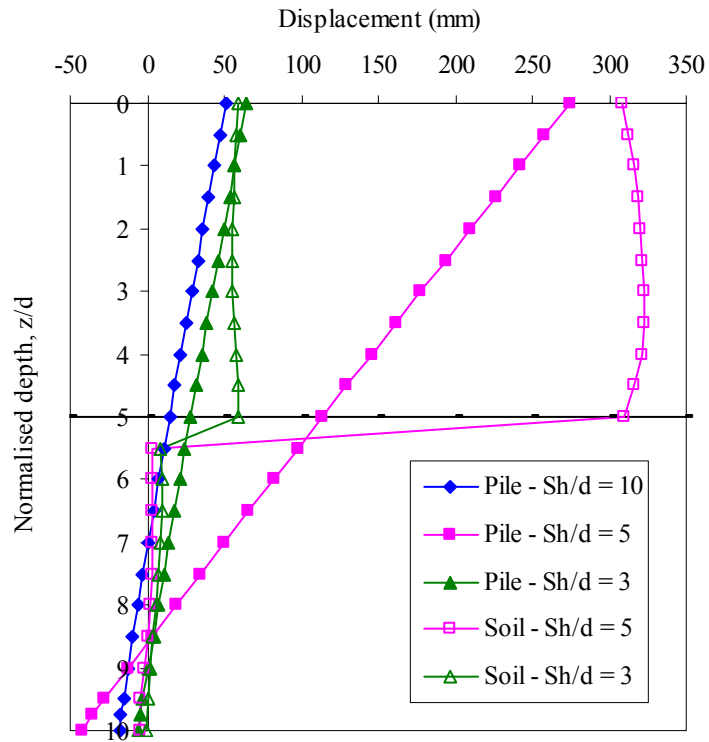


Figure 4.40: Deflection of pile and soil movement on a vertical line through a point located 1 m from pile centre in y-direction, for three different pile spacings after  $2 \times 10^5$   $FLAC^{3D}$  steps

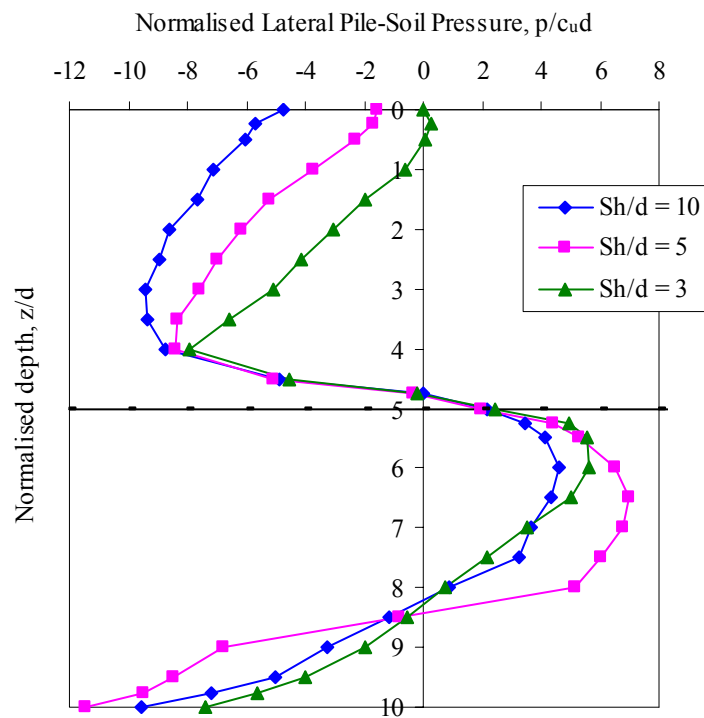


Figure 4.41: Normalised lateral pile-soil pressure versus depth for different pile spacings after  $2 \times 10^5$   $FLAC^{3D}$  steps

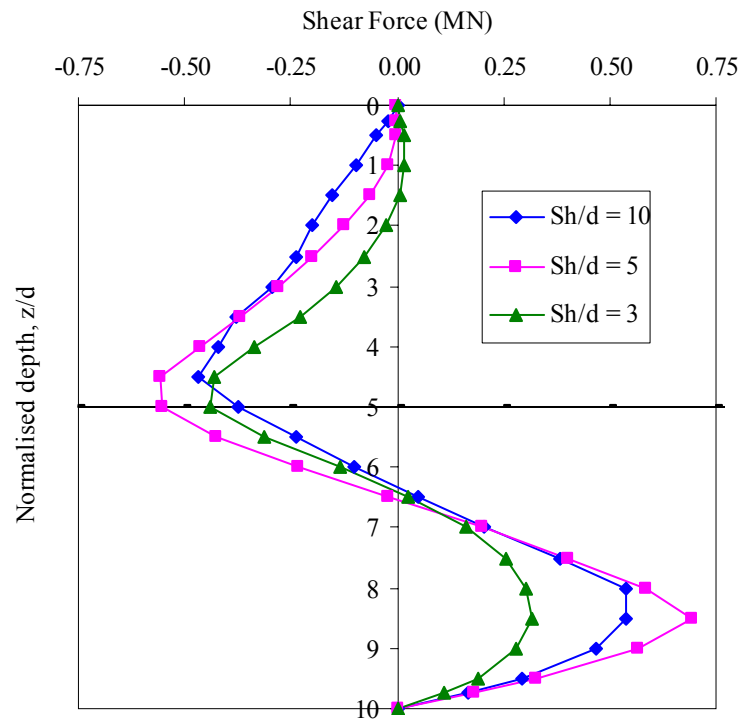


Figure 4.42: Pile shear forces versus depth for different pile spacings after  $2 \times 10^5$   $FLAC^{3D}$  steps

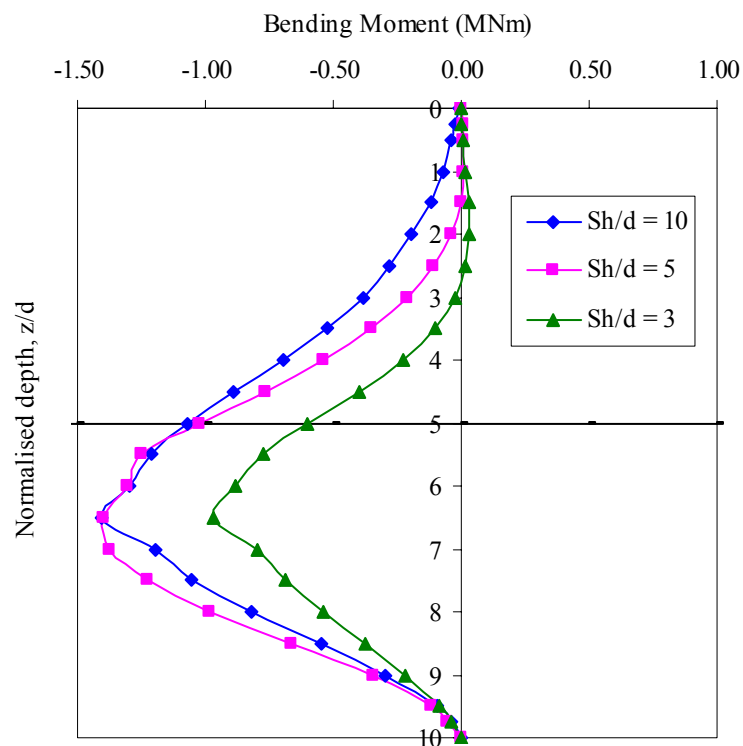


Figure 4.43: Bending moment developed in pile versus depth for different pile spacings after  $2 \times 10^5$   $FLAC^{3D}$  steps

When the spacing between the piles decreases, the behaviour of the piles changes from Viggiani's (1981) mode C mechanism to mode B. According to Viggiani's mode B definition, for ultimate loading state, the movement of pile top exceeds the movement of soil, and as a result a reversed lateral pile-soil pressure develops at the top pile section (Fig. 3.52). This behaviour is evident from Figure 4.41, where a reversed pressure is developed on the top half metre of the pile section, which is almost equal to the length of pile that has exceeded the soil movement (Fig. 4.40).

Pile shear forces and bending moments developed in the pile versus depth for the different pile spacings are shown in Figures 4.42 and 4.43 respectively. They also show that the behaviour of the piles change from Viggiani's mode C to mode B with decreasing pile spacing. The maximum shear force at the pile section passing through the slip plane, is developed for  $S_h/d = 5$  pile spacing, not for  $S_h/d = 10$ . Although the piles spaced at  $S_h/d = 5$  stabilise a narrower width of the slope compared with the piles spaced at  $S_h/d = 10$ , as explained earlier, these piles work hard to stabilise the slope, compared with the piles spaced at  $S_h/d = 10$ . If the behaviour of piles spaced at  $S_h/d = 3$  is contrasted with the piles spaced at  $S_h/d = 5$ , the piles in the former case stabilise a narrower strip of soil and this leads each piles to develop a lower maximum shear force.

The effect of pile spacing on the behaviour of piles spaced in one and two rows are investigated in the next chapter. Variations in the development of ultimate lateral pile-soil pressures along the pile shaft with pile spacing, in the development of maximum stabilising force with the pile spacing, and in the mechanism behind the complex pile-soil interaction are also explored in the next chapter.

## 4.5 Summary

The main aim of the *FLAC*<sup>3D</sup> analyses presented in this chapter was to modify some of Viggiani's (1981) assumptions such as a horizontal ground surface and slip plane, and a zero strength slip plane, so that the applicability of these analyses can be widened.

The analyses carried out to investigate the effect of slip plane strength showed that it has a considerable influence on the pile behaviour. For mode A, increasing the strength of the slip plane interface moves the mode of pile deformation from translation to rotation; but does not significantly change the ultimate lateral pile-soil pressure. In mode B and C, the relative movement between the unstable and stable soil layers decreases as the strength of the slip plane increases, causing a reduction in pile rotation. The strength of the slip plane also significantly affects the performance of piles installed into sloping ground. When the strength of the slip plane decreases, the tendency for movement of the downslope soil increases, and as a result it offers less support to the pile. The analyses carried out to understand the effect of slope angle show that sloping ground only significantly influences the pile above a certain angle. Below that value, the pile behaves in the same manner as for horizontal ground. However, the magnitude of the 'significant' slope angle depends on unit weight of the soil, the depth of the slip plane, and the strength of the slip plane for an undrained analysis.

When a finite slope with zero slip plane strength is allowed to fail by gravity alone, the soil close to the slip plane in the unstable layer moves more than the shallow surface soil. This behaviour is more realistic, because in previous analyses velocity control boundary was employed to the left and right side boundaries and thus free downslope movement was restricted. For the chosen soil properties and when full strength was given to the slip plane, the finite slope was stable. Extended analyses carried out to understand the effect of centre-to-centre pile spacing showed although geometry of the pile configuration is equivalent to Viggiani's (1981) mode B definition, the behaviour of piles spaced too far from each other (i.e. isolated piles) is similar to Viggiani's mode C definition. However, this behaviour changes to mode B definition with decreasing pile spacing. The behaviour of piles with the pile spacing and the mechanism behind this pile-soil interaction problem is investigated carefully in the next chapter.

The analyses were carried out with increasingly realistic boundary conditions, starting from the behaviour of a pile installed on a flat ground and laterally loaded by an imposed displacement, to a piled infinite slope laterally loaded by an imposed displacement, and finally to a gravity driven failure in a piled finite slope. Finally, the analyses presented in this chapter clearly demonstrate how the strength of the slip plane and the slope angle influences the Viggiani (1981) mechanisms for the piles used to stabilise a slope.



## Chapter - 5: Pile-Soil Interaction Effects of Pile Groups

### 5.1 Introduction

Piles are generally installed in one or more rows across a potential sliding mass with a spacing dictated by the pile geometry and bending capacity, and the load they are required to resist. When the piles are grouped closely together pile-soil interaction effects significantly reduce the ultimate lateral load carrying capacity of each individual pile (Broms, 1964; Randolph, 1981; Chen and Poulos, 1997). Therefore the solution obtained for a single pile may not be applicable to each pile in a pile group. Because of the high cost and logistical difficulty of conducting full scale lateral load tests on pile groups, relatively few data are available to quantify group interaction effects (Brown and Shie, 1990b).

Full scale pile load tests in clay (Brown *et al.*, 1987) and clayey silt (Rollins *et al.*, 1998) have been reported for actively loaded pile groups. There has been no full scale lateral load test of passively loaded pile groups. However, there are many case histories available (Ito and Matsui, 1975; Evangelista *et al.*, 2004; Carder and Barker, 2005; Smethurst and Powrie, 2007) in which passively loaded discrete piles used to stabilise slope failures have been instrumented to monitor their behaviour. In general, the discrete piles used to increase the stability of slopes are designed for serviceability rather than ultimate load conditions. Therefore, the behaviour observed from field monitored piles may not help to understand the pile behaviour under ultimate load conditions. Also, the lateral loads developed on instrumented piles are usually determined indirectly using bending strain or displacement data and a curve fitting process, and therefore the exact load may not be obtained as the bending moment is related to the assumed structural properties of the pile.

Numerical modelling is economical compared with full scale field experiments on a pile group, and can be used to gain an improved understanding of pile-soil and inter-pile interaction effects. It may not be still practicable to determine general rules for the evaluation of the optimum spacing between piles based on finite element analyses because of the large number of variables involved (Carder, 2005). However, three dimensional models can provide details of general interaction mechanisms and effective design guidance for specific cases. Three dimensional finite difference analyses using *FLAC*<sup>3D</sup> were carried out to investigate the behaviour of one and two infinitely long pile rows subjected to lateral soil movements. The influence of the centre-to-centre spacing between piles in a row ( $S_h$ ) and the distance between two pile rows ( $S_v$ ) was studied.

## 5.2 Interaction effects between single row of piles

The centre-to-centre spacing between two piles in a row (referred to here as the pile spacing) can make a significant difference to the serviceability and ultimate behaviour of each individual pile. In terms of stabilising the sliding soil, the pile spacing must be designed to provide the required stabilising force to the slipping mass while minimising the opportunity for flow of soil between them (Carder, 2005). A number of  $FLAC^{3D}$  analyses were carried out to understand the behaviour of a single row of piles with different pile spacing, and are presented in the following sections.

### 5.2.1 $FLAC^{3D}$ analyses

To maintain consistency of the mesh structure while changing the pile spacing, a  $FLAC^{3D}$  mesh was generated as follows: a 1 m diameter ( $d$ ) semi-circular hole was formed at the centre of a 2 m long  $\times$  1 m wide  $\times$  10 m high soil block made up of radial elements as shown in Figure 5.1(b), into which the pile was later inserted. The neighbouring soil was then built up of rectangular blocks of appropriate width, placed around the radial block containing the pile.

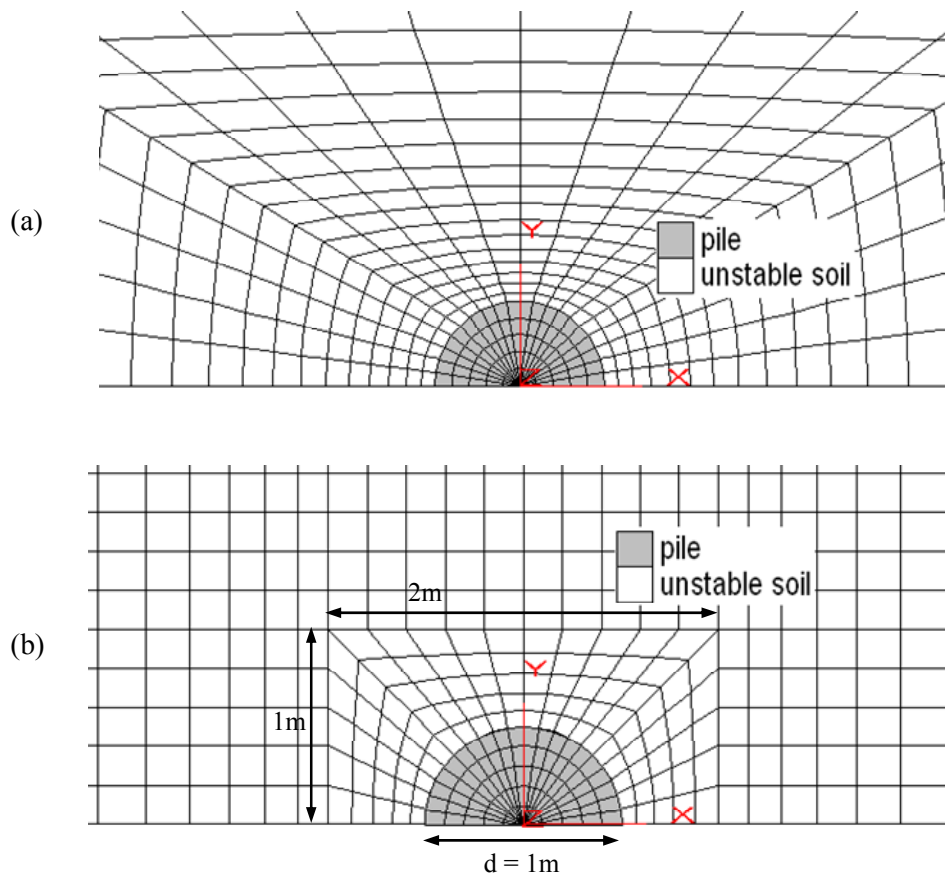


Figure 5.1: Plan view of  $FLAC^{3D}$  model (a) mesh used in Chapter 3 analyses; (b) modified mesh developed for pile group analyses

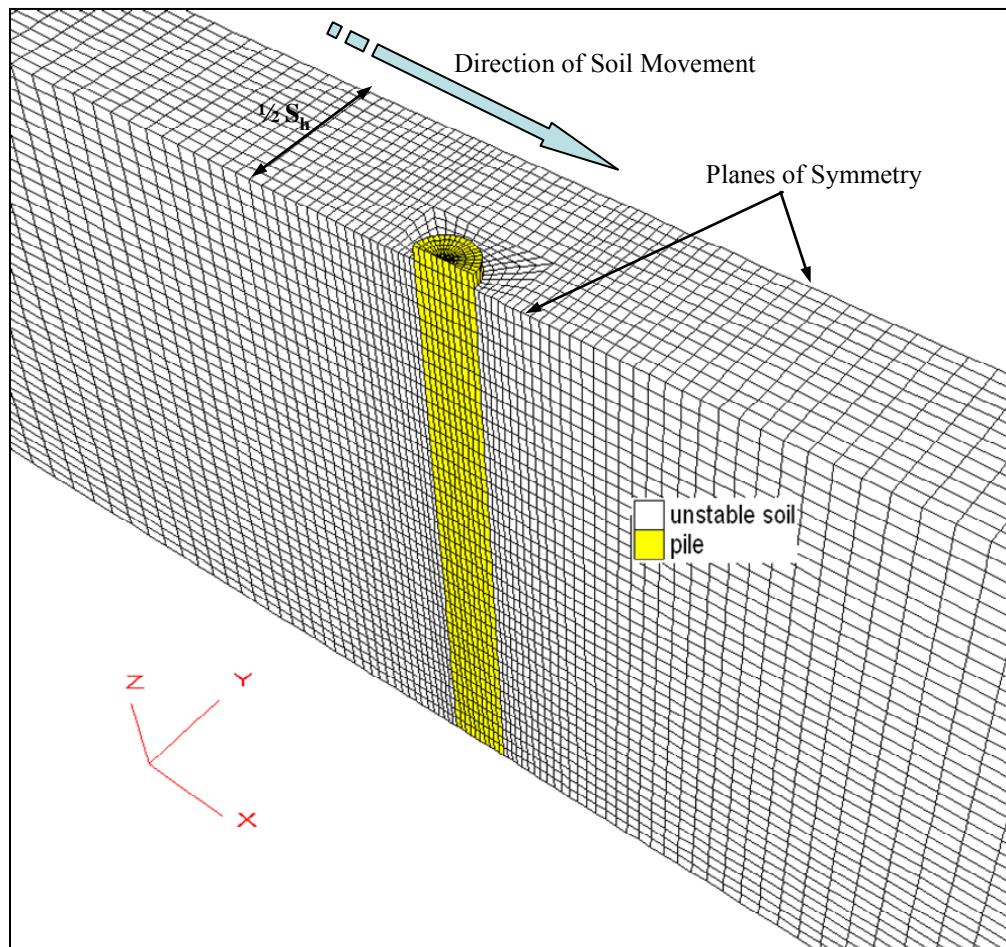


Figure 5.2:  $FLAC^{3D}$  mesh showing the piles in a row at  $S_h/d = 5$  spacing

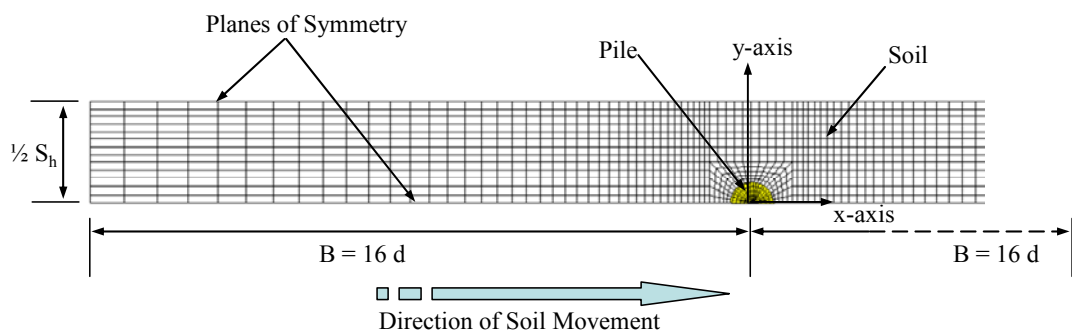


Figure 5.3: Plan view of  $FLAC^{3D}$  mesh used for single pile row analyses

A 32 m long, 10 m high *FLAC*<sup>3D</sup> mesh was modelled as shown in Figure 5.2, representing a single infinitely long pile row. To save computational time, only one layer of soil was modelled assuming the presence of a lower rigid layer into which the piles are firmly embedded. Two boundaries were used to represent the planes of symmetry through the pile centreline and through the soil midway between piles. This geometric arrangement allows investigation of the effect of pile spacing by adjusting the distance  $\frac{1}{2} S_h$  between the two planes of symmetry (Fig. 5.3), where  $S_h$  is centre-to-centre spacing between the piles. The left and right side boundaries were placed at a distance of  $16d$  from the pile centre to minimise boundary effects.

The piles were fixed at the base of the mesh and pile heads were unrestrained. The boundary and initial conditions, and the material properties, were the same as in Section 3.6.2. A pile-soil interface having the full soil strength was used in these analyses to accommodate slippage between the pile and surrounding soil elements. A 300 mm (or  $0.3d$ ) soil movement was imposed on the left and the right boundaries in the  $x$ -direction in three stages (i.e. in 100 mm increments), by applying a ‘velocity’ of  $2 \times 10^{-7}$  m/step as in previous analyses, to investigate pile-soil interaction effects in the ultimate state.

### 5.2.2 Results and discussion

The variation in computed deflections, shear forces, bending moments and ultimate lateral pile-soil pressures ( $p_u$ ) with pile spacing is shown in Figure 5.4. All four parameters (deflection, shear force, bending moment and ultimate lateral pile-soil pressure) decrease as the centre-to-centre spacing ( $S_h$ ) decreases. A particularly significant reduction occurs in all four parameters for the piles spaced at  $S_h/d = 1.1$ . For pile spacings of  $S_h/d = 1.1$  and 2 the trend of variation of the normalised ultimate lateral pile-soil pressure ( $p_u/c_u d$ ) with depth is different than for the other spacing configurations (Fig. 5.4d).

It is interesting to examine the relationship between the ultimate lateral pile-soil pressure and the pile spacing. When a pile is loaded laterally, higher pressures are developed in front of the pile and lower pressures behind it. When the pile-soil system reaches the ultimate state, the soil will flow round the pile from in front to behind, with a mechanism of soil movement indicated by Randolph and Houlsby’s (1984) classical theory, developed based on Broms’s (1964) original work. When the pile spacing is large, a bigger deforming region can form around the pile since the soil can easily flow through the gaps between piles (Fig. 5.5a). This aids the development of a higher ultimate lateral pile-soil pressure on the pile, causing the piles to deflect more. This behaviour agrees with Randolph and Houlsby’s (1984) theoretical analyses in which they demonstrate that a higher limiting pressure is developed on the pile, if the deforming region is big.

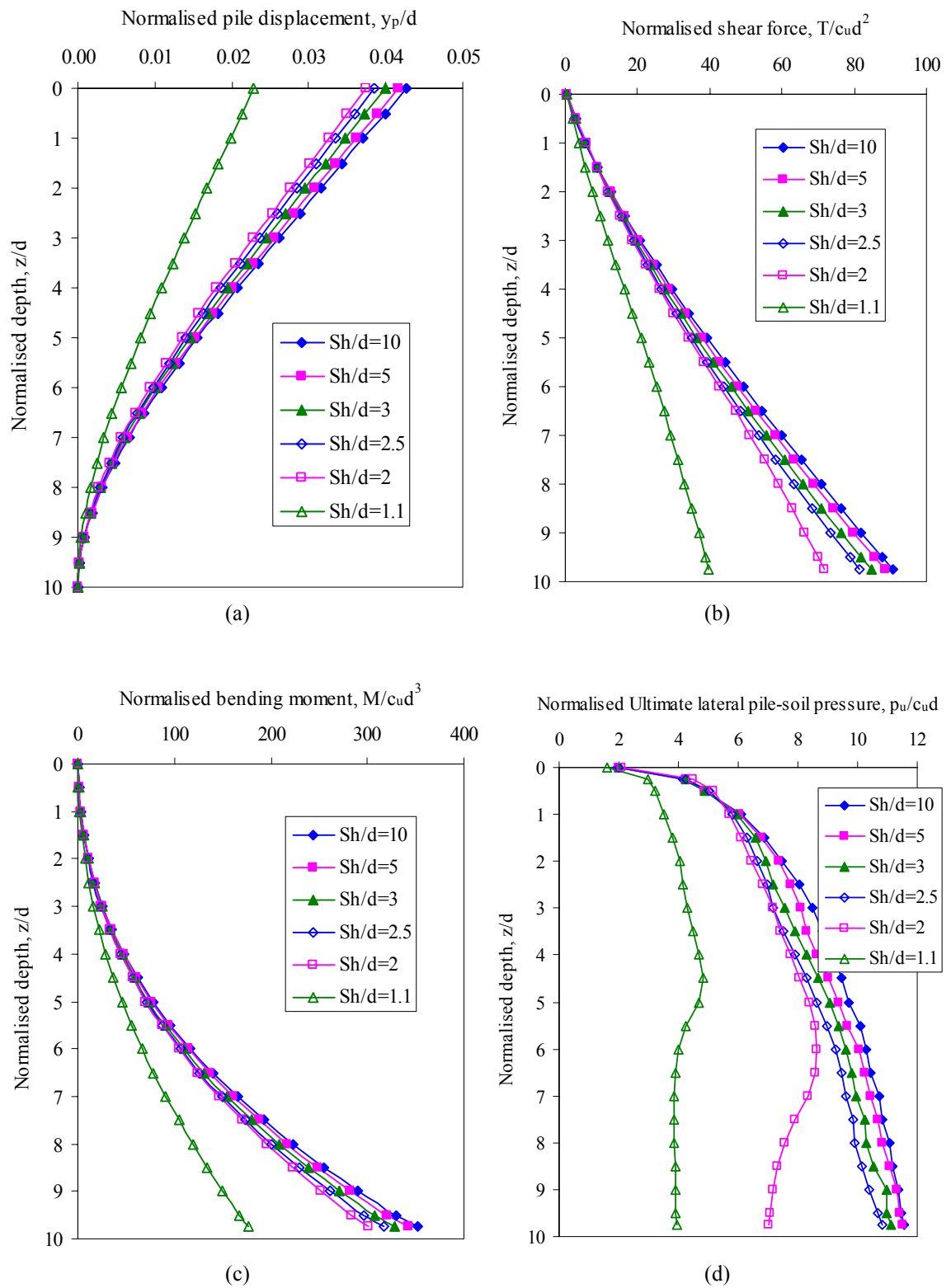


Figure 5.4: Pile behaviour at different pile spacings for a soil boundary displacement of 300 mm: (a) normalised pile displacement; (b) normalised shear force; (c) normalised bending moment; and (d) normalised ultimate lateral pile-soil pressure

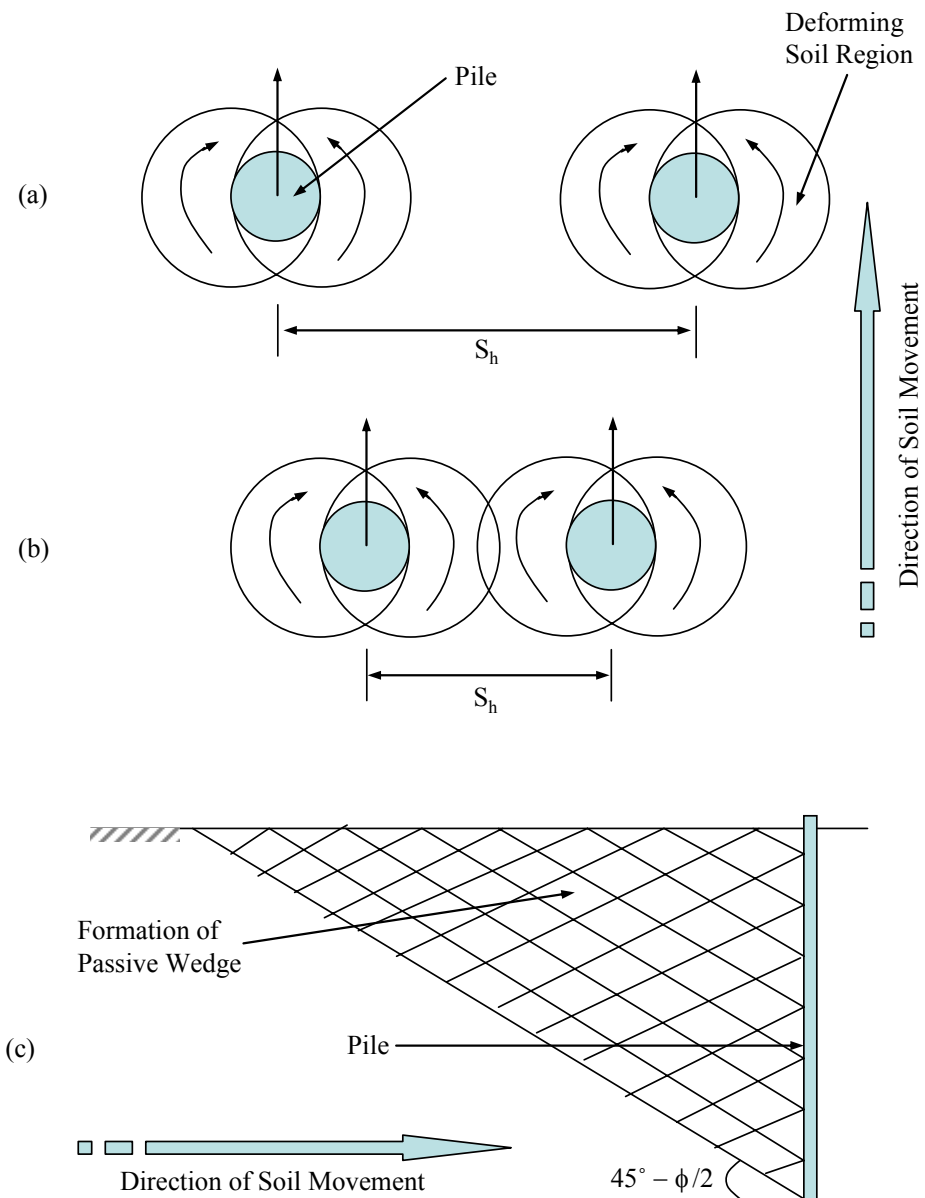


Figure 5.5: (a) Soil flow around the pile and piles act individually; (b) Soil flow around the pile but deforming soil regions start to interact; and (c) Formation of passive wedge in front of closely spaced piles

As the piles become even closer together, the deforming regions are constrained by the adjacent piles (Fig. 5.5b), which changes the interaction mechanism from Randolph and Houlsby's (1984) to formation of a passive wedge in front of the pile row (Fig. 5.5c), causing the ultimate lateral pile-soil pressure to reduce. Once a passive wedge forms the pressure on each pile reduces as the spacing gets closer, since each pile supports a narrower strip of slope.

The modified displacement vectors for pile spacings  $S_H/d = 2$  and 5 were plotted to investigate the formation of passive soil wedge in front of the pile row, and are shown in Figure 5.6. Figure 5.6(a) clearly shows the formation of a passive soil wedge mechanism for the closely spaced piles. This passive wedge mechanism disappears as the pile spacing increases, and is converted to Randolph and Houlsby's (1984) flow mechanism as explained earlier.

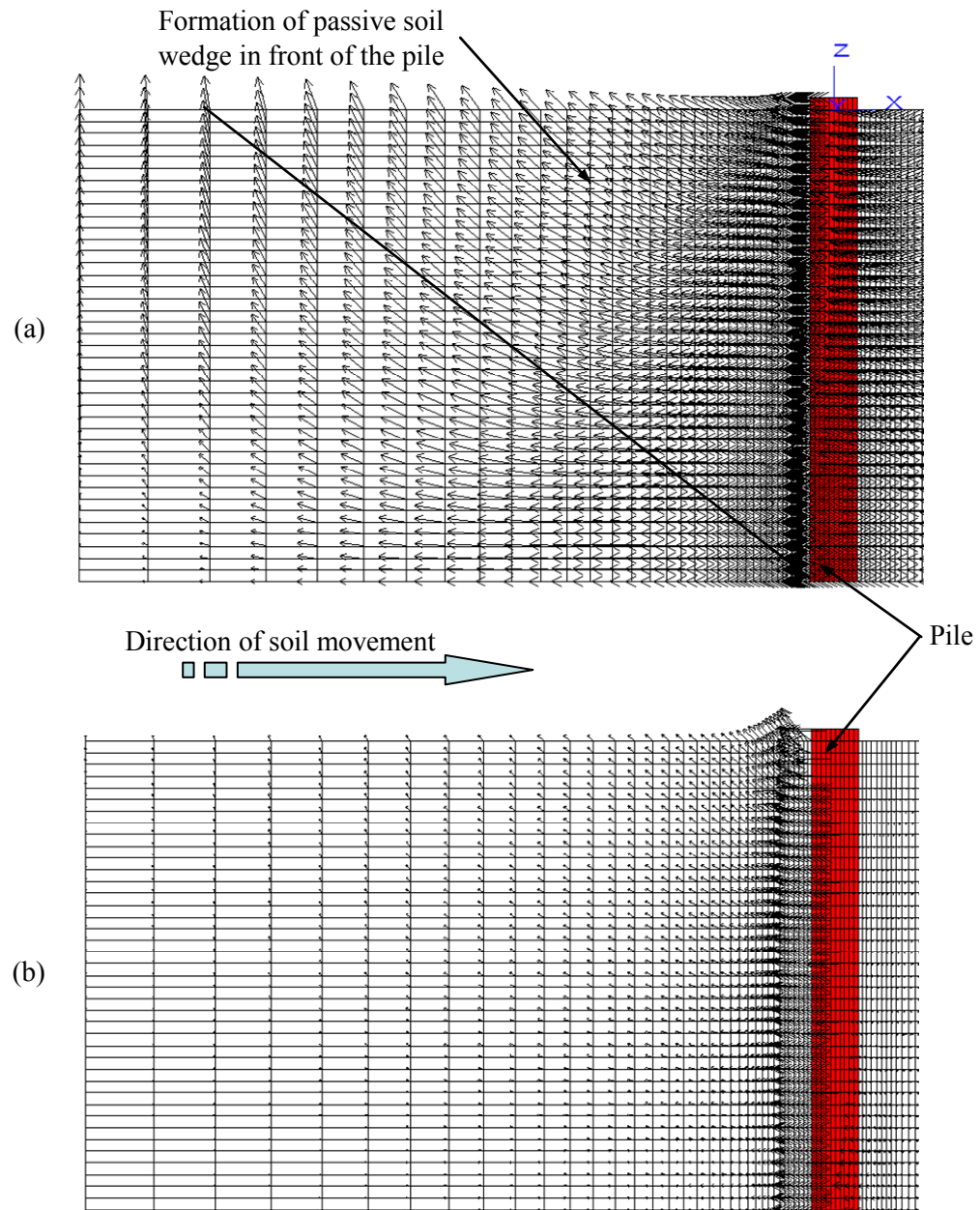


Figure 5.6: Relative pile-soil displacement vectors (= displacement vectors, after 300 mm boundary soil displacement – 300 mm displacement, in x-direction) plotted on the plane through pile axis and parallel to the soil movement ( $y = 0$ ) for the discrete piles spaced at: (a)  $S_H/d = 2$ ; and (b)  $S_H/d = 5$



The variation of ultimate lateral pile-soil pressure with pile spacing calculated from the *FLAC*<sup>3D</sup> analyses agrees well with Chen and Poulos (1993) for a spacing greater than  $2d$  but differs for pile spacings less than  $2d$ . Chen and Poulos reported ultimate lateral pile-soil pressures at  $2d$  spacing slightly greater than for a single isolated pile (Fig. 2.20). This may result from the square cross section pile they modelled, since the deforming region created by the sharp corners of a square pile may well be different from that for a circular shape pile. It is also likely that the plane stress analysis they carried out is incapable of identifying the correct pile-soil interaction (i.e. a passive wedge mechanism can not form). The  $p_u/c_u d$  calculated from the current analyses and 3D analyses carried out by Brown and Shie (1990b) both show a considerable reduction in  $p_u/c_u d$  from the value for an individual pile when the piles are spaced at  $S_H/d = 2$  (Figs. 2.27a and 5.4d).

Figure 5.7(b) shows the deformation of soil around the pile, in particular the lateral soil movement on a vertical line through the node G located 1 m away from the pile centre in plan (Fig. 5.7a). By comparing Figures 5.4(d) and 5.7(b), it is possible to state that with more soil flow through the gap between the piles, a greater ultimate lateral pile-soil pressure is developed. For example, the movement of soil around the piles spaced at  $3d$  is less than for a  $5d$  spacing, and the ultimate lateral pile-soil pressure developed is also less for  $3d$  than for  $5d$  spacing. With piles at a  $2d$  spacing, the soil is almost trapped between the piles with little movement along the vertical line through the Point G as these piles create a strong stabilisation mechanism between them, and a comparatively low ultimate lateral pile-soil pressure is developed on the piles.

A further interesting observation from these analyses is that movement of the soil below a certain depth is larger than the applied boundary soil displacement (Fig. 5.7b), for the analyses with the piles at greater than  $3d$  spacing. When the piles are spaced at  $5d$ , the lateral pile-soil pressure reaches its ultimate value most quickly at deeper levels (Fig. 5.8a). This is probably the result of a higher vertical confining stress and because pile is unable to deflect close to the base; this caused the deeper soil to reach the ultimate state and start to flow around the piles, exceeding the applied boundary soil displacement (Fig. 5.8b). This effect does not occur at the shallow depths, maybe because the soil surface is unconfined. In the  $S_H/d = 2$  analysis,  $p_u$  is lower than has been observed elsewhere (for example, Brown and Shie, 1990b), but the mechanism is very constrained at deeper levels and very little soil flow around the pile is observed (Fig. 5.8d). Figure 5.7(c) shows the relative soil displacement  $y_r = y_s - y_p$ , (where  $y_s$  is the lateral movement of the soil at Point G and  $y_p$  is pile deflection). The relative soil displacement is less than the applied boundary soil displacement for  $S_H/d$  less than 2.5, while it is greater for larger spacings below a depth of about  $6d$ .



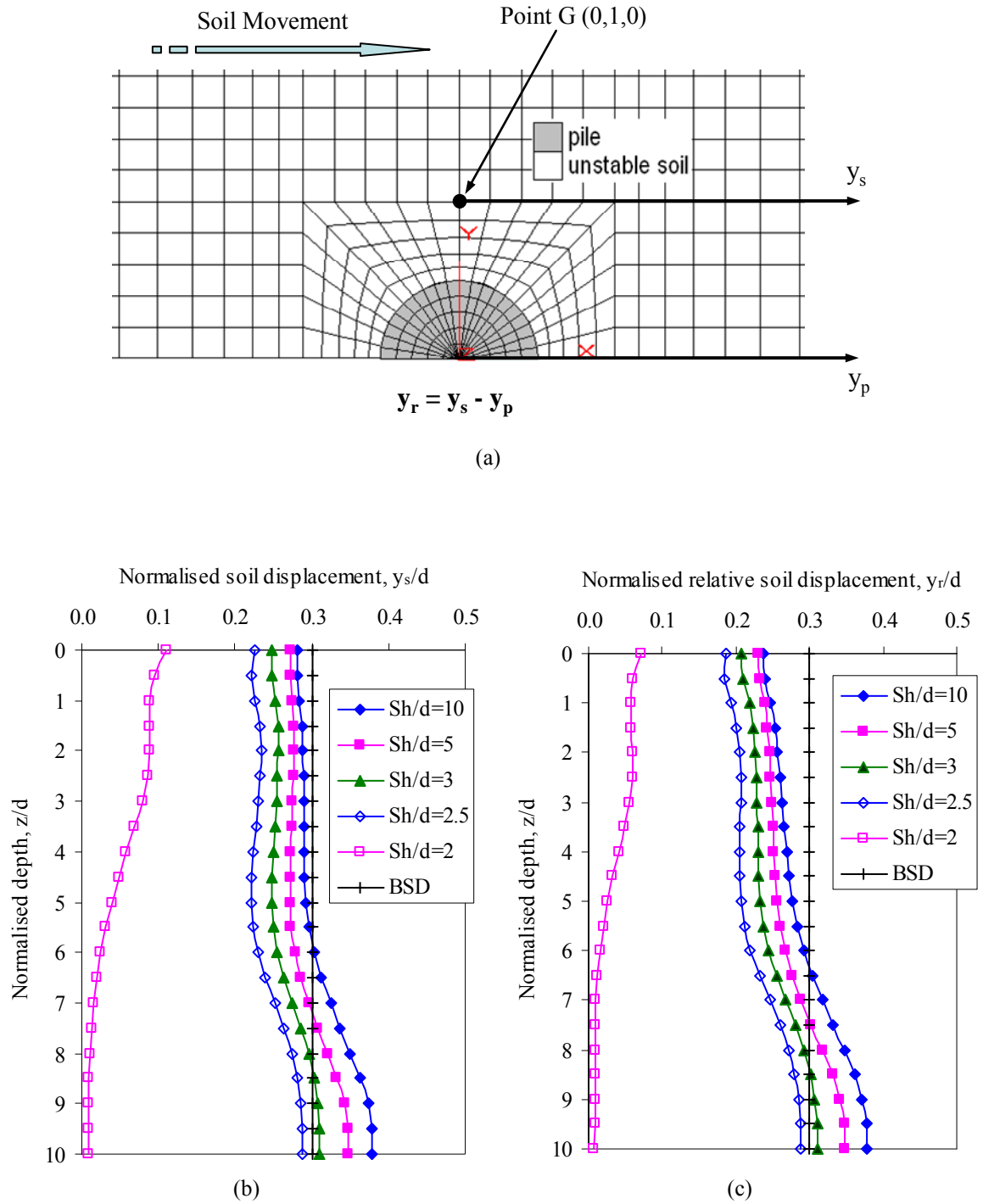


Figure 5.7: (a) Plan view of the mesh showing the location G at which soil movement has been recorded; (b) Movement of soil through Point G in  $y = 1$  m plane for 300 mm of boundary soil displacement; and (c) Relative soil movement at different pile spacings for soil boundary displacement of 300 mm

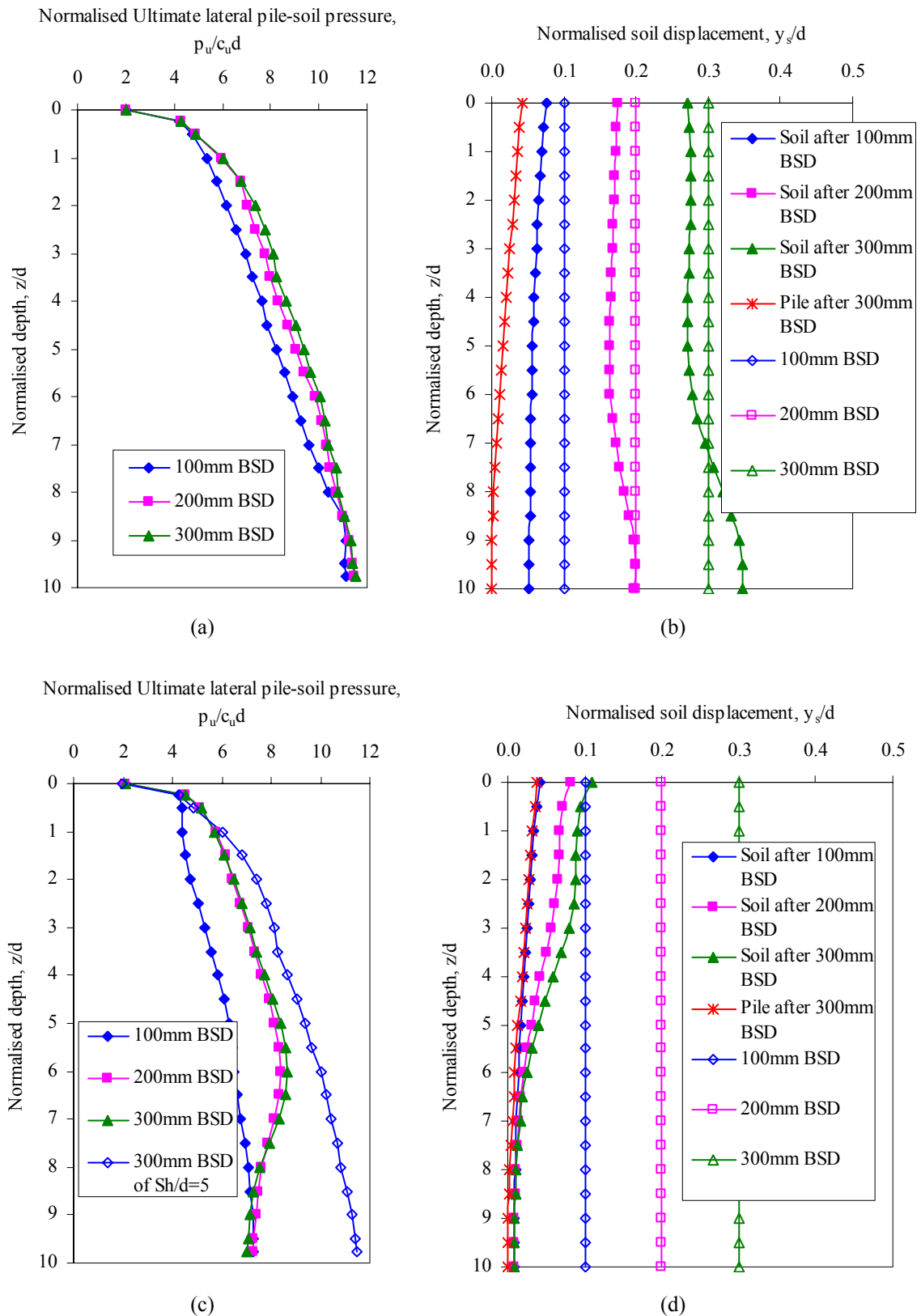


Figure 5.8: Development of normalised ultimate lateral pile-soil pressure for piles spaced at: (a)  $S_h/d = 5$ , (c)  $S_h/d = 2$ ; Movement of soil measured vertically below Point G in the direction of the applied boundary soil displacement for piles spaced at: (b)  $S_h/d = 5$ , (d)  $S_h/d = 2$

The displacement contours of the soil in the  $x$ -direction (i.e. the loading direction) for piles spaced at  $2d$  and  $5d$  are shown in Figure 5.9. The lateral soil movement or flow between the piles is high when the spacing is  $5d$  (Fig. 5.9b) than for the closer piles at  $2d$ , as the soil appears to become trapped in between adjacent piles with decreasing pile spacing. Figure 5.10 shows the vertical displacement contours for the models with piles spaced at  $2d$  and  $5d$ . When the piles are closely spaced as for  $S_H/d = 2$ , the upslope soil tends to move vertically from deeper levels since it cannot easily pass through the piles. However, only the shallower soil in front and close to the pile moves vertically at greater pile spacing as the laterally moving soil is able to flow through them.

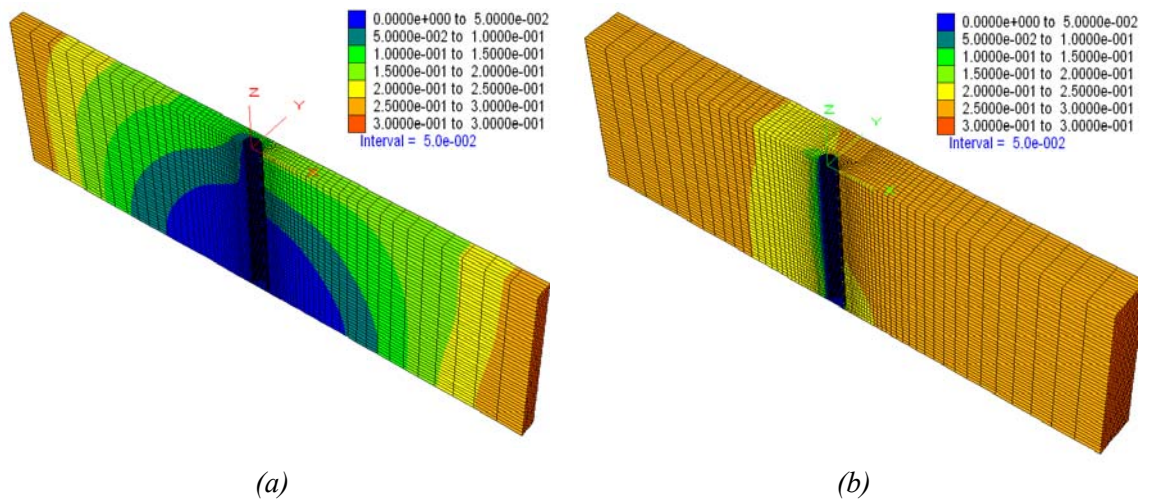


Figure 5.9:  $x$ -displacement contours at 300 mm boundary soil displacement (a) piles at  $2d$  spacing; (b) piles at  $5d$  spacing. Label values are in metre.

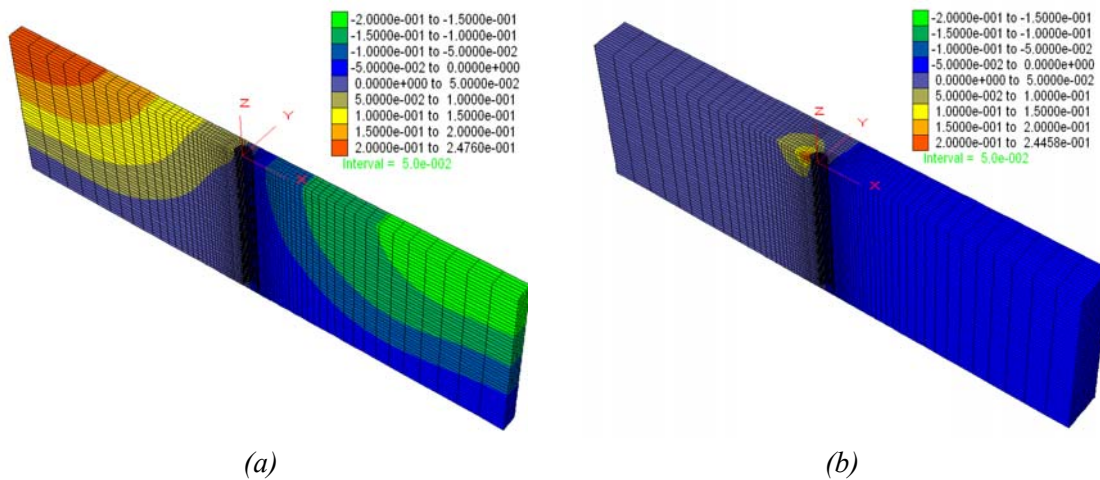


Figure 5.10:  $z$ -displacement contours at 300 mm boundary soil displacement (a) piles at  $2d$  spacing; (b) piles at  $5d$  spacing. Label values are in metre.

Figures 5.11 and 5.12 show the ultimate lateral pile-soil pressure developed on each pile at different spacings and the ultimate lateral pile-soil pressure per metre run of the slope along the direction of the pile row (Eq. 5.1) respectively, for 300 mm of boundary soil displacement. By comparing the figures, it is possible to say that for this situation (for  $S_h/d > 2$ ), increasing pile spacing leads  $p_u$  to increase and  $p_u/S_h$  to decrease. This demonstrates that to stabilise a landslide, the largest ultimate resistance is provided by a row of piles installed fairly close together.

$$p_{u,s} = \frac{p_u}{S_h} \quad \text{Equation 5.1}$$

Where,

- $p_u$  = ultimate lateral pile-soil pressure (unit: N/m)  
= force acting on the pile per unit length along the axis
- $p_{u,s}$  = scaled ultimate lateral pile-soil pressure (unit:  $\text{N/m}^2 = \text{N/m/m}$ )  
=  $p_u$  per metre run of slope along the pile row
- $S_h$  = centre-to-centre spacing between piles in a row

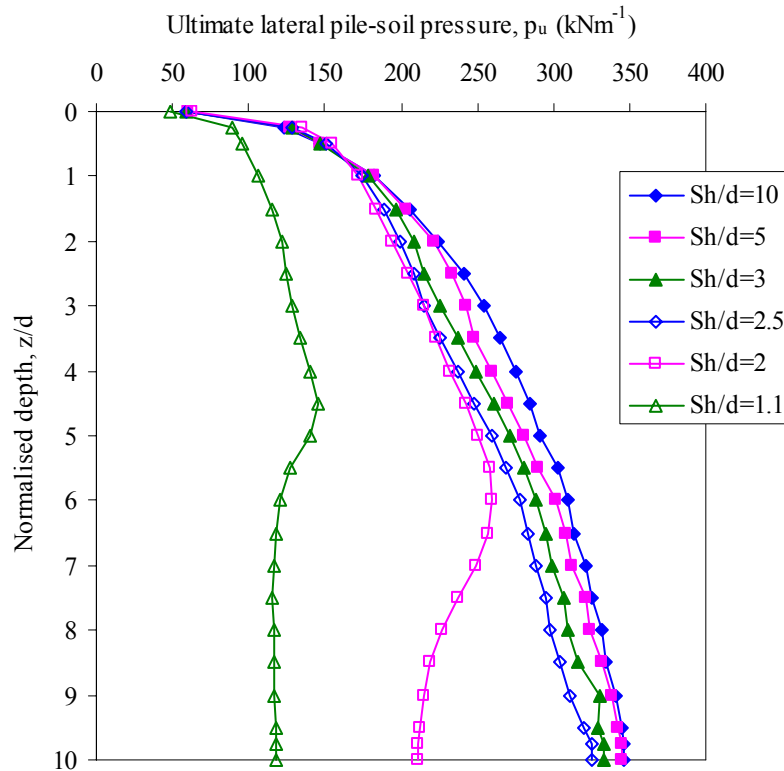


Figure 5.11: Ultimate lateral piles-soil pressure developed on the piles with different pile spacing, after 300 mm of boundary soil displacement

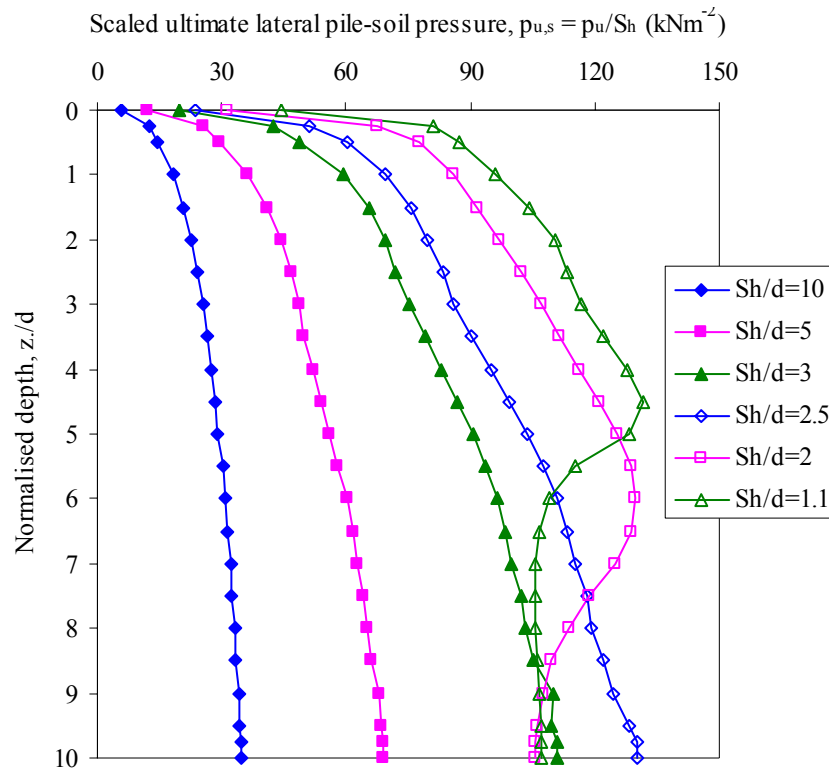


Figure 5.12 Scaled ultimate lateral pile-soil pressure for different pile spacing after 300 mm of boundary soil displacement

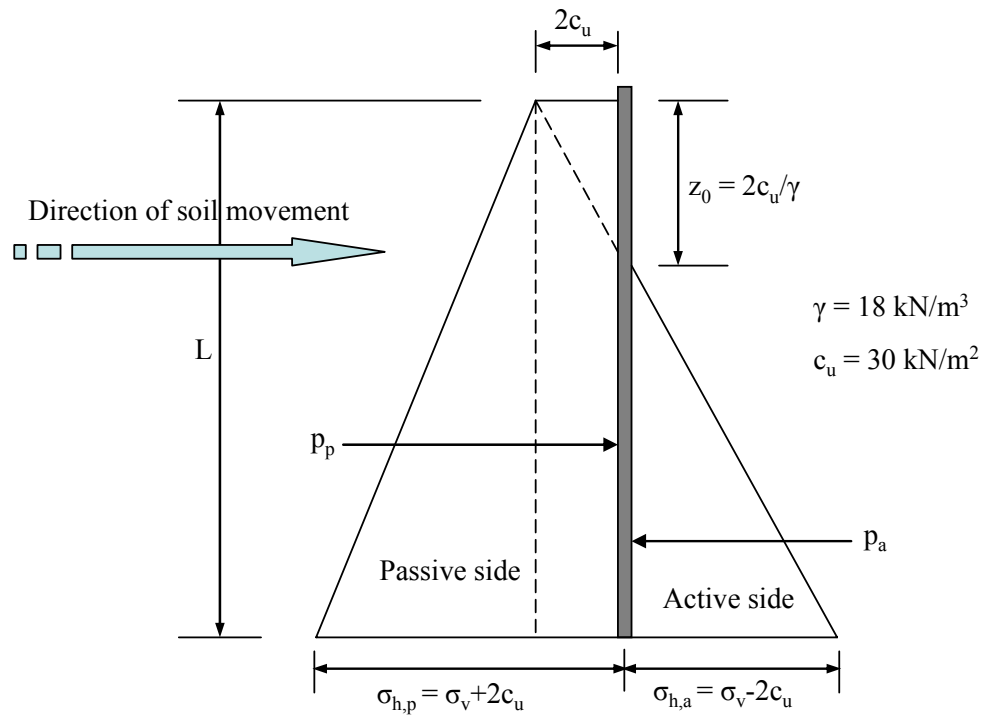


Figure 5.13: Active and passive pressure distribution on a solid retaining wall

As discussed earlier the pile-soil interaction mechanism changes from flow to a passive wedge as the spacing between the pile decreases, and closely spaced piles behave like a solid retaining wall. A 10 m high infinitely long solid retaining wall with zero wall friction (Fig. 5.13) is considered as a basis for comparison with the theoretical retaining wall pressures with those developed for closely spaced discrete piles. The total net thrust acting on the soil retaining wall  $p_{rw}$  (= stabilising force provided by the retaining wall per metre run along the wall) was calculated from Equations 5.2-5.4, and then was normalised by  $c_u L$  (where,  $c_u = 30$  kPa and  $L = 10$  m) to plot the normalised total thrust acting on the ‘solid retaining wall’ in Figure 5.14.

The effects of the formation of a tension crack between the pile wall and the soil in the active side of the retaining wall were taken into account to calculate the pressure acting on the active side of the retaining wall (Eq. 5.3). This was necessary, because gapping was allowed to occur behind the pile (i.e. on the active side) in the  $FLAC^{3D}$  analyses to represent passively loaded pile behaviour more realistically. The depth of soil in tension on the active side of the retaining wall  $z_0$  is dependent of unit weight of the soil  $\gamma$ , and hence  $p_p$ ,  $p_a$  and  $p_{rw}$  are also a function of  $\gamma$ . Changes in  $\gamma$  over the likely range for clays (18-22 kN/m<sup>3</sup>) do not significantly change the total net thrust acting on the soil retaining wall ( $p_{rw}$ ), but it is worth noting that  $p_{rw}$  is not independent of  $\gamma$  if a tension crack forms between the retaining wall and the soil.

$$p_p = \frac{1}{2} \gamma L^2 + 2c_u L \quad \text{Equation 5.2}$$

$$p_a = \frac{1}{2} (\gamma L - 2c_u) \left( L - \frac{2c_u}{\gamma} \right) \quad \text{Equation 5.3}$$

$$p_{rw} = p_p - p_a \quad \text{Equation 5.4}$$

Where,

$p_p$  = total thrust due to passive stresses on the solid retaining wall

$p_a$  = total thrust due to active stresses on the solid retaining wall

$p_{rw}$  = total net thrust acting on the solid retaining wall (Unit: kN per metre length of wall)

The total thrust acting on a 10 m long pile  $p_{pw,ult}$  (= the maximum stabilising force provided by discrete piles per metre run of soil along the direction of the pile row) at different spacings was calculated by integrating the area covered by each curve in Figure 5.12 using an EXCEL spreadsheet, and is plotted in Figure 5.14 with the label ‘discrete pile row’ after being normalised by  $c_u L$ . The ultimate lateral pile-soil pressure ( $p_u$ ) developed for a single isolated pile with full strength or rough pile-soil interface was calculated based on Fleming *et al.*'s (1994) equations (Eqs. 5.5-5.7), and then divided by the pile spacing and normalised by  $c_u L$ . This is shown in Figure 5.14 as ‘isolated pile’.

$$p_u = 2c_u d \quad \text{at the soil surface, } z = 0 \quad \text{Equation 5.5}$$

$$p_u = [2 + ((11.94 - 2)z/3d)]c_u d \quad \text{for depths } z \leq 3d \quad \text{Equation 5.6}$$

$$p_u = 11.94c_u d \quad \text{for depths } z \geq 3d \quad \text{Equation 5.7}$$

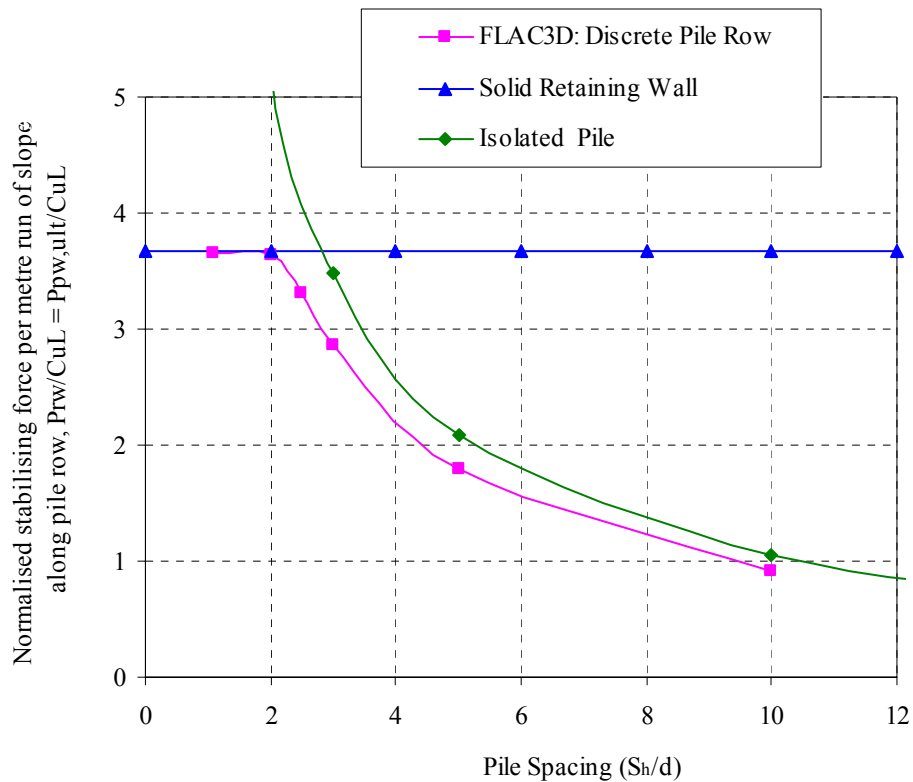


Figure 5.14: Comparison of normalised stabilising force with increasing pile spacing, where  $c_u = 30 \text{ kPa}$ ,  $L = 10 \text{ m}$ ,  $d = 1 \text{ m}$  and  $\gamma = 18 \text{ kN/m}^3$

Figure 5.14 shows that the normalised stabilising force per metre run of the slope provided by closely spaced piles ( $S_p/d < 2$ ) is equal to the normalised total thrust calculated for a solid retaining wall. This confirms the previous analysis which showed that when the piles are spaced at  $S_p/d = 2$ , they create a strong stabilisation mechanism, as a passive wedge forms in front of the closely spaced piles, and pressures developed per metre run of slope along the pile row should be equal to the pressures developed for a solid retaining wall. The stabilising force calculated from  $FLAC^{3D}$  analyses falls below the corresponding isolated pile solution based on Fleming *et al.* (1994), with the reduction in  $p_u$  with decreasing pile spacing ignored assuming that the flow mechanisms for adjacent piles do not interact. From these analyses, it can be deduced that for slope stabilisation by restricting soil movement through the piles at the ultimate limit state, discrete piles have to be installed with a centre-to-centre spacing  $2d$  or less. The maximum stabilising force per metre run of slope, as the piles are brought closer together, is reached at about  $2d$ , and there is not much point then in placing them closer together than  $2d$  centre-to-centre spacing in terms of increasing the stabilising force per metre run.

The stabilising force provided by each pile is a function of the undrained shear strength of the soil. The results presented in Figure 5.14 show the stabilising force for the soil having  $c_u = 30$  kPa. Further numerical analyses were carried out for a soil having  $c_u = 60$  kPa while all other parameters remained as explained in Section 5.2.1, to investigate the effect of undrained shear strength on the normalised stabilising force. The analyses show that for a given pile spacing, the normalised stabilising force provided by each pile per metre run of slope decreases as the undrained shear strength of the soil increases (Fig. 5.15). Also, the difference in normalised stabilising force between the analyses with  $c_u = 30$  kPa and  $c_u = 60$  kPa decreases with increasing pile spacing. In other words, it is possible to say that the difference is greater in closely spaced piles, i.e. when a passive wedge mechanism forms; and the difference decreases when the passive wedge mechanism changes to flow type mechanism. In Figure 5.15, the normalised stabilising force for piles spaced at  $S_p/d = 1.1$  of  $c_u = 60$  kPa analysis is lower than for  $S_p/d = 2$ ; this seems unlikely, and may be due to the boundary effects.



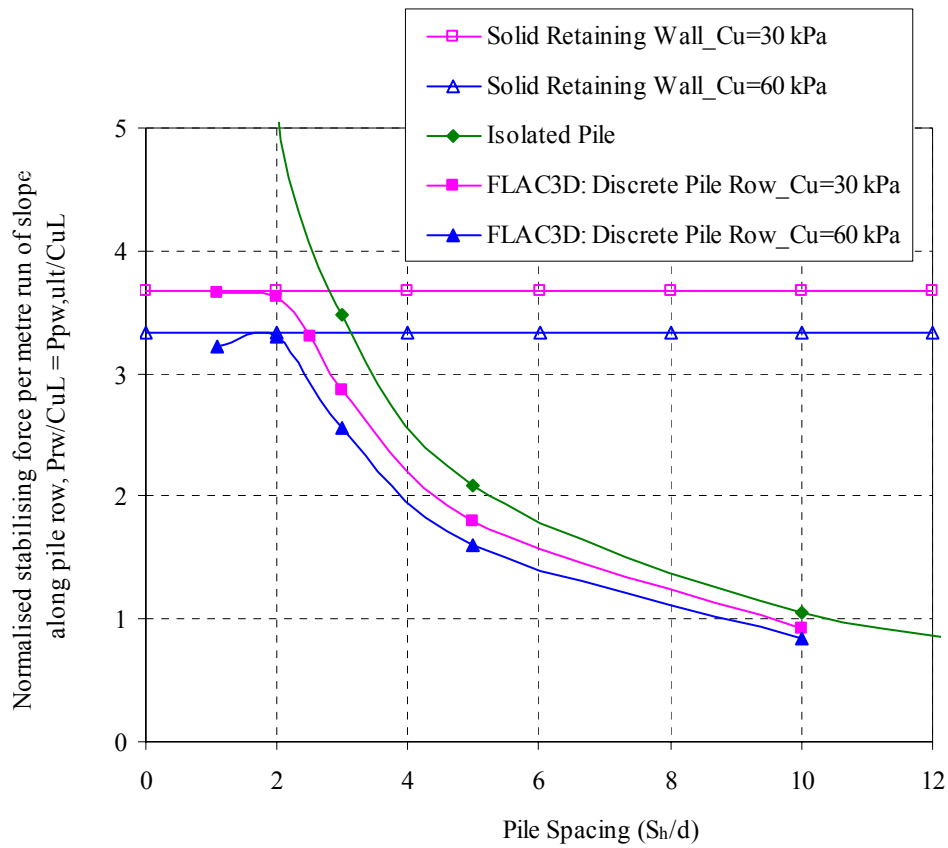


Figure 5.15: Comparison of normalised stabilising force with increasing pile spacing for soils with  $c_u = 30$  kPa and 60 kPa (Stabilising forces normalised by appropriate  $c_u$  values)

The normalised stabilising force calculated for a solid retaining wall using Equations 5.2-5.4, also falls when  $c_u$  increases. The reason for this is that when  $c_u$  increases the depth of soil in the state of tension in active side of the retaining wall  $z_0 = 2 c_u/\gamma$  (Fig. 5.13) also increases, changing the pressure distribution on the active side. This effect is evident from Figure 5.16. The figures also show that the depth of soil in tension  $z_0$  increases when  $c_u$  of the soil increases.

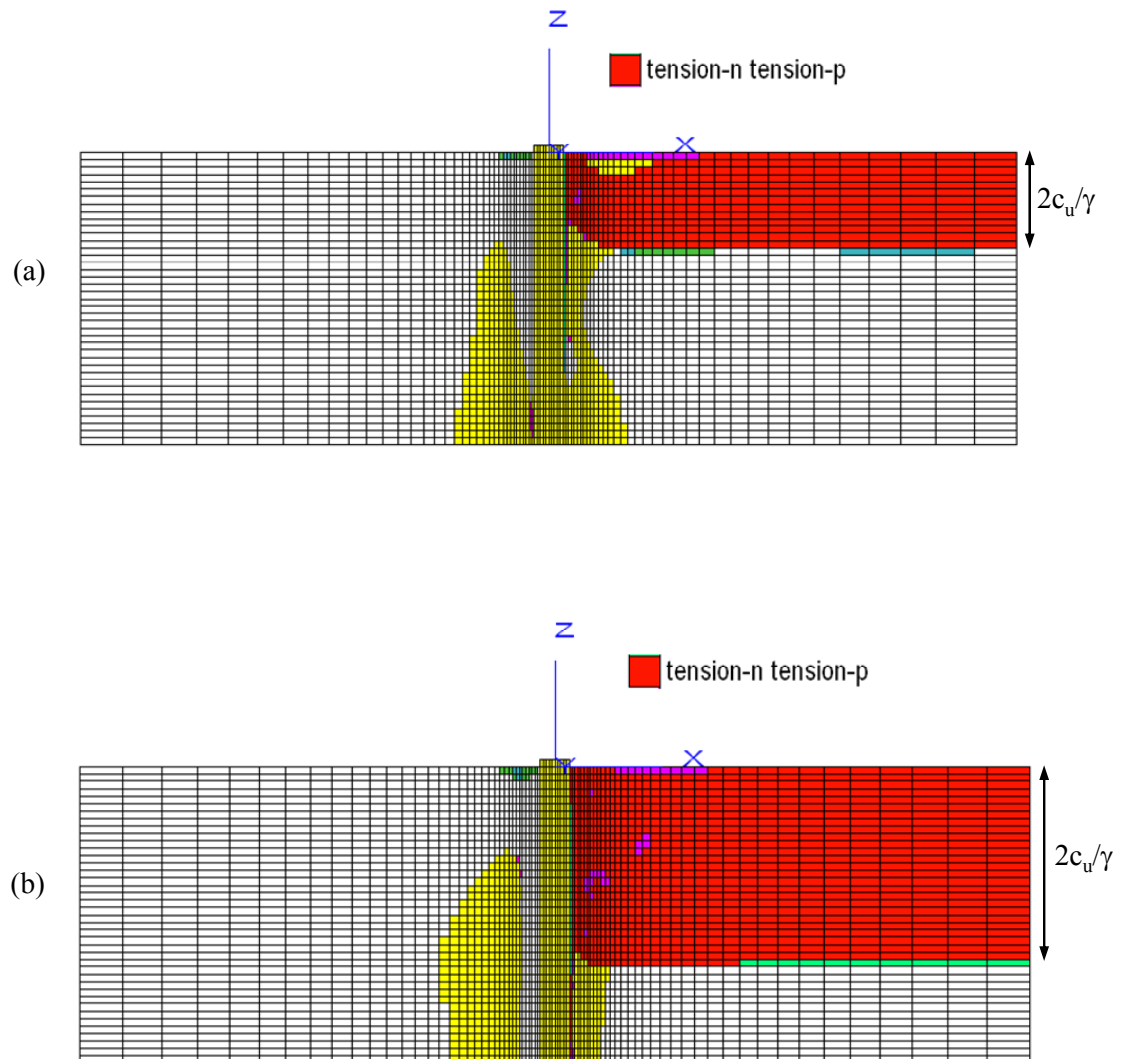


Figure 5.16: Block state of  $FLAC^{3D}$  model at 300 mm boundary soil displacement for piles at 2  $d$  spacing: (a) model with  $c_u = 30$  kPa; and (b) model with  $c_u = 60$  kPa

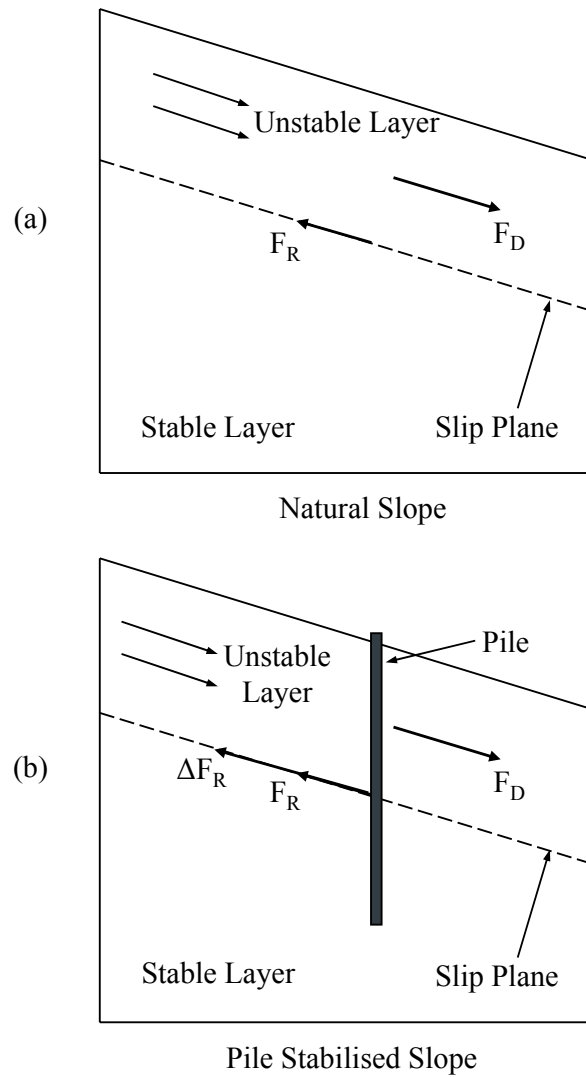


Figure 5.17: Diagrams shows how pile increases factor of safety (FoS) of unstable slope

$$FoS_{\text{Natural}} = \frac{\sum F_R}{\sum F_D} \quad \text{Equation 5.8}$$

$$FoS_{\text{Increased}} = \frac{\sum F_R + \Delta F_R}{\sum F_D} \quad \text{Equation 5.9}$$

Where,

$F_R$  = resisting force provided by per metre run of slope

$F_D$  = disturbing force caused by per metre run of slope

$\Delta F_R$  = stabilising force provided by pile to per metre run of slope

The factors of safety ( $FoS$ ) of a natural slope and a pile stabilised slope can be determined using Equations 5.8 and 5.9, respectively. When a pile is installed into the ground, it provides an additional resisting force  $\Delta F_R$  (here called the stabilising force). Therefore, a pile which provides a higher  $\Delta F_R$  is more effective at increasing the  $FoS$  of the unstable slope. The stabilising force provided by every pile per metre run of slope along the pile row is equal to the shear force developed in the pile at the slip plane, divided by the centre-to-centre pile spacing. The variation in stabilising force with pile spacing calculated from the developed ultimate lateral pile-soil pressure was plotted in Figure 5.14. The stabilising force calculated using the pile shear force is compared with the pressure calculation in Figure 5.18. The stabilising force calculated from the shear forces is slightly less than that calculated using the lateral pile-soil pressures. This is because, the piles have been modelled with a number of elements (40 tiers of vertical elements for 10 m long pile) that balances acceptable numerical modelling accuracy against computation time, so that a small error remains in the maximum shear force.

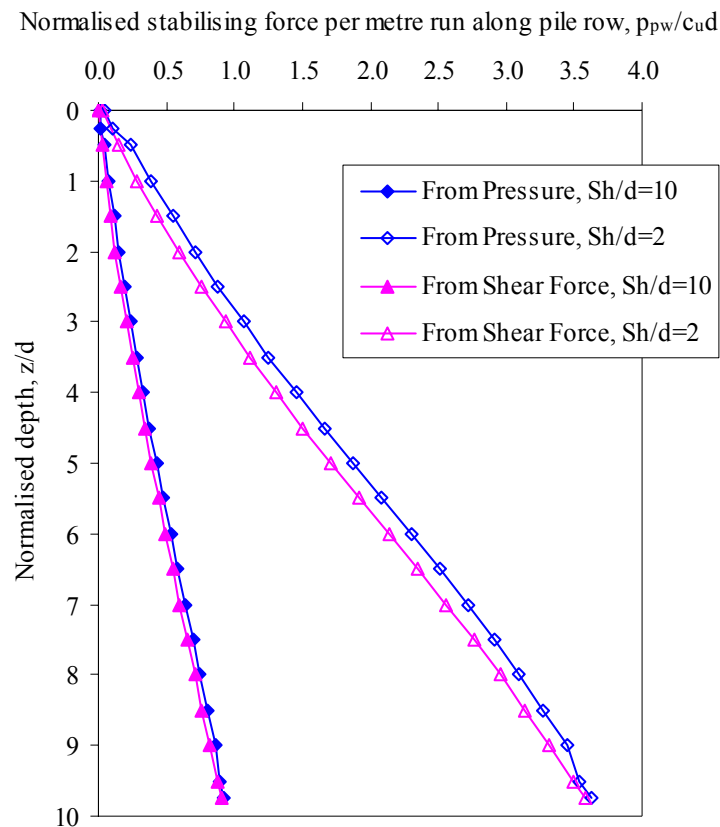


Figure 5.18: Comparison of normalised stabilising force calculated using ultimate lateral pile-soil pressure and maximum shear force, where  $c_u=30$  kPa and  $d=1$  m

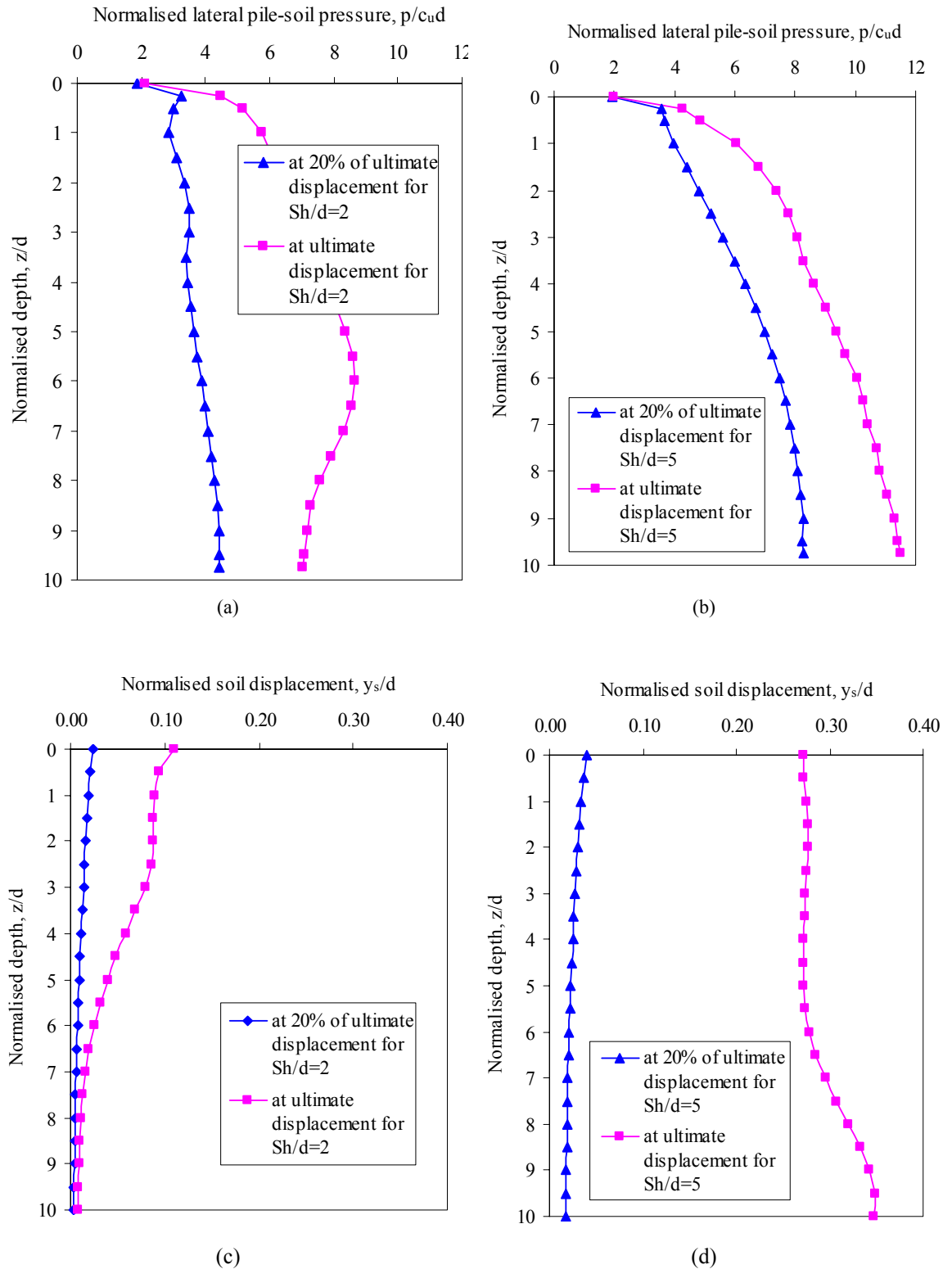


Figure 5.19: (a) & (b) The normalised lateral pile-soil pressure developed on pile at 20% of ultimate displacement for  $S_h/d = 2$  and 5; (c) & (d) The soil movement measured through Point G with depth at 20% of ultimate displacement. 300 mm of boundary soil displacement was assumed to be sufficient to develop the ultimate load

All the above analyses were carried out to understand the pile behaviour at the ultimate limit state. However, in reality stabilising piles are unlikely to reach the ultimate limit state load, and they are generally designed for loading in serviceability conditions. *FLAC<sup>3D</sup>* analyses were carried out to investigate the pile behaviour at 20% of ultimate displacement (i.e. 60 mm), where 300 mm of boundary soil displacement was assumed to be needed to develop the ultimate load. Figures 5.19(a) and (b) show the lateral pile-soil pressure for the piles spaced at  $S_h/d = 2$  and 5, and Figures 5.19(c) and (d) show the measured soil movement along a vertical line through Point G (Fig. 5.7a) with depth. At 20% of the ultimate boundary soil displacement, the lateral pile-soil pressure reaches 72% of  $p_u$  at the bottom of pile for  $S_h/d = 5$ , and 62% for  $S_h/d = 2$ . The soil displacements measured through point G for the piles spaced at  $S_h/d = 5$  are shown in Figure 5.19(d), from which it is possible to say that an acceptable stabilising mechanism is formed in between adjacent piles at 20% of the ultimate boundary soil displacement; and therefore a bigger centre-to-centre pile spacing can be adopted for the design of discrete piles for serviceability loading states.

This point was investigated further by plotting the variation of normalised stabilising force per metre run of slope with pile spacing for 20% of the ultimate boundary soil displacement, as shown in Figure 5.20. The figure clearly shows that the difference between the stabilising forces provided by the piles spaced at  $2d$  and  $10d$  increases with increasing boundary soil movement, and reaches the maximum for the ultimate loading state. As previously explained, the closely spaced piles provide a stabilising force equivalent to the force obtained from a soil retaining wall at the ultimate loading state because of the formation of a passive wedge in front of the pile row. The effect of the passive wedge stabilising mechanism is less for serviceability loading states, and therefore the piles spaced at  $S_h/d = 2$  do not provide a significantly higher stabilising force for serviceability loading states. The difference between the stabilising force provided by the piles spaced at  $S_h/d = 2$  and 3 or 5 is small. These results confirm the earlier conclusion that for serviceability loading states, a bigger pile spacing can be adopted.

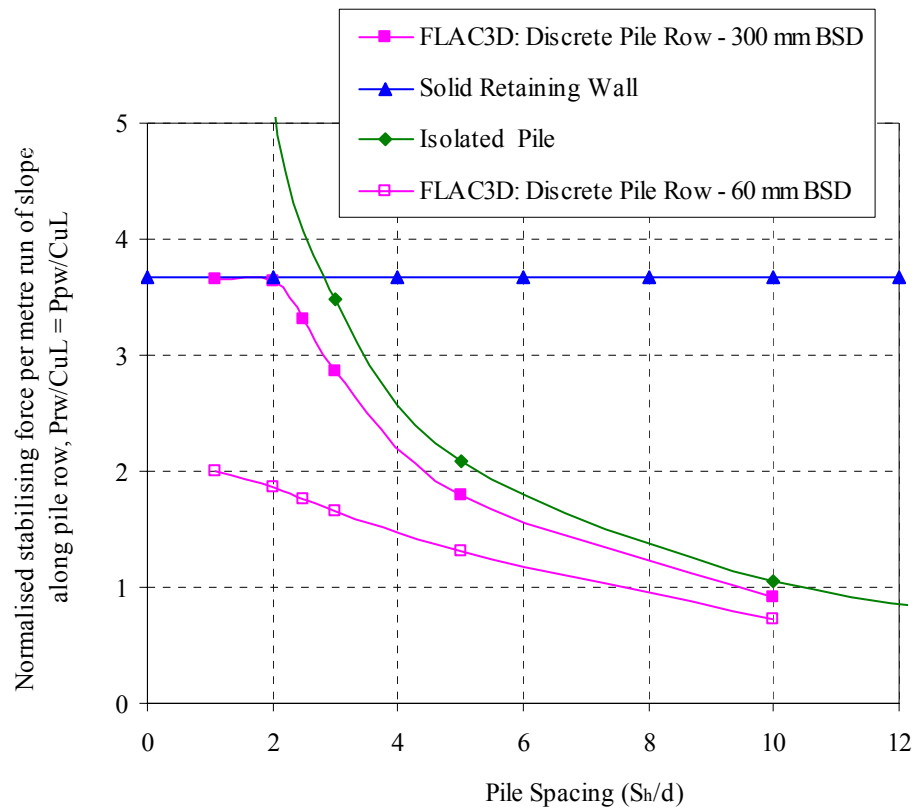


Figure 5.20: Comparison of normalised stabilising force with increasing pile spacing for 20% of ultimate boundary soil movement and ultimate boundary soil movement, where  $c_u = 30 \text{ kPa}$ ,  $L = 10 \text{ m}$ ,  $d = 1 \text{ m}$  and  $\gamma = 18 \text{ kN/m}^3$

### 5.3 Interaction effects between two rows of piles

The previous analyses have shown that a single row of piles does not prevent the flow of soil through the piles at the ultimate limit state unless they are placed at a spacing of  $2d$  or less. Therefore, it is worth investigating the pile-soil interaction mechanism of two pile rows at ultimate load, especially for higher pile spacings in the direction perpendicular to soil movement.

To avoid confusion in naming the pile rows, the following terminologies are used. The pile row which has the nearest displacement boundary pushed towards it is named ‘upslope’ or ‘upper’ row, and the row which has the displacement boundary pulled away from it is named ‘downslope’ or ‘lower’ row (Fig. 5.21). Although in the analyses the two pile rows were installed in a moving soil with a flat ground surface, the pile rows are still named as ‘upslope row’ and ‘downslope row’ to clearly differentiate their position relative to the soil movements. The spacing between the piles in the direction perpendicular to the soil movement is denoted ‘ $S_h$ ’ while the spacing parallel to the soil movement is denoted ‘ $S_v$ ’.

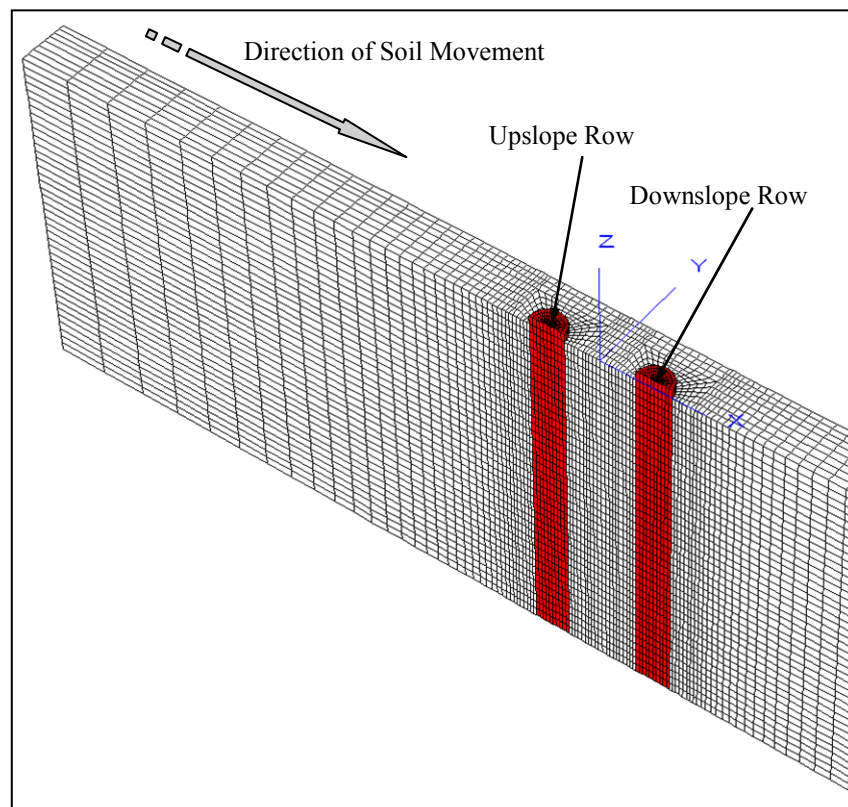


Figure 5.21:  $FLAC^{3D}$  mesh showing two pile rows spaced at  $S_h/d = 3$  and  $S_v/d = 3$



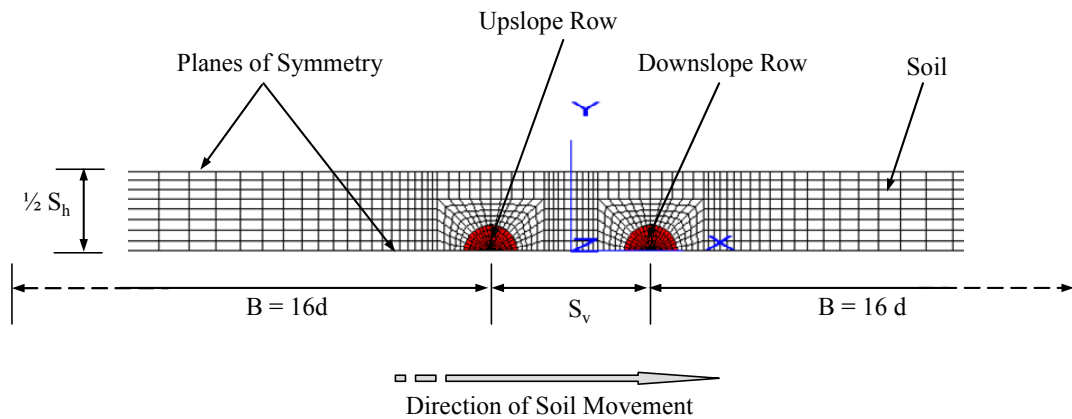


Figure 5.22: Plan view of two infinitely long rows of piles

### 5.3.1 $FLAC^{3D}$ analyses

The  $FLAC^{3D}$  model used to carry out the analyses is shown in Figure 5.21. The boundary conditions, constitutive models and material properties were the same as in the previous analyses. Four different pile group combinations were selected as shown in Table 5.1.

Case	$S_h/d$	$S_v/d$
1-A	3	3
1-B	3	5
2-A	5	3
2-B	5	5

Table 5.1: Pile group arrangements

### 5.3.2 Results and discussion

The deflection, shear force, bending moment and ultimate lateral pile-soil pressure plots from the current analyses are compared with the behaviour of a single pile row. The effects of  $S_v$  on the pile behaviour when the piles are spaced at  $S_h/d = 3$  and  $S_h/d = 5$ , are analysed as Case-1 and Case-2, respectively.

### 5.3.2.1 Case – 1 ( $S_h/d = 3$ )

As may be expected, the maximum deflection, shear force, bending moment and ultimate lateral pile-soil pressure developed in individual piles are significantly reduced when two rows are installed (Fig. 5.23). For both values of  $S_v/d$ , the upslope piles deflect slightly more than the downslope piles. As  $S_v/d$  decreases, the difference between the deflections of the upslope and downslope piles also decreases, so that at  $S_v/d = 3$  both rows seem to move together, but deflect more than the upslope piles spaced at  $S_v/d = 5$  (Fig. 5.23a). A slightly higher shear force and bending moment is developed at the base of the upslope pile row for the ultimate load (Figs. 5.23b and 5.23c). However, these differences are small. In general, the spacing in the direction of loading  $S_v$ , does not much influence the shear force and bending moment in the piles within the range investigated.

The reduction in the normalised ultimate lateral pile-soil pressure as a function of the spacing between pile rows is shown in Figure 5.23(d). There is a crossover in the relative magnitudes of the normalised ultimate lateral pile-soil pressure of the upslope and downslope piles at a depth of about  $4.5 d$  below ground level. Below  $4.5 d$  depth, the greater ultimate lateral pile-soil pressure is carried by the downslope piles and above, by the upslope piles.

Figure 5.24 shows the lateral movement on a vertical line through the Points ‘Up’ and ‘Down’ located 1 m away from the pile centres, after 300 mm of boundary soil displacement. A very effective stabilising mechanism has been developed in this pile group configuration compared with a single pile row at  $S_h/d = 3$ . A slightly bigger soil movement is apparent in the upslope row than in the downslope row, especially at shallow depths. This might be expected, since the upslope piles directly face the laterally moving soil, while the downslope row is sheltered to some extent by the upslope row.

Figure 5.25(a) shows the displacement contours in the  $x$ -direction for two pile rows spaced at  $S_h/d = 3$  and  $S_v/d = 3$ . If compared with Figure 5.25(b), the two pile rows (with the same  $S_h/d$  as single row) create a zone between the pile rows in which a very little soil movement occurs. Careful inspection of Figure 5.25(a) shows that the soil movement at ground level along the upslope pile row is slightly bigger than along the downslope row, confirming the measured soil movement as shown in Figure 5.24(b). For  $S_h/d = 3$ , the soil movement through the Point ‘Down’ decreases as  $S_v/d$  increases; however, the difference is very small (Fig. 5.24b). It is important to note that the numerical results presented here aim to analyse the pile group behaviour for 300 mm of boundary soil displacement.

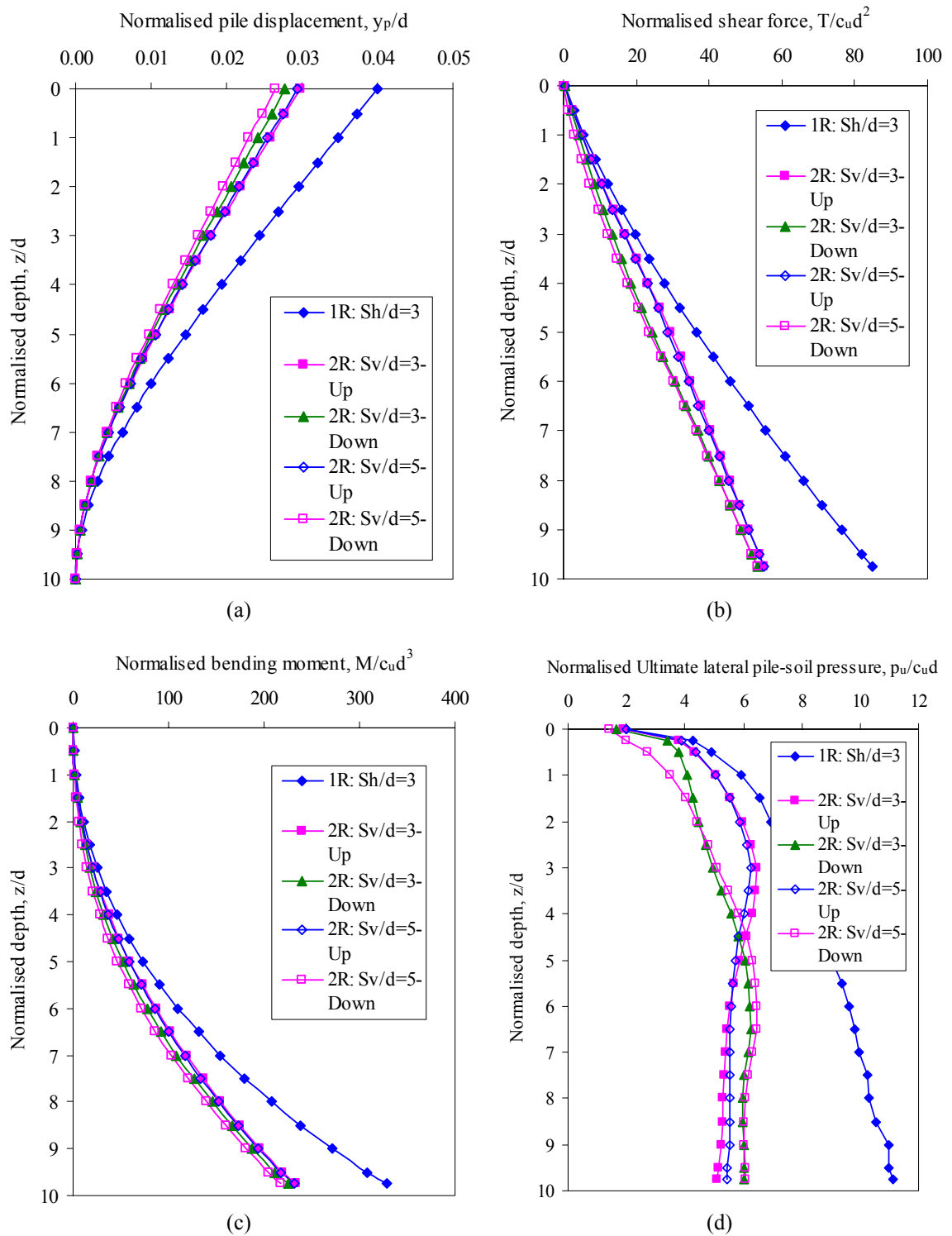


Figure 5.23: Behaviour of two pile rows at different  $S_v/d$  pile spacings for soil boundary displacement of 300 mm. The spacing between piles along the pile row,  $S_h = 3d$  : (a) normalised pile displacement; (b) normalised shear force; (c) normalised bending moment; and (d) normalised ultimate lateral pile-soil pressure

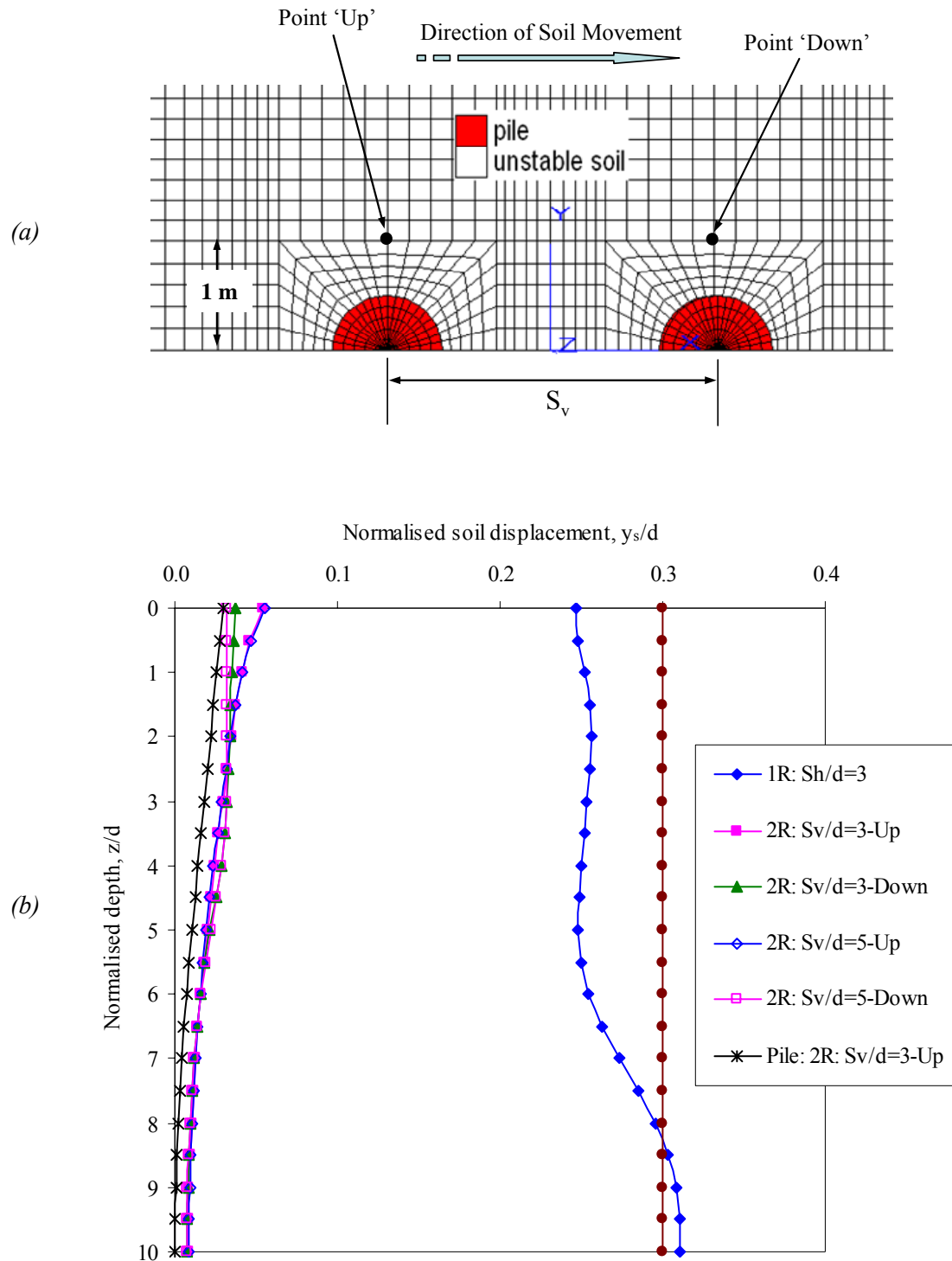


Figure 5.24: (a) Mesh showing where soil movement was monitored; (b) Movement of soil at 1 m away from pile centres in the  $y = 1$  plane after 300 mm of boundary soil displacement for  $S_h/d = 3$  arrangement

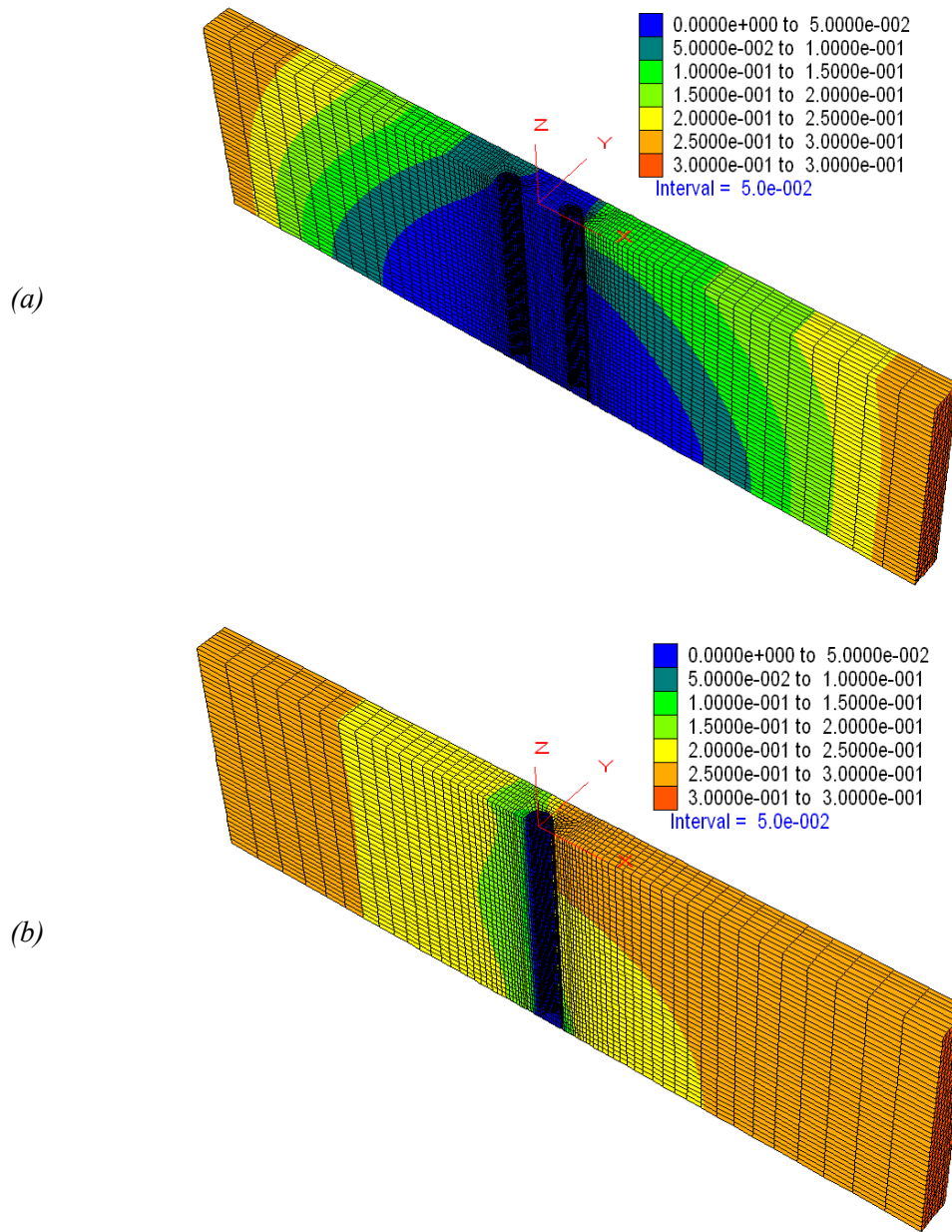


Figure 5.25: (a)  $x$ -displacement contours at 300 mm boundary soil displacement for two pile rows spaced at  $S_h/d = 3$  and  $S_v/d = 3$ ; (b)  $x$ -displacement contours at 300 mm boundary soil displacement for single pile row at  $3d$  spacing. Label values are in metre.

The analyses carried out to investigate the behaviour of single pile row showed that the passive wedge mechanism forms in front of piles installed at a spacing of  $2d$  or less (Fig. 5.6). For a spacing greater than  $2d$ , the mechanism changes to the Broms (1964) / Randolph and Houlsby (1984) flow mechanism. Figure 5.26(a) shows the modified displacement vectors of the two pile rows spaced at  $S_h/d = 3$  and  $S_v/d = 3$ , from which it is obvious that a passive wedge has developed in front of the upslope row. This may be contrasted with Figure 5.26(b) in which the

mechanism of passive wedge formation is less apparent and the soil flows around the pile. The formation of the passive wedge in front of the two pile rows at  $S_h/d = 3$  is the reason for the small soil movement in between the pile rows in Figure 5.25(a).

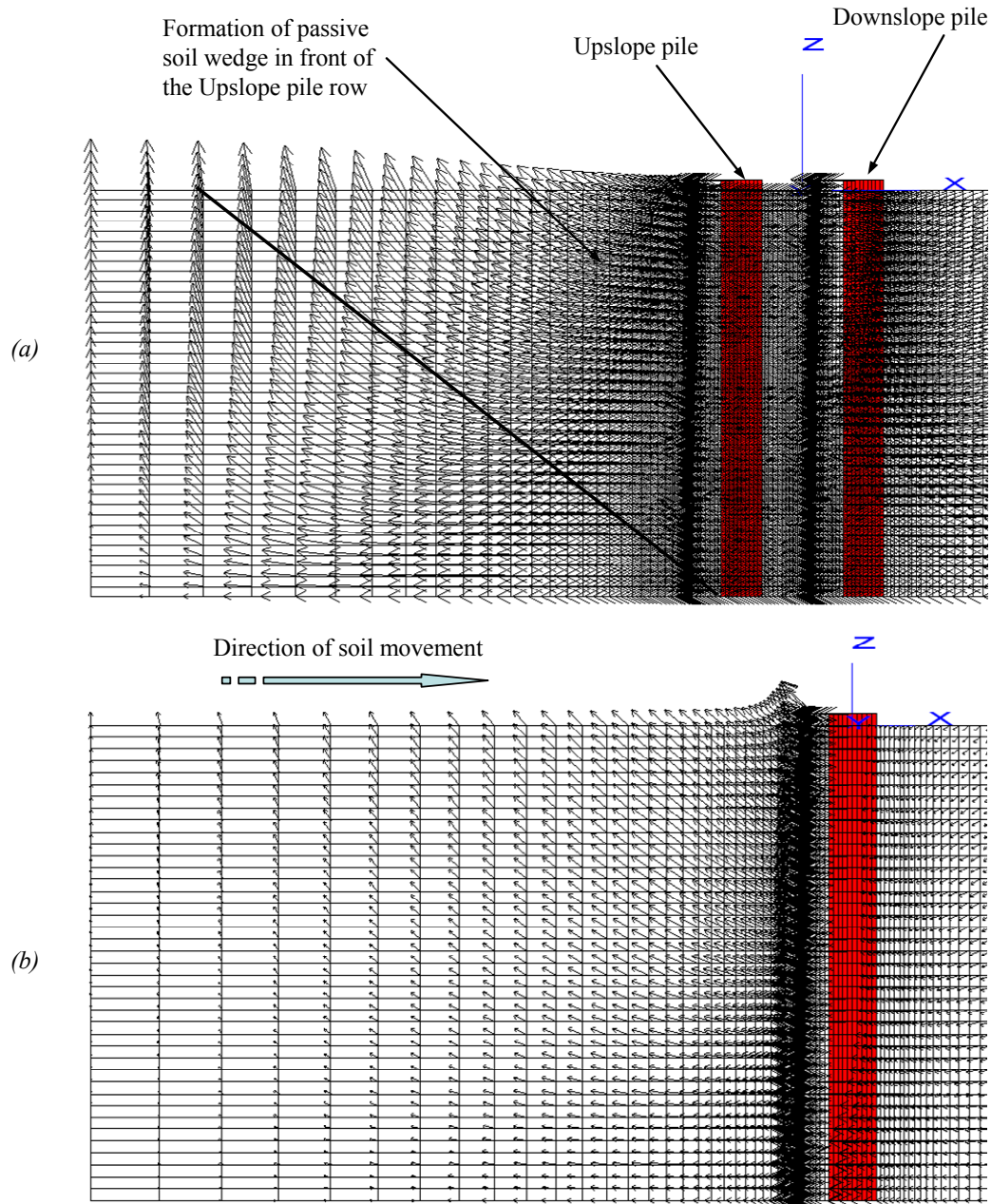


Figure 5.26: Relative displacement vectors (= displacement vectors, after 300 mm boundary soil displacement – 300 mm displacement, in x-direction) plotted on the plane through pile axis and parallel to the soil movement ( $y = 0$ ) (a) for the discrete piles spaced at  $S_h/d = 3$  and  $S_v/d = 3$ ; (b) for single discrete pile row spaced at  $S_h/d = 3$

If Figure 5.23(d) is compared with Chen and Poulos's (1993) 2D plane strain analyses of actively loaded piles (Fig. 2.21) for the pile group arrangement  $(S_H/d, S_V/d) = (3, 3)$ , the difference in  $p_u/c_u d$  above about  $4.5 d$  depth is similar in that pressures are greater on the upslope piles. However, the  $p_u/c_u d$  for the downslope piles exceeds the  $p_u/c_u d$  for the upslope piles below  $4.5 d$  depth in the current  $FLAC^{3D}$  analysis.  $p_u/c_u d$  is not much affected by the increase in  $S_V$  in the  $FLAC^{3D}$  analysis, while in the 2D plane strain analyses  $p_u/c_u d$  increases for downslope piles. The key reason why Chen and Poulos's results vary from the  $FLAC^{3D}$  analysis is because 2D plane strain analyses do not incorporate the 3D surface effects that cause such large differences in pressure with depth.

### 5.3.2.2 Case – 2 ( $S_H/d = 5$ )

The effect of  $S_V$  on two rows of piles spaced at  $S_H/d = 5$  is analysed in this section and their behaviour is shown in Figure 5.27 for 300 mm of boundary soil movement. Figure 5.27 clearly shows that the reduction in the deflection, shear force, bending moment and ultimate lateral pile-soil pressure is smaller when  $S_H/d = 5$ , than when  $S_H/d = 3$  (Fig. 5.23). Figure 5.27(a) shows that the highest deflection is at the top of the downslope row when  $S_V/d = 5$  which is greater than the deflection of single pile row, and the lowest is when  $S_V/d = 3$ . As the downslope row with  $S_V/d = 3$  deflects least, the lowest shear force and bending moment are developed in the same pile row. The highest bending moment is developed in the downslope row for  $S_V/d = 5$ . However, there is not much difference between these, if contrasted with  $S_H/d = 3$ .

Figure 5.27(d) compares the development of normalised ultimate lateral pile-soil pressure for different pile group arrangements after 300 mm of boundary soil displacement. The piles spaced at  $S_V/d = 5$  have  $p_u/c_u d$  close to that for a single pile row, while a considerable reduction occurs in the piles with a spacing  $S_V/d = 3$ . The same result was found by Brown and Shie (1990b) using 3D finite element analyses (Fig. 2.28), although their analyses were carried out for active loading. The reason for the smaller reduction in  $p_u/c_u d$  with increasing  $S_V$  is that after a certain  $S_V$ , both pile rows tend to behave independently.

The soil movement on a vertical line through the Points marked 'Up' and 'Down' shows that the soil movement increases as  $S_V/d$  decreases (Fig. 5.28b). However, this movement is much greater than for compared with the  $S_H/d = 3$  pile group arrangement (Fig. 5.24b). From this, it is possible to say that the formation of an 'interlocking' or 'soil locking' mechanism between the piles in the  $S_H/d = 5$  arrangement is not as clear as when  $S_H/d = 3$ , for the ultimate state (Figs. 5.29a and 5.25a).

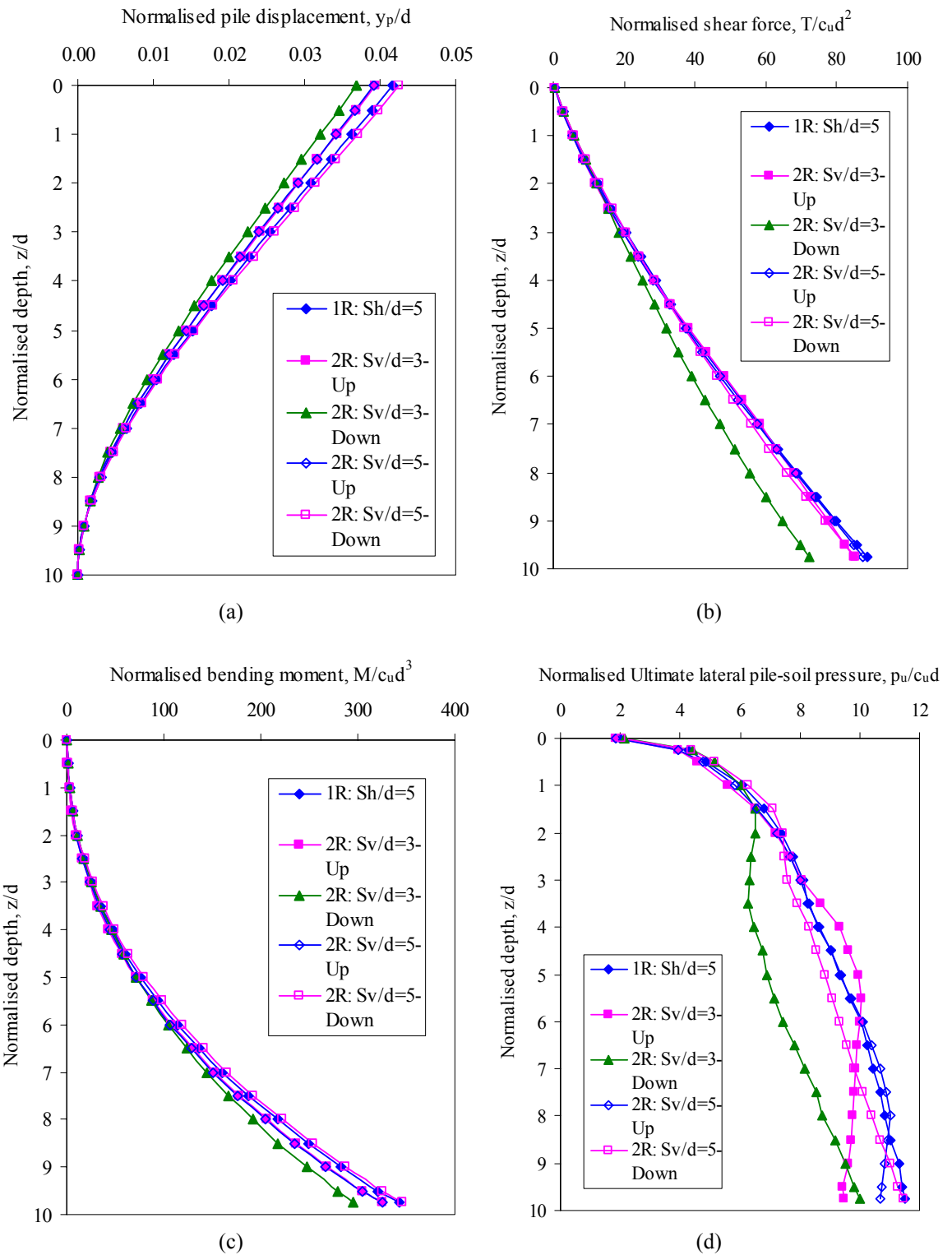


Figure 5.27: Behaviour of two pile rows at different  $S_v/d$  pile spacings for soil boundary displacement of 300 mm. The spacing between piles along the pile row,  $S_h = 5d$  : (a) normalised pile displacement; (b) normalised shear force; (c) normalised bending moment; and (d) normalised ultimate lateral pile-soil pressure



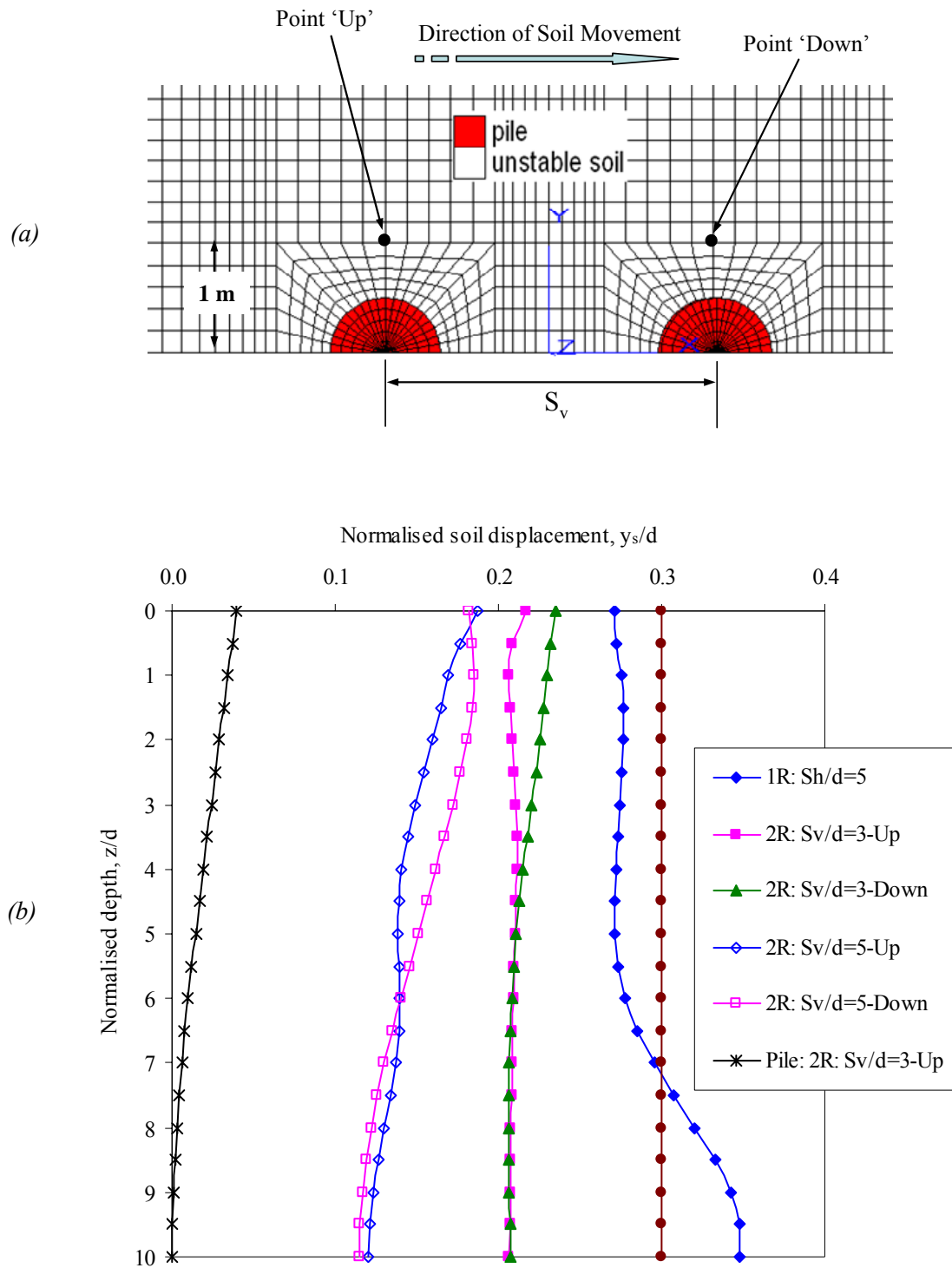


Figure 5.28: (a) Mesh showing where soil movement was monitored; (b) Movement of soil at 1 m away from pile centres in the  $y = 1$  plane after 300 mm of boundary soil displacement for  $S_h/d = 5$  arrangement

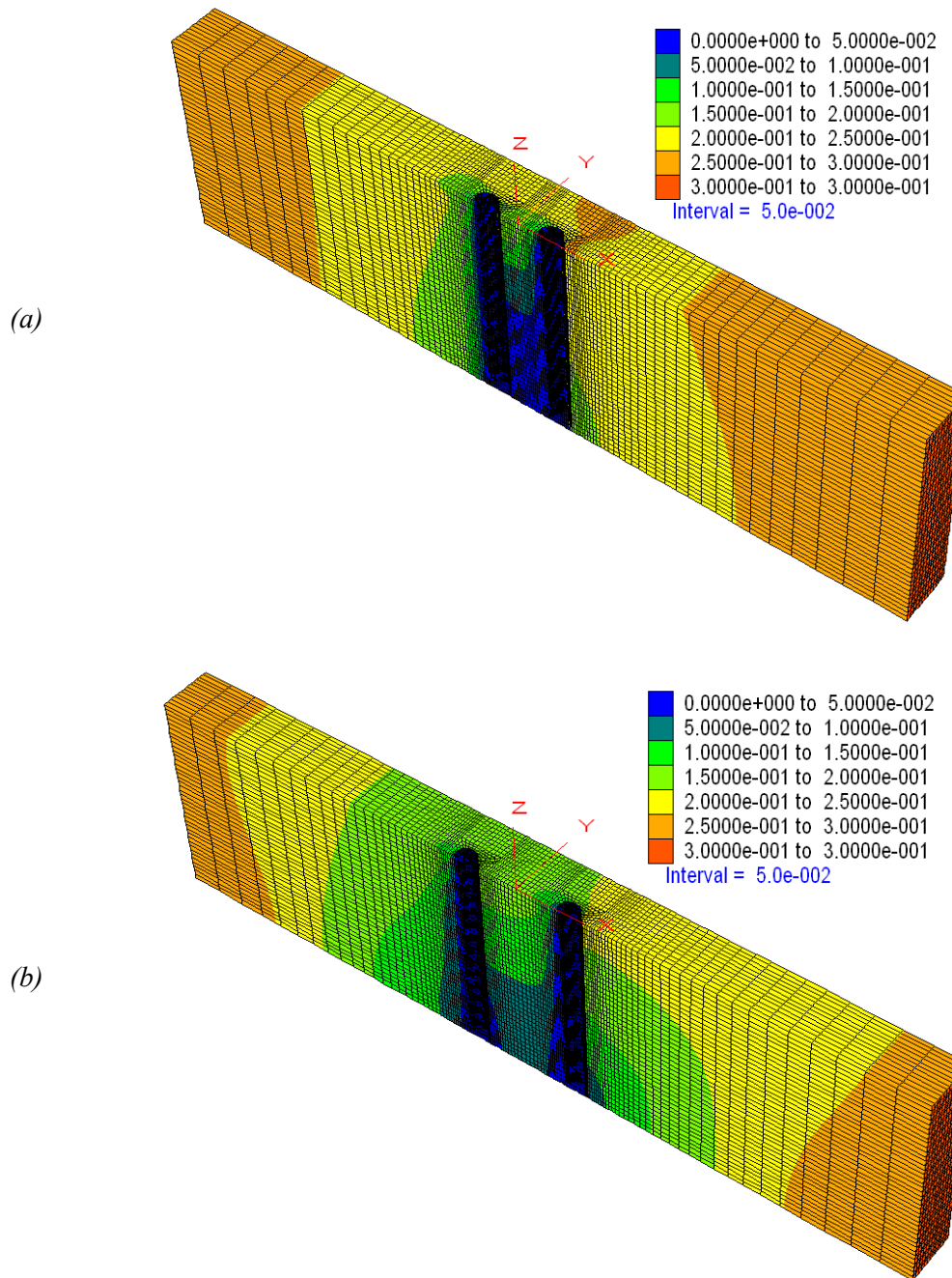


Figure 5.29:  $x$ -displacement contours at 300 mm boundary soil displacement for two pile rows spaced at (a)  $S_h/d = 5$  and  $S_v/d = 3$ ; (b)  $S_h/d = 5$  and  $S_v/d = 5$ . Label values are in metre.

For  $S_h/d = 5$ , the soil movement through the piles is greater when  $S_v/d = 3$  than when  $S_v/d = 5$  (Fig. 5.28b). This behaviour is more evident in Figure 5.29, in which the  $x$ -displacement contours have been plotted after 300 mm of boundary soil displacement. When  $S_v/d = 3$ , more soil has flowed through the piles as can be seen in Figure 5.29(a). However, these soil movements are much higher than for the  $S_h/d = 3$  pile group arrangement (Fig. 5.24b). This is

because, as explained earlier, the stabilisation mechanism developed in front of the upslope piles is the passive wedge for the  $S_h/d = 3$  arrangement, and is not influenced by the increase in spacing  $S_v$ . When  $S_h/d$  reaches 5, the stabilisation mechanism changes from a passive wedge to soil flow, and as a result a greater soil movement occurs through the piles. Interestingly, for the  $S_h/d = 5$  arrangement, the magnitude of soil movement through the piles depends on the spacing  $S_v$  unlike when  $S_h/d = 3$ , and increases with decreasing  $S_v$ .

The normalised stabilising resistance provided by one and two discrete pile rows per metre along the slope are compared with the solid retaining wall, and the isolated pile calculations in Figure 5.30. Figure 5.30 clearly shows that the double rows provide a larger stabilising resistance than a single row at the same spacing, and the double row with  $S_h/d = 3$  provides a larger resistance than that with  $S_h/d = 5$ . When two pile rows are installed with a spacing  $S_h/d = 3$ , the developed maximum stabilising resistance was equal to the force calculated from the soil retaining wall. This is because, as explained earlier, when the two pile rows are spaced at  $S_h/d = 3$ , the mechanism developed in front of the upslope pile row is similar to a passive wedge.

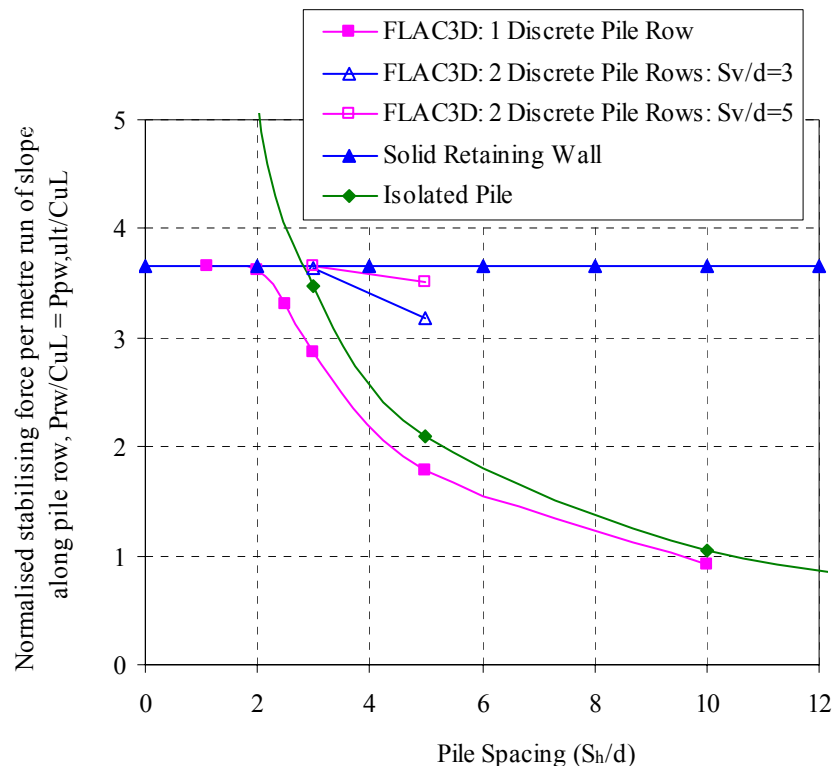


Figure 5.30: Comparison of normalised stabilising force per metre run of slope along pile row with increasing pile spacing in single and double discrete pile rows, where  $c_u = 30 \text{ kPa}$ ,  $L = 10 \text{ m}$ ,  $d = 1 \text{ m}$   $\gamma = 18 \text{ kN/m}^3$

In terms of stabilising a slope using discrete pile rows, two main criteria have to be satisfied in selecting the pile spacings: the piles have to be installed to provide a sufficient stabilising force to resist the laterally moving soil, and to allow acceptably small soil movements through them. When the two pile rows are spaced at  $S_h/d = 3$ , the movement of soil through the piles is very small and is independent of spacing  $S_v$  (Fig. 5.24b). Also, this pile group arrangement provides a stabilising force equivalent to the force obtained from a solid retaining wall (Fig. 5.30). When the spacing  $S_h/d$  increases to 5, the soil movement through the piles is larger than when  $S_h/d = 3$  (Fig. 5.28b). Although this pile group arrangement provides a higher stabilising force than a single pile row spaced with the same  $S_h/d$ , it may not be preferred to stabilise the slope for ultimate loading state, due to the occurrence of higher soil flow through the piles (Fig. 5.28b).

However, as previously explained, the difference between the stabilising force provided by the closely and widely spaced piles and the flow of soil through the piles decrease with decreasing boundary soil displacement. Therefore, a bigger spacing between piles in a row ( $S_h$ ) can be adopted for the stabilising pile design at the serviceability loading state.

If the performance of a single pile row is compared with that of two pile rows at the ultimate loading state, the single pile row spaced at  $S_h/d = 2$  and the two piles rows spaced  $S_h/d = 3$  provide a stabilising force equivalent to the force obtained from a solid retaining wall (Fig. 5.30). For both cases, soil movement through the piles remains very small, as a passive wedge type stabilisation mechanism forms in front of the piles. Therefore, both of these pile group arrangements can be adopted for a stabilising pile scheme for the ultimate loading state.

However, when the number of piles required is considered, the two pile rows with  $S_h/d = 3$  requires more piles than the single row with  $S_h/d = 2$ . For example, if the slope is 12 m long, 7 piles are needed to stabilise it using a single row, and three more piles are needed to stabilise it using the double row. Therefore, when identical piles (i.e. same length, diameter and material properties) are used in the single and the double rows, the stabilisation scheme using the double pile rows will cost more than the single pile row. If the maximum shear force in the pile is considered, a normalised shear force  $T/c_u d^2$  (where  $c_u = 30$  kPa and  $d = 1$  m) of 71.67 was developed in the single pile row (Fig. 5.4b), while around 54 was developed in one of the rows in the double pile row (Fig. 5.23b). Therefore, the stabilising piles used in a double row can be designed to be slightly weaker (one way of achieving this is by reducing the pile diameter), and in this way the total cost of the double row pile scheme may reduced, perhaps to below that of single pile row scheme.

## 5.4 Summary

The major findings from the analyses carried out to understand the behaviour of one and two pile rows are:

(a) for the single pile row,

- (1) The pile deflection, shear force, bending moment and ultimate lateral pile-soil pressure increase with increasing centre-to-centre pile spacing. When the piles are placed further apart, the size of the deforming soil region is larger as it is possible for the full soil flow mechanism to form around the pile. As the pile spacing decreases, the deforming regions interact and are constrained by the adjacent piles while the flow mechanism continues to exist. When the piles become closer together, the deforming regions are fully constrained by the adjacent piles, and as a result the pile-soil interaction mechanism changes from soil flow to a passive wedge as in front of a solid retaining wall (Fig. 5.5).
- (2) A significant reduction in the ultimate lateral pile-soil pressure is observed when the piles are placed at  $2d$  spacing or less, and for the  $S_H/d = 1.1$  and 2 analyses the ultimate lateral pile-soil pressure is found to be greater at intermediate depths than at a deeper level. In all other cases the ultimate lateral pile-soil pressure increases with depth (Fig. 5.4).
- (3) The piles spaced at  $2d$  or less are likely to establish a stabilising mechanism which prevents the soil flow through the piles even for the ultimate limit state (Fig. 5.19c). When the piles are placed at a spacing greater than  $2d$ , a larger soil movement through the piles is observed at the ultimate load (Fig. 5.19d), as the stabilising mechanism changes from a plane passive wedge to soil flow through the piles.
- (4) The normalised stabilising force provided by closely spaced discrete piles matches the stabilising force exerted by a retaining wall, since the failure mechanism of the soil in closely spaced discrete piles and a retaining wall is the same passive wedge mechanism. As would be expected, the stabilising force per metre run along the pile row decreases with increasing pile spacing.
- (5) The discrete piles spaced with a bigger spacing establish an acceptable stabilising mechanism especially at deeper levels for a serviceability loading state (i.e. for a small boundary soil displacement). The closely spaced piles provides a much greater stabilising force for the ultimate loading state, because of the formation of a passive wedge stabilising mechanism in front of the piles. However, the extent of passive wedge formation decreases with decreasing boundary soil displacement, and the difference between the stabilising force provided by the piles spaced at  $S_H/d = 2$  and 3 or 5 is small for serviceability loading state. Therefore, a bigger pile spacing can also be adopted to stabilise the slopes for serviceability loading states.

(b) for the double pile rows,

- (1) The reduction in the deflection, shear force, bending moment and normalised ultimate lateral pile-soil pressure from the single row of piles is considerably higher for  $S_h/d = 3$ , than with  $S_h/d = 5$  (Figs. 5.23 and 5.27). This is because, when  $S_h/d = 3$ , the failure mechanism developed in front of the upslope pile row is a passive wedge, and soil is prevented from flowing through the piles. When the spacing  $S_h$  increases to  $5d$ , the passive wedge mechanism changes towards a flow type mechanism as theoretically illustrated by Randolph and Houlsby (1984), which is not as effective in stopping the soil movements through the piles.
- (2) Due to this change of mechanism, the soil movement along vertical lines through the Points 'Up' and 'Down' shows that the piles spaced at  $S_h/d = 5$  are less effective than  $S_h/d = 3$  at developing a strong stabilising mechanism to prevent the soil flow through the piles for the ultimate load condition (Figs. 5.28b and 5.24b).
- (3) In the pile group with  $S_h/d = 3$ , the normalised ultimate lateral pile-soil pressure developed on the upslope pile row is greater than on the downslope row above  $4.5d$  depth. Below this depth the pressures swap round resulting in the downslope piles experiencing higher ultimate lateral pile-soil pressures.
- (4) Although the pile group spaced at  $S_h/d = 5$  provides a higher stabilising force than a single pile row, it is not useful to stabilise the slope at the ultimate loading state as the soil movement through the piles is considerably higher. The pile group arrangement with  $S_h/d = 3$  develops a strong stabilising mechanism in between the pile rows by providing a higher stabilising force per run of slope and by preventing the soil flow through the piles. From this, it can be said that the formation of a strong stabilising mechanism is dependent more on the spacing  $S_h$  than on  $S_v$ . However, a bigger pile spacing  $S_h$  can be adopted to stabilise the slopes for serviceability loading states.
- (5) The double pile rows provide a much higher stabilising resistance than the equivalent single pile row (i.e. for the same  $S_h/d$ ). An equivalent stabilising mechanism developed by single row of piles at  $S_h/d = 2$  is achieved by the two pile rows spaced at  $S_h/d = 3$ , and the stabilising resistance per metre run along the slope is equal to the force given by a solid retaining wall at this pile group arrangement. However, more piles are needed for the double pile rows than for the single pile row, if  $S_h/d = 3$  and 2 are chosen for the double and single rows respectively.

The current  $FLAC^{3D}$  analyses have demonstrated and explained the behaviour of single and double pile rows such as the variation of ultimate lateral pile-soil pressure and the development of stabilising force with different pile spacings, which were not correctly modelled or revealed by 2D plane stress analyses.

## Chapter - 6: Back Analysis the Observed Performance of the Pile Stabilised Landslide at Telford

### 6.1 Introduction

In this chapter, the performance and behaviour of the discrete piles used to stabilise a landslide near Ironbridge, Telford are back analysed using the finite difference computer code *FLAC<sup>3D</sup>*. The numerical results are compared with field data to test the robustness of simplified finite difference analyses for use in the design of pile stabilised slopes and to improve the design framework.

### 6.2 Background to the site

The instrumented site is located just less than a mile downstream from the world's first iron bridge, known simply as the Ironbridge (Fisher and Clark, 1997), and comprises the northern valley side stretching upwards from the River Severn (Fig. 6.1). Numerous landslides have taken place in this area (Henkel and Skempton, 1954), and the signs of a possible large landslide on the northern side of the River Severn first appeared in 2004 (Fig. 6.2).

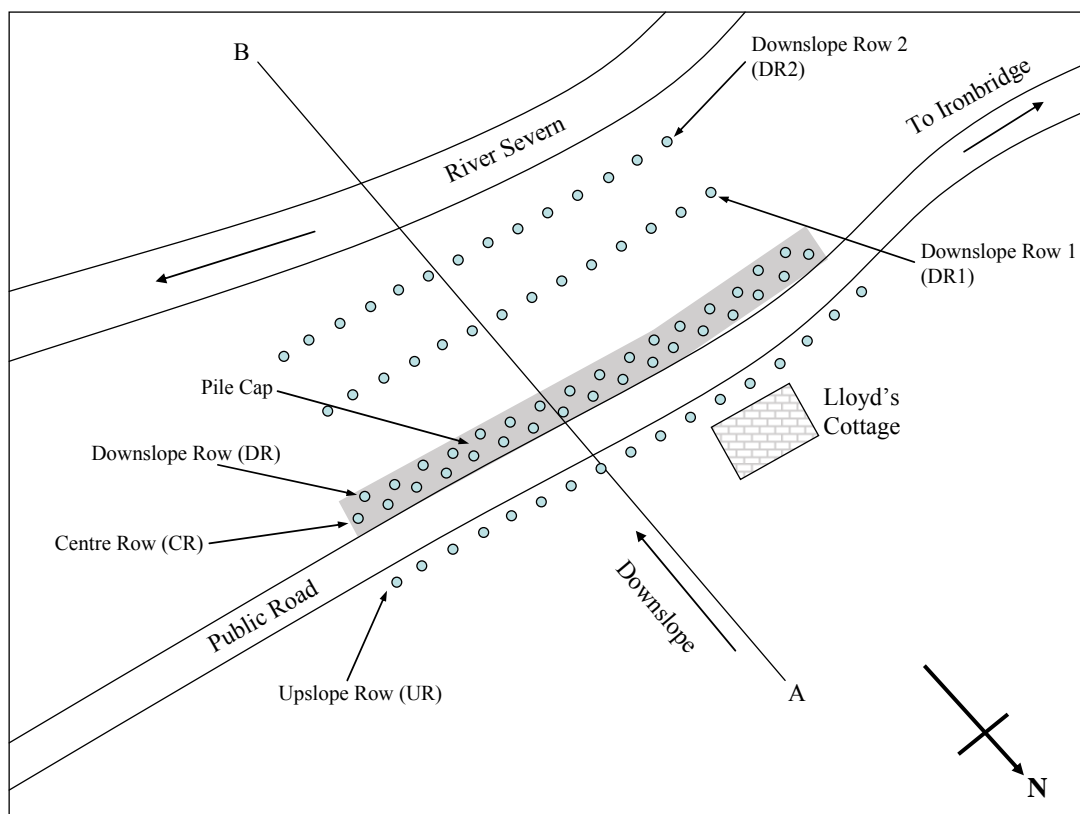


Figure 6.1: Site plan of Lloyd's cottage landslide (not to scale)

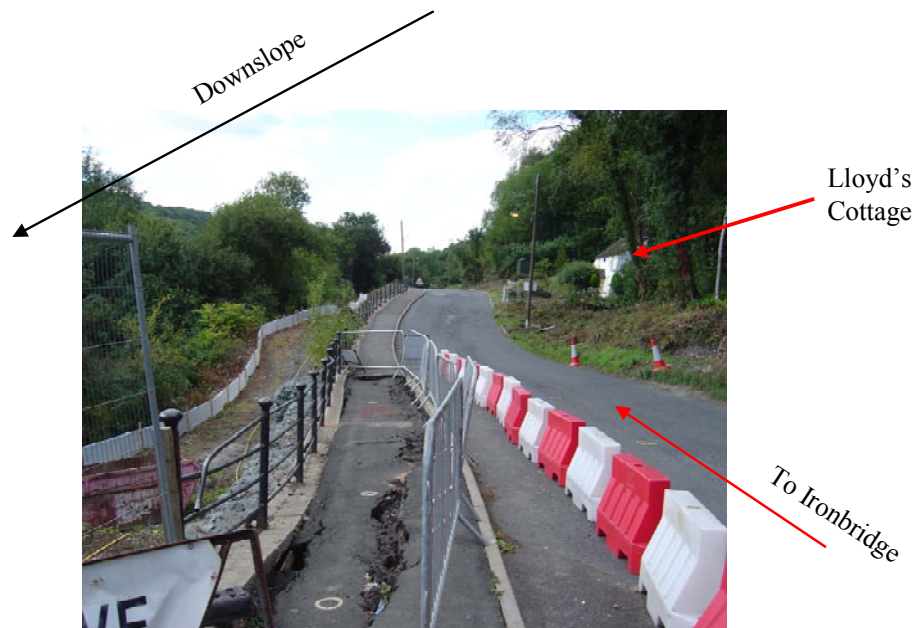


Figure 6.2: Damage to The Lloyd's Road caused by development of a large landslide in 2004 near Ironbridge, Telford. (Photograph Dr J Smethurst)

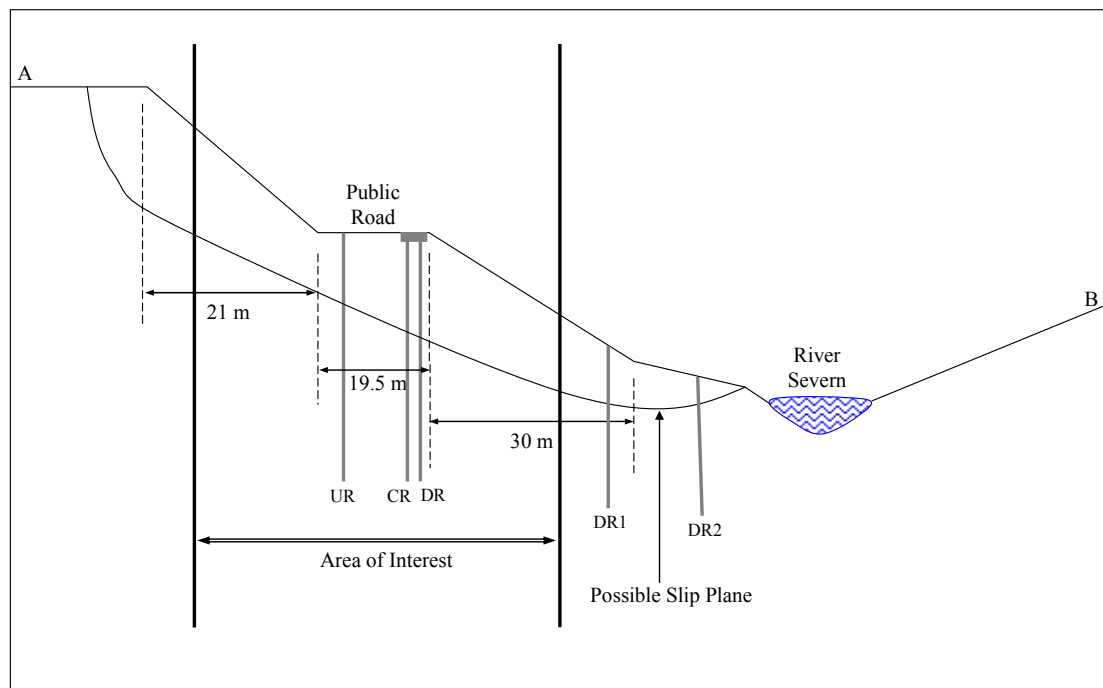


Figure 6.3: Cross-section of the site through A-B (not to scale)



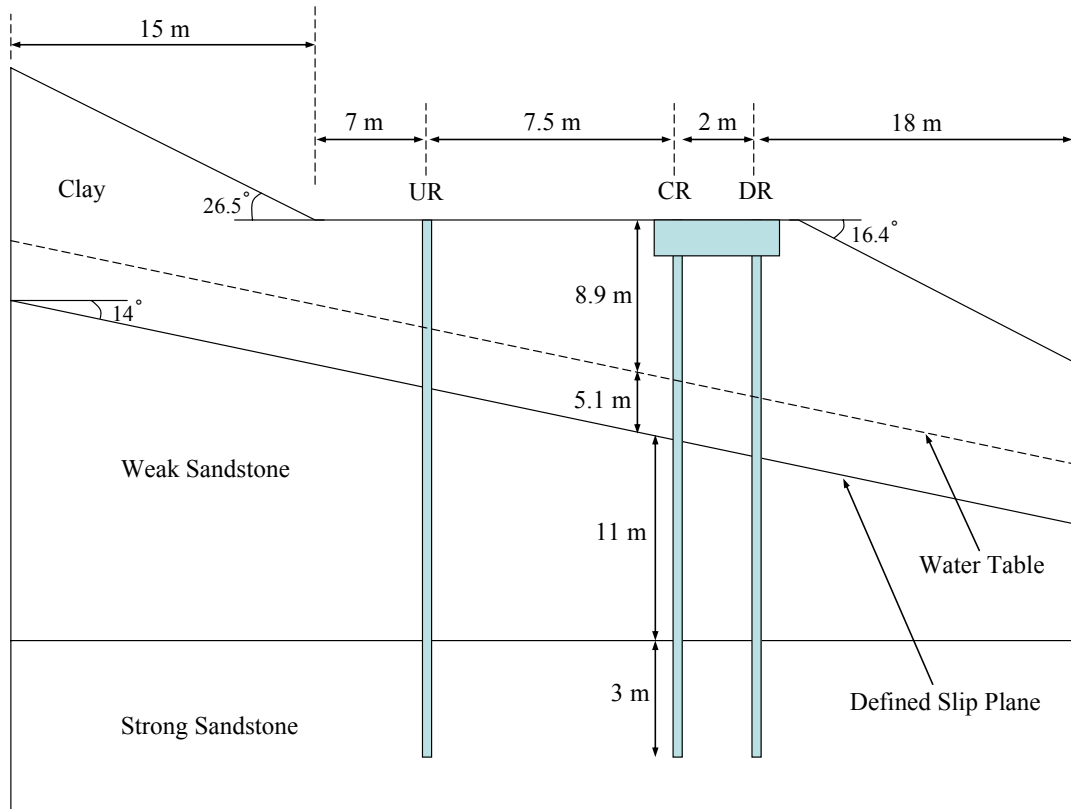


Figure 6.4: Simplified slope geometry used to model  $FLAC^{3D}$  mesh

Figure 6.3 shows cross-section A-B of the site. In this numerical study, only the area shown as ‘area of interest’ was modelled, since these numerical analyses were aimed mainly at understanding the behaviour of the piles used to stabilise the slope. The geological sequence of this area is complex with many thin weak clay and sandstone layers throughout the sequence, and was simplified to a layer of gravelly clay underlain by layers of weak and strong sandstone (Fig. 6.4). The ground investigation report (High-Point Rendel Ltd, 2005) identified a slip plane at around 14 m below ground level at a location close to the central pile row (Fig. 6.4).

### 6.3 Instrumentation and field monitoring

Some of the piles used to stabilise the landslide were fully instrumented with inclinometers and vibrating wire strain gauges. Flushable vibrating wire piezometers and inclinometers were placed into the ground to measure the variation in pore water pressures and ground movements respectively. Instrumentation was carried out by Dr J Smethurst of the University of Southampton, and the behaviour of the piles has been continuously monitored since their installation.

The deflection of the piles was measured using inclinometer tubes installed within them. The bending moments developed in the pile were determined using the strain gauge data; however, uncertainties arise as a result of a number of concrete processes such as cracking and shrinkage that influence the performance of the gauges; it is also necessary to estimate a value of Young's modulus for the concrete to use in the calculation of bending moment.

#### 6.4 Back analyses the pile group behaviour using *FLAC<sup>3D</sup>*

The observed performance of the discrete piles used to stabilise a landslide at Telford is back analysed in the following sections.

Cylindrical piles of diameter  $d = 0.88$  m and length  $L = 28$  m were installed in three rows. The piles installed in the centre row (CR) and the downslope row (DR) were connected together using a rigid pile cap. As shown in Figure 6.5, the centre row and downslope row piles were installed in 'zigzag' arrangement to prevent soil flow through the piles. Two planes of symmetry were exploited in the analyses; in this way, the width of the slope needed to be modelled numerically was reduced to 4.5 m.

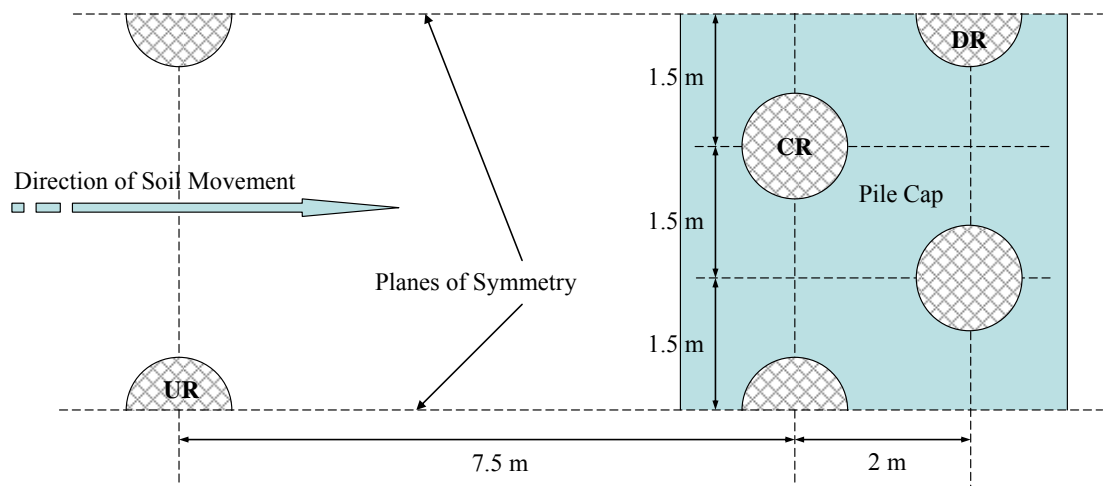


Figure 6.5: Plan view of positions of pile group

### 6.4.1 Grid generation

The  $FLAC^{3D}$  mesh was modelled on the basis of the geometry shown in Figure 6.4. Interface elements were placed in between the clay and weak sandstone layers to represent a defined slip plane. Interface elements were also placed between the piles and the soil, and between the pile cap and the soil. 28 m long, 0.88 m diameter piles were installed in three rows as shown in Figure 6.7. As mentioned earlier, the piles installed in the centre row and in the downslope row were connected together using a rigid pile cap (Figs. 6.6 and 6.7).

To model the pile cap, a soil block with similar dimensions to the pile cap was excavated (Fig. 6.8), and the interface elements were then attached to the soil surfaces. The pile cap was modelled above the ground surface and moved down to complete the geometry. The pile cap was fully attached to the piles.

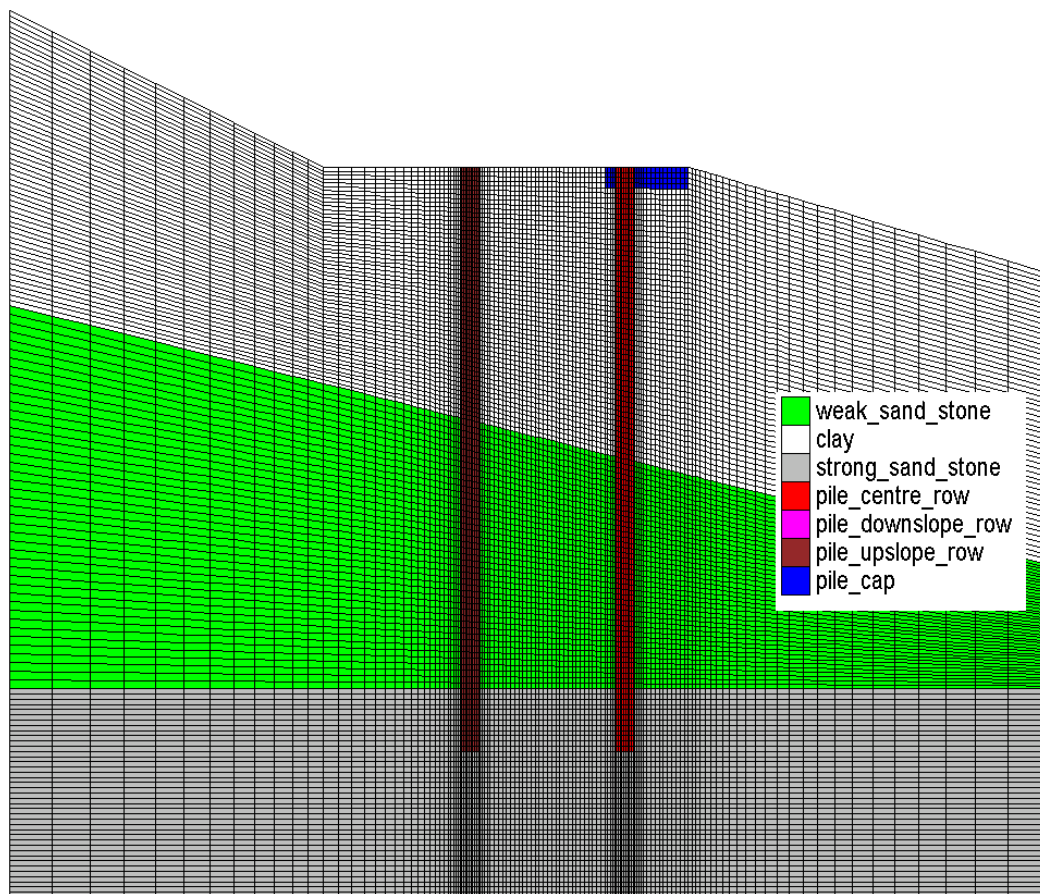


Figure 6.6:  $FLAC^{3D}$  model used to back analyse the behaviour of stabilising piles installed at Ironbridge, Telford

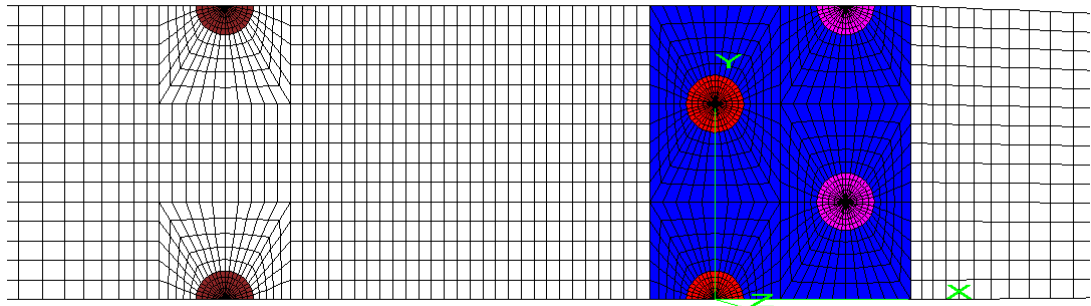


Figure 6.7: Plan view of  $FLAC^{3D}$  mesh showing positions of piles and location of pile cap

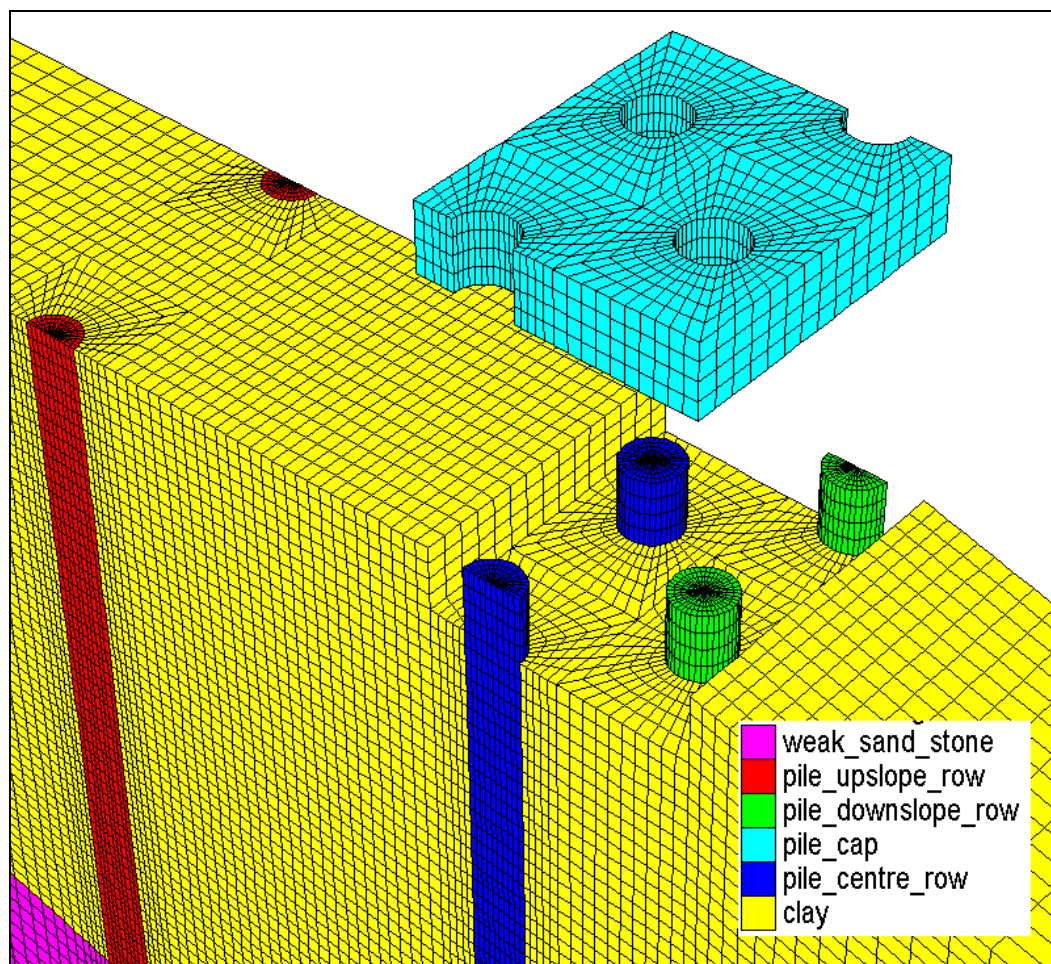


Figure 6.8:  $FLAC^{3D}$  model showing installation of pile cap

### 6.4.2 Constitutive models and material properties

The piles and the soils were modelled as linear elastic and elastic-Mohr-Coulomb plastic materials respectively. The properties of the piles used for the *FLAC*<sup>3D</sup> analyses are given in Table 6.1. Drained conditions were adopted for the soils as the pile stabilised landslide was analysed to understand its long term performance. Assumed plastic strength properties of the soil layers and their densities are shown in Table 6.2. The Young's modulus of the clay was taken as 10 MPa based on Das (1994). Values of 19.3 GPa and 0.38 for the Young's modulus and Poisson's ratio of the strong sandstone respectively were used, based on Goodman (1980). The ground investigation report shows that the middle layer is made up of heavily fractured sandstone (High-Point Rendel Ltd, 2005), for which it was difficult to estimate appropriate elastic and strength parameters. Therefore, two different distributions of the Young's modulus were assumed for the weak sandstone layer (i.e. the middle layer). Table 6.3 shows the elastic-strength properties used in the analyses.

Length (m)	28
Diameter (m)	0.88
Young's Modulus (GPa)	35
Poisson's Ratio	0.2
Bulk Modulus (GPa)	19.44
Shear Modulus (GPa)	14.58
Density (kg/m <sup>3</sup> )	2500

Table 6.1: Properties of the pile

Material Properties	Clay	Weak Sand Stone	Strong Sand Stone
Density (kg/m <sup>3</sup> )			
Dry density	1750	-	-
Saturated density	1900	1900	1900
Strength Properties:			
Drained shear strength (kPa)	5	5	5
Friction angle	21°	30°	40°

Table 6.2: Assumed plastic-strength properties of the soil layers

<i>Material</i>	<i>Young's modulus (MPa)</i>	<i>Increase in Young's modulus with depth (MPa/m)</i>	<i>Poisson's ratio</i>
Clay	10	0	0.3
Weak Sand Stone			
Case 1	20	0	0.3
Case 2	20	7.27	0.3
Strong Sand Stone	$19.3 \times 10^3$	0	0.38

Table 6.3: Elastic-strength properties of the soil layers

As before, the interface stiffness was set to be ten times that of the stiffest neighbouring element. The interface representing the slip plane was assigned the following drained parameters: effective cohesion = 5 kPa and friction angle =  $21^\circ$  based on failure taking place in the clay soil. The pile-soil friction was set to the drained shear strength of the surrounding soil, corresponding to a perfectly rough interface. The measurements from the piezometers in the slope showed the ground water to be hydrostatic, below a water table 8.9 m below ground level as indicated in a bore-hole located close to the centre pile row (Fig. 6.4).

### 6.4.3 Initial and boundary Conditions

The nodes on the base of the completed mesh were restrained in all three directions while the nodes on the top face were free to move. The nodes on the faces representing planes of symmetry were prevented from moving in the  $y$ -direction. The nodes on the right and left faces were prevented from moving in the direction of the applied soil movements (i.e. in the  $x$ -direction) during gravity loading, and the nodes on these faces on the clay layer (Fig. 6.6) were freed to move during lateral loading.

Jaky (1944) suggested a relationship to calculate the *in situ* lateral stresses of a normally consolidated soil (Eq. 6.1). *In situ* stresses were initialised according to this relationship.

$$K_0 = (1 - \sin \phi') \quad \text{Equation 6.1}$$

Where,

$K_0$  = *in situ* earth pressure coefficient

$\phi'$  = effective angle of friction of the soil

#### 6.4.4 *FLAC<sup>3D</sup>* analyses

To prevent instability during gravity loading, high shear and tensile strengths were temporarily assigned to the clay and weak sand stone layers, which were then reduced to their actual values once the self weight stresses had been initialised in the mesh. After the model had been brought into equilibrium under gravity loading, the addresses of required nodes and elements were stored so that stress and displacement outputs could be calculated. The nodes on the left and right faces of the clay soil block were released to move in the  $x$ -direction, and a velocity of  $1 \times 10^{-6}$  m/step from left to right and parallel to the slip plane was applied over  $1 \times 10^5$  steps to move the soil boundaries by 100 mm. 100 mm of boundary soil displacement was enough to move the pile head of the centre row pile to match with the corresponding field data.

In the field, the upslope pile row was installed first, and after few months the centre and downslope pile rows were installed. However, in this numerical study, pile installation effects (including the installation sequence) were not taken into account and was assumed that all piles were installed at the same time. This assumption may cause the back-analysis results to differ from the field behaviour. *FLAC<sup>3D</sup>* analyses were initially carried out to try to replicate the broad behaviour of stabilising piles such as deflection and bending moment patterns with depth, and are presented in the following section.

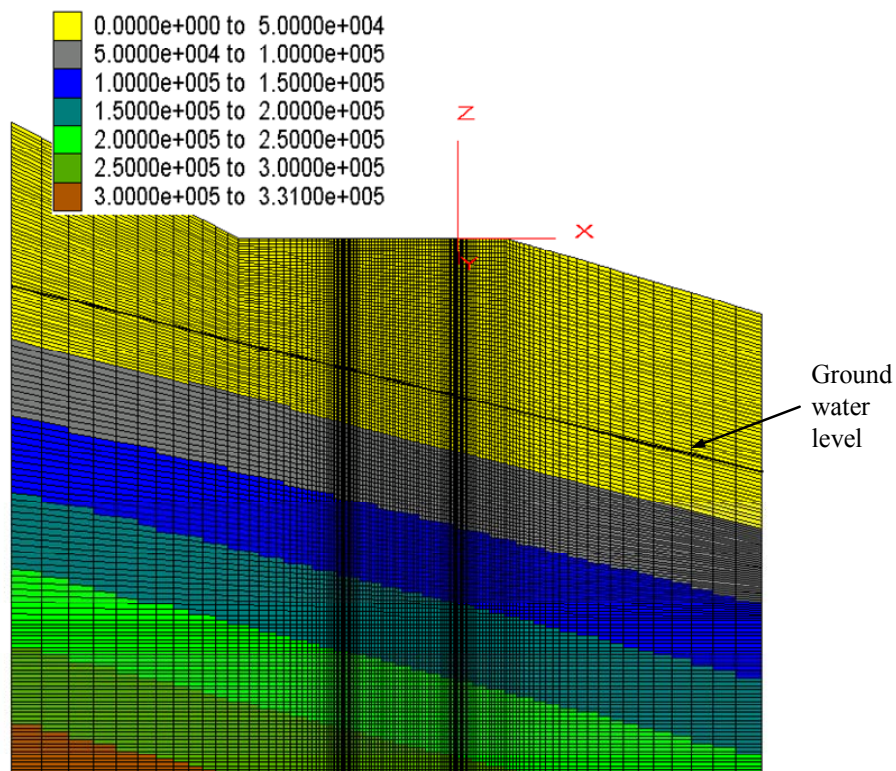


Figure 6.9: *FLAC<sup>3D</sup>* mesh showing equilibrium of pore water pressure after gravitational loading



### 6.4.5 Results and discussion

The numerically calculated deflection of the centre pile row (assuming that the Young's modulus of the weak sandstone layer is constant with depth and is equal to 20 MPa) is compared with the data obtained from the inclinometer tubes in Figure 6.10(a). The deflection of the pile top is slightly higher in the  $FLAC^{3D}$  analysis. Comparison of the numerical and field results suggests that the pile used for numerical analyses has a higher stiffness or Young's modulus than the actual pile. This may be true: the stiffness of the pile in the numerical model was calculated assuming that the concrete does not crack with bending. However, in reality concrete will crack after a few millimetres of lateral deflection, hence the stiffness of the concrete will reduce and the flexibility of the pile will increase.

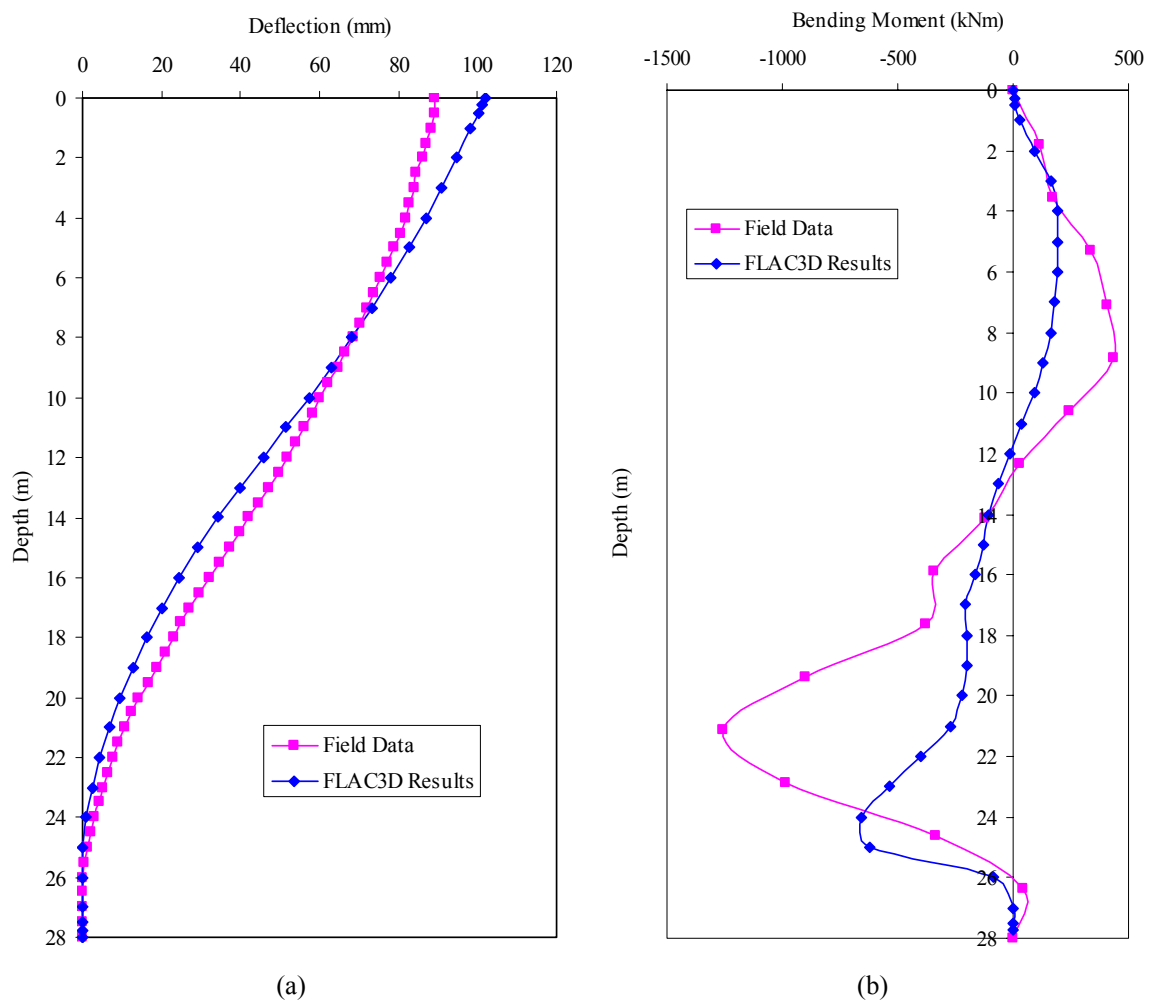


Figure 6.10 : Comparison of pile behaviour (centre row) plotted from field data and  $FLAC^{3D}$  results (a) pile deflection versus depth; and (b) bending moment developed in the pile versus depth. Field data was analysed by Bicocchi, 2010).



Another reason for the higher deflection of the pile top in the  $FLAC^{3D}$  analysis may be related to the strength of the slip plane. In this analysis, an effective cohesion of 5 kPa and an effective friction angle of  $21^\circ$  were assigned to the slip plane. As found in earlier analyses, the strength of the slip plane plays a vital role in pile behaviour. Reducing the strength of the slip plane may change the soil movement profile, resulting in the soil transferring a higher load to the pile. The deflection of the pile section embedded below 14 m BGL may increase little more when the strength of the slip plane is reduced, and may then match with the deflection curve plotted from inclinometer data.

Figure 6.10(b) compares the pile bending moments calculated in the  $FLAC^{3D}$  analyses with the field data obtained from strain gauges. The bending moments calculated in the  $FLAC^{3D}$  analysis are low compared with the field data. The maximum bending in the pile was measured at about 21 m BGL, while the numerical results show it at about 25 m BGL. In this numerical analysis, the soil layer below 25 m BGL (i.e. the strong sandstone) was assigned a very high stiffness; compared with the a constant stiffness of 20 MPa assigned to the middle of weak or degraded sandstone. However, in reality, the stiffness of a soil layer may increase linearly or parabolically with depth. If this effect is considered in the numerical analysis, the depth at which the maximum bending moment develops in the pile might move upward, closer to the depth at which the bending moment reached a maximum in the field data.

It is important to note that the bending moment at the pile top is zero in Figure 6.10(b). Generally a higher bending moment is developed at the pile top when the pile is fully connected to a rigid pile cap. However, both the field monitored data and numerical results show similar bending moment values over the top 3 m portion of the pile. In reality, it can be quite difficult to construct a full moment connection between pile and cap, and this may be the case for the real pile and pile cap. However, a rigid connection was modelled in the  $FLAC^{3D}$  analysis; interestingly, the numerical results also show that the bending moment at the connection point is zero. This behaviour can also be caused by rotation of the whole pile cap along with the top of the pile section, for which a bending moment does not need to be developed at the connection point. However, this behaviour could not be verified, since the movement of pile cap relative to a stationary reference point was not monitored.

A  $FLAC^{3D}$  analysis was carried out to investigate the effect of stiffness variation within the weak sandstone layer. It was assumed that Young's modulus of the weak sandstone layer is 20 MPa at the clay/weak sandstone interface and increases linearly with depth at a rate of 7.27 MPa/m (see Case-2 in Table 6.3) to the weak sandstone/strong sandstone interface. The deflection of the pile section embedded into the middle layer decreases when the stiffness of the

middle layer increases linearly with depth (Fig. 6.11a). As would be expected, the depth at which the maximum bending moment is developed in the pile moves to 17 m BGL from 24 m BGL (Fig. 6.11b). However, the bending moment profile calculated using  $FLAC^{3D}$  still significantly differs from the field data, especially below 16 m BGL. Therefore, in addition to the influence of the stiffness, there are additional factors affecting the actual pile behaviour. One of them may be the location of weakened slip plane and its shape. In this numerical model, an inclined, planar slip plane was assumed based on the information available in the borehole logs and ground investigation report. A careful inspection of borehole logs reveals that there is a possibility for a compound slip plane (i.e. not only one slip plane; but several at different depths with different strengths). This has not been investigated in this thesis, but could be carried out in future.

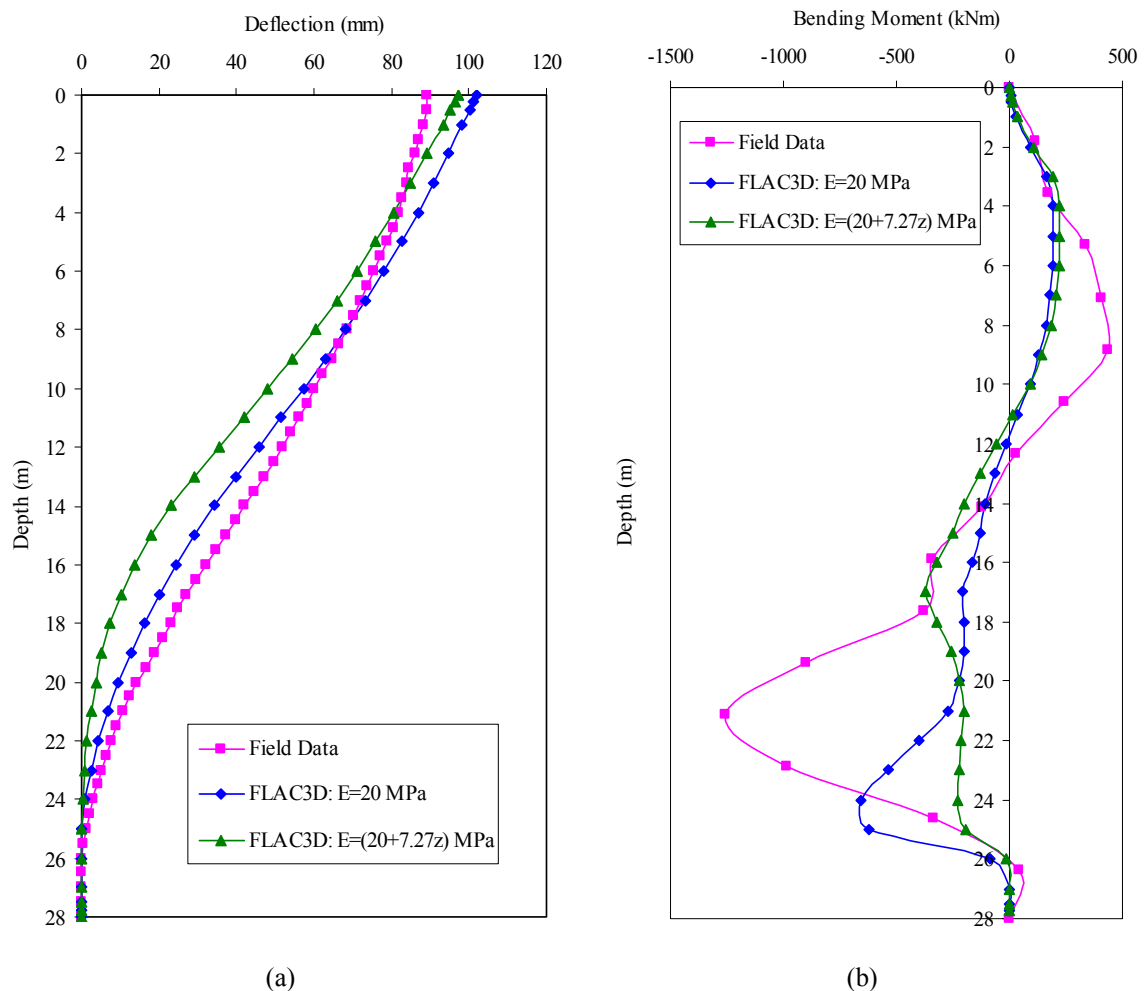


Figure 6.11: Comparison of pile behaviour (centre row) plotted from field data and different  $FLAC^{3D}$  results (a) pile deflection versus depth; and (b) bending moment developed in the pile versus depth. Field data was analysed by Bicocchi, 2010).

Figure 6.12 shows the deflection profiles of all three pile rows with depth. According to the field measurements, the movement of pile top is greatest in the downslope row and smallest in the upslope row. The same order is found from the numerical analyses also; but, the values are different, especially in the upslope row. As mentioned earlier, the upslope row piles were installed first in the field, and after few months the other two rows were installed. However, the field measured deflection of the upslope pile row plotted in Figure 6.12 is plotted from the day the centre pile row was installed. Because of this, the deflection of the upslope pile plotted here may not represent the actual full pile deflection profile, as the piles started to pick up load from the day they were installed. Therefore, the deflection of the upslope pile may be greater than the values shown in Figure 6.12, and can be expected that they may match the pile deflection calculated from the *FLAC<sup>3D</sup>* analysis.

Figure 6.13(a) shows the development of pile shear forces with depth for the two different profiles of Young's modulus in the middle soil layer. In this numerical study, a defined slip plane was modelled at 14 m BGL at the location of the centre pile row. The clear soil movement that occurs along this defined slip plane causes the pile to develop a higher shear force at this depth (Fig. 6.13a). The maximum shear force in the pile section is developed at around 25 m BGL; this is because the very strong sandstone layer is present below this depth, and the pile cantilevers from this. The development of lateral pile-soil pressure with depth is shown in Figure 6.13(b), which shows that the direction of lateral pile-soil pressures switch at the location of the defined slip plane. However, the development of lateral pile-soil pressure close to the strong sandstone layer is not consistent with the shear force profile. As explained earlier, the behaviour of the piles have been investigated numerically after displacing the left and right side boundaries of the clay layer. To move the boundaries by 100 mm, a velocity of  $1 \times 10^{-6}$  m/step were applied over  $1 \times 10^5$  steps. It seems that the numerical model did not reach equilibrium at this point (i.e. the maximum unbalanced force within the model is quite zero). An analysis with smaller applied velocity (e.g.  $1 \times 10^{-7}$  m/step velocity over  $1 \times 10^6$  steps) may give a better result. This could be carried out in future.

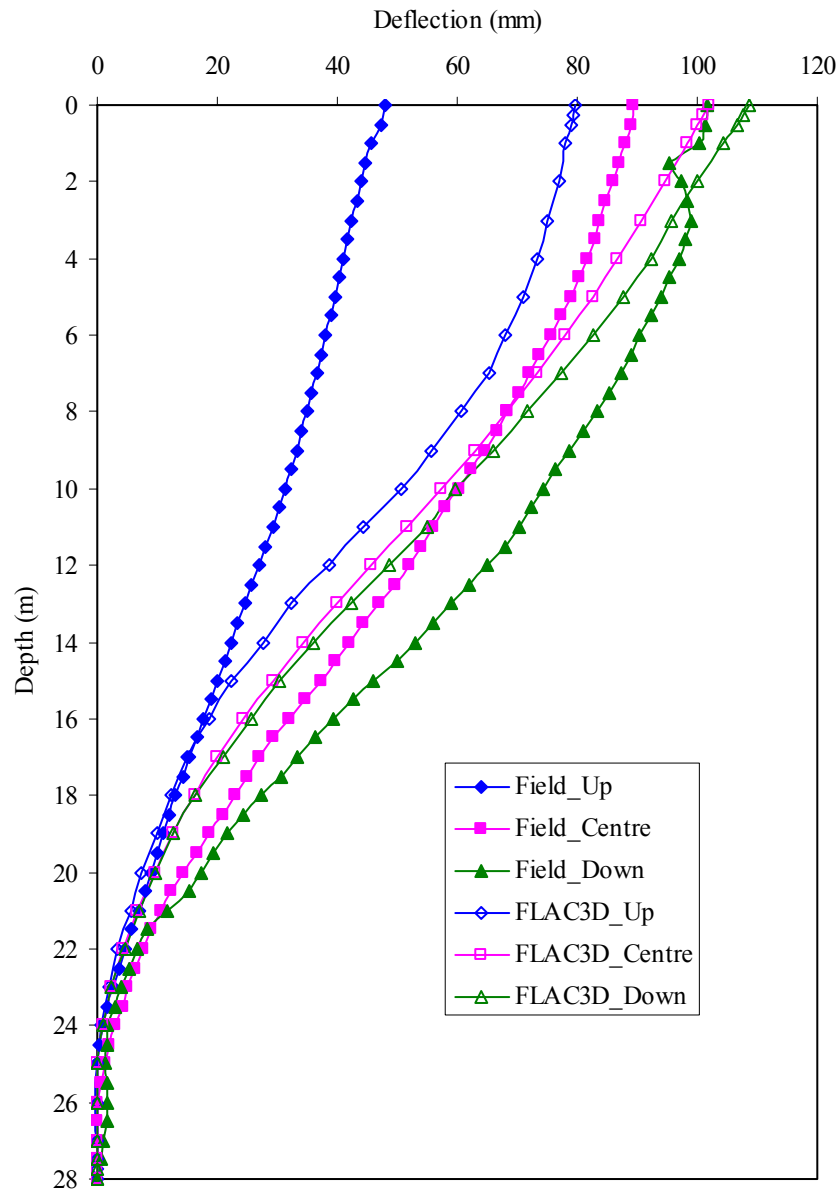


Figure 6.12: Comparison between the field data and the FLAC<sup>3D</sup> result of pile deflections of all three pile rows

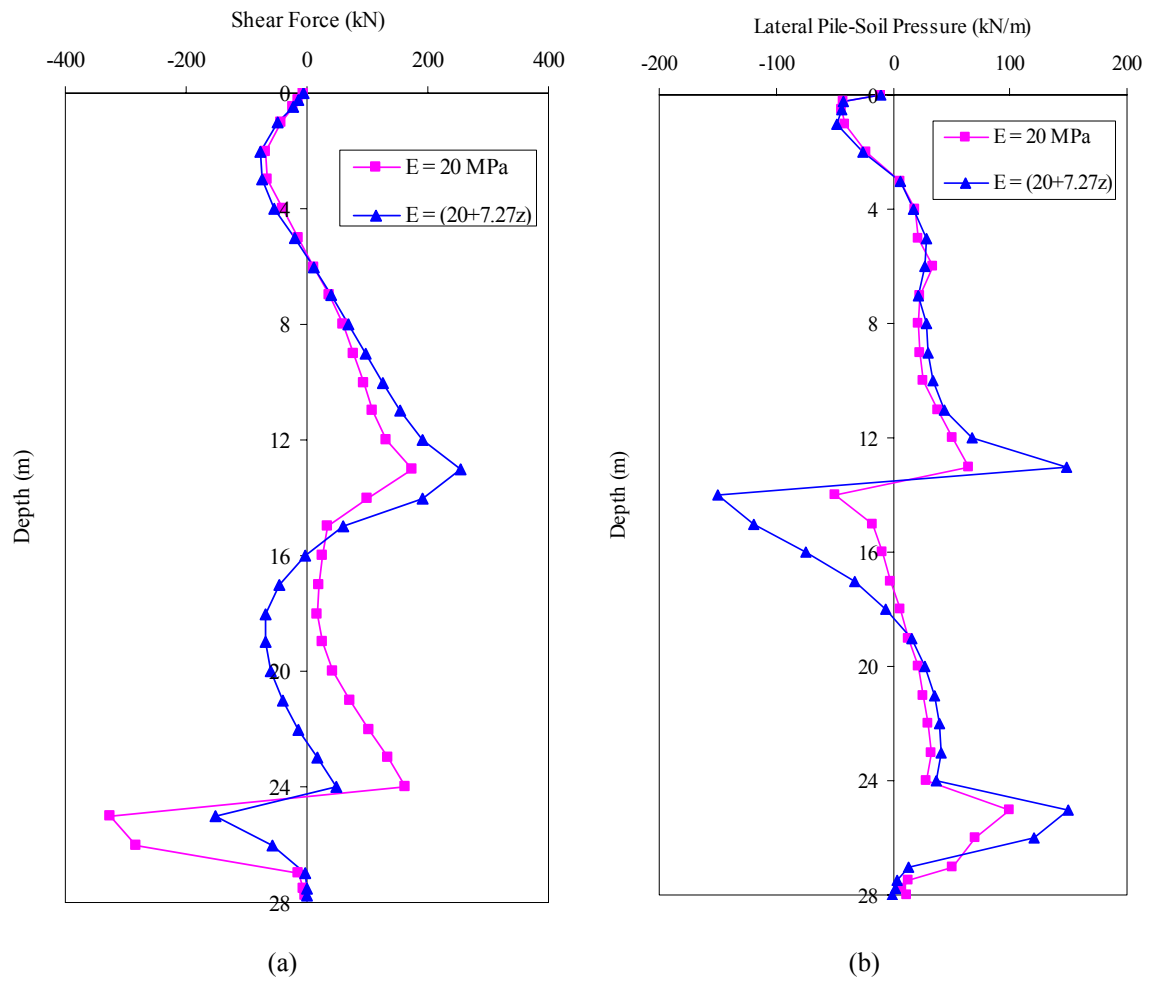


Figure 6.13: Comparison of pile behaviour (centre row) for two different stiffness variations of weak sand stone layer: (a) pile shear forces versus depth; and (b) lateral pile-soil pressures developed in the pile versus depth

## 6.5 Summary

The behaviour of rows of piles used to stabilise a landslide near Ironbridge, Telford has been back analysed numerically. A  $FLAC^{3D}$  model was developed according to the information available in the ground investigation report and the use of some engineering judgement in determination of some parameters. The ground was simplified into three different soil layers: a layer of weak gravelly clay, underlain by layers of weak and strong sandstone, with a defined slip plane between the clay and the weak sandstone layers.

The  $FLAC^{3D}$  model showed a reasonably good match with the pile deflections plotted from the field measurements. The shape of the  $FLAC^{3D}$  bending moment plot was similar to that from the field strain gauge data, but the bending moment values were slightly less for the  $FLAC^{3D}$  analysis. This may be because the stiffness of the pile was calculated assuming that concrete does not crack for any lateral deflection. However, in reality, concrete will crack after some millimetres of lateral deflection, and hence the stiffness of the pile will reduce.

A number of  $FLAC^{3D}$  analyses were carried out to help understand the behaviour of passively loaded piles used to stabilise complex and large landslides. This is important, because only deflection and bending moment can be measured directly from field instrumentation. Other important parameters such as development of the shear forces and lateral pile-soil pressures along the pile shaft cannot be measured directly from field. Numerical modelling using appropriate geotechnical finite element or finite difference computer codes, for example  $FLAC^{3D}$ , is a way of investigating them. However, the reliability of the numerical results depends entirely on the selection of material properties of the pile and soil layers.

The ground investigation report did not provide all of the data required such as the exact strength and stiffness properties of all of the soil layers, and soil properties were selected for the  $FLAC^{3D}$  analyses based on the available literature (e.g. Henkel and Skempton, 1954; Goodman, 1980) and the borehole logs. It is believed that the depth of the weakened slip surface, the shape of it (whether it is planar, or circular or compound), and its strength parameters are the main factors that should be more carefully investigated for reliable numerical outputs in this case. As found in previous analyses, the strength of the slip plane heavily influences the behaviour of the stabilising piles. Therefore, further numerical analyses may be required to understand the effect of the strength of slip plane, and this could be done in future. In addition to this, a new  $FLAC^{3D}$  mesh could be developed, with a compound slip plane (i.e. at around 25 m BGL close to the upslope pile row and 20 m BGL close to the centre pile row). In this model, it may be possible to simplify the geology so that only two soil layers will be modelled: a layer of weak gravelly

clay underlain by strong sandstone (Fig. 6.14). The piles could also be assigned a stiffness value calculated including the effect of concrete cracking.

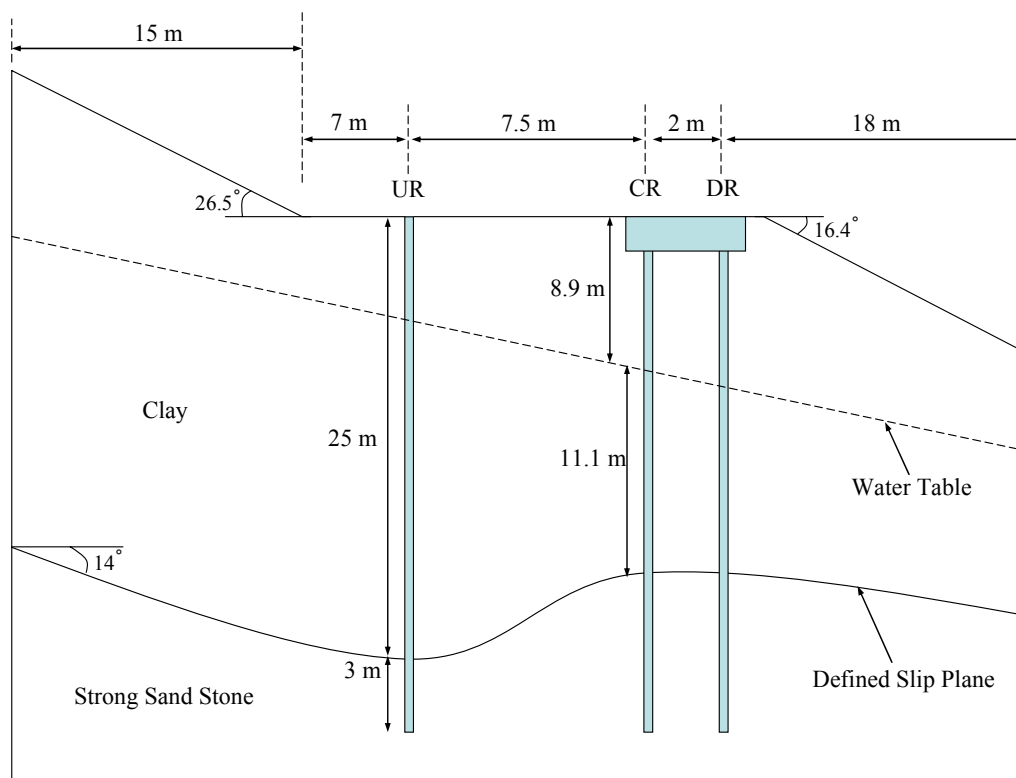


Figure 6.14: New slope geometry showing the compound slip plane

Finally, the numerical analyses presented in this chapter have shown that the finite difference computer code *FLAC<sup>3D</sup>* can be used to back analyse complex pile stabilised landslides, in a way not possible by simple limit equilibrium analysis. However, detailed material properties, and the location of weakened slip planes and their strength parameters, are very important input parameters if accurate outputs are to be obtained.

## Chapter - 7: Conclusions and Future Work

### 7.1 Conclusions

The results of a number of  $FLAC^{3D}$  analyses have been presented in this thesis. These have provided new insights into complex pile-soil interaction effects for a single isolated pile and a group of piles. The three-dimensional numerical models developed to carry out these analyses are able to model the full pile-soil interaction problem including three dimensional and surface effects, which cannot be understood fully using two dimensional analyses. Three dimensional models are a powerful tool for parametric studies of factors influencing the behaviour of laterally loaded piles such as the strength of the slip plane, the strength of the pile/soil interface, and the effect of sloping ground. In addition, the models can be used to aid the design of pile stabilised slopes, in particular to calculate the required stabilising force per metre run of the slope, and to choose the optimum centre-to-centre spacing between the piles.

Detailed  $FLAC^{3D}$  analyses were carried out to understand the behaviour of passively loaded single and groups of piles used to stabilise slopes, and were presented in Chapters 3-5. The observed performance of a pile stabilised landslide at Telford was back analysed and presented in Chapter 6. The major conclusions drawn from each of these chapters are summarised in the following sections.

#### 7.1.1 Chapter 2: Literature review

Although there are a number of uncertainties in the design of laterally loaded piles, this thesis investigated mainly the behaviour and potential failure of piles used to stabilise major landslides, and the load distribution behaviour when rows of piles are used. A brief literature review of these two areas was presented in this chapter. The following major points were drawn from this chapter:

- There is a difference in potential failure mechanisms between a pile loaded ‘actively’ where external loads are applied to the pile head (e.g. Broms, 1964), and piles loaded ‘passively’ via global ground movement (e.g. Viggiani, 1981).
- A number of studies undertaken subsequently to investigate interaction effects in pile group arrangements, especially for clay soil in undrained conditions were reviewed. Researchers have found that when the piles are grouped, they experience a different ultimate lateral pile-soil pressure ( $p_u$ ) than when isolated. However, some of these studies are counter-intuitive and contradictory to the other studies (e.g. Chen and Poulos, 1993 and Chen and Martin, 2002), and therefore further investigations were needed to clearly understand this complex 3D pile-soil interaction.



### 7.1.2 Chapter 3: Failure mechanisms of a single pile

Three-dimensional finite difference analyses were carried out to investigate the response of a single pile subjected to passive loading. The analyses aimed mainly to verify and explore the failure mechanisms for landslide stabilising piles categorised by Viggiani (1981). Based on the results, the following conclusions were made:

- The pile behaviour determined from the numerical models with a rigid pile, a distinct plane of sliding and a horizontal ground surface, matching the assumptions made in the analyses presented by Viggiani (1981), agree well with his theoretical solutions.
- Vertical soil movements associated with the unconstrained ground surface prevent development of the classical theoretical values of normalised ultimate lateral pile-soil pressure ( $p_u/c_u d$ ) within  $5 d$  and  $8 d$  of the ground surface for the zero and full strength pile-soil interfaces respectively. Reduced values of ultimate pressure above the sliding surface in mode B deformation (associated with a pile embedment into the underlying stable layer similar to the depth of the slipping mass) mean that the full theoretical ultimate pressures are not required – and are therefore not generated – below the sliding surface to maintain pile equilibrium. This reduces the ultimate resistance that the mode B pile can provide to the sliding soil to a value below that calculated using the Viggiani (1981) limit equilibrium equations, even when  $p_u = 0$  is assumed over the top  $1.5 d$  of the pile.
- The normalised ultimate lateral soil-pile pressure  $p_u/c_u d$  also remains distant from the classical theoretical values adjacent to the sliding surface. This is a result of vertical soil movement due to large differences in lateral pressure above and below the sliding plane. The proximity of the sliding surface to the base of the pile in mode A deformation (associated with a small pile embedment into the underlying stable stratum) prevents the development of the full theoretical value of  $p_u/c_u d$  on the short pile length below the slip surface. This also reduces the ultimate resistance that a pile behaving in mode A is able to provide to a value below that calculated using the Viggiani (1981) limit equilibrium equations.
- The highest ultimate stabilising force was attained in mode B, however, this was a consequence of maintaining a pile of the same length and varying the depth to the sliding surface in the analyses. For a given depth of slipping soil, mode C (associated with a large pile embedment into the underlying stable stratum), would be expected to provide the largest resistance. Pile displacements are much less for mode C than for mode B, which might be a consideration when serviceability is important. However, for a given depth of unstable soil, the mode C pile will always require a larger embedment depth and would therefore be more expensive to construct.

### 7.1.3 Chapter 4: Extended analyses on the failure mechanisms of single pile

The numerical analyses presented in Chapter 3 contained idealisations such as the ground surface and the slip surface both being horizontal and the strength of the slip plane set to zero. The numerical analyses presented in this chapter removed these assumptions, investigating the applicability of the Viggiani (1981) solutions to more realistic conditions. The following conclusions were drawn from these analyses:

- Analyses carried out with increasing strength on the sliding plane show that for deformation in mode A, the increased strength changes the main mode of pile movement from translation to rotation but does not significantly alter the ultimate lateral pile-soil pressure, pile shear forces and bending moments. In modes B and C, pile rotations and displacements decrease because the increased strength of the sliding surface reduces soil displacements and hence the pile-soil pressures developed above it. The reduced rotation of the mode B pile eliminates the upslope pressure acting at the top of the pile, and causes this mechanism to become more like mode C. The change is most marked as  $c_{int}/c_u$  rises from 0.5 to 1.0 for modes A and C, but as  $c_{int}/c_u$  increases from 0 to 0.5 for mode B.
- Sloping ground only significantly influences the pile behaviour above a certain angle. Below that, the pile behaves in the same manner as for a horizontal ground and sliding surface. The significant angle may be influenced by the stability of the slope, and this in turn is influenced by the unit weight of the soil, the depth of slip plane from the slope surface and the strength of the slip plane for an undrained analysis.
- The ultimate behaviour of a pile in an infinite slope is heavily dependent on the strength of the slip plane. For a given boundary displacement, the deflection of the pile is quite large when  $c_{int}/c_u = 0$ , compared with  $c_{int}/c_u = 0.5$  and 1, where  $c_u = 30$  kPa. This is because a low slip plane strength leads to a greater downslope soil slippage between the controlled displacement boundaries and thus the pile rotates more due to the lack of downslope support.
- When a finite slope with zero slip plane strength is allowed to fail by gravity alone, the soil close to the slip plane in the unstable layer moves more than the shallow surface soil. This behaviour is more realistic, because in previous analyses a displacement control boundary was employed to the left and right side of the model and thus free downslope movement was restricted.
- In a piled finite slope allowed to fail by gravity and with a pile configuration similar to Viggiani's (1981) mode B, the behaviour of piles changes from Viggiani's mode C to mode B with decreasing centre-to-centre pile spacing.

#### 7.1.4 Chapter 5: Pile-soil interaction effects of pile groups

The behaviour of single and double pile rows with increasing pile spacing were analysed in this chapter. The numerical analyses were carried out for passively loaded piles in an undrained soil. No previous work of a similar nature (3D analysis of passively loaded piles) was found in the literature. The analyses presented in this chapter were therefore compared with 3D finite element analysis of actively loaded piles (e.g. Brown and Shie, 1990b), and 2D plane strain analysis of actively loaded piles (e.g. Chen and Poulos, 1993). The *FLAC<sup>3D</sup>* analyses have shown that pile-soil interaction within a group of piles has a significant influence on the ultimate and serviceability performance. The following conclusions were made from these numerical analyses:

- For the single pile row, no significant reduction in the ultimate lateral pile-soil pressure  $p_u$  occurred for a centre-to-centre pile spacing of twice the diameter of the pile ( $d$ ) or greater. Piles spaced at  $2d$  showed some reduction in the ultimate lateral pile-soil pressure, while a significant reduction occurred in the deflection, shear force, bending moment and the ultimate lateral pile-soil pressure for  $S_h/d = 1.1$ . In terms of preventing flow of soil between the piles, the piles spaced at  $2d$  developed an ultimate mechanism with little soil flow between the piles especially at deep levels.
- The ultimate stabilising force given by closely spaced piles ( $S_h/d < 2$ ) per metre along the direction of the pile row was close to the ultimate resistance of a retaining wall, and decreased from this value with increasing pile spacing beyond  $2d$ . The *FLAC<sup>3D</sup>* analyses showed that the stabilisation mechanism developed in front of the closely spaced pile row ( $S_h/d < 2$ ) was a passive wedge as developed in front of a solid retaining wall, and therefore the stabilising resistance provided by closely spaced discrete piles equals that of a retaining wall. However, as the spacing between the piles  $S_h$  increases this passive wedge mechanism changes towards the flow mechanism defined by Randolph and Houlsby (1984). This change in mechanism reduces the maximum stabilising resistance provided, per metre run of soil along the slope.
- For the pile group with two rows and  $S_h/d = 3$ , a significant reduction occurred in the deflection, shear force, bending moment and ultimate lateral pile-soil pressure from a correspondingly spaced single pile row. Little soil flow occurred between the piles in this configuration even in ultimate state, independent of the range of  $S_v/d$  tested (3 and 5). For  $S_h/d = 5$ , a slight reduction in the deflection, shear force, bending moment and ultimate lateral pile-soil pressure in downslope pile row were calculated for  $S_v/d = 3$ .
- For  $S_h/d = 3$ , failure occurs via formation of a passive wedge; for the analyses with  $S_h/d = 5$ , failure is tending to form via a flow of soil around the piles. Considering the movement of soil through the piles and the total stabilising resistance provided by each

pile to the soil, it can be concluded that for  $S_h/d = 3$ , the increase in the spacing  $S_v$  within the range  $S_v/d = 3$  to 5 does not affect the formation of the mechanism (failure occurs via a passive wedge). For  $S_h/d = 5$ , although a higher spacing in  $S_v$  (i.e.  $S_v/d = 5$ ) helps to provide a higher stabilising resistance to the soil, this pile group arrangement results in considerably greater soil flow through the piles.

- In terms of designing a stabilising pile scheme for maximum force per metre run of slope, more piles are needed for the two pile rows at  $S_h/d = 3$ , than for the single pile row at  $S_h/d = 2$ . Therefore, the scheme with two pile rows costs more, if piles identical to those for the single row are used. If the maximum shear force developed on the pile is considered, a higher shear force is developed on the piles in the single row than on the piles in the double row. The piles used in the double row could therefore be less strong and this could be achieved by reducing the pile diameter or the amount of reinforcing steel.
- Finally, the  $FLAC^{3D}$  numerical analyses presented in this Chapter showed that three dimensional analyses are essential to gain a full understanding of pile-soil interaction. This is because the pile-soil interaction is a three dimensional problem by nature, and therefore the numerical analyses using plane strain or stress approaches cannot really demonstrate accurate behaviour. For example, formation of the surface passive wedge cannot be captured by 2D plain strain analysis with an assumed horizontal plane and the mechanism of soil flow through the piles cannot be reproduced by 2D plain strain analysis with an assumed vertical plane.

### 7.1.5 Chapter 6: Back analysis of pile stabilised landslide at Telford

The behaviour of rows of piles used to stabilise a landslide near Ironbridge, Telford were back analysed, and the numerical results were then compared with available field data. The  $FLAC^{3D}$  model was developed based on the information available in the ground investigation report and the use of some engineering judgement in determination of some parameters. However, some of the assumptions may not be correct and as a result, the numerical results vary slightly from the field data. On the whole, it is possible to say that the  $FLAC^{3D}$  model back analyses the behaviour of piles used to stabilise the landslide reasonably well. The conclusions from the back analyses are given below:

- The deflection of the centre row of piles in the numerical model agrees reasonably with the pile deflection curve plotted from the field data. However, from careful observation of these plots, it is possible to say that the numerical pile looks slightly stiffer than the actual pile. This may be true: the stiffness for the numerical pile was calculated assuming that the concrete does not crack with bending of the pile. However, in reality,

the concrete will crack after some millimetres of lateral deflection and thus the stiffness of the pile will reduce.

- The  $FLAC^{3D}$  model was developed based on the information available on the ground investigation report. It was assumed that the ground is simplified into three soil layers: a layer of gravelly clay underlain by weak and strong sandstones; and that there is a defined weakened slip plane along the gravelly clay/weak sandstone interface. However, it may be possible that the ground may be better approximated by two soil layers with a compound slip plane. It is believed that further analysis of field data and updated model assumptions may give a better numerical comparison to the field data.
- The  $FLAC^{3D}$  analyses carried out to back analyse the piles used to stabilise a landslide at Ironbridge, Telford have showed that a  $FLAC^{3D}$  model is capable of analysing the behaviour of a pile stabilised landslide. Accuracy of the numerical results was improved when more accurate geometry and material properties were given to the  $FLAC^{3D}$  model.

## **7.2 Future Work**

There are a number of extensions that can be made to this work to make it more applicable to a wider range of scenarios. Four major areas of future work have been identified and are explained briefly below.

### **7.2.1 Pile-soil interaction of asymmetrically spaced pile group**

The  $FLAC^{3D}$  analyses presented in Chapter 5 investigate the behaviour of one and two rows of piles spaced in a symmetrical arrangement. However, in practice, when two rows of piles are used, they would be more likely installed in a zigzag pattern to form an asymmetrical pile group arrangement. It is expected that this type pile group arrangement may be more efficient compared with the two rows of piles in a symmetrical arrangement. This could be investigated numerically by adapting the existing pile spacing model.

### **7.2.2 Long term behaviour of pile group**

The behaviour of piles installed in a clay soil in undrained conditions was investigated in Chapter 5. Many slopes are modelled using long-term drained parameters and it would be helpful to investigate the behaviour of piles under these conditions. Further numerical analyses could be carried out to extend the applicability of the analyses presented in Chapter 5. The long term behaviour of pile rows placed in a clay or in a sandy soil could be investigated.

### **7.2.3 Formation of plastic hinges (failure of the pile)**

In the numerical analyses in this thesis, it was assumed that the piles were designed with sufficient bending capacity (i.e. the yield moment of the pile is always higher than the maximum bending moment that can develop anywhere within the pile), and only the soil fails as it attains its ultimate lateral pile-soil pressure. It would be interesting to investigate the failure of the piles due to the formation of one or two plastic hinges. The principles of plastic design of structures may be used in practice to distance the real piles from hinge formation.

### **7.2.4 Extended analyses on the pile stabilised landslide at Ironbridge, Telford**

As explained in Section 6.5, two further modifications could be made to the  $FLAC^{3D}$  model to increase the reliability of the numerical results. The stiffness of the piles could be re-calculated by considering the effect of concrete cracking. Secondly, the shape of the defined slip plane could be modified to represent a compound slip plane. It is expected that a updated  $FLAC^{3D}$  model may better back analyse the real pile behaviour.

## References

- Allison J A, Mawditt J M and Williams G T (1991) The use of bored piles and counterfort drains to stabilize a major landslip - a comparison of theoretical and field performance, *In: Slope Stability Engineering*, Thomas Telford, London, pp. 369-376.
- Banerjee P K and Davies T G (1978) The behaviour of axially and laterally loaded single piles embedded in non-homogeneous soils, *Geotechnique*, Vol. 28, No. 3, pp. 309-326.
- Bicocchi N (2010) Interpretation of strain gauge data from reinforced concrete structures in the ground, *MPhil-PhD Transfer Report*, University of Southampton, UK.
- Bjerrum L (1967) Progressive failure in slopes of over consolidated plastic clay and clay shales, *Journal of the Soil Mechanics and Foundations Division, ASCE*, Vol. 93, No. SM5, pp. 3-49.
- Bransby M F and Springman S (1999) Selection of load-transfer functions for passive lateral loading of pile groups, *Computers and Geotechnics*, Vol. 24, pp. 155-184.
- Broms B B (1964) Lateral resistance of piles in cohesive soils, *Journal of the Soil Mechanics and Foundations Division, ASCE*, Vol. 90, No. SM2, pp. 27-63.
- Brown D A and Shie C F (1990a) Three dimensional finite element model of laterally loaded piles, *Computers and Geotechnics*, Vol. 10, pp. 59-79.
- Brown D A and Shie C F (1990b) Numerical experiments into group effects on the response of piles to lateral loading, *Computers and Geotechnics*, Vol. 10, pp. 211-230.
- Cai F and Ugai K (2000) Numerical analysis of the stability of a slope reinforced with piles, *Soils and Foundations*, Vol. 40, No. 1, pp. 73-84.
- Cai F and Ugai K (2003) Response of flexible piles under laterally linear movement of the sliding layer in landslides, *Canadian Geotechnical Journal*, Vol. 40, pp. 46-53.
- Carder D R (2005) Design guidance on the use of a row of spaced piles to stabilise clay highway slopes, *TRL Report-632*, Transport Research Laboratory, Crowthorne, Berkshire, UK.

- Carder D R and Barker K J (2005) Performance of a single row of spaced bored piles to stabilise a Gault Clay slope on the M25, *TRL Report-627*, Transport Research Laboratory, Crowthorne, Berkshire, UK.
- Chen C Y and Martin G R (2002) Soil-structure interaction for landslide stabilizing piles, *Computers and Geotechnics*, Vol. 29, pp. 363-386.
- Chen L and Poulos H G (1993) Analysis of pile-soil interaction under lateral loading using infinite and finite elements, *Computers and Geotechnics*, Vol. 15, pp. 189-220.
- Chen L T and Poulos H G (1997) Piles subjected to lateral soil movements, *Journal of Geotechnical and Geoenvironmental Engineering*, Vol. 123, No. 9, pp. 802-811.
- Chmoulian A Y (2004) Briefing: Analysis of piled stabilisation of landslides, *Proceedings of the Institution of Civil Engineers - Geotechnical Engineering*, Vol. 157, No. GE2, pp. 55-56.
- Chow Y K (1996) Analysis of piles used for slope stabilization, *International Journal for Numerical and Analytical Methods in Geomechanics*, Vol. 20, pp. 635-646.
- CPI (1992) Users Manual for Program ERCAP, Coffey Partners International Pty Ltd, North Ryde, Australia.
- Cubrinovski M, Kokusho T and Ishihara K (2006) Interpretation from large-scale shake table tests on piles undergoing lateral spreading in liquefied soils, *Soil Dynamics and Earthquake Engineering*, Vol. 26, pp. 275-286.
- Das B M (1994) *Principles of Geotechnical Engineering*, PWS Publishing Company, Boston.
- Dawson E M and Roth W H (1999) Slope stability analysis with FLAC, *In: FLAC and Numerical modeling in Geomechanics*, Balkema, Rotterdam, pp. 3-9.
- De Beer E E and Wallays M (1970) Stabilization of a slope in schist by means of bored piles reinforced with steel beams, *Proceeding of the 2nd International Congress on Rock Mechanics*, Beograd, pp. 361-369.
- Durrani I K (2006) Numerical modelling of discrete pile rows to stabilise slopes, *PhD Thesis*, University of Nottingham, UK.



- Durrani I K, Ellis E A and Reddish D J (2008) Numerical modelling of lateral pile-soil interaction for a row of piles in a frictional soil, *Proceedings of the 1st International Conference on Advances in Transportation Geotechnics*, Nottingham, pp. 291-298.
- Ellis E A, Durrani I K and Reddish D J (2010) Numerical modelling of discrete pile rows for slope stability and generic guidance for design, *Geotechnique*, Vol. 60, No. 3, pp. 185-195.
- Evangelista A, Lirer S, Pellegrino A, Ramondini M and Urciuoli G (2004) Interpretation of field measurements for slope stabilising piles, *Proceedings of the 9th International Symposium on Landslides*: Taylor & Francis Group, London, pp. 1593-1598.
- Fan C C and Long J H (2005) Assessment of existing methods for predicting soil response of laterally loaded piles in sand, *Computers and Geotechnics*, Vol. 32, pp. 274-289.
- Fisher J and Clark G M (1997) Bridging the Ironbridge Gorge – The Jackfield Bridge, Shropshire: planning and development, *Proceedings of the Institution of Civil Engineers - Structures & Buildings*, Vol. 122, pp. 104-116.
- Fleming W G K, Weltman A J, Randolph M F and Elson W K (1994) *Piling Engineering*, Blackie and Son, Bishopbriggs.
- Fourie A B (1996) Predicting rainfall-induced instability, *Proceedings of the Institution of Civil Engineers - Geotechnical Engineering*, Vol. 119, pp. 211-218.
- Frank R and Pouget P (2008) Experimental pile subjected to long duration thrusts owing to a moving slope, *Geotechnique*, Vol. 58, No. 8, pp. 645-658.
- Fukuoka M (1977) The effects of horizontal loads on piles due to landslides, *Proceeding of the Specialty Session 10, 9th International Conference on Soil Mechanics and Foundation Engineering*, Tokyo, pp. 27-42.
- Gabr M A and Borden R H (1990) Lateral analysis of piers constructed on slopes, *Journal of Geotechnical Engineering, ASCE*, Vol. 116, No. 12, pp. 1831-1850.
- Goodman R E (1980) *Introduction to Rock Mechanics*, John Wiley and Sons, New York.
- Griffiths D V and Lane P A (1999) Slope stability analysis by finite elements, *Geotechnique*, Vol. 49, No. 3, pp. 387-403.

- Hayward T, Lees A, Powrie W, Richards D J and Smethurst J A (2000) Centrifuge modelling of a cutting slope stabilised by discrete piles, *TRL Report-471*, Transport Research Laboratory, Crowthorne, Berkshire, UK.
- Henkel D J and Skempton A W (1954) Landslide at Jackfield, Shropshire, in a heavily overconsolidated clay, *Proceedings of the European Conference on Stability Slopes*, Vol. 1, pp. 90-101.
- Hong W P and Han J G (1996) The behavior of stabilizing piles installed in slopes, *Proceeding of the 7th International Symposium on Landslides*, Rotterdam, pp. 1709-1714.
- Hulme M, Jenkins G J, Lu X, Turnpenny J R, Mitchell T D, Jones R G, Lowe J, Murphy J M, Hassell D, Boorman P, McDonald R and Hill S (2002) Climate change scenarios for the United Kingdom, *The UKCIP02 Scientific report*, Tyndall Centre for Climate Change Research, School of Environmental Sciences, University of East Anglia, Norwich, UK.
- Itasca (1998) Fast Lagrangian Analysis of Continua in 2 Dimensions, Version 3.4: Users Manual, Itasca Consulting Group, Minneapolis, USA.
- Itasca (2006) Fast Lagrangian Analysis of Continua in 3 Dimensions, Version 3.1: Users Manual, Itasca Consulting Group, Minneapolis, USA.
- Ito T and Matsui T (1975) Methods to estimate lateral forces acting on stabilising piles, *Soils and Foundations*, Vol. 15, No. 4, pp. 43-59.
- Jacky J (1944) The coefficient of earth pressure at rest, *Journal of the Union of Hungarian Engineers and Architects*, pp. 355-358 (in Hungarian).
- Krahn J (2003) The limits of limit equilibrium analyses, *Canadian Geotechnical Journal*, Vol. 40, pp. 643-660.
- Leroueil S, Locat J, Vaunat J, Picarelli L, Lee H and Faure R (1996) Geotechnical characterization of slope movements, *Proceeding of the 7th International Symposium on Landslides*, Rotterdam, pp. 53-74.
- High-Point Rendel Ltd (2005) Ironbridge Gorge Report – The interpretation of ground investigations at Jackfield and the Lloyds, Ironbridge, Telford, *Report Ref. R/2088/01*.
- Martin G R and Chen C Y (2005) Response of piles due to lateral slope movement, *Computers and Structures*, Vol. 83, pp. 588-598.

- Matlock H and Reese L (1960) Generalized solutions for laterally loaded piles, *Journal of the Soil Mechanics and Foundations Division, ASCE*, Vol. 86, No. 5, pp. 63-91.
- Miao L F, Goh A T C, Wong K S and Teh C I (2006) Three-dimensional finite element analyses of passive pile behaviour, *International Journal for Numerical and Analytical Methods in Geomechanics*, Vol. 30, pp. 599-613.
- Nash W A (1972) *Schaum's Outline of Theory and Problems of Strength of Materials*, McGraw-Hill, New York.
- Ng C W W, Zhang L and Nip D C N (2001) Response of laterally loaded large-diameter bored pile groups, *Journal of Geotechnical and Geoenvironmental Engineering, ASCE*, Vol. 127, No. 8, pp. 658-669.
- Oasys (2004) ALP, Version 18.0: Users Manual, Oasys Ltd, London, UK.
- Pan J L, Goh A T C, Wong K S and Selby A R (2002) Three-dimensional analysis of single pile response to lateral soil movements, *International Journal for Numerical and Analytical Methods in Geomechanics*, Vol. 26, pp. 747-758.
- Pan J L, Goh A T C, Wong K S and Teh C I (2002) Ultimate soil pressures for piles subjected to lateral soil movements, *Journal of Geotechnical and Geoenvironmental Engineering*, Vol. 128, No. 6, pp. 530-535.
- Potts D M, Kovacevic N and Vaughan P R (1997) Delayed collapse of cut slopes in stiff clay, *Geotechnique*, Vol. 47, No. 5, pp. 953-982.
- Poulos H G (1995) Design of reinforcing piles to increase slope stability, *Canadian Geotechnical Journal*, Vol. 32, No. 5, pp. 808-818.
- Poulos H G (1999) Design of slope stabilising piles, *In: Slope Stability Engineering*, Eds: Yagi, Yamagami and Jiang, Balkema, Rotterdam, pp. 83-100.
- Poulos H G and Davis E H (1980) *Pile Foundation Analysis and Design*, John Wiley and Sons, New York.
- Powrie W (2004) *Soil Mechanics: Concepts & Applications*, Spon Press, London and New York.
- Randolph M F (1981) The response of flexible piles to lateral loading, *Geotechnique*, Vol. 31, No. 2, pp. 247-259.

- Randolph M F and Houlsby G T (1984) The limiting pressure on a circular pile loaded laterally in cohesive soil, *Geotechnique*, Vol. 34, No. 4, pp. 613-623.
- Reese L C, Cox W R and Koop F D (1974) Analysis of laterally loaded pile in sand, *Proceeding of the 6th Annual Offshore Technology Conference*, Houston, Paper No. 2080.
- Reese L C, Wang S T, Arrellaga J A and Hendrix J (1996) Computer Program GROUP for Windows, Version 4.0: Users Manual, Ensoft Inc, Austin, Tex.
- Rollins K M, Olsen K G, Jensen D H, Garrett B H, Olsen R J and Egbert J J (2006) Pile spacing effects on lateral pile group behavior: Analysis, *Journal of Geotechnical and Geoenvironmental Engineering, ASCE*, Vol. 132, No. 10, pp. 1272-1283.
- Rollins K M, Peterson K T and Weaver T J (1998) Lateral load behavior of full-scale pile group in clay, *Journal of Geotechnical and Geoenvironmental Engineering*, Vol. 124, No. 6, pp. 468-478.
- Selby A R and Arta M R (1991) Three-dimensional finite element analysis of pile group under lateral loading, *Computers and Structures*, Vol. 40, No. 5, pp. 1329-1336.
- Skempton A W (1970) First-time slides in over-consolidated clays, *Geotechnique*, Vol. 20, No. 3, pp. 320-324.
- Skempton A W and Weeks A G (1976) The Quaternary history of the Lower Greensand escarpment and Weald Clay Vale near Sevenoaks, Kent, *Philosophical Transactions of the Royal Society of London*, Vol. A283, pp. 493-526.
- Smethurst J A (2003) The use of discrete piles for infrastructure slope stabilisation, *PhD Thesis*, University of Southampton, UK.
- Smethurst J A and Powrie W (2007) Monitoring and analysis of the bending behaviour of discrete piles used to stabilise a railway embankment, *Geotechnique*, Vol. 57, No. 8, pp. 663-677.
- Sommer H (1977) Stabilization of a creeping slope in clay with stiff elements, *Proceeding of the 7th European Conference on Soil Mechanics and Foundation Engineering*, Brighton, pp. 269-274.
- Vaughan P R and Walbancke H J (1973) Pore pressure changes and the delayed failure of cutting slopes in overconsolidated clay, *Geotechnique*, Vol. 23, No. 4, pp. 531-539.

- Viggiani C (1981) Ultimate lateral load on piles used to stabilize landslides, *Proceeding of the 10th International Conference on Soil Mechanics and Foundation Engineering*, Stockholm, Vol. 3, pp. 555-560.
- Wang W L and Yen B C (1974) Soil arching in slopes, *Journal of the Geotechnical Engineering Division, ASCE*, Vol. 100, No. GT1, pp. 61-78.
- Weeks A G (1969) The stability of natural slopes in south-east England as affected by periglacial activity, *Quarterly Journal of Engineering Geology*, Vol. 2, pp. 49-61.
- Yang Z and Jeremic B (2005) Study of soil layering effects on lateral loading behavior of piles, *Journal of Geotechnical and Geoenvironmental Engineering*, Vol. 131, No. 6, pp. 762-770.
- Yoon B S and Ellis E A (2008) Centrifuge modelling of slope stabilisation using discrete pile row, *Proceedings of the 1st International Conference on Advances in Transportation Geotechnics*, Nottingham, pp. 349-354.
- Zacharopoulos A (2010) Piles in unstable ground, *PhD 9 Months Report*, University of Southampton, UK.
- Zhang L, Silva F and Grismala R (2005) Ultimate lateral resistance to piles in cohesionless soils, *Journal of Geotechnical and Geoenvironmental Engineering*, Vol. 131, No. 1, pp. 78-83.

